Defense Nuclear Agency
Alexandria, VA 22310-3398

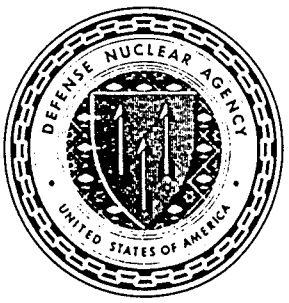

DNA-TR-91-132

SPEAR-1 Payload and SPEAR-2 External Diagnostic Package

W. John Raitt
Utah State University
Center for Atmospheric and Space Sciences
Logan, UT 84322-4405

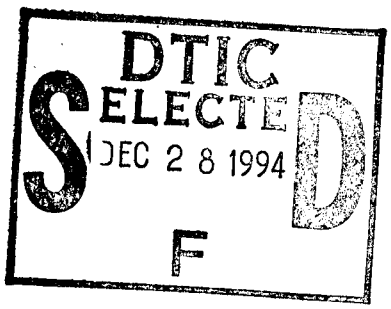

June 1992

Technical Report

CONTRACT No. DNA 001-87-C-0015

Approved for public release;
distribution is unlimited.

REPORT DOCUMENTATION PAGE

Form Approved
OMB No. 0704-0188

1. AGENCY USE ONLY (Leave blank)	2. REPORT DATE	3. REPORT TYPE AND DATES COVERED
	920601	Technical 870310 - 910830

4. TITLE AND SUBTITLE
SPEAR-1 Payload and SPEAR-2 External Diagnostic Package

5. FUNDING NUMBERS
C - DNA 001-87-C-0015
PE - 63224C
PR - SF
TA - SD
WU - DH028960

6. AUTHOR(S)
W. John Raitt

7. PERFORMING ORGANIZATION NAME(S) AND ADDRESS(ES)
Utah State University
Center for Atmospheric and Space Sciences
Logan, UT 84322-4405

8. PERFORMING ORGANIZATION REPORT NUMBER

9. SPONSORING/MONITORING AGENCY NAME(S) AND ADDRESS(ES)
Defense Nuclear Agency
6801 Telegraph Road
Alexandria, VA 22310-3398
RAEV/Beatty

10. SPONSORING/MONITORING AGENCY REPORT NUMBER
DNA-TR-91-132

11. SUPPLEMENTARY NOTES
This work was sponsored by the Defense Nuclear Agency under RDT&E RMC Code B7664D SF SD 00183 PRPD 1950A 25904D. Additional support and funding provided by the Strategic Defense Initiative Organization

12a. DISTRIBUTION/AVAILABILITY STATEMENT
Approved for public release; distribution is unlimited.

12b. DISTRIBUTION CODE

13. ABSTRACT *(Maximum 200 words)*

This report describes the development, test and results from the sounding rocket payloads in the program "Space Power Experiments Aboard Rockets" (SPEAR). The report addresses the complete payload designated SPEAR-1, successfully flown in December 1987, and the external diagnostics package included in the payload designated SPEAR-2 which was launched in July 1990.

SPEAR-1 used an internal 45kV power supply to differentially bias a pair of deployed spheres relative to the main payload structure. Although volume discharges were seen when the payload was tested in a space simulated chamber, no significant discharges or arcs were observed when the payload was operated in the ionosphere at altitudes up to 370km. Failure of a payload grounding device to be exposed resulted in an electrically bipolar system. For the configuration flown it was concluded that the LEO space environment was an adequate insulator.

The external diagnostic package of the SPEAR-2 payload was instrumented to study the interaction of the high voltage and high current loads with the vehicle environment using imaging optical techniques, EMP detectors, and measurements of the environment pressure, plasma

14. SUBJECT TERMS		15. NUMBER OF PAGES
SPEAR-2	Space Power	176
Rocket Payload	Diagnostic Testing	16. PRICE CODE

17. SECURITY CLASSIFICATION OF REPORT	18. SECURITY CLASSIFICATION OF THIS PAGE	19. SECURITY CLASSIFICATION OF ABSTRACT	20. LIMITATION OF ABSTRACT
UNCLASSIFIED	UNCLASSIFIED	UNCLASSIFIED	SAR

CLASSIFIED BY:

N/A since Unclassified

DECLASSIFY ON:

N/A since Unclassified

9. SPONSORING/MONITORING AGENCY NAME(S) AND ADDRESS(ES) (Continued)

Director
Strategic Defense Initiative Organization
Pentagon
Washington, D.C. 20301-7100

13. ABSTRACT (Continued)

density, and energetic charged particle fluxes. Although no useful flight data were collected from the mission, valuable measurements were obtained during testing and integration, including a full payload test in a large space simulation chamber.

SUMMARY

The SPEAR 1-2 program greatly advanced our understanding of the HV interaction with a vacuum/plasma environment. This environment was provided by a space simulation chamber for SPEAR-1 and SPEAR-2, and by the actual LEO space environment for SPEAR-1. The comparison of SPEAR-1 chamber test results and the flight results helped in understanding how space simulation chambers could be configured to avoid the gross differences in operation in the chamber compared to space. It also demonstrated that even the largest space chamber is no substitute for performing active experiments in the unbounded plasma of the true LEO space environment.

SPEAR-1 provided new data on currents flowing between the environment and exposed electrodes for biassing in the 10's kV range. The results showed that the current levels were rather low, and no volume or localized discharges occurred above an altitude of about 100 km. This showed that for the open configuration of the SPEAR-1 HV system, the LEO space environment provided adequate insulation for loads attached to HV space power systems.

We showed that the sounding rocket approach provides a short turn-around to perform a specific test, even when the technology being used was new to sounding rocket applications. Minimizing documentation, quality control yet still maintaining adequate engineering standards provided the means of performing a significant space power related experiment at relatively low cost and with short time from inception to flight.

SPEAR-2 resulted in valuable data being obtained on the fabrication and conditioning needed to prepare realistic space power components for operation while exposed to a vacuum/plasma environment.

The EDP performed well during testing. We demonstrated the capability to use fiber optics in HV systems, both by the transmission of coherent images to cameras located at a protected site, and to provide communication to an isolated subsystem deployed in a potentially hazardous location. All systems functioned in the space simulation chamber, except the LLLTV cameras due to a problem in the instrumentation section not maintaining its pressure, and also the cameras not meeting their specification of operating at 2 psi. This problem was subsequently corrected before flight by building pressurized enclosures for each of the two LLLTV cameras.

The loss of the flight data was disappointing for the EDP instruments because we believe the HV/HC system interaction would have been different in space as opposed to simulated space as was observed for SPEAR-1. However the configuration of SPEAR-2 was such that the chamber/space comparison may not have been so different as the SPEAR-1 tests showed. Until the chamber/space comparison is made, there is still a strong case to be made for flying a realistic HV load into the LEO environment to study its interaction, if the possibility of utilizing HV systems at LEO altitudes is still in the long term planning in both the civil and the defense arenas. In addition there is very little information about the interaction of HV with the space environment for the supersonic motion of a payload in LEO orbit.

TABLE OF CONTENTS

Section		Page
SUMMARY		iii
LIST OF ILLUSTRATIONS		vi
1	INTRODUCTION	1
2	USU CONTRIBUTION TO THE SPEAR PROGRAM	3
	2.1 SPEAR-1	3
	2.2 SPEAR-2	4
3	SPEAR-1 EXPERIMENT	6
4	SPEAR-2 EXTERNAL DIAGNOSTICS PACKAGE	8
	4.1 Introduction	8
	4.2 Instrument descriptions	11
	4.3 Results	30
5	FUTURE WORK	36
	5.1 HV-Environment Interaction	36
	5.2 Spacecraft Grounding	38
	5.3 General Considerations	38
APPENDIX		
A	SPACE POWER EXPERIMENTS ABOARD ROCKETS (SPEAR-1)	A-1
B	HOW TO USE THE SPEAR-1 FORMATTING CALIBRATING PROGRAM	B-1
C	SPEAR-1, COLLECTION OF ALL DISCHARGE/CURRENT AND VOLTAGE PLOTS	C-1

LIST OF ILLUSTRATIONS

Figure		Page
4.1	SPEAR-2 payload showing location of external diagnostic package sensors.	41
4.2	SPEAR-2 load section diagram showing location and fields-of-view of the video camera, still camera and photometer optical heads.	42
4.3	SPEAR-2 load section diagram cross section showing location and fields-of-view of the video camera, still camera and photometer optical heads.	43
4.4	SPEAR-2 fiber optics optical head design (used on imaging fiberscopes 1 through 7; See Figures 4.2 and 4.3).	44
4.5	SPEAR-2 fiber optics optical head design (used on imaging fiberscope 8; See Figures 4.2 and 4.3).	45
4.6	SPEAR-2 optical imaging system beam-splitter.	46
4.7	SPEAR-2 photometer high-voltage mode data acquisition timeline.	47
4.8	SPEAR-2 photometer processor map channel functional block diagram.	48
4.9	SPEAR-2 photometer processor accumulator functional block diagram.	49
4.10	SPEAR-2 sensor deployment system showing location of EMP sensors, Langmuir probe, particle detector clusters and charge probe.	50
4.11	SPEAR-2 EMP detector log amplifier channel block diagram.	51
4.12	SPEAR-2 EMP digitizer channel block diagram.	52
4.13	SPEAR-2 particle detector assembly.	53
4.14	SPEAR-2 Langmuir probe assembly.	54
4.15	SPEAR-2 Langmuir probe functional block diagram.	55
4.16	SPEAR-2 charge probe.	56
4.17	SPEAR-2 optical imaging system views of load section.	57
4.18	SPEAR-2 photometer accumulator serial data plot.	58
4.19	SPEAR-2 photometer pulse map output for one HV operation at 231.33 seconds.	59
4.20	SPEAR-2 D-dot data sampled at 200 nS sampling interval.	60

LIST OF ILLUSTRATIONS (Continued)

Figure		Page
4.21	SPEAR-2 D-dot data from high current event.	61
4.22	SPEAR-2 B-dot data sampled at 200 nS sampling interval.	62
4.23	SPEAR-2 B-dot data from high current event.	63
4.24	SPEAR-2 particle detector output plot.	64
4.25	SPEAR-2 Langmuir probe output plots.	65
4.26	SPEAR-2 Neutral pressure gauge output plots.	66
4.27	SPEAR-2 Fluxgate magnetometer output plots.	67

SECTION 1

INTRODUCTION

At the inception of the Space Power Experiments Aboard Rockets (SPEAR) program the increasing maturity of the national space program had led to proposals for the incorporation of space platforms containing high energy defensive systems into the national defense plan. The overall purpose of the SPEAR program was to provide a better understanding of how these systems would interact with the space environment, leading to the development of engineering design guidelines for the development of future operational systems. Since many of the systems under consideration were heavy and bulky, most of the emphasis was to be on system-space interactions at low earth orbit altitudes (LEO).

Some of the systems under consideration involved the conversion of large amounts of energy in short periods of time, in other words the handling of high energy on the space platform. If the energy involved was electrical energy, then often the high energy would be equated with high voltage. This consideration led to the prime thrust of the SPEAR program being to study the interaction of high voltages with the LEO space environment. Of particular interest was to determine if the "vacuum" of space at LEO could provide adequate insulation to charged conductors that the leakage currents were negligible, implying that no significant bulk discharges or localized arcing took place.

Theoretical models of the interaction were rather limited at the start of the SPEAR 1-2 project. The work of Langmuir and Blodgett dating from the 1920s gave an analytical description of HV-plasma interaction ignoring magnetic field effects. Parker and Murphy studied the same problem by a strict conservation of momentum and energy in the presence of a magnetic field, but without allowance for collisions or collective plasma effects. Linson modified the Parker-Murphy model to allow some cross-field currents due to plasma instabilities.

Prior to and during the SPEAR 1-2 program advances were being made in the numerical modeling of the HV - space interaction with programs such as NASCAP-LEO and POLAR. These programs took advantage of rapidly developing computer technology to enable irregular shapes and complex surface geometries and properties to be modeled.

The theoretical models predicted widely varying results for the current collected when voltages in the 10's kV range were exposed to the ionospheric plasma. Experimental

data was limited, and mainly secondary results obtained from charged particle beam experiments in space which were subject to the disturbing influence of the particle beam.

It was therefore proposed that the SPEAR program would investigate HV-space interactions using differential biassing of a space platform in the 10's kV range. Measurements of the currents collected by exposed biased collectors and diagnosis of the effect on the platform and its environment would help refine the theoretical models, and also provide a basis for an engineering guide to the handling of HV in the LEO space environment.

The approach taken in the SPEAR 1-2 program was to develop two sounding rocket payloads to take HV systems to the LEO altitude range from 100 - 370 km. SPEAR-1 was a science oriented payload using simple geometry to study the current collected when a sphere was biassed to 45kV relative to the vehicle. The vehicle was intended to remain close to ionospheric potential by the operation of an active plasma contactor device. SPEAR-2 was intended to demonstrate that components with configurations and mounting schemes closer to an actual system could operate successfully in the space environment without the need for excessive insulation.

In order to be able to study the interaction of the selected elements of the biassed systems with the space environment, both SPEAR-1 and SPEAR-2 protected their prime HV power source from the environment in pressurized sections of the payload. The experiments were therefore performed on the loads to the protected power systems rather than the power systems themselves.

SECTION 2

USU CONTRIBUTION TO THE SPEAR PROGRAM

Utah State University was tasked to develop the SPEAR-1 payload to the point of delivering a working system to the major integrator at (then) AFGL for complete system integration, testing and flight preparation. The testing included the standard environment tests as well as a space simulation chamber test at the NASA Plum Brook facility which was planned and directed by USU. USU was also responsible for experiment preparation and system configuration for the launch phase and for the data handling tasks associated with the various instruments and sensors carried on the payload.

The role of USU in the SPEAR-2 project was more peripheral than for SPEAR-1. We were tasked to provide an external diagnostics package which would monitor the effect of HV and high current (HC) discharges in the load section of the payload external to the sensors incorporated in the load section components.

2.1 SPEAR-1.

SPEAR-1 was designed to achieve the following measurements:

- Bias one of two spheres deployed at 3m from the rocket body to up to 45kV relative to the vehicle.
- Monitor the currents and voltages in the HV system at low (1mS) and high (200nS) time resolution.
- Provide visual images of the light resulting from volume and local discharges caused by the high bias voltage.
- Connect the vehicle to the ionosphere by a low impedance path provided by a hollow cathode plasma contactor.
- Monitor the vehicle potential by a combination of charged particle detectors and boom mounted floating probes.
- Monitor the neutral pressure close to the vehicle.
- Monitor the ambient ionospheric electron density close to the vehicle.
- Monitor plasma waves resulting from the disturbance produced by the HV exposure to the ionosphere.

- Verify the orientation of the geomagnetic field in the reference frame of the payload.

The measurements were to be achieved by a payload developed for launch by a Black Brant 10 sounding rocket. This put a size constraint on the payload to be accommodated in a cylindrical volume of 17" in diameter and no longer than 300". The hardware had to be ruggedized to withstand the steady acceleration and the vibration levels associated with a rocket launch.

An important part of the development of the SPEAR-1 payload was a comprehensive test of the integrated system in a large space simulation chamber. This test was performed at the NASA Plum Brook facility using the newly refurbished chamber-B. The tests of the flight payload were preceded by a mockup test which provided valuable data to assist in the planning of the flight payload.

In order to have a quiescent background ionospheric plasma it was required to launch the payload into the mid-latitude ionosphere. The high altitude requirement for the payload limited the choice of the launch site to a coastal rocket range, so it was decided not to include any recovery equipment in the payload. The selected launch site was the NASA Wallops Island range, VA, and NASA personnel provided support for the launch operations.

The launch of the payload was successfully achieved on December 14, 1987 at 01:45 GMT (13 Dec. 1987 20:45 EST) and reached an apogee of 369 km 351 sec after lift off.

2.2 SPEAR-2.

The external diagnostics package of SPEAR-2 was designed to achieve the following measurements:

- Optical images of light emission from discharges around exposed HV/HC components in the load section of the payload.
- Measurement of ambient pressure in the vicinity of the load section of the payload.
- Measurement of the ambient ionospheric electron density close to the vehicle.
- Level of EMP signals in the instrumentation section of the payload, sampled sufficiently rapidly to reconstruct the dE/dt and dB/dt waveforms in three axes.

- Determination of vehicle charging by charged particle detectors and a dielectric charge probe.
- Verification of the orientation of the geomagnetic field in the reference frame of the payload.

The payload was planned to be launched by an Aries sounding rocket which allowed a diameter of 48" to be available for payload components. The components and their mountings were designed with the knowledge that they would have to survive the acceleration and vibration associated with a rocket launch.

The external diagnostics were to be located in two parts of the payload. The pressure gauge and the optical heads for the imaging system were to be in the load section. This resulted in a need to maintain strict electrical isolation for those components from their data handling units located in the instrumentation section of the payload. The remainder of the sensors were located in the instrumentation section of the payload, those sensors requiring high voltage were in a part of the section which could be evacuated on the pad, the others were in a part which was planned to maintain a pressure of 2 psi throughout the flight.

The integrated flight payload was tested in the very large space simulation chamber at NASA Plum Brook designated the SPF facility. A comprehensive series of tests were performed related to conditioning the exposed HV/HC components in preparation for reproducing a flight sequence in the chamber.

As for SPEAR-1 it was desirable to have a quiescent mid-latitude background ionosphere for the planned measurements. In this case, however, we were able to choose the mid-latitude launch site on land since the Aries is guided on its ascent, and, therefore, has a much lower landing position dispersion than the unguided Black Brants. The SPEAR-2 launch site was selected to be White Sands Missile Range, NM.

The payload was launched on July 26, 1990 at 05:51 GMT (July 25, 1990 23:51 MDT) the Aries guidance system developed a problem, and the flight was aborted about 30 sec after launch for safety reasons. The vehicle never initiated any of its prime measurement cycles, and the payload was destroyed on impact with the ground.

SECTION 3

SPEAR-1 EXPERIMENT

The SPEAR-1 experiment used two 2.5 μF capacitors charged to one of several voltages as the HV biassing source for two spheres deployed to a distance of about 3m from the payload. The capacitors provided a compact HV source with a large current capacity. In this experiment it was limited to a maximum of 20 amps, providing adequate current to support volume discharges or arcs for short time should they occur. The intention was to ground the vehicle to the ionosphere by a hollow cathode plasma contactor, but failure of a cover to be removed from the device resulted in the experiment changing from the planned unipolar system to a bipolar system, the rocket body being driven to several thousand volts negative while the sphere was driven positive.

The development, testing and flight results from SPEAR-1 were reported in 1988, and a copy of the technical report is attached as appendix B, together with plots of the current-voltage characteristics for each of the capacitor discharges during the flight in appendix C.

The principal results obtained from the SPEAR-1 experiment were as follows:

- The exposure of 10's kV positive or negative to the nighttime LEO environment resulted in no significant discharges or arcs above about 100km altitude.
- The leakage currents to space were quite low, well represented by a resistor with a value 500kΩ to 1MΩ for the SPEAR-1 geometry. The space environment could therefore be regarded as an insulator for systems handling currents in the ampere range.
- Although the bipolar effect was an interfering factor, the evidence points to the plasma currents to the charged parts of the system to be limited by the geomagnetic field.
- The release of gas from an ACS nozzle while the vehicle was negatively charged appeared to provide a low impedance path to the ionosphere by the generation of local plasma within the gas jet.
- The payload demonstrated the capability to utilize high energy, high voltage capacitors on a space platform.

Further analysis of SPEAR-1 data was suspended due to funding problems with SPEAR-2 which were becoming acute as the SPEAR-1 data analysis was about to build up. There are some additional analyses which could still usefully be performed with the SPEAR-1 data. These will be addressed at the end of the report.

SECTION 4

SPEAR-2 EXTERNAL DIAGNOSTICS PACKAGE

4.1 INTRODUCTION.

The purpose of the SPEAR-2 external diagnostics package (EDP) was to study the effect of high voltage (HV) and high current (HC) discharges on the SPEAR-2 payload (exclusive of monitoring the performance of the load and power section instrumentation) and the interaction of those discharges with the internal and external payload environment. In particular, the instrumentation was selected to study optical signatures of the presence of arcs and/or discharges at the surfaces and in the immediate environment of exposed, biased elements of the power system; pulsed electromagnetic fields resulting from the operation of the HV and HC systems; energetic charged particles in the vicinity of the instrumentation section; and the ambient neutral pressure, plasma density and geomagnetic field at the payload.

Figure 4.1 illustrates the SPEAR-2 payload configuration and identifies the location of the EDP subsystem. Optical heads for the eight imaging systems and the photometer, and the self-contained neutral pressure gauge, were in the load section of the payload. The EDP sensor section, aft of the power generation section, contained the sensors intended for deployment into the space environment through ejectable doors in the payload skin. The sensor section was maintained under vacuum on the pad, since it was connected to the evacuated load section through tubes carrying the coherent fiber optic bundles forward into the load section. Aft of the EDP sensor section was the EDP electronics section. Although initial plans called for the electronics section to be maintained at 2 psi, difficulties in sealing resulted in a decision to allow this section to be evacuated.

When an arc or a volume discharge occurs, multiplicative ionization and excitation occurs and the associated relaxation of the atoms and molecules results in light emission over a wide range of wavelengths. The SPEAR-2 EDP used sensitive optical devices to detect this light, and an optical imaging system to identify the emission region.

The rapidly varying currents and electric fields associated with the HV and HC discharges into the loads, as well as currents flowing as a result of arcing or other unanticipated current paths, will generate electric and magnetic fields. If these fields have a very high intensity in the vicinity of the payload instrumentation section they could upset

electronics associated with the communications and control of the payload. We therefore included sensors to monitor these levels a short distance outside the payload skin.

The interaction of high electrostatic and induced potentials with the space plasma environment can accelerate the plasma particles to high energies. The EDP included sensors to detect the presence of fluxes of energized particles impinging on the payload. This array of differential electrostatic analyzers was to measure the energy spectra of both positive ions and electrons from a few eV up to 30keV.

The ambient neutral gas and plasma conditions around the payload play an important role in the development of arcs and discharges resulting from exposed, biased electrodes. The EDP included a neutral pressure monitoring system located close to the power load section of the payload, designed to respond to pressure pulses with a mS time period. A Langmuir probe in the EDP sensor section was to monitor the ambient electron density and temperature as the payload progressed along its trajectory. Finally, the EDP included a fluxgate magnetometer to monitor the attitude of the vehicle, and to respond to any perturbations of the magnetic field at a lower level than the EMP sensors.

Table 1 summarizes the 10 different instruments making up the SPEAR-2 external diagnostics package.

Table 1. SPEAR-2 external diagnostics package instrument complement.

Instrument	Qty	Loc*	Notes
LLLTV Camera	2	E	White light, 8 images; optical heads in power section; uses fiber optics for image transmission
35mm Camera	2	E	White light, 8 images; optical heads in power section; uses fiber optics for image transmission
Photometer	1	S	391.4nm; photon-counting, photon-mapping
EMP D• Sensor	1	S	3-axis; 200nS time-resolution waveform capture
EMP B• Sensor	1	S	3-axis; 200nS time-resolution waveform capture
Charged Particle Detectors	2	S	1eV-30KeV ions and electrons, multiple view directions, 32mS energy scan period
Thermal Plasma Probe	1	S	Ion and electron density, electron temperature in ionospheric range (n:10^4-10^7, T:500 - 5000K)
Charge Probe	1	S	Vehicle potential changes
Neutral Pressure	1	P	Range: 10 to 10^{-7} torr, high time resolution
Magnetometer	1	S	3-axis fluxgate; ambient geomagnetic field measurements

* E=EDP Electronics Section; S=EDP Sensor Section; P=Payload Power Section

4.2 INSTRUMENT DESCRIPTIONS.

4.2.1 *Optical Imaging Systems.*

4.2.1.1 Purpose. The SPEAR-2 EDP used two low-light-level television (LLLTV) cameras and two 35-mm still-frame film cameras to record images of emissions from the HV/HC components. The cameras were located in the EDP electronics section, and eight optical heads in various locations in the load section defined the cameras' fields of view, conveying the images to the cameras via coherent fiber optic bundles. Each image was recorded simultaneously by a LLLTV camera and a film camera. The film cameras, given their relatively long exposure time, integrated all emission during a HV/HC discharge selection, while the LLLTV cameras gave the 30mS time resolution provided by the frame scanning rate. We employed no special gating of the imaging CCD; each CCD cell integrated light for a full frame interval to maximize sensitivity.

One of the optical heads was positioned to view away from the payload in the direction of the plasma ejection from the HC load provided by the plasma accelerator. This head's objective was to record the evolution of the accelerated plasma cloud as a function of the orientation of the ejection direction relative to the geomagnetic field.

4.2.1.2 Heritage. SPEAR-1, flown in December 1987, represented the prior state of art in using LLLTV images to study the spatial distribution and intensity of light emission from HV arcs and discharges in space. The SPEAR-1 camera, similar to those used on SPEAR-2, operated successfully, but lacked the coherent fiber optic bundle we used in SPEAR-2 to convey the image to a remotely located camera.

The camera packaging developed for SPEAR-1 enabled the HV associated with the image intensifier to be maintained at one atmosphere. This development proved valuable in the SPEAR-2 program for reasons described later.

4.2.1.3 Design Considerations. The most innovative part of the imaging optical system was the use of a coherent fiber optic bundle to convey images formed at the forward end of the payload to recording cameras located in the EDP electronics section. Locating the cameras well aft of the load section protected them from potential damage from the high-

voltage environment, and provided isolation to reduce the possibility of conducted destructive emissions from the load section to the telemetry encoders and electronics.

Eight optical head assemblies in the load conditioning section provided eight separate images of such elements as the pulse forming network, the transformer, the klystrode, the plasma accelerator inductor, the voltage divider and the plasma jet emerging from the plasma accelerator. Each optical head assembly was adjustable and consisted of an imaging lens and an adjustable convex mirror, except that the optical head viewing the plasma discharge had no mirror. The combination of lens and adjustable convex mirror provided a generous selection of viewing angle and subject for each image, even after the head was mounted in the load section. Figures 4.2 and 4.3 illustrate the locations and fields of view of the optical heads, and Figures 4.4 and 4.5 illustrate the optical heads designed for SPEAR-2.

Each optical head assembly focused an image on the image plane of the distal end of a coherent fiber optics bundle; the coherent bundle transmitted this image to the pressure bulkhead. At the bulkhead, the end of each bundle forms one quadrant of a hermetically-sealed four-part image plane; two such image planes, held in place by circular flanges, thus contained all eight images in two separate "superimages." On the pressure side of the bulkhead, a beamsplitter divided the superimage beam emerging from the image plane, sending half of it to a video camera and half to a 35mm camera. One video and one film camera thus identically recorded one set of four images from the load section, and the second film and video camera record the second set of four images.

The beamsplitter dividing the 4-part superimages between the LLLTV and still cameras presented a considerable design challenge. As finally constructed, the beamsplitter interfaced to both the LLLTV camera and a standard ruggedized 35mm film camera within the cramped confines of the EDP electronics section, and yet allowed access to the film cameras from outside the payload after assembly. Figure 4.6 illustrates the beamsplitter designed for SPEAR-2.

The coherent fiber optic bundles employed another innovative design feature. Standard fiber optics are enclosed in a stiff shield that both protects the delicate fibers and provides a rugged mounting surface. However, since in SPEAR-2 the fiber optic bundles had to traverse a large area where maintaining a high vacuum was important, we found the standard design practice unsuitable. Not only would a standard shield, by mechanically enclosing the fibers bundles, create a potential "virtual leak," but it would also offer a potential path by which any arcs or discharges in the load section could propagate to the EDP sensors and electronics.

To overcome the problems inherent in standard fiber optic design, we worked with our fiber optic subcontractor to develop a two-part bundle enclosure. The entire length of each of the eight fiber optic bundles was enclosed in a loosely-braided fiberglass sheath. This sheath was rugged enough to protect the fibers from abrasive damage, yet porous enough to allow the bundles to outgas to a high degree during evacuation.

Although the braided cover removed the potential virtual leak problem, however, it was not stiff enough to permit us to tie or clamp the bundle to the payload structure without crushing the fibers. Therefore, before putting the fiberglass cover in place we installed several stiff Teflon sleeves, each about 2" long, around each bundle of fibers at approximately 1-foot intervals. We then put the fiberglass braid over the entire assembly. Each sleeve bore two circumferential grooves on its outer surface, allowing us to use cable ties to secure the entire fiber optic bundle along its length to the payload structure. The sleeves were short enough to permit thorough outgassing. Also, exercising care, one could slide the sleeves along the bundle, which enabled us to tailor our mounting to the actual configuration of the payload during integration.

4.2.1.4 Flight System. The optical imaging system used two Nikon F3HP 35mm film cameras, each equipped with a Nikon 50mm f/1.8 lens, a 250-exposure film magazine, battery-operated film advance and rewind and external shutter control. We used high-speed (~ 1000 ASA) film with a spectral response of 350-680 nm (3M color print film), and an exposure time of 1 second. A camera controller housed in the EDP electronics section operated the shutter, exposing a single frame for each one-second, 50-pulse HV sequence and a single frame for each of the HC sequences. The camera controller initiated the shutter sequence in response to timing signals received from the main payload controller. The exposed film was to be removed after payload recovery.

The imaging system also used two English Electric Valve P45930 video cameras, each equipped with an Angenieux 40mm f/1.8 lens and a Generation II microchannel-plate image intensifier with a 350-900 nm spectral response. The video system provided one frame approximately every 30 mS; the video signal was telemetered to ground station receivers for recording.

4.2.1.5. System Failures. A design failure of the imaging optical system arose out of the LLLTV cameras not meeting one of their specifications. We believed the camera image intensifiers would operate without arcing at a pressure of 2 psi. However during testing it

was found that the intensifiers failed at about 8 psi. This problem, compounded with difficulty in maintaining a pressure differential of 2 psi in the EDP electronics section, resulted in the need to design and build pressurized housings for the two LLLTV cameras late in the payload development. We drew upon the SPEAR-1 design to correct the situation speedily. Unfortunately, however, we were not able to complete the LLLTV camera enclosures before the space chamber testing at Plum Brook, so no interior TV images were obtained from that phase of the program.

4.2.1.6 Future Design Guidelines. In a future design of the fiber optic bundles we would attempt to reduce the number of lost pixels apparently arising from the breaking of individual fibers when the four individual bundles making up one set were swaged together. We would also recommend that more attention be paid to the outgassing characteristics of the fiber optic bundles, and to the likelihood of their providing a conductive channel to propagate arcs. The question of whether an attempt should be made to completely seal them or whether, as in the SPEAR-2 design, they should be as open as possible needs further study.

The film cameras performed well, but to help keep track of the many frames generated during testing, we would add a time/date/sequence number annotating back to the film cameras.

4.2.2 *Photometer.*

4.2.2.1 Purpose. A narrow field-of-view photometer filtered at 391.4nm recorded the near-UV component of any optical emissions in the vicinity of the HV transformer and the pulse-forming network. Although this system was not an imaging system, it had the considerable advantage of 200nS time resolution in the photon mapping mode, rather than the ~30mS resolution of the video cameras.

The pulse stream from the photomultiplier was directed both to an accumulated-count monitor and pulse-mapping system. The pulse-mapping system recorded the occurrence of one or more pulses in a 200nS time window as a 1-bit in a memory. The contents of this memory thus provided a time history of the development of light emission with a sub-microsecond time resolution for high light intensities.

Although the photometer's field of view was directed at the pulse transformer, the instrument was sensitive to reflected light from discharges occurring elsewhere in the

power load section. This feature made its output a valuable confirmation of other indicators of arcs and discharges in the load section.

4.2.2.2 Heritage. The pulse counting photometer design has been flown on many previous rocket flights. The pulse mapping system was developed for the NASA CHARGE-1 and -2 sounding rocket payloads, but was refined considerably for SPEAR-2.

4.2.2.3 Design Considerations.

- Fiber optic transfer of light pulses to the photometer.

To minimize both the opportunity for a high-voltage discharge damaging the photometer and the possibility of EMI/C effects corrupting photometer data, the photometer and its electronics were located on the main EDP bulkhead, well aft of the power section. Optical input passed to the photometer by means of a fiber optic link to the load section. Locating the electronics at a distance from the high power environment considerably eased design constraints on the data and signal processing system.

An optical head in the load section focused any light emitted or reflected from vicinity of the transformer and pulse-forming network onto one end of a fiber-optic bundle, which conducted the light to the photometer. Electrical output signals from the photometer passed through a hermetically-sealed bulkhead connector to the electronics box for processing. Figures 4.2 and 4.3 illustrate the location of the photometer's optical head and its field of view.

- High Speed pulse mapping system.

In the high voltage mode, the pulsed-power system emits a series of high-voltage pulses: fifty 3μs pulses, fifty 10μs pulses and fifty 50μs pulses. Each series of fifty pulses takes one second, and the entire sequence takes six seconds. The six- second sequence is driven first at 50kV, then at 80kV and finally at 100kV. The SPEAR-2 photometer system provided photon mapping as a function of time at very high resolution (200nS) during these high voltage emission events.

The output from the photometer in response to a photon event is a 40nS pulse. The photometer mapping channel records the photometer output during successive 200nS windows, placing the events captured during each window into successive addresses in semiconductor memory as 8-bit words. The presence of one or more 40nS pulses within a 200nS window is recorded as a logical "one," and the absence of a 40nS pulse is recorded as a logical "zero."

In the high voltage case, the mapping system starts recording photometer output in response to the same triggers that initiate the first seven of the fifty pulses in each of the three pulse-width regimes, and thus the memory contains a history of photon events immediately following 21 of the 150 HV pulses (seven each at 3μs, 10μ s and 50μ s). The first 20 post-trigger sampling intervals each last for 156.2μs and contain 781 200nS sampling windows; the 21st sampling interval is 152.8μs long and contains 764 windows. The system thus provides up to 6248 bits per trigger (i.e., up to 781 8-bit words), and a total of 131,072 bits available to store photon event data at 200nS time resolution. The 8-bit words are transmitted to the telemetry encoder in a serial digital data stream upon command at the end of each six-second pulse sequence. Figure 4.7 illustrates the photometer high voltage data acquisition timeline.

The photometer map data processing channel uses a unique catching cell designed to insure that all photon events were captured and stored without ambiguity or multiple-counting, regardless of when the event occurred relative to a 200nS clock window. Since the output of the photometer is a fixed 40nS pulse, we established three different electronics paths to map these pulses into memory. The first path records a single pulse occurring within an 200nS acquisition window, the second path records multiple pulses occurring during the same window, and the third catches a photon event pulse that bridges two acquisition windows. The events are latched, a logical "or" is performed, and the result stored as an 8-bit word into an individual memory cell. Since the data system can acquire pulse widths as small as 24nS, the time resolution of the system is a constraint imposed only by the response time of the selected photometer. Figure 4.8 is a functional block diagram of the photometer processor map channel.

In the high current mode, the pulsed-power system emits a single high-current pulse, during which time the photometer system recorded all available data. The acquisition window in this case is not 156.2μS but 26.21mS.

Each map channel is controlled by its own high-speed state machine which directs the caching of the photon map data. This same state machine controls the serial digital interface and mark byte generation.

4.2.2.4 Flight System. The SPEAR-2 photometer used a Hanamatsu R647-04 photon-counting photomultiplier with a spectral response from 300 to 650 nm, peaking at ~420 nm. The photometer filter had a half-power bandwidth of ~10 nm, peaking at ~400 nm.

The system provided five orders of dynamic range from 500R to 1000 kR. Output data formed a serial pulse train with a fixed 40 nS pulse-width.

The photometer was enclosed in a sealed container in the EDP sensor section, and the electronics and signal conditioning were on the opposite side of the pressure bulkhead in the EDP electronics section, both well aft of the payload's power section.

In addition to the innovative high-speed pulse mapping system described above, the photometer data system had a photon counting system based on a 16-bit accumulator. The counter accumulated photon "hits" from the photometer output and was sampled and reset on the basis of the TM major frame rate. Figure 4.9 is a functional block diagram of the photometer processor accumulator.

Integration testing at Space Data Division and environmental and space simulation tests conducted at NASA's Plum Brook Test Facility showed that the photometer system design was a successful one. None of these tests produced any evidence of failure anywhere in the photometer system. Using multi-layer boards in the data system was extremely beneficial in conserving space and minimizing noise susceptibility.

4.2.2.5 Future Design Guidelines. Advances in memory chip technology make possible increasing the amount of memory available in the pulse mapping system without increasing the system size. Increasing memory size would allow us to speed up the sampling rate and provide a higher time resolution of events occurring in the load section during the high voltage and high current experiments. Moreover, it would allow us to sample more than the first seven microsecond-length pulses. However, such a change would require higher telemetry bit rates to accommodate the increased data.

Increasing the width of the accumulators in the photon counting system would provide a larger dynamic range. Also, a calibration source inside the system could provide a very quick health check of the accumulator data channels. This calibration check should be designed for command from the umbilical and the payload controller, to be useful in final countdown checkouts.

4.2.3 *Electromagnetic Pulse Detectors.*

4.2.3.1 Purpose. Sensors to measure the rates of change of **B** and **D** within the sensors were deployed in clusters of three to measure three orthogonal components of the field derivatives. The sensor outputs were conditioned by compression amplifiers to provide a

wide dynamic range. A linked boom system was used to deploy the sensors in opposite directions through ports in the payload skin.

The outputs of the sensor compression amplifiers were peak-detected and sampled at 1000 samples per second continuously. In addition the six channels were also sampled in a snapshot mode at a sample interval of 200nS for a time window corresponding to seven of the 50 pulses of the HV pulsing sequence. The stored samples were telemetered to the ground at a slower rate during the period between HV pulsing operations.

4.2.3.2 Heritage. The SPEAR-2 scientific objectives required us to measure electric and magnetic field changes that were both very rapid and potentially of large magnitude. Since the mid- 1960s, EG&G has been a leader in developing EMP and SGEMP sensors to measure similar effects in nuclear test experiments. More recently, researchers have adapted some of the sensors EG&G developed to measure the effects of lightning. Because of the similarity of measurement goals, we investigated sensors built by EG&G to measure field changes in the SPEAR-2 experiment. We were able to obtain accurate broadband sensors with simple transfer functions as a means of measuring electromagnetic field changes arising from the SPEAR-2 high voltage and high current events.

4.2.3.3 Design Considerations.

- Deployment System.

SPEAR-2 Science objectives required that the EMP sensors be immersed in the field surrounding the payload, and that the three sensors in each set be deployed orthogonally. Because SPEAR-2 was to be a recoverable payload, however, the probes could not extend beyond the payload skin during recovery for fear of their becoming tangled in parachute shrouds. Thus we were faced with designing a deployment system that either jettisoned the probes or withdrew them inside the payload at the end of the mission. The latter system proved least complex and became the system of choice. This same system simultaneously deployed the Langmuir probe as Section 5.3 discusses.

The probes themselves were in the EDP sensor section, as illustrated in Figure 4.1, and deployed on opposite sides of the spacecraft (45° and 225°) through doors that were jettisoned. As the drawing in Figure 4.10 shows, the probes in the stowed position were quite close together, but when fully extended they splayed apart in such a way as to be mutually orthogonal. The cable-drive deployment system incorporated a floating track that

remained planar despite pressure- induced deformation of the bulkhead to which it was mounted, assuring that the probes would deploy under any predicted vehicle stress.

The drive motor responded to signals from the main payload controller to deploy and retract the probes. Because the drive motor had to operate in vacuum, we used a TRW 400 Hz induction motor to avoid potential problems associated with brush-type dc motors operating in vacuum.

- Field Sensors.

We used two different types of field sensors on SPEAR-2, the first such use of these sensors in a rocket experiment. The first probe type was a D-dot free-field hollow spherical dipole (HSD) sensor, capable of measuring the normal component of the displacement current (dD/dt). The second probe type was a B-dot multi-gap loop (MGL) sensor, which measured the temporal rate of change of a magnetic field in free space (dB/dt). Both types of probe are passive, requiring no external power, and very light weight.

Each sensor is coupled with a differential balun, also provided by EG&G, which transforms the balanced 100 ohm signal from the differential (free-space) field sensor to an unbalanced 50-ohm signal for input to a 50 ohm coaxial cable. The balun changes the input signal of V_0 across 100 ohms to an output signal of $V_0/2$ across 50 ohms. Half of the input power is dissipated in the balun so that the insertion loss is 3dB. From the balun, signals pass directly to signal processing electronics.

- High Speed Data Acquisition System.

Signals leaving the baluns pass first to pseudo-logarithmic compression amplifiers for signal conditioning, and then to digitizers which sample and store data for delivery to the telemetry system.

The log amps provided an efficient means of compressing data to accommodate the wide dynamic range of input signals from the sensors. We used Analog Module model 381 logarithmic compression amplifiers, which provided low phase shift and linearity over a 90 dB range. The log amp systems also supply the signal conditioning and scaling necessary for the digitizers to operate properly. The data processing system also incorporated a unique peak detection system, which captured both the low and high peaks in the field fluctuations. The peak detection data is directly available in the telemetry data stream, sampled at 500 samples per second. Figure 4.11 is a functional block diagram of the log amplifier channel.

From the log amp system, data passed to the high-speed digitizers as conditioned signals in the range of +/- 0.5V. We designed the digitizers to take data for two different cases: the high voltage sequence and the high current sequence.

In the high voltage mode, the pulsed-power system emits a series of high-voltage pulses: fifty 3-μS pulses, fifty 10μS pulses and fifty 50μS pulses. Each series of fifty pulses takes one second, and the entire sequence takes six seconds. The six- second sequence is driven first at 50kV, then at 80kV and finally at 100kV.

In the high voltage case, the digitizers start recording data in response to the same triggers that initiate the first seven of the fifty pulses in each of the three pulse-width regimes, and thus the memory contains a history of field configuration "snapshots" immediately following each of the first seven triggers at each pulse width, or 21 samples at each voltage level. The first 20 post-trigger sample intervals each last for 156.2μ s and contain 781 200nS sampling windows; the 21st is 152.8μ s and contains 764 windows. The system thus provides up to 6248 bits per trigger (i.e., up to 781 8-bit digitized words), and a total of 131,072 bits available to store data at 200nS time resolution. The 8-bit words are stored in parallel in 16 Kbytes of memory, and transmitted to the telemetry encoder in a serial digital data stream upon command at the end of each six-second pulse sequence.

In the high current mode, the pulsed-power system emits a single high-current pulse. In this mode, the digitizer provides a continuous sample window started by one external trigger and ending in 16 Kbytes of memory being filed. The sample window remains open for 3.277mS. A functional block diagram of the SPEAR-2 EMP digitizers appears in Figure 4.12.

All data taking events are controlled by the external payload controller. The main interface in the digitizer to the payload controller is through an optically isolated EPLD. This system enabled us to put all the control logic into a localized chip, freeing up board space for other components. Since the controller was so compact, each individual channel was separately controlled from the main control lines, making each channel independent.

An external test connector interface to the digitizers allows us to run known waveforms into the digitizers rather than the sensor signals from the log amps. This feature provides for an internal health check for the digitizers, memory chips, EPLD state machine, command interface, and telemetry read out and command.

4.2.3.4 Flight System. The SPEAR-2 EMP detector system comprised six EMP detectors (three B-dot and three D-dot sensors), two identical multi-channel log amplifiers, and

multi-channel digitizing/cache memory electronics systems. The data path for the sensors starts with the sensors themselves and then flows through the EG&G differential baluns into the log amps for signal conditioning of the raw sensor data. Signals then pass to the digitizers where the data are sampled and stored for delivery to the telemetry system.

The EMP detectors were housed in the EDP sensor section and deployed through doors described earlier. The EMP log amplifiers and digitizers were located in the pressurized EDP electronics section. All the electronics boxes were designed with great care to insure noise immunity. Using multi-layer circuit cards greatly improved the systems' noise tolerance and overall system performance.

The EMP Data system provided important data on the effects of high voltage and high current experiments at both Space Data, during integration testing, and at NASA's Plum Brook Test Facility during vacuum chamber testing. Using multi-layer circuit boards and mother-boards, similar to those used in computers, provided very quiet, noise-immune electronics. The EMP system showed no failures during testing operations, which reassures us that the instruments would have performed as well during flight.

4.2.3.5 System Failures. We experienced no design failures in the EMP system or in the boom deployment system.

4.2.3.6 Future Design Guidelines. The SPEAR-2 data system was a new system, and its performance suggests some areas for improvement in future similar data systems. One area of improvement is to include enhanced self-test capability. Self-testing the current system during integration at Space Data produced some ambiguous data. Including a separate, independent test trigger would provide better control of the test timing.

We would want to encode the state machine transitions into the mark data, and to have them be some of the most significant bits. This would provide improved visibility into the state transitions when we were watching strip chart output during system cycling. In addition, mark data need to delineate each pulse sampled, and to include payload controller state information.

In future designs, we would hope to take advantage of recent advances in silicon technology, which has greatly increased the amount of memory available on very small chips. We could thus expand the amount of memory in our systems, making possible taking more science data or using much faster data sampling rates for the same period of

operational time. This expansion, however, would place greater demands on the telemetry bit rate or frame resources in order to accommodate the increased data.

4.2.4 *Charged Particle Detectors.*

4.2.4.1 Purpose. Two clusters of electrostatic differential energy analyzers detected any flux of energetic positive ions and electrons in the vicinity of the platform. A pair of electron detectors measured electron fluxes in two energy bands with a total energy span of a few eV up to 30keV. Each band was divided into 32 energy steps, and a total count of particles falling within the energy step was accumulated for 1mS. The two bands were swept together resulting in a time resolution of 32mS for a complete spectrum. A similar arrangement existed to analyze the positive ion fluxes.

The energetic particle detectors would respond to instantaneous fluxes resulting from system discharges, but the energy sweeps were not synchronized with the HV/HC activities so the energy channel would be randomly selected from those scanned. However any residual fluxes lasting more than 32mS would show up as a change in the spectrum of the particles.

4.2.4.2 Heritage. The SPEAR-1 payload incorporated a similar set of charged particle detectors. The instrument flown on SPEAR-2 had no significant design changes, but it had a more restricted set of view directions than the instrument flown on SPEAR-2.

4.2.4.3 Design Considerations. An innovation introduced into the SPEAR-2 implementation of the charged particle detectors was to incorporate a pulse mapping channel freed when descoping of the payload removed one of the two photometers originally planned. This arrangement enabled tracking the development of charged particle fluxes to the vehicle with a time resolution of 200 nS. Unfortunately, it was not possible to synchronize the sweep of the charged particle detector with the application of HV to the load, so the data would have been taken from different energy steps for different discharges.

We improved the instruments' field of view by deploying them through openings uncovered when the payload doors were jettisoned. This deployment allowed the sensors to view very close to parallel to the longitudinal axis of the payload.

4.2.4.4 Flight System. The particle detector system consisted of four differential electrostatic analyzers, two covering the energy range from 1 eV to 3 KeV and two covering the range from 500 eV to 30 KeV. These four sensors were positioned in two pairs on opposite sides of the spacecraft in the EDP Sensor Section, and each pair consisted of one low-range and one high-range analyzer. They were mounted in a deployable bracket that was to push the sensor heads through an opening in the sensor section skin uncovered when the doors were jettisoned. The sensor heads protruded slightly beyond the skin, providing a 100° conical field of view. Figure 4.1 shows the location of the sensors in the payload, Figure 4.10 illustrates the location of the particle detector sensors radially in the EDP sensor section, and Figure 4.13 is a drawing of one of the sensor pair assemblies.

The detectors' output went to an electronic system common to both clusters that used a microprocessor both to control the different analyzers' energy scanning and to manage collecting and formatting data for the spacecraft telemetry system.

4.2.4.5 System Failures. The particle detectors suffered from no known design failures. However, the sensor developer expressed concern that the prolonged exposure of the channel plate detectors to the atmosphere during a delay in the program may have resulted in their degradation. It is not possible to test the detectors and evaluate his concern without placing them in a vacuum system and exposing them to a charged particle flux. During the Plum Brook test, which was the first opportunity we had to evaluate the particle detectors after the delay, the detectors responded to charged particle fluxes in the chamber as expected. However, we had no means of establishing if a sensitivity change had occurred.

4.2.4.6 Future Design Guidelines. In order to reduce the possibility of detector contamination during the period between final laboratory tests and vacuum chamber or flight use, the instrument should be designed to be sealed and backfilled with a dry, inert gas.

The possibility of vacuum chamber test contamination of the sensors requires a calibration check prior to launch. A final calibration check was difficult to accomplish for SPEAR-2. To alleviate the need for calibration, we suggest that a radioactive source be included to stimulate the detectors with a known particle energy spectrum during final vacuum testing.

A pulse stream to the accumulators to activate them without vacuum conditions would provide another instrument health check. The pulse stream would be independent of

any external GSE input and could be controlled by command while the payload was completely sealed.

4.2.5 *Langmuir Probe.*

4.2.5.1 Purpose. The source of charged particles to trigger multiplicative ionization associated with arcs and discharges is the naturally occurring ionospheric particles. They also provide part of the return current to try to neutralize charge build-up on the vehicle and prevent it charging to high electrical potentials. Thus it is important to monitor the number density of these particles. The Langmuir probe used on this flight was biased to monitor primarily the ambient electron density with mS time resolution. However, it was swept in potential once per second to enable the electron temperature to be determined.

Perturbations in probe current can be interpreted as changes in electron density. The changes may result from increased plasma production resulting from HV/HC operations, or due to the potential of the vehicle changing. In either case the probe will show a change in the thermal plasma environment on a mS time scale.

4.2.5.2 Heritage. The type of Langmuir probe flown on SPEAR-2 was typical of many such instruments flown on a variety of sounding rocket payloads. The physical configuration of the probe and the electronics used was a duplicate of those flown on SPEAR-1.

4.2.5.3 Design Considerations. SPEAR-2 Science objectives required that the Langmuir probe be immersed in the plasma surrounding the payload. Because SPEAR-2 was to be a recoverable payload, however, the probe could not extend beyond the payload skin during recovery for fear of its becoming tangled in parachute shrouds. Thus we were faced with designing a deployment system that either jettisoned the probe or withdrew it inside the payload at the end of the mission. The latter system proved least complex and became the system of choice. This same system simultaneously deployed the EMP sensors as discussed in the section on the EMP sensors.

The probe was located in the EDP sensor section, as illustrated in Figure 4.1, and deployed through an opening at 90° through an opening uncovered when a door was jettisoned at altitude. The cable-drive deployment system incorporated a floating track that remained planar despite pressure-induced deformation of the bulkhead to which it was

mounted, assuring that the probe would deploy under any predicted vehicle stress. The drive motor responded to signals from the main payload controller to deploy and retract the probes. Figure 4.10 illustrates the Langmuir probe's location on the EDP bulkhead. Figure 4.14 illustrates the Langmuir probe in its deployment carriage.

4.2.5.4 Flight System. The Langmuir probe used on SPEAR-2 had cylindrical geometry. A cylinder 11.49" (291.8mm) long with a diameter of 0.0625" (1.59mm) formed the probe collecting area. This created a total collection area of 14.6cm^2. and an electron current at zero bias of about 1.5μA for an electron density of 10^6 cm^{-3} at 1000K.

A short guard electrode connected to the probe electronics shielded the sensing electrode as shown in figure 4.15. The probe current fed a logarithmic amplifier and the a differential amplifier. Both amplifiers were synchronized to the waveform function generator to provide separate signals for the ion and electron currents. The waveform generator provided a probe biasing signal which remained constant at a positive bias of 5 volts for 1.5 sec, then swept down to -1 volts, then up to 5 volts again during a period of 1 second.

The fixed bias period provided a means of monitoring rapid changes in the electron density, while the sweep provided a measurement of the ion density and electron temperature. The repetition period of the voltage sweep is adequate to provide a height profile of the ionospheric parameters over the vehicle trajectory.

4.2.5.5 Design Failures. A recently-developed high-speed operational amplifier had been incorporated in a compression amplifier design. Under certain circumstances of temperature and input conditions, this operational amplifier oscillated. Replacing the operational amplifiers with earlier types resolved the problem.

4.2.5.6 Future Design Guidelines. The sweep rate of the instrument is rather slow, resulting in a poor time resolution for electron temperature measurements. The circuitry could benefit from more modern components to increase the bandwidth, yet retain the low noise level necessary to measure the low currents collected by the probe.

4.2.6 *Charge Probe.*

4.2.6.1 Purpose. The charge probe, in addition to being sensitive to platform potential changes, monitored the speed of those changes (within the limits of the telemetry system), and also sensed the polarity of changes in platform potential. Vehicle potential changes are inferred by observing the charge redistribution on the probe's small dielectric surface, deployed flush with the payload skin, which responds to changes in vehicle potential with respect to the undisturbed ionosphere. Absolute interpretation of the potential of this type of probe is rather difficult, owing to the lack of good knowledge of how the outer surface of the dielectric contacts the ionospheric plasma. However, experience with this probe on a number of space vehicles ranging from sounding rockets to the space shuttle indicates that it can provide a useful measure of both the rate and polarity of change in potential.

4.2.6.2 Heritage. The design of both the probe and the electronics was based on flight proven instruments and was representative of our state-of-the-art instrumentation for this particular system.

4.2.6.3 Design Considerations. No special considerations were needed for the design of this system. Predictions of the expected vehicle potential were within the range of our standard design, so a previous sounding rocket charge probe system was built, tested and incorporated in the EDP instrument package.

4.2.6.4 Flight System. The charge probe deployed through an opening uncovered when the doors are jettisoned at altitude, as illustrated in Figure 4.1, and at full deployment was flush with the payload skin. Signals from the probe are monitored through the telemetry system with a time resolution of approximately 1mS. The probe was not intended to retract prior to re-entry, but being flush with the skin posed no entanglement threat. Figure 4.10 illustrates the probe's location on the EDP bulkhead, and Figure 4.16 is a drawing of the charge probe sensor.

4.2.6.5 Design Failures. The charge probe experienced no design failures.

4.2.7 *Neutral Pressure Monitors.*

4.2.7.1 Purpose. The neutral pressure was monitored by sensors covering a total dynamic range of 10 torr to 10^{-7} torr. The pressure measuring package was mounted near the HV components in the load section of the payload, as Figure 4.1 illustrates. Its only connection to the instrumentation section was to convey the gauge output to the telemetry through active fiber optic links.

The sensors would have monitored background pressure from the pad up to operational altitudes, recording the pressure drop as the payload doors open. In addition, the gauge would have responded to pressure bursts on a mS time scale resulting from gas evolving during arcs and localized discharges at the exposed HV biased conductor surfaces. The gauges monitored load section pressure during chamber tests, and also monitored pressure for the extended vacuum period prior to launch operations.

4.2.7.2 Heritage. The cold cathode ionization gauge duplicated the instrument flown on SPEAR-1. It was, however, packaged differently and interfaced to a fiber-optic data transmission system described below. Ensuring the gauge's fast start, as was required in SPEAR-1, was unnecessary for SPEAR-2 because the gauge was operating at lift-off.

4.2.7.3 Design Considerations. Prior to SPEAR-2, a capacitance manometer gauge had not been used in a spacecraft application. A significant effort went into making it rugged enough to withstand the mechanical environment anticipated during launch. The gauge successfully underwent rigorous environmental testing in the course of development, and performed very well during the launch. It took over pressure measurements from the cold-cathode ion gauge when the excessive accelerations encountered during ascent caused some leakage into the load section.

The pressure gauge, located in the HV/HC payload section remote from power and telemetry, was entirely self-contained. Internal sealed batteries provided power to activate the gauge during flight, and the gauge transmitted analog signals proportional to gas pressure over an analog fiber optic link to a receiver/signal conditioning interface unit in the EDP electronics section. During all pre-launch activities, a dedicated umbilical supplied

battery charging power and control for the transition from external to internal power prior to launch.

The ionization gauge aperture was designed to give rapid time response to pressure changes This was achieved by maximizing the diameter of the aperture to the gauge and keeping the length as short as possible consistent with the envelope constraints, and the accommodation of a gate valve to isolate the gauge from ambient atmospheric pressure.

4.2.7.4 Flight System. The neutral pressure gauge was designed to measure the neutral particle flux in the HV/HC section between 10 and 10^{-7} torr. The gauge consists of two sensors: a capacitance manometer covering the pressure range between 10 and 10^{-3} torr, and a cold-cathode ionization gauge covering the range between 10^{-3} and 10^{-7} torr. The sensors were designed and developed to have a relatively high time resolution for low-pressure measurement. Pressure output was monitored with a time resolution of 1mS, and laboratory tests showed that the pressure gauges themselves have a time resolution between 5mS and 10mS.

The ionization gauge was protected from atmospheric pressure by a vacuum gate valve. The use of this valve enabled the gauge to be used to monitor the pressure of the load section during testing, and be able to protect the gauge when the pressure in the load section was cycled.

4.2.7.5 Design Failures. The analog fiber optic link used to transfer the pressure gauge telemetry signals from the load module to the telemetry section showed a tendency to introduce small dc offsets in the signals. The offsets were only a small percentage of the full scale signal, so it was decided not to pursue the problem during payload development. Furthermore, the effect was not reproducible. and it was unclear whether the electronics, fiber optic connectors or the fiber itself produced the effect.

4.2.7.6 Future Design Guidelines. As designed, we had to remove the umbilical connection to the neutral pressure gauge and seal the connector compartment 45 minutes prior to launch. In the future, we would modify the umbilical design so that the vehicle flies away from the umbilical.

The DC offset in the fiber optic link should be studied carefully. If no viable solution to the offset problem is identified, consideration should be given to using digital data transmission through the optical fibers.

4.2.8 *Magnetometer.*

4.2.8.1 Purpose. The fluxgate magnetometer was included to monitor the geomagnetic field direction as a means of verifying that the attitude maneuvers were completed satisfactorily. Field strength measurements also recorded changes in the magnetic field induced by currents flowing in the load section, at a level below that detectable by the EMP B-dot sensors.

4.2.8.2 Heritage. The magnetometer was a commercial unit designed for spaceflight applications. It has a long heritage of flights on many payloads.

4.2.8.3 Design Considerations. No innovative concepts emerge in connection with our use of the Develco magnetometer on SPEAR-2. The main design consideration related to the provision of an isolated power supply to maintain the integrity of the grounding philosophy of the payload to keep signal and power returns separate except for a single point connection.

4.2.8.4 Flight System. The system sensor was a model 9200C 3-axis fluxgate magnetometer manufactured by Develco, Inc., and designed for spaceflight. The sensor was enclosed in an aluminum box that served as a Faraday cage, and was mounted on the electronics side of the EDP bulkhead. The +28V power supply was in a separate box on the same side of the bulkhead. Magnetometer analog output to the telemetry system (one 0-5 Vdc signal for each of three axes) was sampled at 50 Hz.

4.2.8.5 Design Failures. No design failures were encountered with the magnetometer system.

4.3 RESULTS.

The failure of the guidance system on the SPEAR-2 flight precluded any flight HV interaction flight data being obtained. However, those instruments which made measurements during the ascent operated correctly and provided data from lift off to impact. The instruments were also tested in the integrated payload during the Plum Brook space simulation chamber tests. In this section we will present examples of the measurements from each of the instruments described in the earlier section.

4.3.1 *Optical Imaging System.*

An example of the eight images formed by the fiber-optic imaging system is shown in Figure 4.17. The images were obtained during the system integration phase, and illumination was from the ambient laboratory lighting through the load section door apertures. The results were obtained from the two Nikon film cameras viewing the coherent fiber optic bundles. In each picture the four distinct images can clearly be seen corresponding to the view directions of each of the eight fiber-optic head units.

The upper group in Figure 4.17 shows (clockwise from upper left) views of the rail gun inductor, a PFN component, the view in direction of the rail gun plasma cloud, and the HV bushing used in determining the HV transformer output voltage. The lower group in Figure 4.17 (clockwise from upper left) shows PFN area, the klystrode bushing and two views of windings on the HV transformer.

During the vacuum test at NASA Plum Brook, we were unable to operate the LLLTV cameras due to an ambient pressure problem discussed earlier. However, the film cameras were operational, and we were able to detect examples of arc discharge images during the flight sequence simulations. Localized arcs in the HV transformer were often observed as white dots on a dark background. The different positions of the white dots at the arc location clearly showed spatial variability in the location of the arcs. The lower sensitivity of the film camera compared to the LLLTV prevented the surrounding structure being visible, but comparison with earlier shots taken during the illuminated phase would enable the locations of the arcs on the transformer to be defined.

After the TV cameras were packaged in pressurized containers we were able to operate them again under reduced pressure, and TV images were obtained during ascent, prior to the vehicle cut-down. The image was obtained at T+9secs. The illumination in the load section was not ideal for viewing the structure, but various HV items could just be

resolved. The images could have been enhanced using a computer, and had the flight been successful it was planned to do this as a means of providing spatial references to locate the position of arc discharges in the fields-of-view of the eight imaging systems.

The LLLTV images were obtained from launch until impact. A study of the animated images showed that the view in one of the dissected images clearly indicated reaction of either the viewed component or the optical head to the unexpected acceleration motion of the vehicle. The image showed considerable displacement for several seconds around, T+30 seconds, however the other images remain fixed throughout the brief flight of the vehicle.

4.3.2 *Photometer.*

Figure 4.18 shows an example of the photometer accumulator channel output plotted as a function of mission elapsed time (MET). The data was obtained during the flight sequence test performed in the NASA Plum Brook space simulation chamber. The large increase for the MET period 231-2 secs results from a 1 sec HV pulsing experiment. The HV was applied as 100 kV pulses of 50 μ S duration repeated at 50 Hz. The time resolution of the plot is not adequate to resolve the individual HV pulses. The signal spike at 242 sec MET is a calibration pulse, and the data gap following the calibration pulse is the result of an error in one of the time words on the data tape.

It is not clear whether the emission of light from a discharge associated with the HV pulse train was in the field-of-view, or reflected from elements of the HV transformer at which the photometer was aimed.

The photometer data showed good correlation with evidence of discharge from the HV system monitors. The counting rate showed a correlation with the intensity of the discharge monitored both by LLLTV systems and the HV output current. As the power system became conditioned increasing combinations of HV and pulse width did not induce arcs or discharges, and this fact was corroborated by the photometer output which remained at the noise level for those cases.

An example of the high resolution photometer output from the pulse mapping system is shown in Figure 4.19. The number of photon events in each 8-bit byte of the pulse map were summed to produce a number from 0 to 8 counts in a time window of 1.6 μS. The figure shows a plot to its full resolution of 1.6 μS windows. The y-axis shows the number of counts per 1.6 μS, and the x-axis shows the elapsed time after 232.33 sec MET in μS.

We have selected one burst of activity by the photometer. The onset of counts just after 17.5 μS corresponds to the first of seven pulses in the beginning of a 50 pulse HV experiment. Each window for the seven pulses is 156.2 μS long. Thus the highest counts, covering about 300 μS, correspond to the first two pulses the photometer responded for the full 156 μS, much longer than the longest HV pulse of 50 μS. After the two pulses, there was a decrease in photometer activity, perhaps illustrating that surface conditioning occurred within the first two pulses.

4.3.3 *Electromagnetic Pulse Detector.*

During the flight sequence performed in the NASA Plum Brook space simulation chamber, the EMP detectors were deployed, and responded to electric and magnetic fields generated as a result of the HV and HC discharges.

Figure 4.20 shows two sequences of D-dot data sampled at high speed (200 nS sampling interval) and sent to the vehicle telemetry system at a much lower rate from a cache memory. The constant level at 255 is fill data between memory dumps. Thus the MET represents the time the data was sent to the telemetry system. The sampling time approximately corresponds to the time the data changes from fill data to actual data.

The first group of measurements corresponds to data from the D-dot probe when a HV experiment was performed. The cache memory dumped shows the 50 Hz pulsing of the HV. It consists of 3 groups of 7 pulses for each of the three voltages applied to the HV load for the MET corresponding to the start time of the memory dump. The panels correspond to the x-, y- and z- axes of the D-dot sensors. The increasing activity in the EMP signal as the voltage increases from left to right within the sequence can clearly be seen.

The second group of measurements corresponds to the EMP D-dot field when the plasma accelerator was operated. In this mode of operation, the data represents a continuous sequence of 200 nS samples for the complete data window of 3.3 mS.

Figure 4.21 shows an extended view of the D-dot data corresponding to the operation of the HC experiment in which D-dot is plotted as a function of actual sample time from the initiation of the HC experiment; these plots correspond to the right-hand portion of the plots in Figure 4.22. Large variations in D-dot during the initial 1.5 mS correspond to the acceleration period of the railgun pellet prior to its emergence from the muzzle.

Figures 4.22 and 4.23 are in the same format as Figures 4.20 and 4.21 but contain data from the B-dot sensor. In general the B-dot sensor showed little sensitivity to HV discharges, suggesting that the currents flowing in these discharges were not very high. On the other hand the B-dot sensor showed considerable activity during the HC experiment. Again the data are expanded and plotted against sample time in Figure 4.23. In this case we see that the B field signature shown little effect for the first 0.6mS. This relatively quiescent period is then followed by an active period until it becomes quiescent again at about 1.5mS. It is speculated that the active period corresponds to the emergence of plasma from the muzzle of the rail gun and the establishment of unbalanced electric currents in the region outside the gun structure.

4.3.4 *Charged Particle Detectors.*

The charged particle detectors were deployed and the HV applied to the channel plates allowing particle counts to be measured during the flight sequence test in the NASA Plum Brook space simulation chamber.

The channel plates had been exposed to ambient laboratory environment for a period of about one year, and there was a concern that water vapor contamination of the channel plates may have rendered them inoperative. However, the lower two panels in Figure 4.24 shows repeatable data from two of the charged particle detector channels.

Figure 4.24 shows the energy monitor in the upper panel, and counts from two of the detectors in the lower panel. Each panel shows its data plotted as a function of MET. The two channels are for ion data corresponding to two different view directions. The lower panels indicate particle count spectra showing higher counts at the low and high energy ends of the energy sweep. This raw data does not take account of the varying energy bandwidth (E) from low to high energies, and must be divided by this parameter to produce spectra shapes corresponding to differential energy spectra for the particles. This correction has the effect of increasing the low energy end of the spectrum relative to the high energy end due to the instrument parameter $\Delta E/E$ being constant.

4.3.5 *Langmuir Probe.*

Figure 4.25 shows data from the Langmuir probe during the flight sequence operated in the space simulation chamber at NASA Plum Brook. The upper panel shows that the HV biassing experiments interfere with the sweep generator, when a sequence of HV pulses was applied to the load at about 231-2 secs MET.

An anomalous feature of the data occurred during the fixed bias period when both the ion and electron channels showed high noise levels. This phenomenon was not seen before or after the chamber test when the plasma currents to the probe were simulated by a fixed resistor.

4.3.6 *Charge Probe.*

No data were obtained from the charge probe due to the payload being grounded in the Plum Brook chamber, and insufficient altitude being attained during the flight.

4.3.7 *Neutral Pressure Gauge.*

Figure 4.26 shows the neutral pressure measurements inside the SPEAR-2 load section as a function of time from lift-off. The upper panel shows data from the capacitance manometer gauge, the lower panel data from the cold cathode ionization gauge. The data are uncalibrated, and are presented as telemetry volts output from the instrument.

The slow rise in the ionization gauge shows the increasing load section pressure as the cryogenic absorption pump warms up. However, at about 33 secs MET, an event occurred which resulted in a leak to the load section, increasing the pressure beyond the limit detectable by the ionization gauge. The ionization gauge then showed a steady increase in the pressure until the pressure exceeded its operating range.

The small fluctuations in the capacitance manometer gauge resulted from motion of the diagram due to the coning motion of the payload at that phase in its flight. At the point when the ionization gauge went off-scale, the manometer began recording a continued increase in pressure, as well as continued fluctuations probably arising from spacecraft motion, until impact.

We believe the change that occurred at about 33 secs MET was caused by the payload breaking loose from the rocket motor and springing a leak in the load section.

4.3.8 *Magnetometer.*

Figure 4.27 shows the results from the 3-axis fluxgate magnetometer obtained during the brief flight of SPEAR-2. Each panel shows the uncalibrated output of one of the three axes of the magnetometer as a function of time.

For approximately 20 seconds, the magnetometer recorded the geomagnetic field as the rocket rotated during the ACS malfunction. Between 20 and 22 seconds a large amount of motion occurred which apparently resulted in the payload separating from the motor at about 23 seconds. Thereafter the payload started to tumble as it went through its limited trajectory before impacting the ground at about 120 seconds MET.

SECTION 5

FUTURE WORK

In common with other innovative projects, the SPEAR program has raised questions as well as answering some. Further valuable data should be obtained from the SPEAR-3 project, but beyond SPEAR-3 there are other issues which need experimental and theoretical studies to provide a firmer basis to deal with space platform charging, and with the utilization of high power in space with or without the presence of effluent contamination.

At the instrument level we have already addressed a variety of improvements which should be incorporated if similar instruments were to be reflown.

In this section we address broader issues appropriate to the two main, and related, areas for which the SPEAR program was, and is, providing experimental data. The SPEAR-1 and SPEAR-2 projects were largely oriented towards the interaction of exposed conductors biased to high electrical potentials with the platform environment. With the commencement of the SPEAR-3 project the emphasis has shifted more to considerations of grounding biassed vehicles to the ambient ionosphere. Since grounding techniques can involve the release of effluents, this latter issue is also addressed by SPEAR-3.

5.1 HV-ENVIRONMENT INTERACTION.

Although the issue of HV-environment interaction from the point of view of utilizing space platforms for high power systems has been recently reduced in importance in the near term, it is likely that this issue will eventually re-appear when future, more complex systems are deployed.

5.1.1 *Simple Geometry.*

It is necessary to repeat the SPEAR-1 type of experiment for both polarities of differential biassing, and also to extend the maximum potential difference to extend our knowledge of the basic physics of the HV-environment interaction process. It would be very valuable to determine what is the maximum potential difference which can be developed between the vehicle body and the deployed electrode for the relatively simple SPEAR-1 geometry.

The temporal consideration of HV exposure also needs more attention. Due to the relatively long time for a charge sheath around a HV biassed system to reach steady state, a detailed understanding of this process is essential to the utilization of pulsed power systems on space platforms. It is likely that the "insulation" characteristics of the environment will differ greatly for short (yet to be measured) pulses compared to DC biassing. Experimental exploration of the transient behavior for a wide range of parameters including effluent emission should be performed.

An unambiguous method of measuring vehicle potential must be developed and incorporated in all of the HV experiments. Our recommendation is that a deployed, tethered reference electrode is used, being positioned at least 100m from the platform to provide a voltage reference immersed in the undisturbed ionospheric plasma to which the vehicle potential may be referred.

5.1.2 *Complex Geometry.*

Although a great deal was learned from SPEAR-2 about handling insulated complex sub-systems at high potentials in the vacuum environment, the lack of flight data for the interaction with the near unbounded ionosphere plasma is an omission which needs to be corrected. Either SPEAR-2 or a subset of that payload should be flown as part of an on-going program to study HV-system - environment interactions. A new SPEAR-2 type payload would benefit greatly from the substantial amount of information learned from SPEAR-2 even without the culmination of a space flight for SPEAR-2.

Much of the extension of parameters could be achieved by sounding rocket flights. However, the tendency to make the payloads too complex should be resisted. The complex payload is expensive to develop, more prone to failures and while it visits parameter space broadly, there is insufficient time to visit any one parameter depth. It would be preferable to have a pre-approved program of several, less expensive payloads in which the breadth of parameter space is acquired by multiple flights, each flight giving more depth to its particular objective.

Finally there is an urgent need to extend the HV interaction studies to the orbital situation. The move from the sub- or transonic suborbital case to the supersonic orbital case has a significant impact on system plasma interactions. Ram and wake effects became more pronounced, and may aid or defeat HV space insulation. In addition the presence of substantial amounts of effluent from a space platform may destroy some of the advantages

expected from the utilization of plasma and neutral wakes formed by platform structures or plasma shields.

5.2 SPACECRAFT GROUNDING.

Reduction in the electrical impedance between space platforms and the ionosphere is important for both passive spacecraft operating at high latitudes and also for space platforms carrying exposed HV equipment at all latitudes. It is anticipated that certain grounding techniques will also alleviate localized differential charging which offers a threat to the operation of some subsystems susceptible to the EMP developed by electrical arcs.

Grounding techniques will be explored by SPEAR-3. If it is determined than an effluent producing system will be needed, then further measurements will be essential to study the distribution of neutrals and plasma in the effluent cloud. Studies of excitation and ionization resulting in light emission will also be relevant to establishing if optical contamination to platform mounted sensors is likely to be a problem.

The extension of grounding experiments to orbital platforms is an important future direction for similar reasons to those listed earlier for HV-environment interactions.

5.3 GENERAL CONSIDERATIONS.

The three-pronged approach of theory, laboratory testing and space experiment adopted in the SPEAR program has proved to be a powerful approach. The laboratory versus space testing needs continuous monitoring and comparison to enable some of the tests to be performed at lower cost either in laboratory vacuum systems or in large space simulation chambers. However, all of the experiments so far in SPEAR and other programs have demonstrated that for many phenomena associated with HV-space environment interaction (including grounding) their is no substitute for true space.

The rocket payloads should be continued, but with a move to simpler, more specialized payloads. However, if this policy is adopted it will be easier to implement if the simpler payloads are part of a planned sequence of payloads so that the major issues are all expected to be addressed over a period of time. the payloads could then be flown on smaller, lower cost vehicles with a fast turn around for each payload, and the possibility of parallel payload development giving faster programmatic progress.

The orbital experiments would be entirely appropriate for short-lived lower cost orbital platforms. The ideal would be to transfer the sounding rocket payload development

philosophy to orbital payloads. The reduction of extensive quality control and documentation required for long-lived orbital payloads, and the avoidance of meeting very strict safety requirements required for shuttle payloads would have a very significant effect on the costs associated with the transition from SPEAR to SPEAS (Space Power Experiments Aboard Satellites).

FIGURES

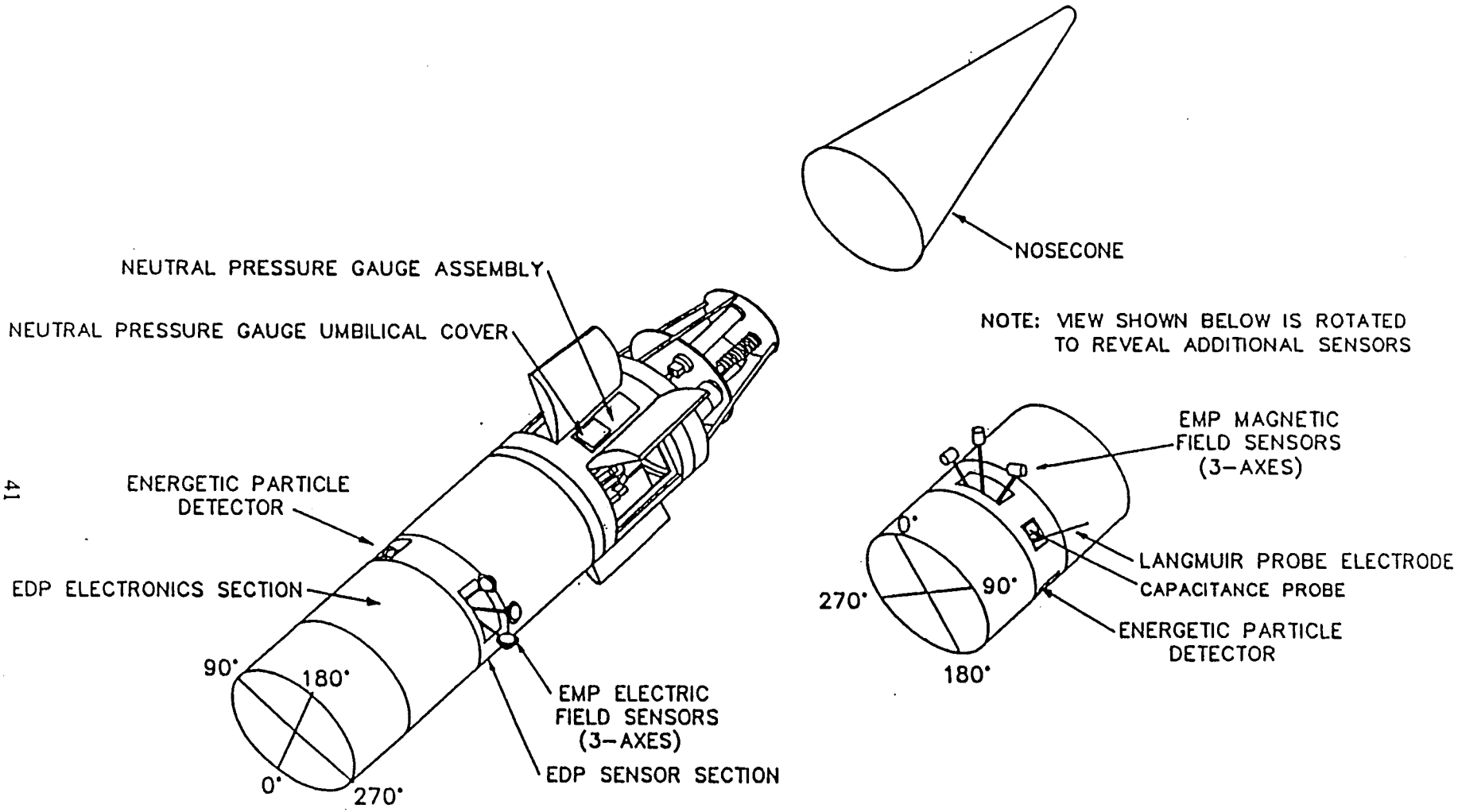

Figure 4.1 SPEAR-2 payload showing location of external diagnostic package sensors.

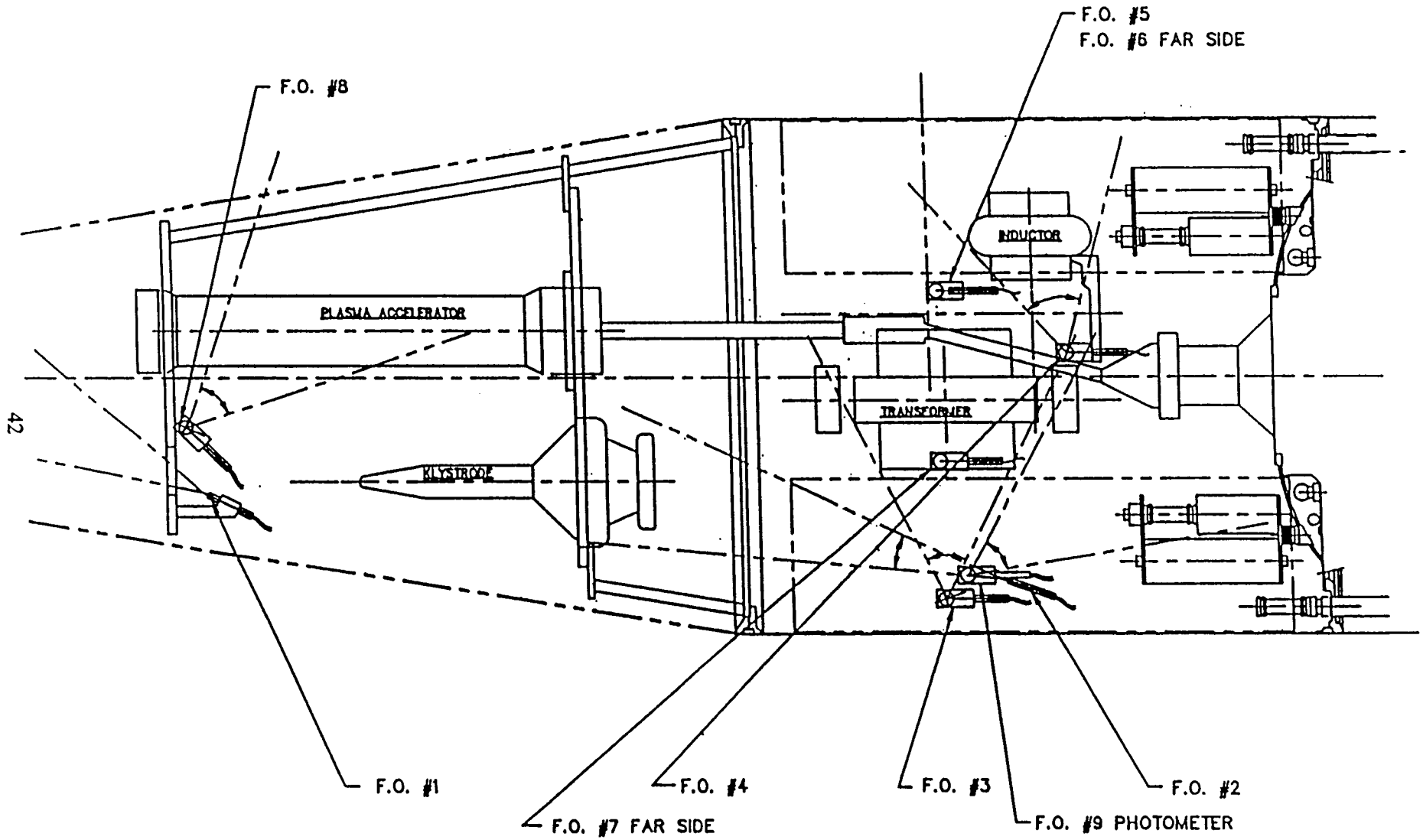

Figure 4.2 SPEAR-2 load section diagram showing location and fields-of-view of the video camera, still camera and photometer optical heads.

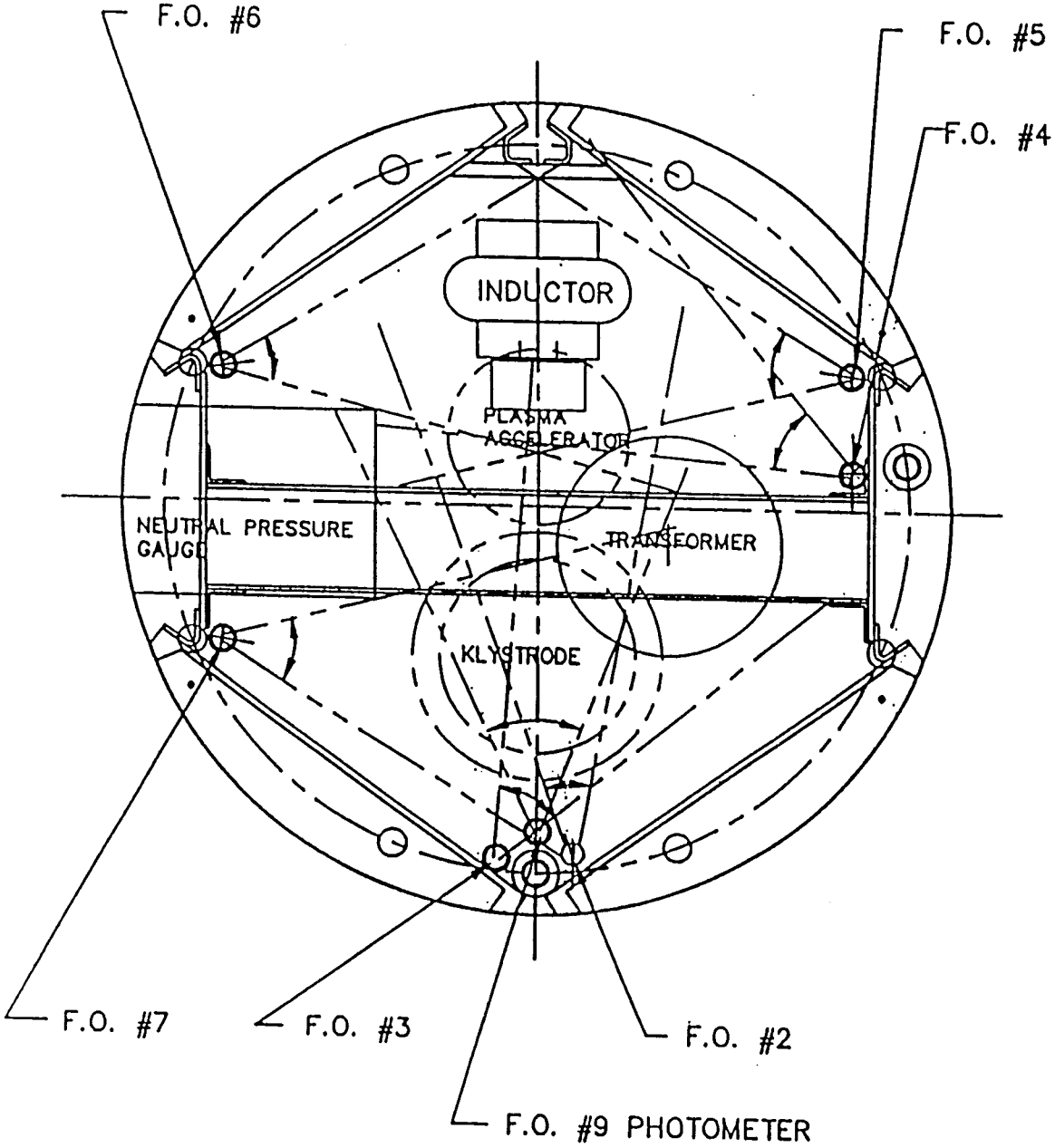

Figure 4.3 SPEAR-2 load section diagram cross section showing location and fields-of-view of the video camera, still camera and photometer optical heads.

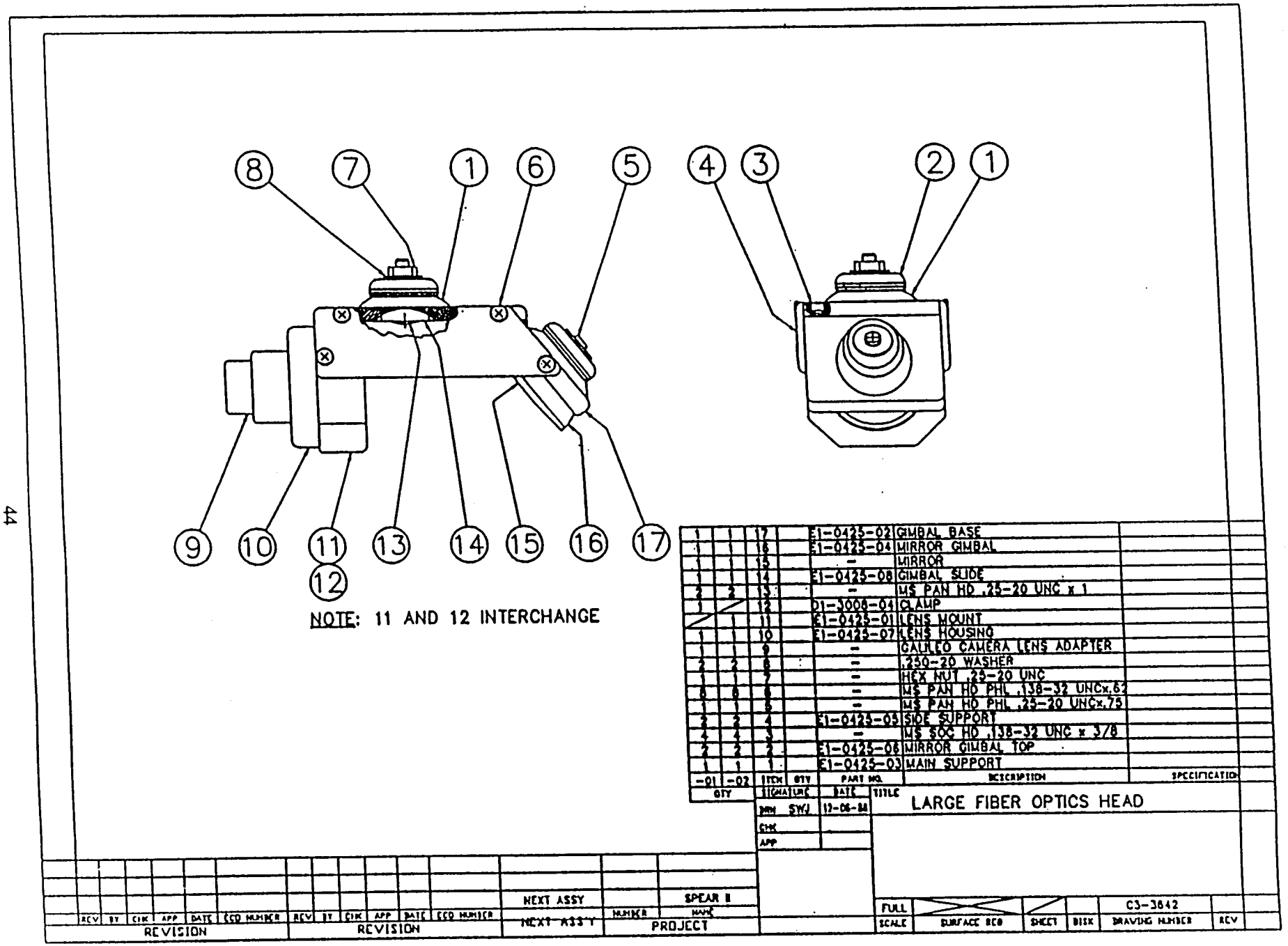

Figure 4.4 SPEAR-2 fiber optics optical head design (used on imaging fiberscopes 1 through 7; See Figures 4.2 and 4.3).

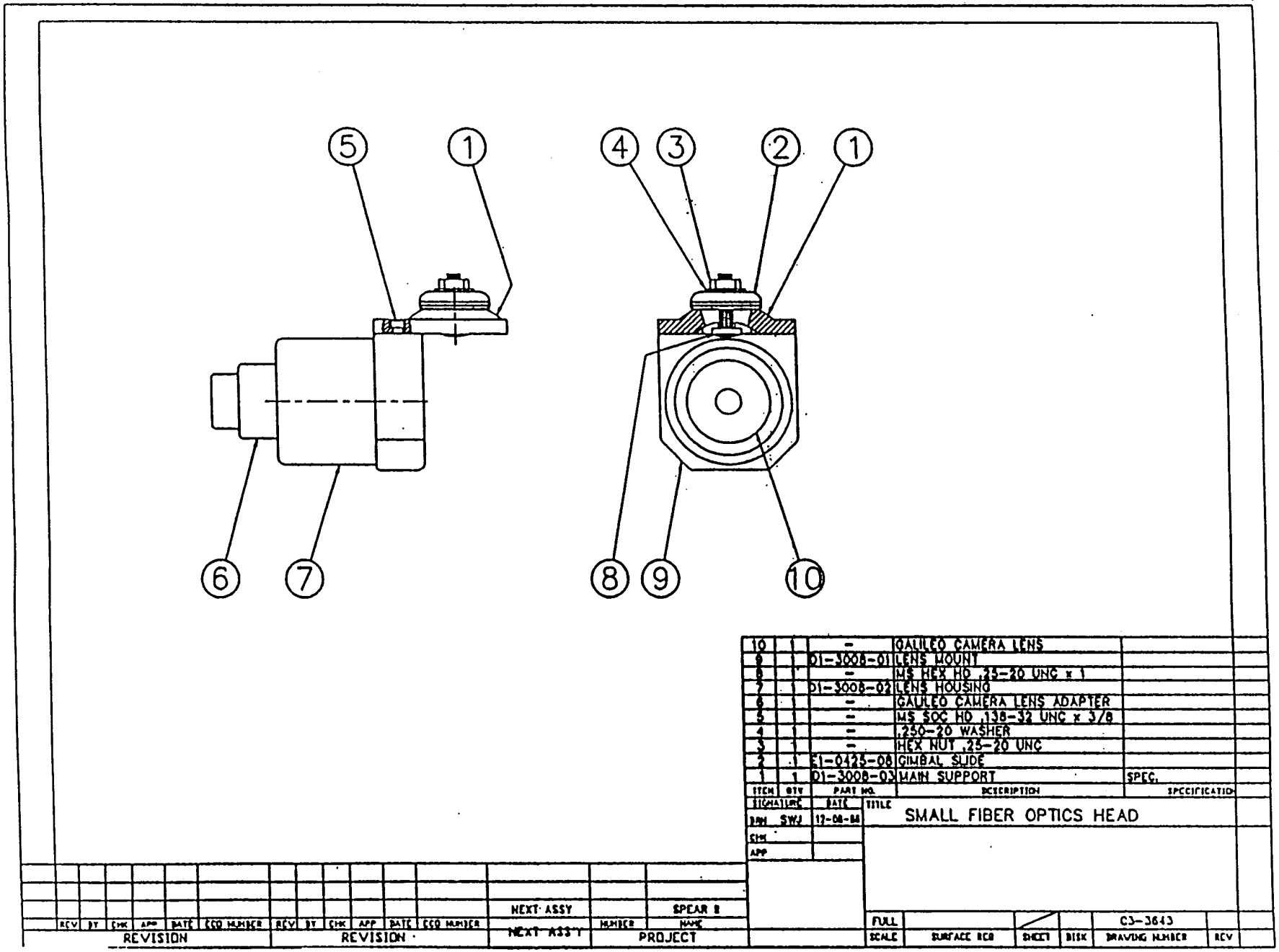

Figure 4.5 SPEAR-2 fiber optics optical head design (used on imaging fiberscope 8; See Figures 4.2 and 4.3).

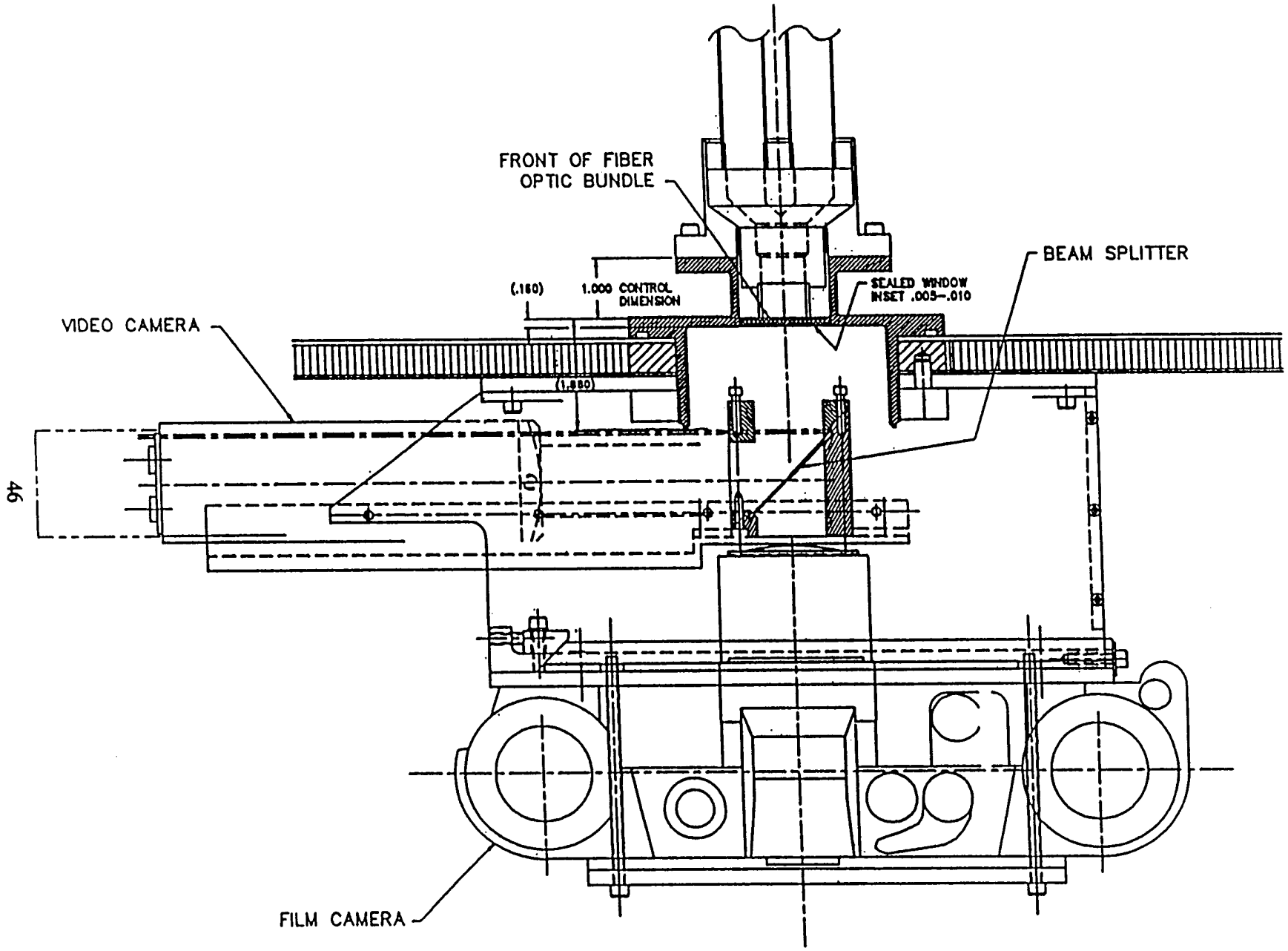

Figure 4.6 SPEAR-2 optical imaging system beam-splitter.

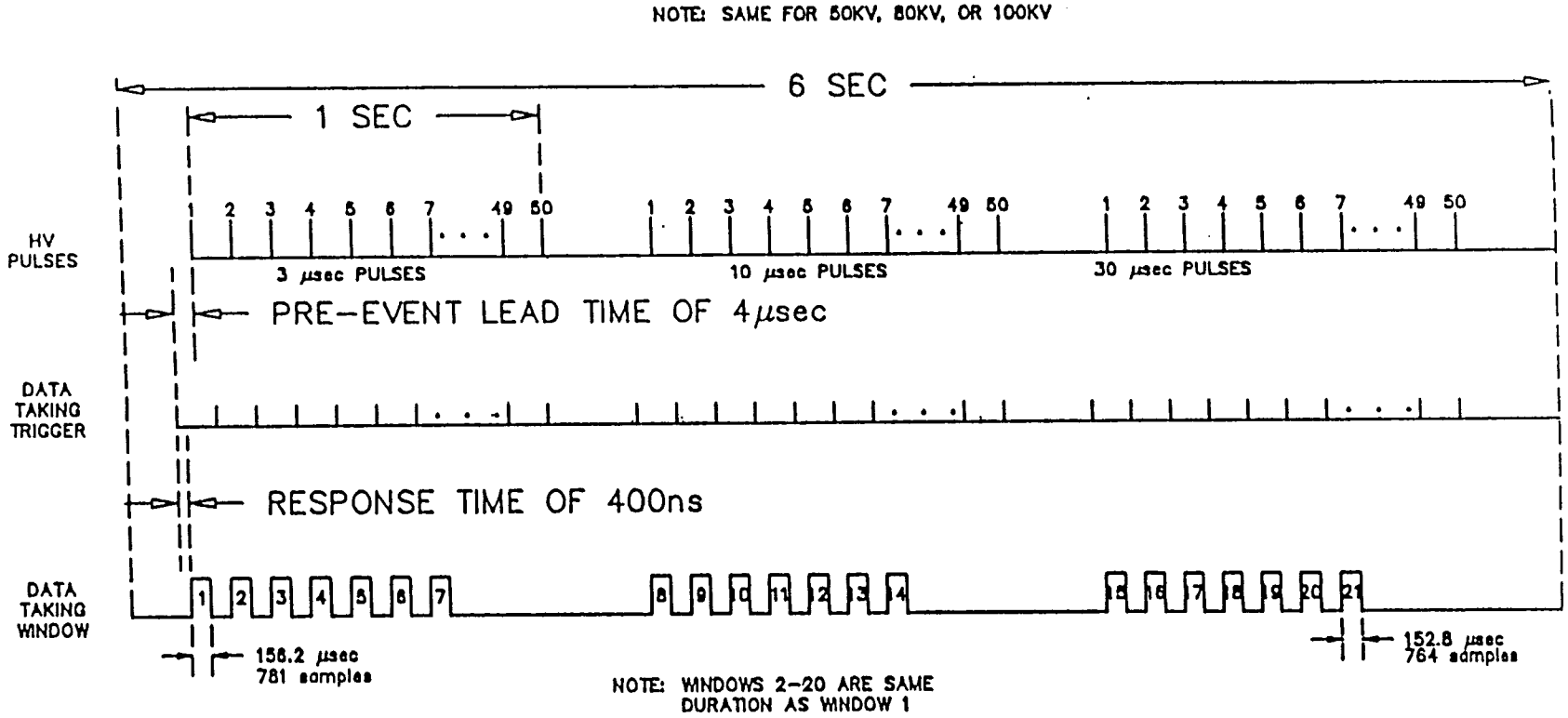

HV MODE DATA ACQUISITION TIMELINE

Figure 4.7 SPEAR-2 photometer high-voltage mode data acquisition timeline.

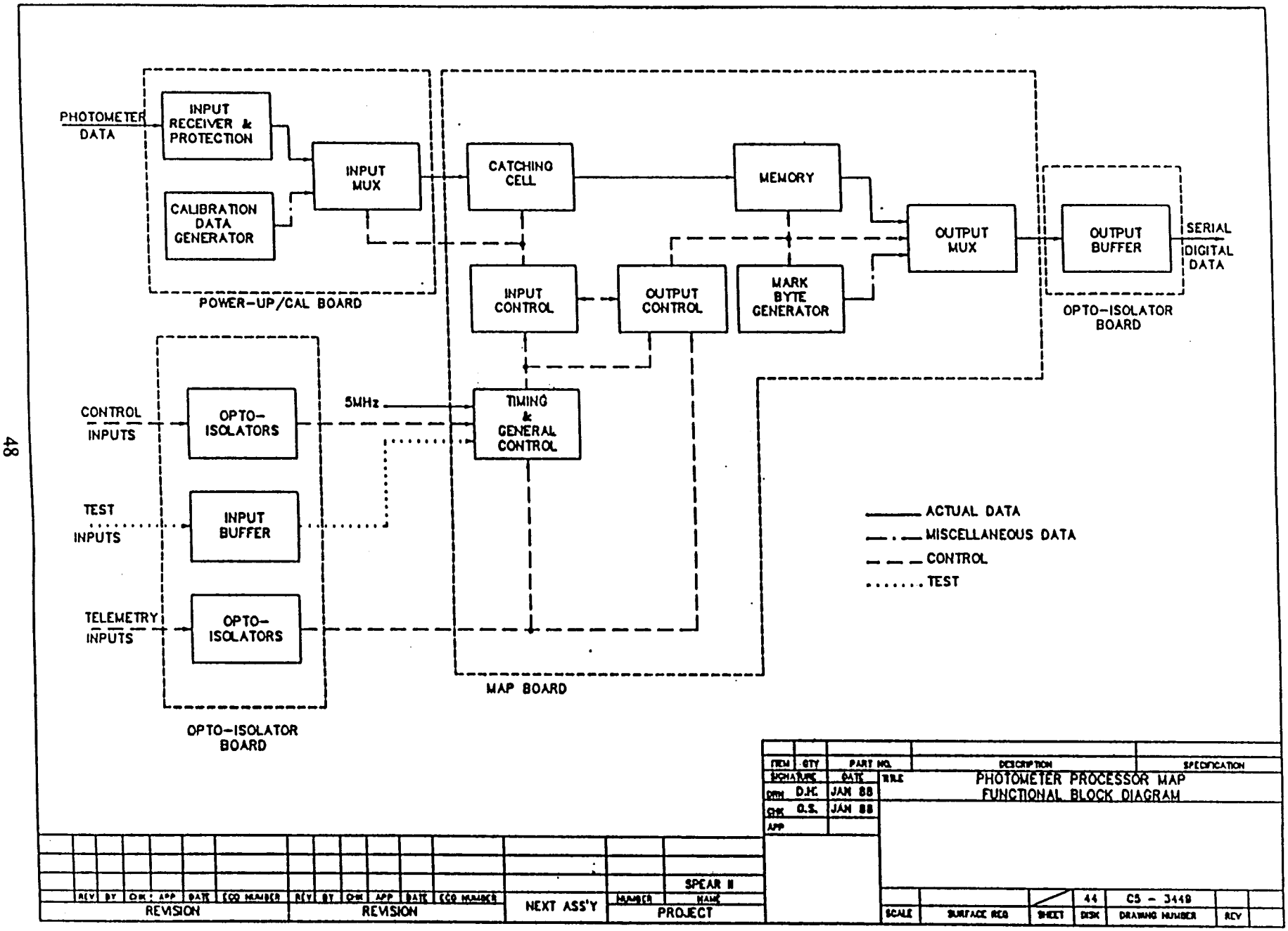

Figure 4.8 SPEAR-2 photometer processor map channel functional block diagram.

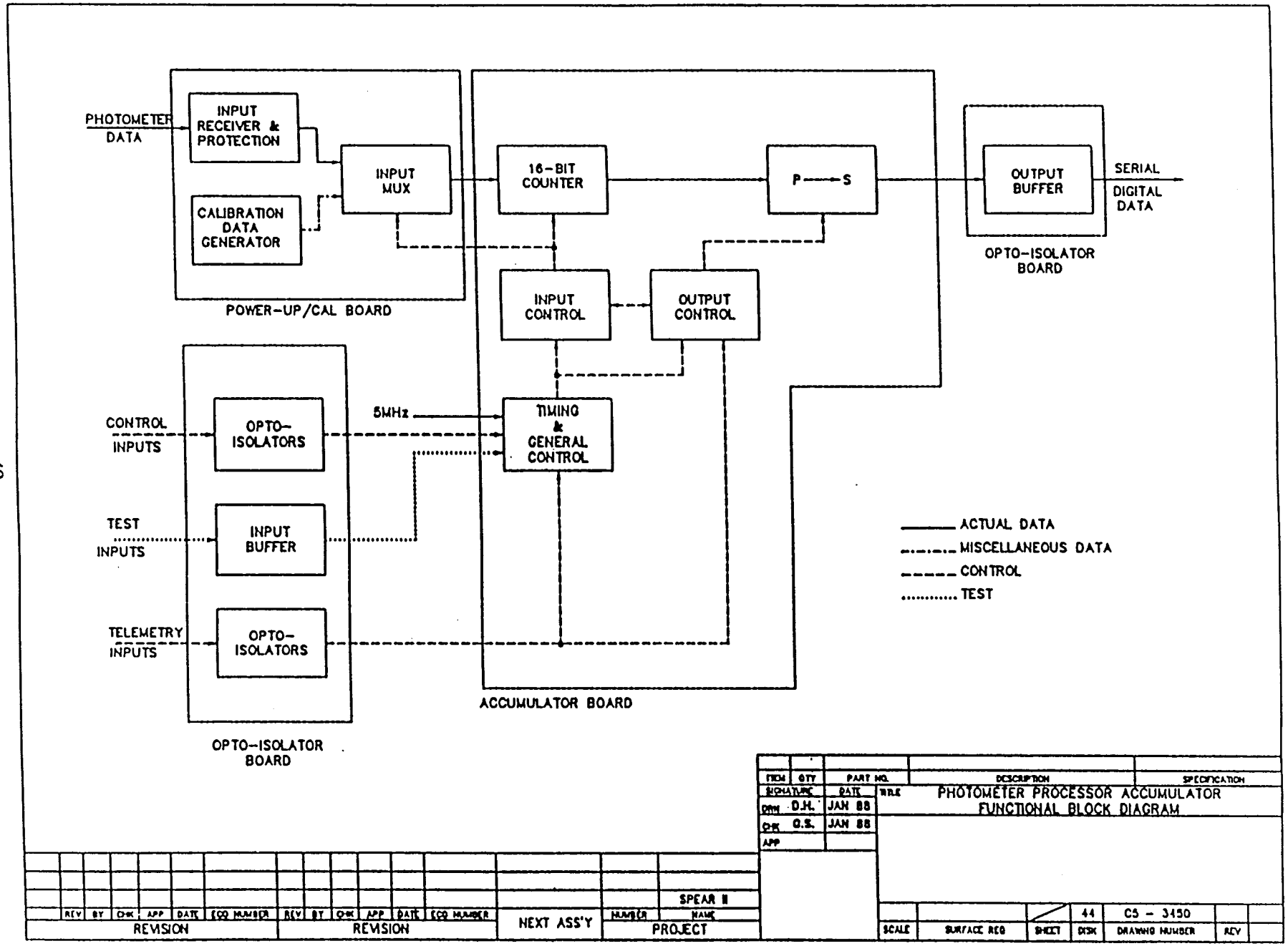

Figure 4.9 SPEAR-2 photometer processor accumulator functional block diagram.

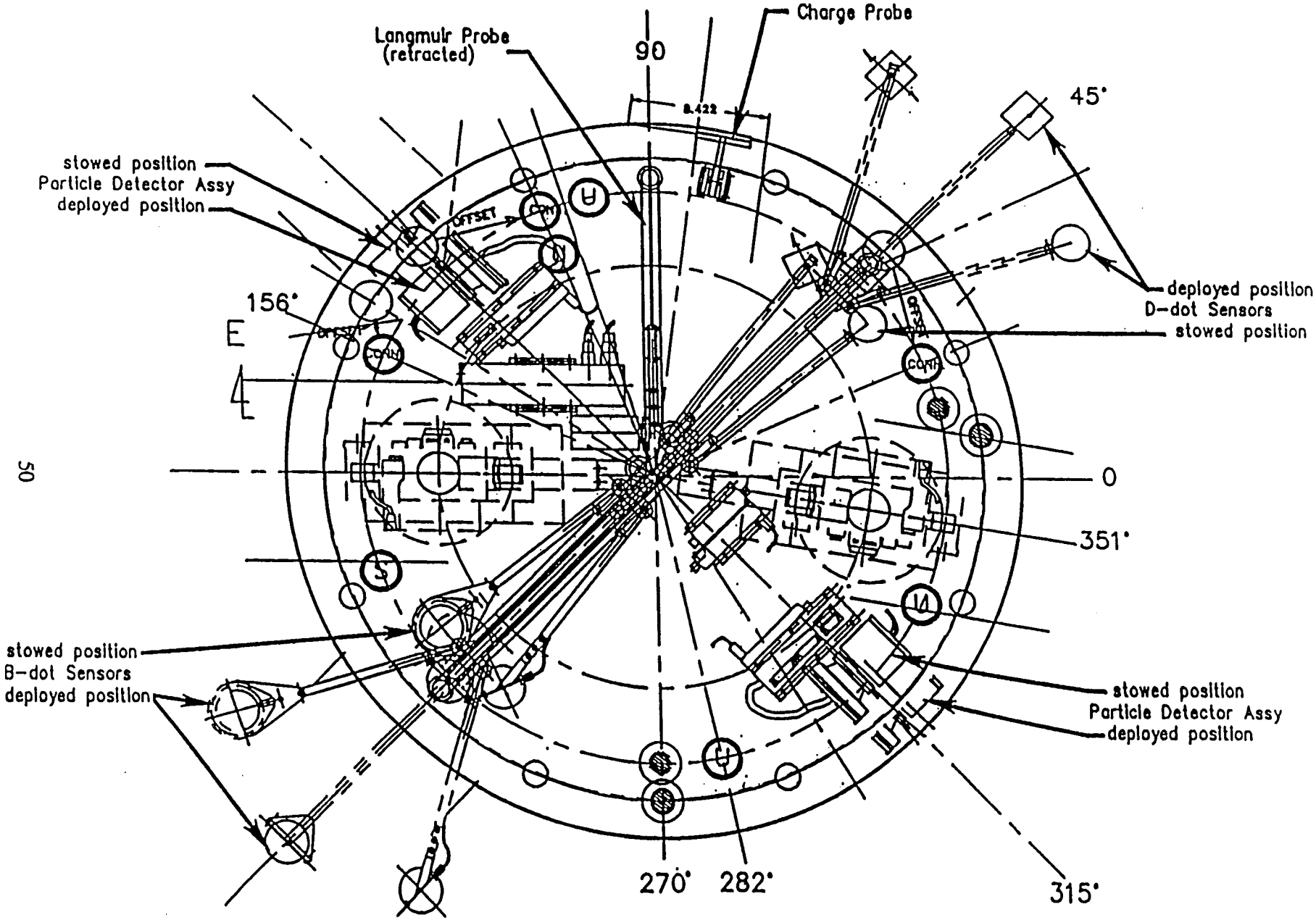

Figure 4.10 SPEAR-2 sensor deployment system showing location of EMP sensors, Langmuir probe, particle detector clusters and charge probe.

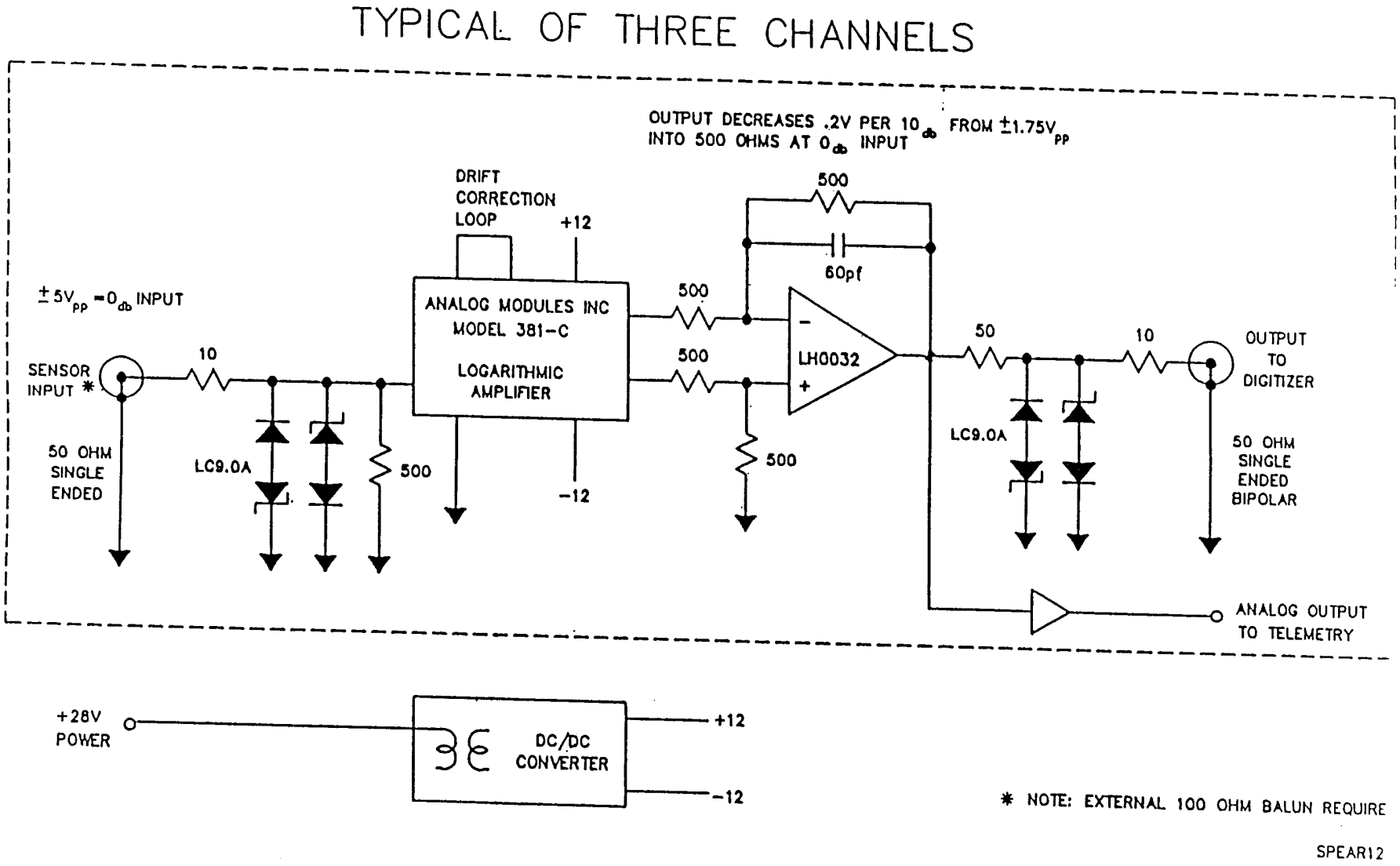

Figure 4.11 SPEAR-2 EMP detector log amplifier channel block diagram.

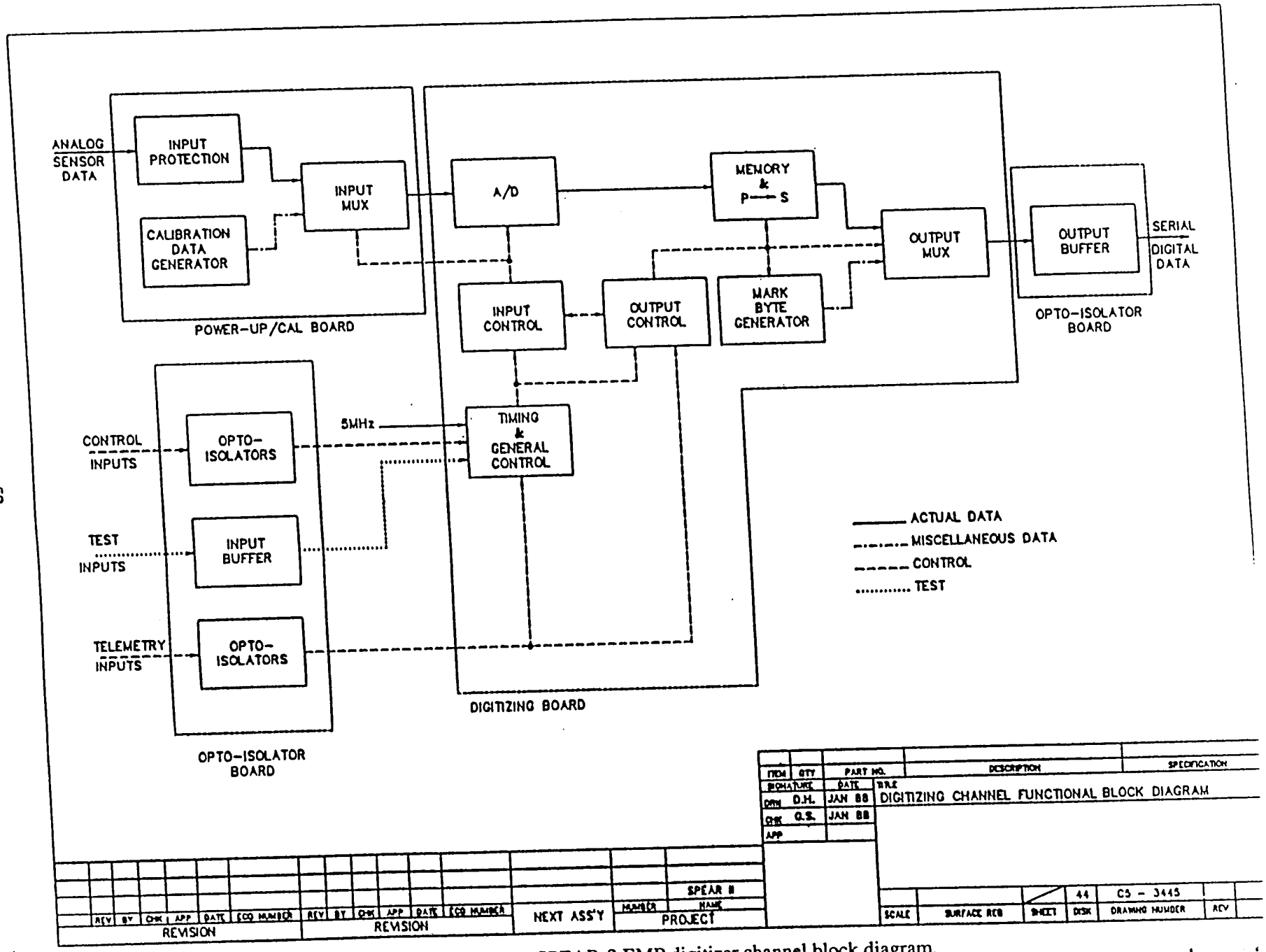

Figure 4.12 SPEAR-2 EMP digitizer channel block diagram.

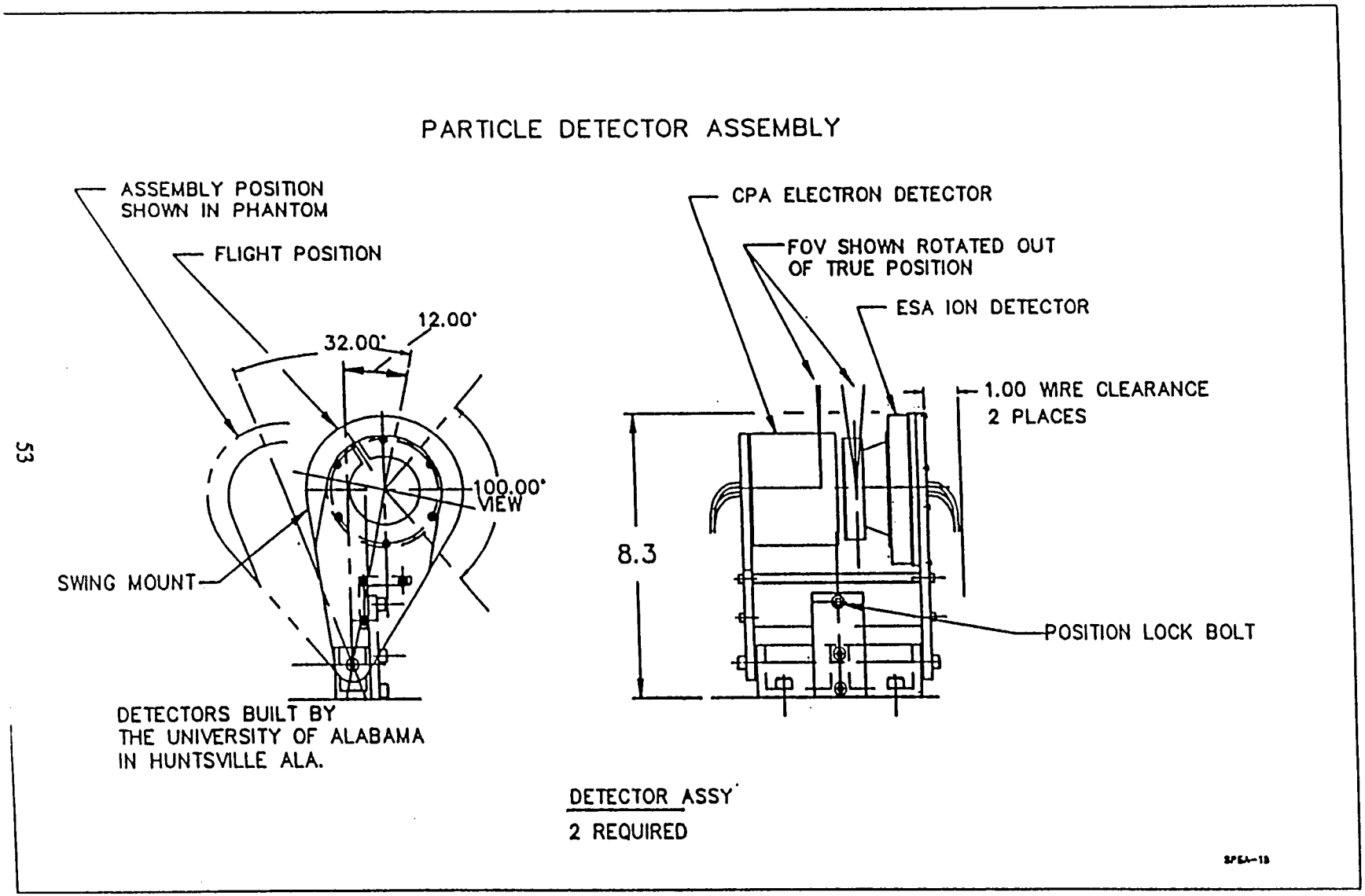

Figure 4.13 SPEAR-2 particle detector assembly.

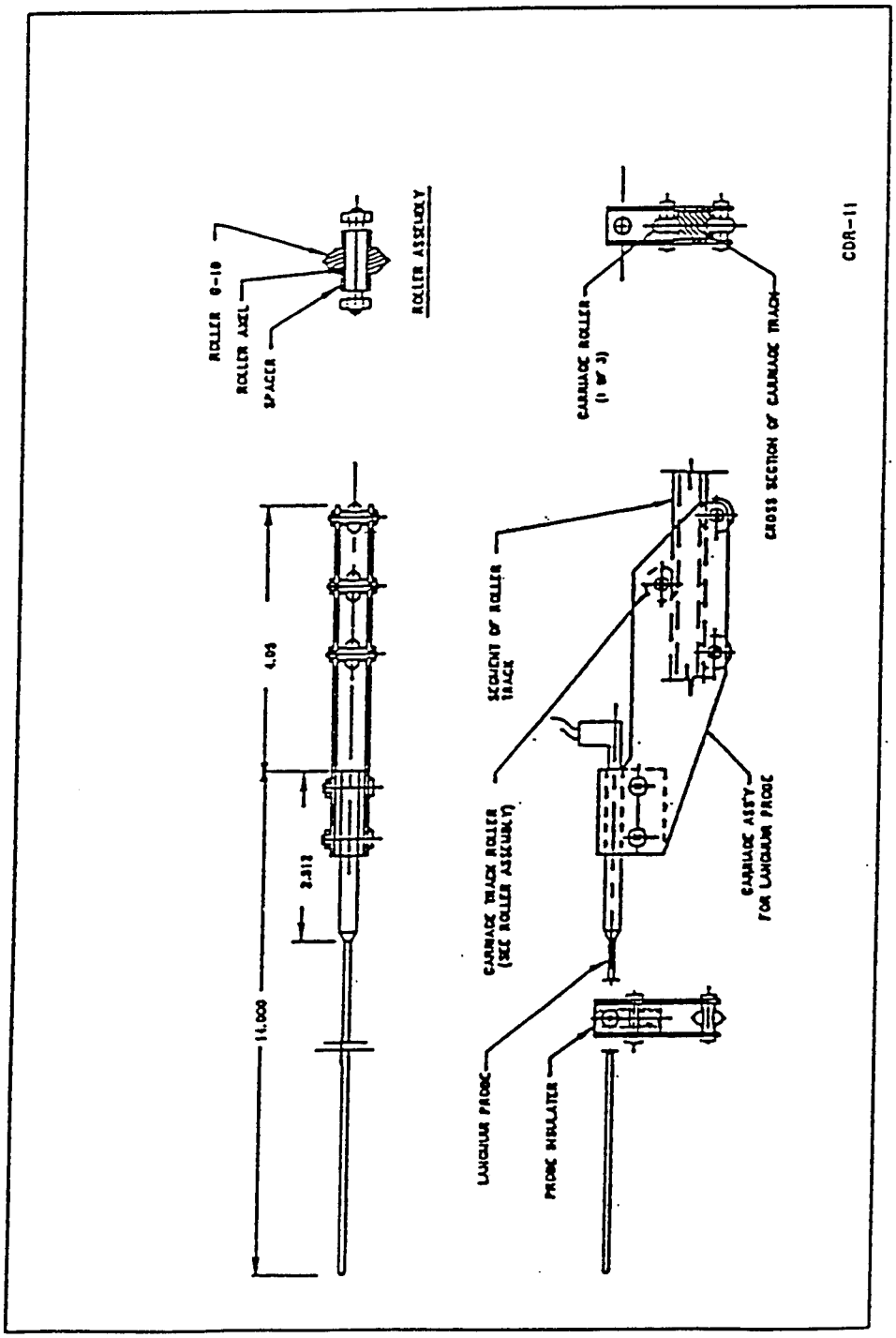

Figure 4.14 SPEAR-2 Langmuir probe assembly.

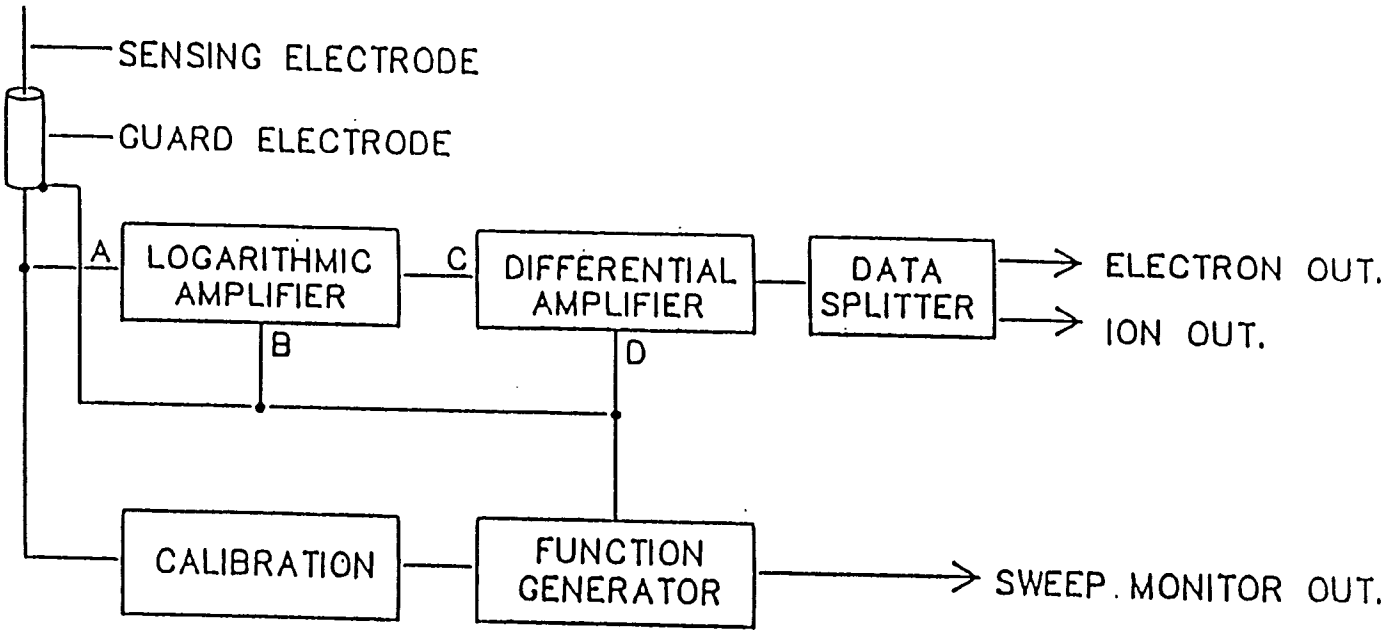

Figure 4.15 SPEAR-2 Langmuir probe functional block diagram.

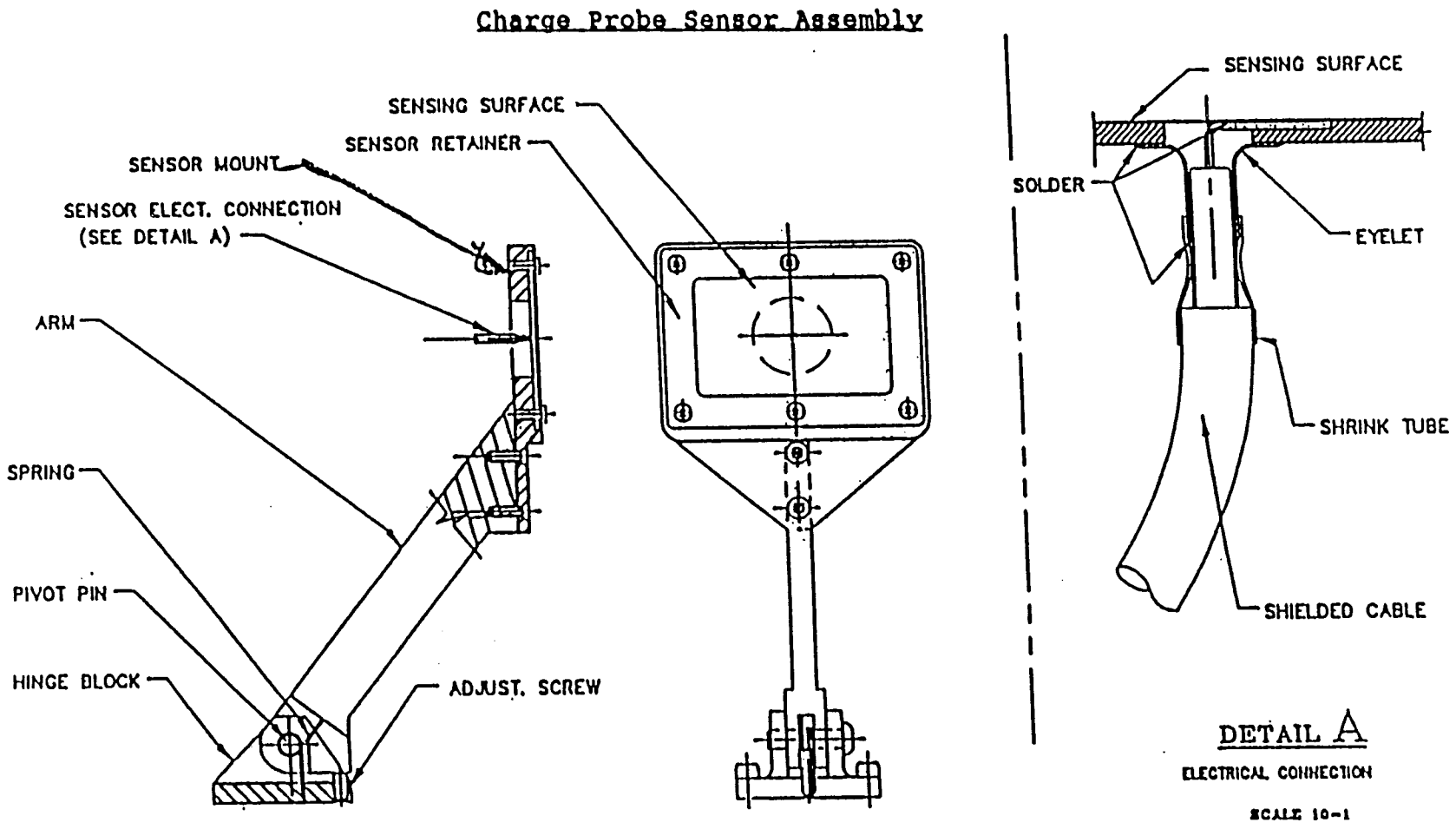

Figure 4.16 SPEAR-2 charge probe.

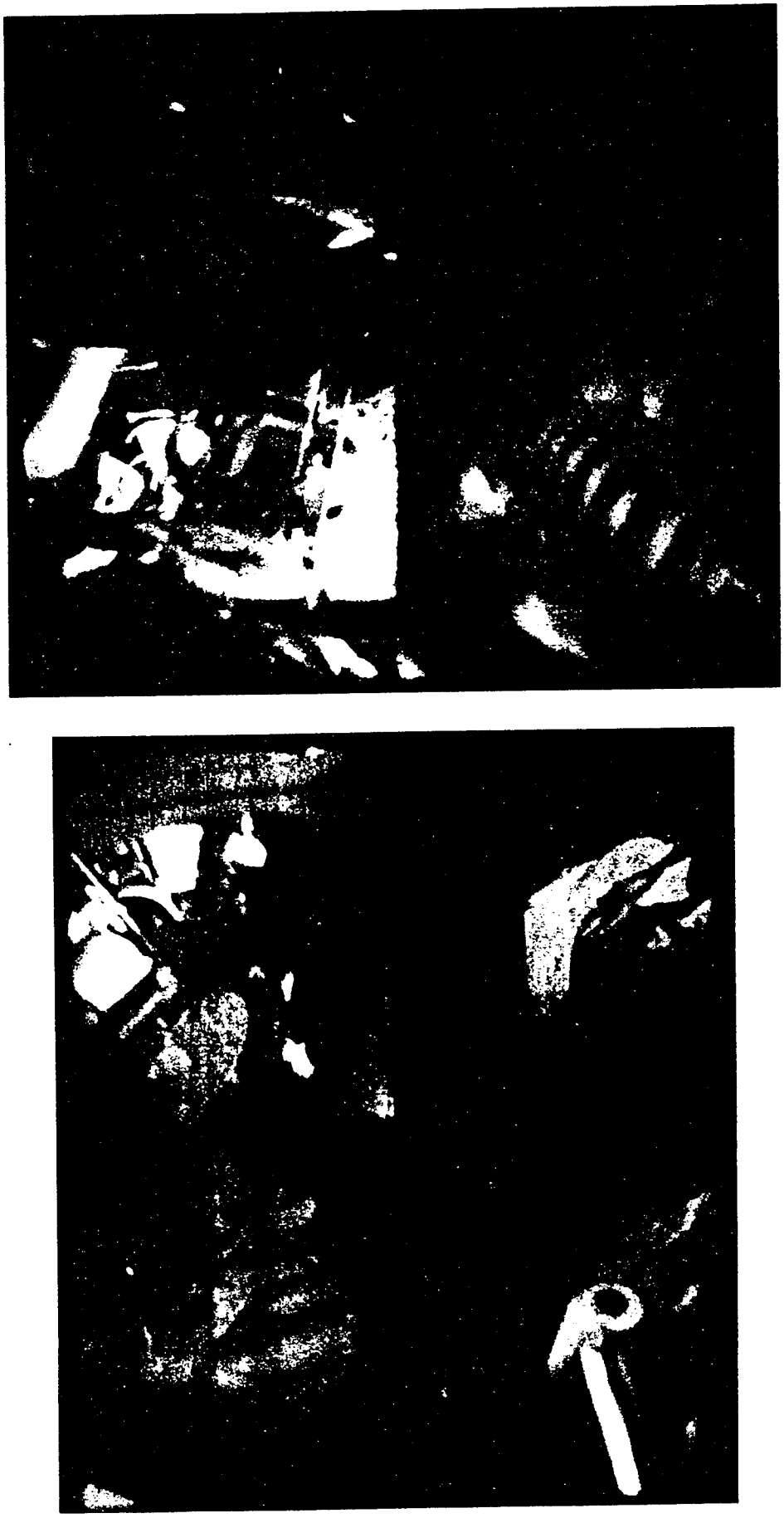

Figure 4.17 SPEAR-2 optical imaging system views of load section

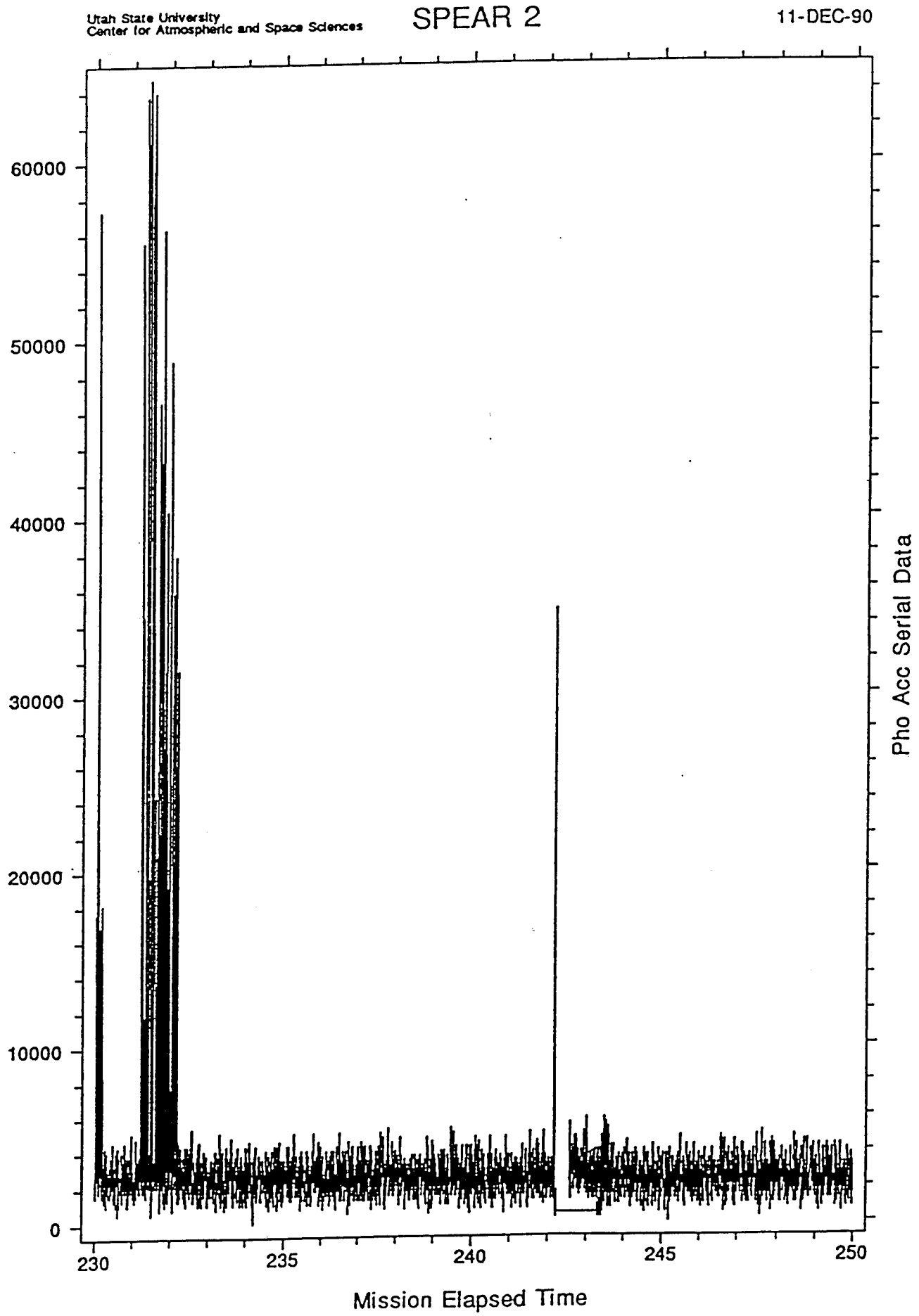

Figure 4.18 SPEAR-2 photometer accumulator serial data plot.

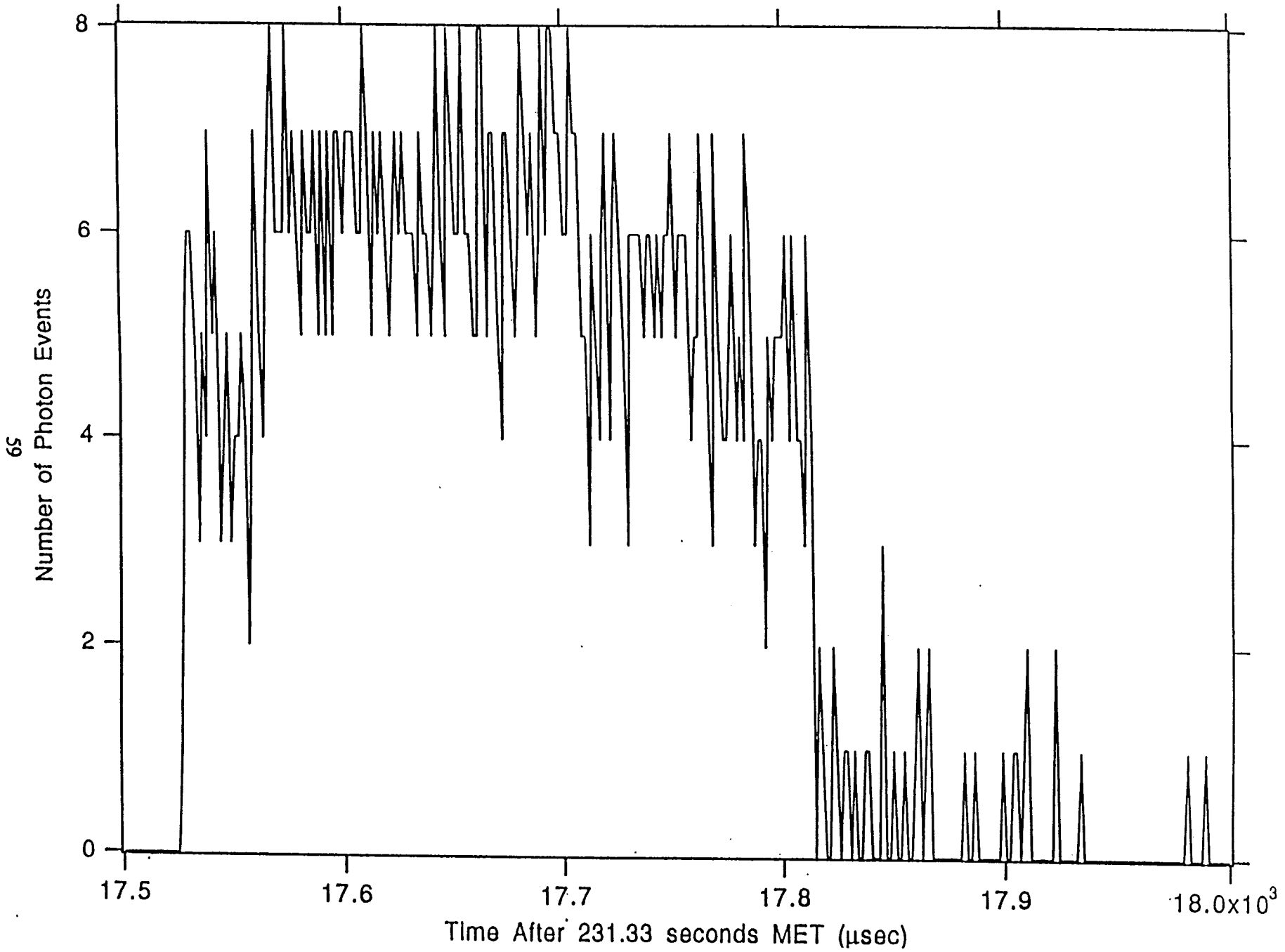

Figure 4.19 SPEAR-2 photometer pulse map output for one HV operaton at 231.22 seconds.

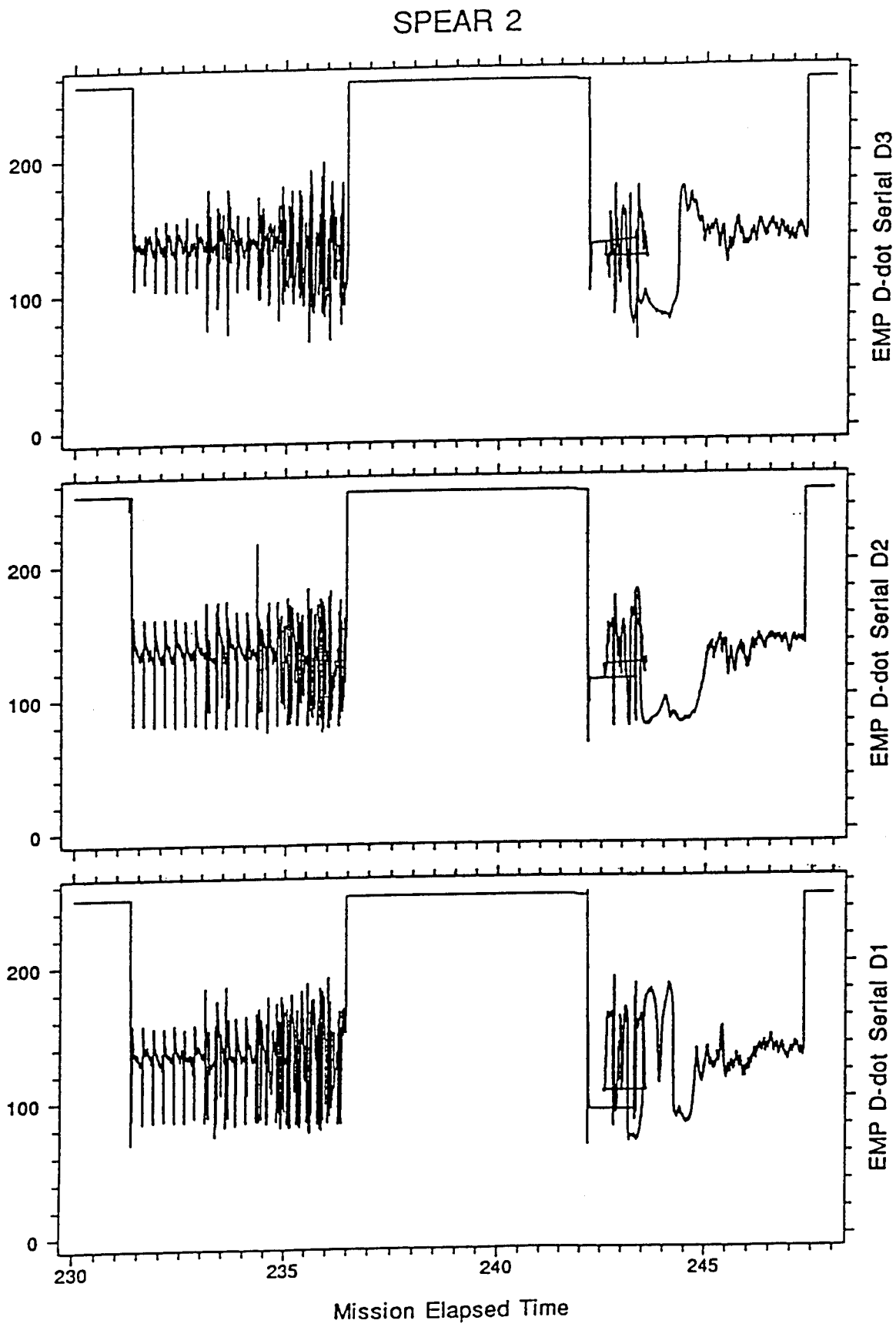

Figure 4.20 SPEAR-2 D-dot data sampled at 200 nS sampling interval.

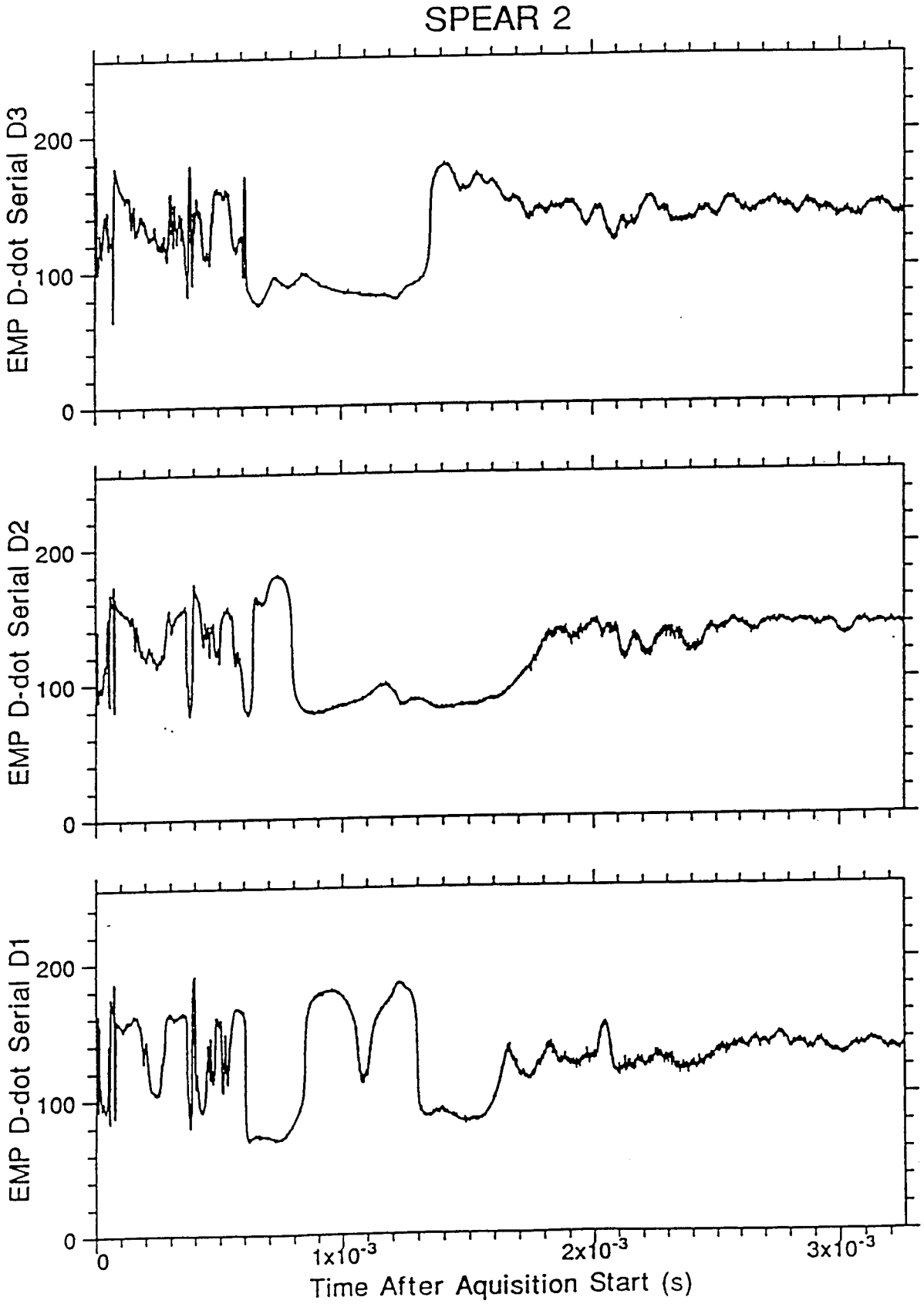

Figure 4.21 SPEAR-2 D-dot data from high current event.

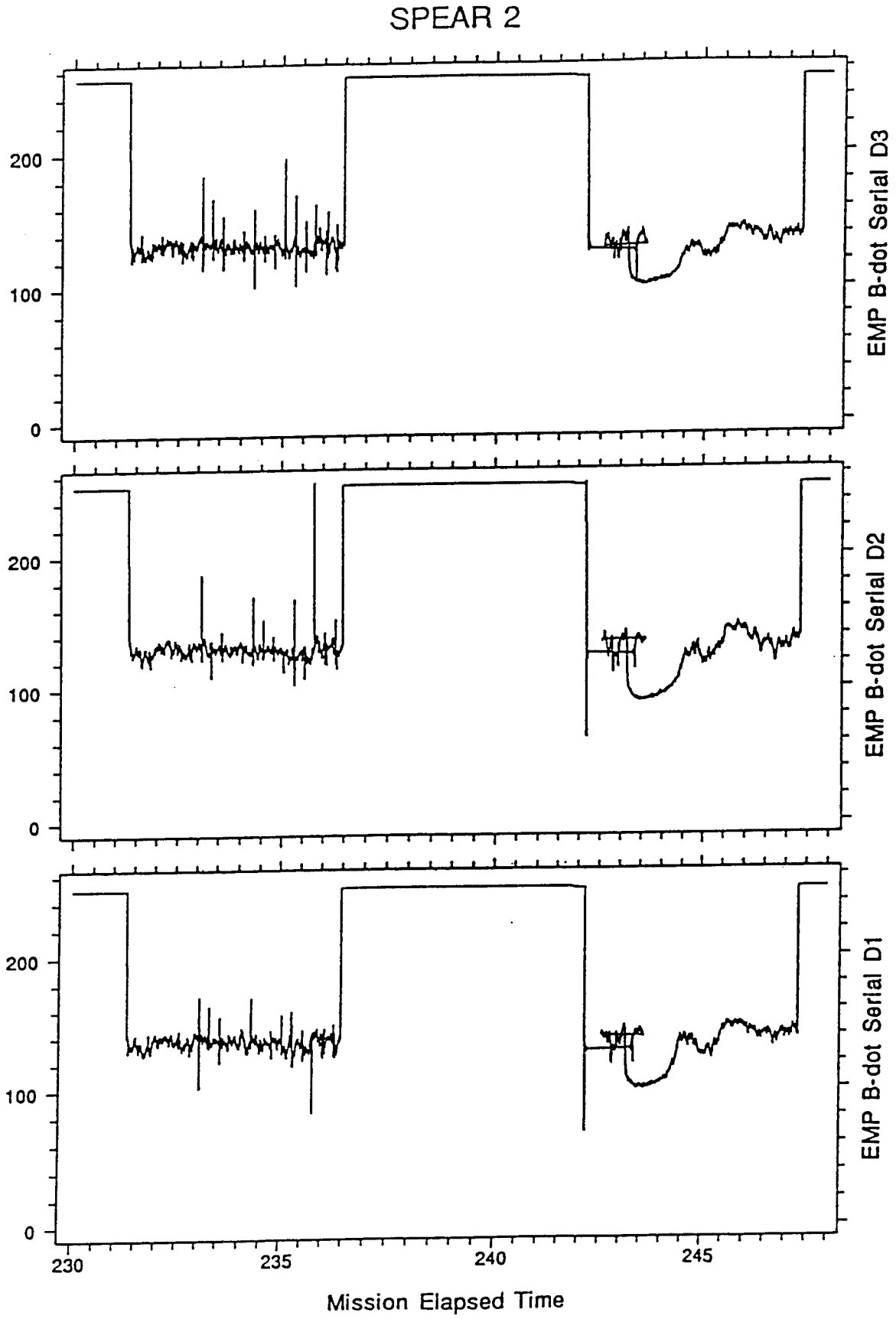

Figure 4.22 SPEAR-2 B-dot data sampled at 200 nS sampling interval.

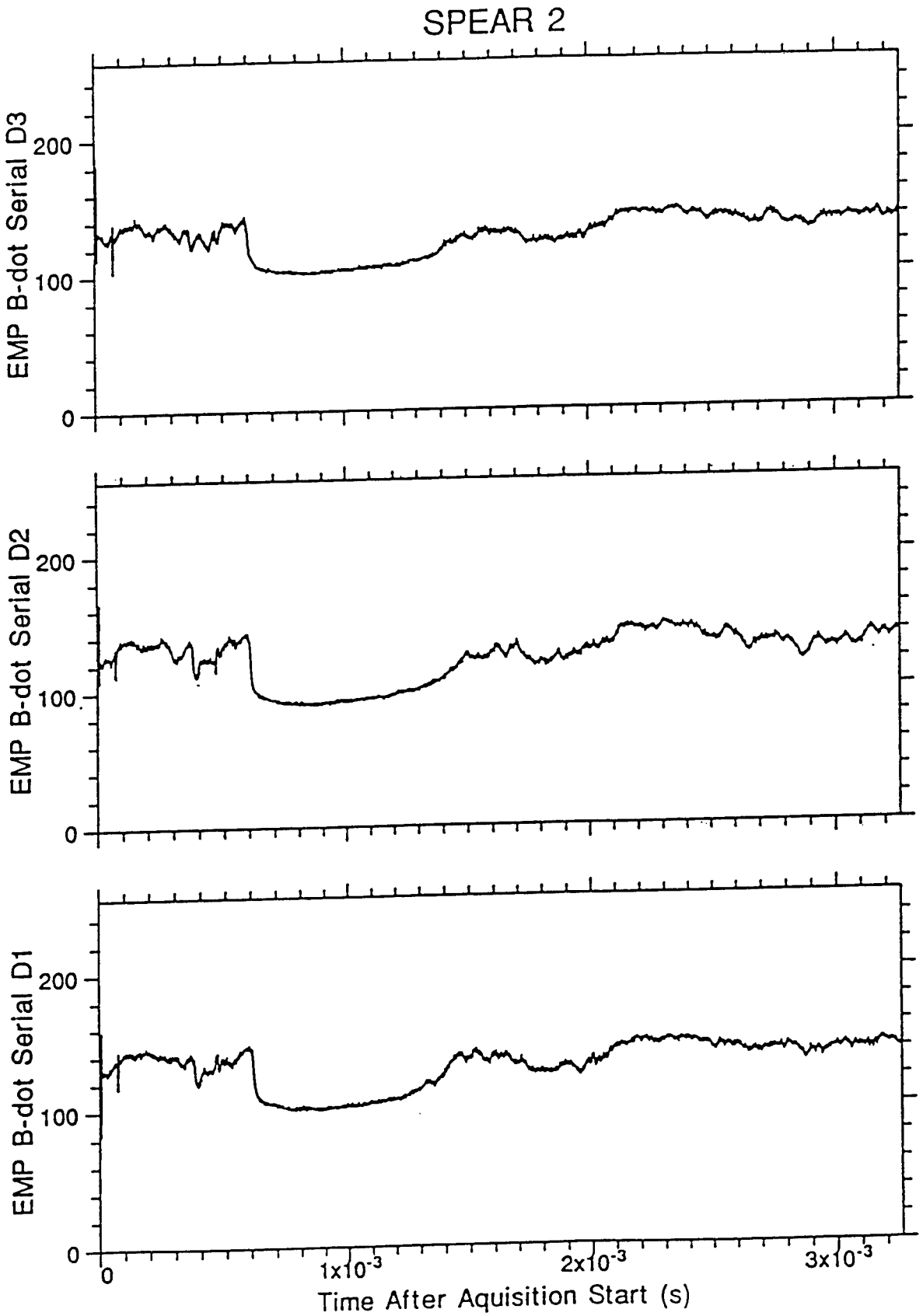

Figure 4.23 SPEAR-2 B-dot data from high current event.

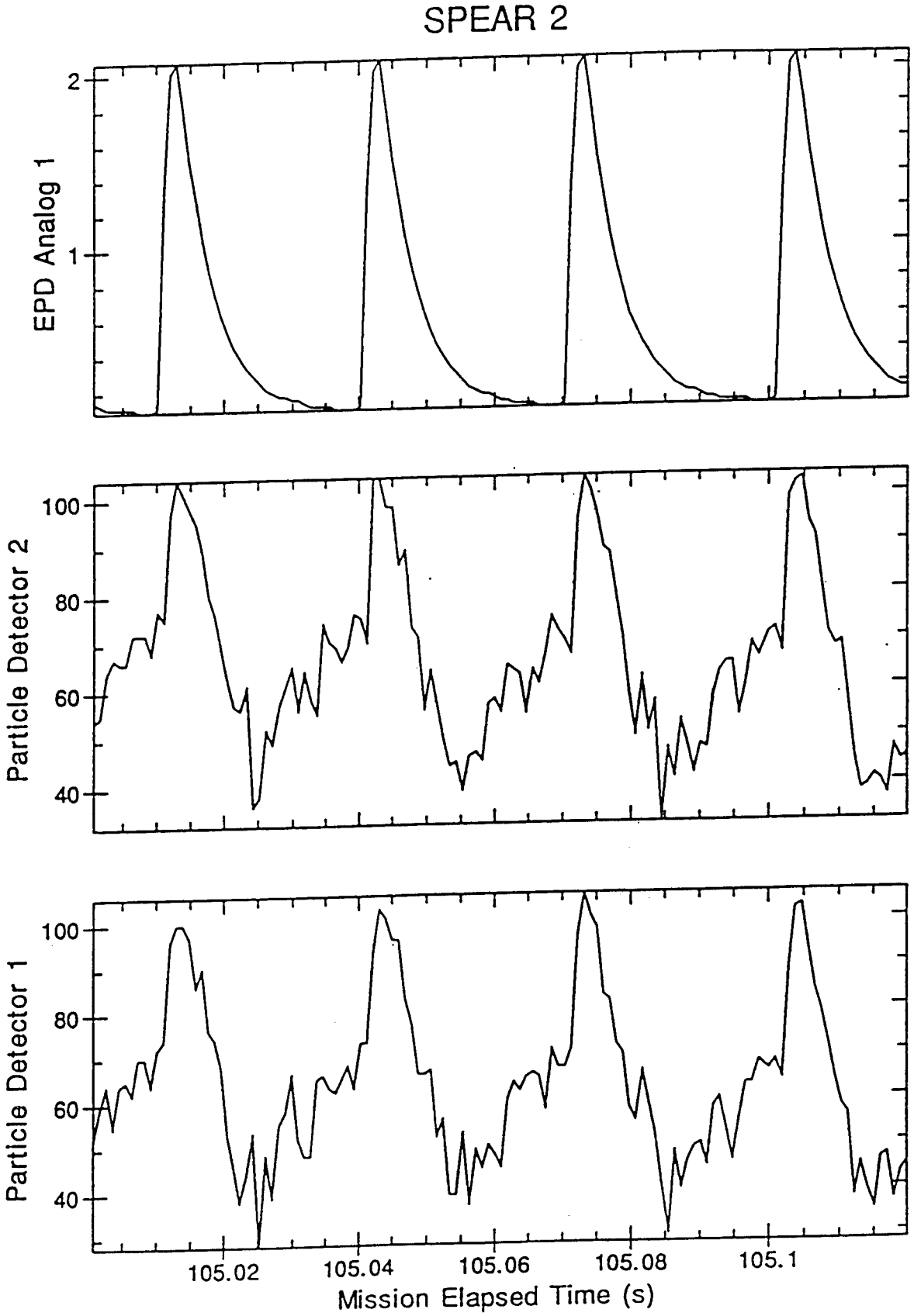

Figure 4.24 SPEAR-2 particle detector output plot.

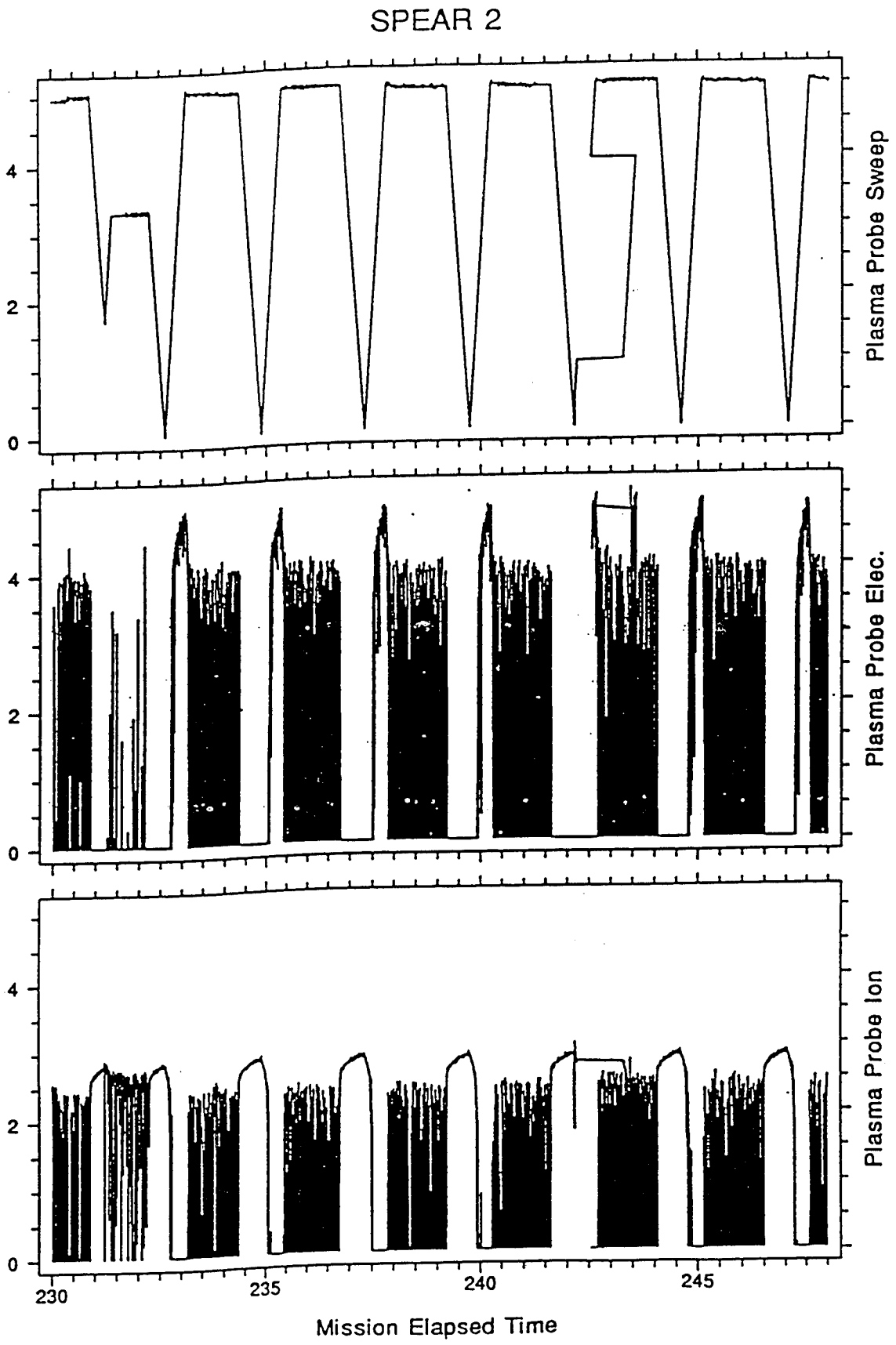

Figure 4.25 SPEAR-2 Langmuir probe output plots.

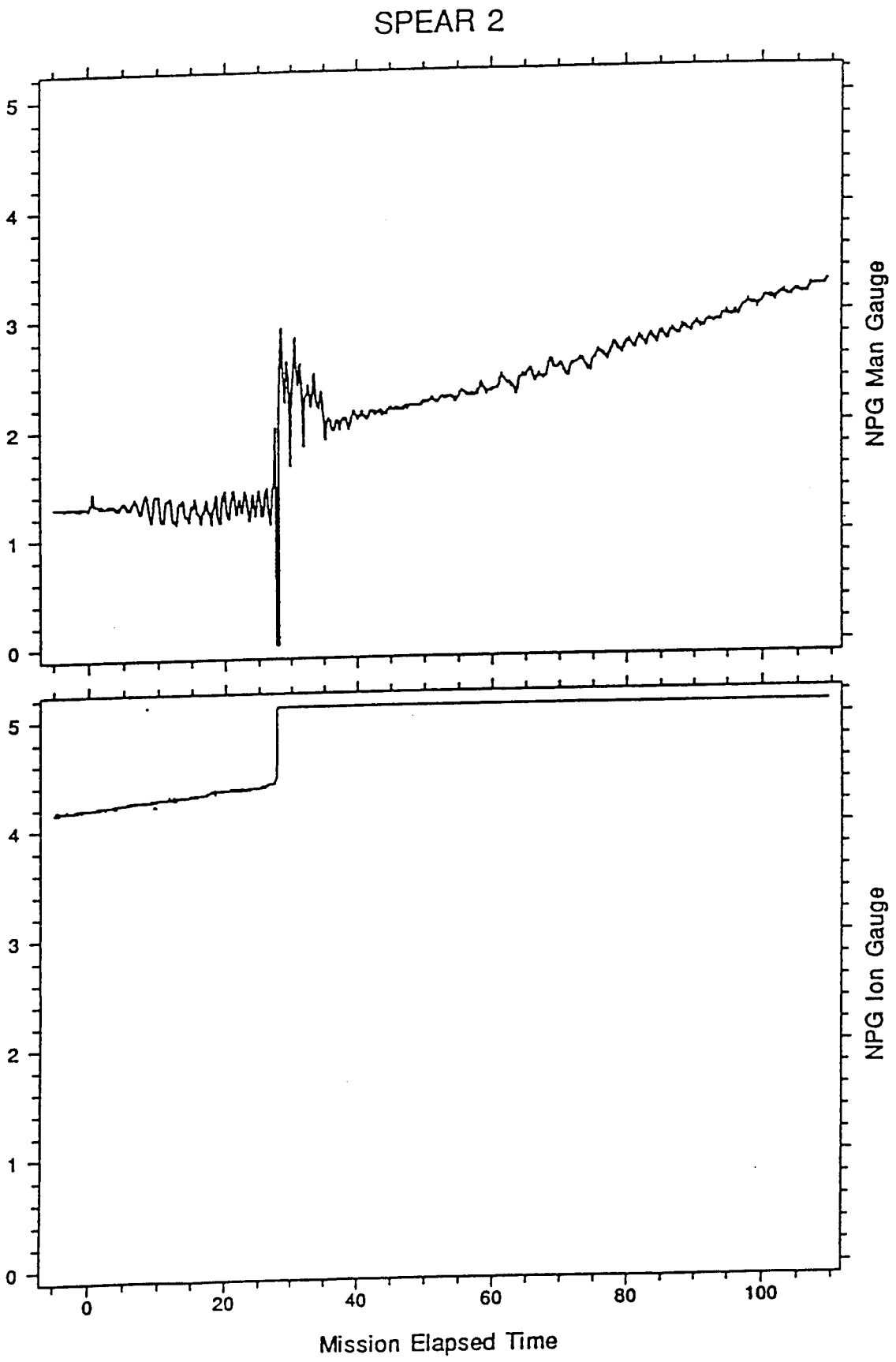

Figure 4.26 SPEAR-2 Neutral pressure gauge output plots.

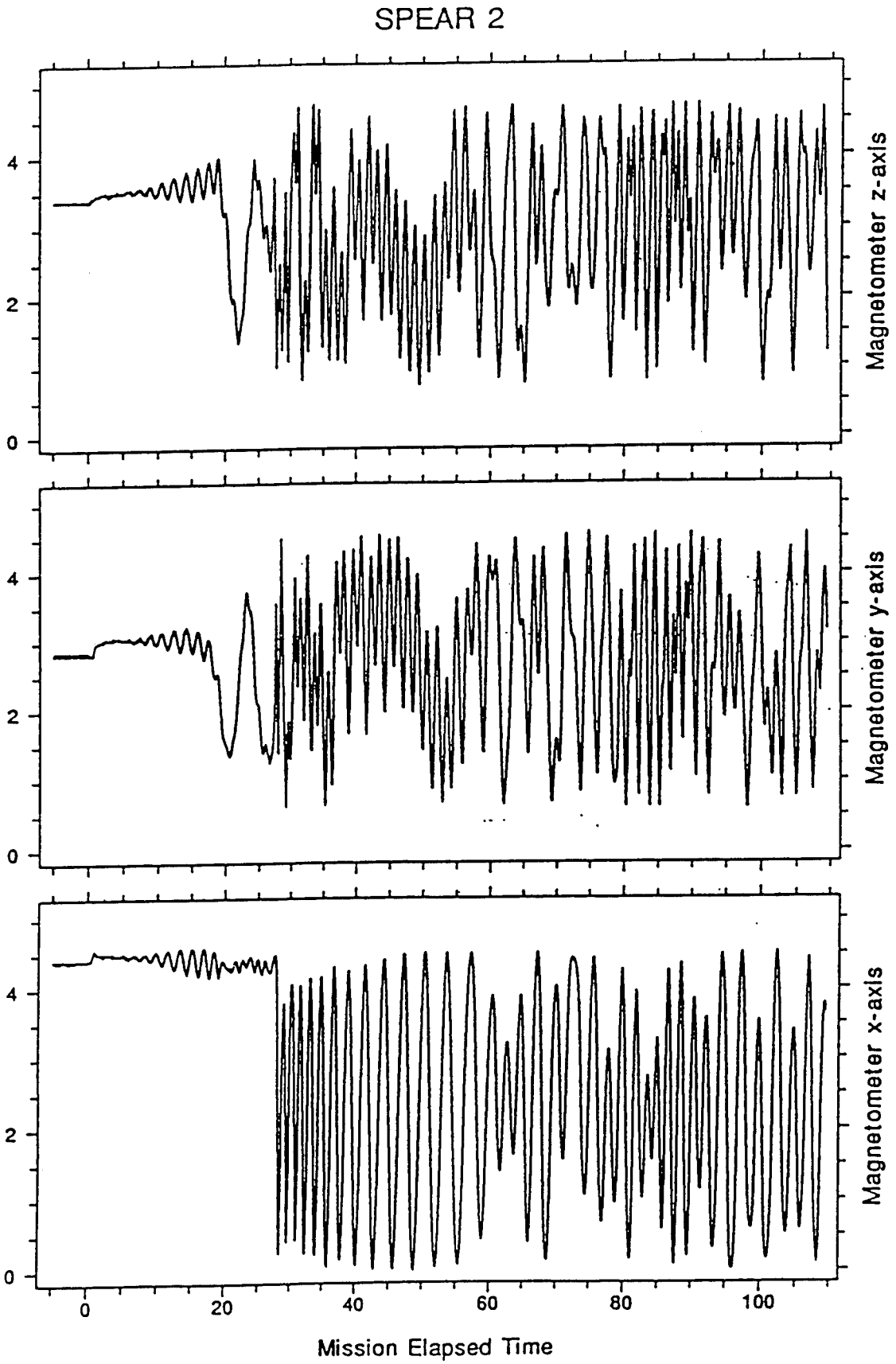

Figure 4.27 SPEAR-2 Fluxgate magnetometer output plots.

APPENDIX A

SPACE POWER EXPERIMENTS ABOARD ROCKETS

(SPEAR-1)

Space Power Experiments Aboard Rockets

(SPEAR-1)

Final Report

to

Defense Nuclear Agency

from

Utah State University

Technical Contract Monitor:
Capt Daniel B. Allred
HQ DNA/RAEV
Washington, D.C. 20305-1000

Tel: (703) 325-1114

Principal Investigator:
Dr. W. J. Raitt
CASS/UMC 4405
Utah State University
Logan, UT 84322-4105

Tel: (801) 750-2983

October, 1988

Table of Contents

1 Introduction 1
2 Instrumentation 3
2.1 Measurement Philosophy 3
2.2 Instrument Complement 3
2.2.1 Spherical Current Collectors and Graded Booms 4
2.2.2 HV Supply and Capacitors 4
2.2.3 Transient Current and Voltage Measurement 5
2.2.4 Regular Current and Voltage Measurement 5
2.2.5 TV Imaging of Current Collector Sheath 5
2.2.6 Photometers 5
2.2.7 Hollow Cathode Plasma Contactor 6
2.2.8 Ambient Neutral Pressure 6
2.2.9 Ambient Plasma Density/Temperature 6
2.2.10 Ion and Electron Detectors 6
2.2.11 VLF and HF Wave Detectors 7
2.2.12 3-axis Magnetometer 7
3 Payload Engineering 7
3.1 Mechanical 7
3.1.1 Payload Skin Section. 8
3.1.2 Boom Deployment System. 8
3.1.3 Graded Booms 8
3.1.4 Current Collecting Spheres 8
3.2 Electrical 9
3.2.1 HV System 9
3.2.2 High Speed Data System 10
3.2.3 Langmuir Probe. 10
3.2.4 Photometers 11
3.3 Integration and Testing 11
4 Data Collection 12
4.1 FM/FM Link 12
4.2 FM/Video Link 13
4.3 FM/PCM link 13
5 Data Processing 14
5.1 SPEAR-1 PCM Data Reduction 14
5.2 Video Processing 15
5.2.1 Single Frame Images 15
5.2.2 TV Frame Image Processing 15
6 SPEAR-1 Chamber Test Results 15
6.1 Introduction 15
6.2 Payload Configuration 16
6.3 Testing Schedule 17
6.4 External Diagnostics 19
6.5 Chamber Test Results 19
6.5.1 Sphere Currents and Voltages 19
7 Flight Summary 19
7.1 Launch 19
7.2 Attitude Program 20
7.3 Flight Timeline 20
7.4 High Voltage Timeline 21
7.5 Instrument Performance 22
7.7 Flight Results 23
7.7.1 Ambient Environment 23

7.7.2 Neutral Pressure 23
7.7.3 Plasma Density 23
7.8 Electric Currents to HV Biassed Spheres 24
7.8.1 Steady State Currents 24
7.8.2 Optical Signatures 25
7.9 Vehicle Charging 26
8 Discussion of Results 26
8.1 Ambient Environment 26
8.2 Plasma Currents 27
8.3 Vehicle Charging 28
9 References 30
10 Figures 31

SPEAR-1

1. Introduction

The Space Experiments Aboard Rockets (SPEAR) program was initiated by the Strategic Defense Initiative Office, Innovative Science and Technology division (SDIO/IST) and is managed by the Defense Nuclear Agency (DNA) to gain further insight into the interaction of high voltage pulsed power systems with the Low Earth Orbit (LEO) space environment.

The program consists of three pronged attachment on the problem involving

i) Theoretical studies and computer model development.
ii) Ground-based vacuum chamber experiments.
iii) Flight experiments utilizing sounding rockets to carry experiments into the LEO environment.

At present two space flights have been authorized, one designated SPEAR-1 was flown in December, 1987, the second designated SPEAR-2 is scheduled for flight in April, 1989. This report will deal with the first space flight in the program, SPEAR-1.

SPEAR-1 was planned to be a short time-scale mission to provide some science-oriented measurements on the HV - space environment interaction to help in the development and interpretation of theoretical models. The model predictions varied from a very low current situation typified by the Parker-Murphy model to the possibility of heavy current discharges between parts of the system or to the ambient ionosphere. The specific science objectives of the SPEAR-1 mission are listed below in Table 1.

Table 1. SPEAR-1 Science Objectives

Objective	Description
1.	To study the altitude and attitude dependence of the *i-v* characteristic of a metallic conductor exposed to the space environment and biassed at up to 10s of kV.
2.	To study the interaction of HV biassed conductors within each other's charge sheaths.
3.	To make diagnostic measurements to aid the development of theoretical models to predict the current collection by conductors biassed to HV in the ionosphere.
4.	To study the effectiveness of a plasma contactor in grounding the power platform to the ambient ionosphere.
5.	To obtain this data in a timely fashion to be useful in the SPEAR-1 program.

The innovative features of the SPEAR-1 payload and the short development time scale led us to adopt a design philosophy to keep the payload as simple as possible, avoid

the use of sophisticated microprocessor control and to utilize previously developed diagnostic instruments whenever possible. The major challenge was to develop a HV power supply capable of generating 10s of kV and delivering 10s of amperes for short periods while still conforming to the volume and weight restrictions imposed by the capabilities of a Black Brant 10 sounding rocket and the requirement to reach an apogee exceeding 300km.

It was decided to generate HV at varying potentials by using a mechanical timer to control the charging period of a HV capacitor. After the predetermined charging time the HV was transferred to a spherical current collector mounted at a distance of about 3m from the rocket body, and having the electric field close to the mounting point of the sphere controlled by using a graded boom at about 1m in length. The general arrangement of HV electrical potentials in the flight system is shown conceptually in Figure 1-1. In order to have better control over the sphere-ionosphere potential (V_{si}) it was planned to maintain the rocket-ionosphere potential (V_{ir}) at a low value by flying a plasma contactor on the rocket to maintain a low impedance connection between the rocket and ionosphere.

The SPEAR-1 development and flight took place over a period of about one year. The key milestones in the program are shown below in Table 2.

Table 2. Key Milestones in SPEAR-1 Program

Activity	Date
1. Project approval	December 1986
2. Authority to proceed	January 1987
3. Payload design review	April 1987
4. Delivery to AFGL for integration	September 1987
5. Payload vacuum chamber test	November 1987
6. Delivery to Wallops Flight Facility	November 1987
7. Flight	December 1987
8. Initial data review	January 1988

Consistent with our philosophy of using flight proven instruments whenever possible, we sub-contracted a number of sub-systems in order to meet the scheduled flight date and maintain high reliability. The sub-contractors and principal vendors to USU and their subsystems are listed below in Table 3.

Table 3. Principal Sub-contractors and Vendors

Sub-system	Supplier
Neutral pressure gauge	University of Iowa
Wave receivers and antennas	Systems Unlimited
Charged particle detectors	University of Alabama, Huntsville
Plasma contactor	SRS Inc.
Telemetry system	Northeastern University
Payload skins	Bristol Aerospace Ltd.
Low light level TV camera	English Electric Valve Co.

2. Instrumentation

2.1 Measurement Philosophy

The prime instrumentation planned for the SPEAR-1 payload was a means of measuring the currents and voltages associated with the application of the high voltages stored on capacitors to the exposed spheres. It was planned to perform this at the regular telemetry sampling rate of 1024 samples/sec and also at a much higher rate of 5×10^6 samples/sec for a short period (200μS) at the start of each discharge period.

The current sensors for the total capacitor current and the current flowing through the graded boom were chosen to be low resistance current sensing resistors connected on the ground side of the circuitry. This method was adopted to avoid development problems of rejecting a common mode voltage of up to 45kV which would have been the case if the current sensor had been located at the sphere.

The current and voltage measurements were supplemented by a number of diagnostic instruments to provide further information on the sheath and system/environment interaction. Optical sensors (imaging and photometric) were included to search for arcs or discharges in the vicinity of the spheres. Wave receivers were included to search for turbulence in the sheath plasma, and an energetic charged particle analyzer was included to monitor the vehicle potential. The ambient environment was monitored in terms of thermal electron density and temperature and neutral gas pressure. A magnetometer was included to monitor the correct execution of the vehicle attitude maneuvers.

In order to prevent the vehicle body being driven to high negative potentials to achieve a current flow to balance that collected by the positively biassed spheres, a low impedance connection between the vehicle and the ionospheric plasma was planned. This connection would be achieved by a hollow cathode plasma contactor device mounted at the end of the payload remote from the biassed spheres.

2.2 Instrument Complement

In order to meet the scientific objectives listed earlier an instrument complement shown below in Table 4 was procured from the institutions indicated in the table.

Table 4. SPEAR-1 Instruments

Instrument	Institution
Two spherical current collectors and graded booms	(USU)
HV power supply and capacitors	(USU)
Transient current and voltage measurement	(USU)
Regular current and voltage measurement	(USU)
TV imaging of current collector sheath	(USU)
Photometer detection of specific emission lines in current collector sheath	(USU)
Hollow cathode plasma contactor	(SRS Inc.)
Ambient neutral pressure at vehicle	(Univ. Iowa)
Ambient plasma density/temperature (Langmuir probe)	(USU)
Ion and electron detectors	(Univ. Ala., HSV)
VLF and HF wave detectors	(Systems Unltd.)
3-axis magnetometer	(USU)

2.2.1 Spherical Current Collectors and Graded Booms

It was required to utilize two current collectors to perform experiments on the mutual interaction of such collectors when their charge sheaths overlapped, and in order to accommodate them within the 17-inch payload diameter, a sphere diameter of 20cm was selected. The spheres were fabricated from aluminum and they were gold-plated over nickel. In order to uniformly grade the electrical potential away from the spheres in the vicinity of their attachment point to their support booms, a grading ring structure was used. This structure consisted of a series of shallow, saucer-shaped rings mounted on the fiber glass support tube in such a way that no electron fluxes accelerated to the spheres could impinge on the fiberglass. The rings were spun from aluminum sheet and nickel plated. The uniformity of the potential was achieved by connecting each ring to its neighbor by a parallel resistor combination having a resistance of about 24kΩ. The 46 rings used in the graded boom resulted in a total resistance of 1.1MΩ down the graded boom for sphere-1 and 980kΩ for the shorter sphere-2 boom. The circuit contribution of this resistance is discussed later.

2.2.2 HV Supply and Capacitors

The high voltages applied to the spheres were derived from 2.5μF capacitors charged to voltages between 6kV and 44kV. A common charging source was used, but thereafter the energy storage charge/discharge control and sphere systems were independent. The capacitor voltage was determined by timing the charge-up period, and the discharge period was also controlled to a fixed time. In some cases the capacitor for sphere-2 was left uncharged to provide for one-sphere operation. After each of the capacitors had been charged to its pre-planned voltage, a common discharge command was sent to each HV relay and the two spheres were connected to their charged HV capacitor supply at nominally the same time (within mechanical relay activation time variability). The capacitors were current limited by 2kΩ resistors in series with the capacitor outputs. The whole timing program was controlled by a mechanical cam/microswitch system to make it less vulnerable to upset by EMI from the capacitor discharge currents. Six combinations of voltages to be applied to the spheres were planned, and the magnitudes of the voltages are shown in Figure 2-1.

The HV generation components, the storage capacitors and the HV relays were flown in a sealed container filled with Sulphur Hexafluoride (SF_6) at atmospheric pressure. The HV was conducted to the spheres by HV coaxial cables which emerged from the HV pressure vessel with no break in either the conductor or the insulation. The outer braiding was intact until the cable entered the grading ring booms, after which it was removed and the cable was passed into the booms and the whole inside potted solid. The upper grading ring was at sphere potential, the lower ring at vehicle ground potential. Thus the only parts of the positive HV system exposed to the LEO environment were spheres and the grading rings. The spheres were gold-plated, the grading rings nickel-plated.

When the capacitors were connected to the spheres fixed resistive loads were also connected across the capacitor to ensure that the capacitors would be nearly completely discharged at the end of the 5 sec discharge period even in the absence of any plasma currents. The current and voltage measuring circuit is shown schematically for one sphere in Figure 2-2, which also indicates plasma impedances contributing to the discharge current. The broken line enclosing the schematic circuit indicates those parts of the circuit within the broken line which were not exposed to the space environment.

2.2.3 Transient Current and Voltage Measurement

In addition to the current and voltage measuring circuits shown in Figure 2-2, the capability for transient voltage and current measuring was included on the payload. The voltage signal was derived from the same source as the regularly sampled signal (HV in Figure 2-2) while the transient current was monitored by the signal from Rogowski coils surrounding sections of the HV cables leading to the spheres. The current and voltage signals were routed to a video digitizer operating at a sample rate of 5MHz, and the first 1024 8-bit samples after a trigger was received were stored in a cache memory. The memory was subsequently read out by the telemetry in a period of 1 sec after a given discharge had occurred. The trigger signal for memory load was generated by the rise in the HV monitor signal after the discharge relay closed.

2.2.4 Regular Current and Voltage Measurement

Figure 2-2 shows the circuit location of the total current monitor i(t), the high voltage monitor HV, and the boom current monitor i(b). These signals were conditioned and sampled by the telemetry system at 1024 samples/sec. The bandwidth of the 1000:1 potential divider was arranged to be compatible with the high speed sampling by using a frequency compensated potential divider, rather than the simplified resistive potential divider shown schematically in Figure 2-2. The i(t) monitor had two sensitivity ranges of 2 amps full scale and 200mA full scale. Both ranges were sampled by the telemetry and no range switching was used.

2.2.5 TV Imaging of Current Collector Sheath

A low light level television (LLLTV) camera was installed on the payload using a wide angle lens to view the two spheres and a region extending to about 5m either side of them. The camera used was an EEV generation 2 unit which incorporates an integral image intensifier viewed by a CCD array detector and has a wavelength sensitivity which peaks in the visible region of the spectrum. No external wavelength filtering was used. The camera generated a standard TV signal which was used to modulate a dedicated telemetry transmitter.

Scene illumination at times between the HV discharges was provided by two light emitting diodes mounted on the camera housing, and directed towards the support boom and spheres. The control of this illumination was provided by a cam on the master control sequencer described earlier.

2.2.6 Photometers

Three pulse counting photometers were mounted to view the region between the two spheres. The units had a narrow field-of-view of about 5^{o} full width, half maximum. Interference filters were used to select the wavelengths of the emissions detected by the photometer. The wavelengths used were 476.5nm, 441.5nm and 391.4nm which correspond to emission lines from Ar^{+}, O^{+} and N_2^{+} respectively. The O^{+} and N_2^{+} lines were selected to study absolute intensities and temporal variations of emission from the dominant atmospheric constituents near apogee and at the lower parts of the descent respectively. The Ar^{+} line was selected to see if there was significant gas buildup in the vicinity of the spheres from the gas emitted by the operation of the hollow cathode plasma contactor.

2.2.7 Hollow Cathode Plasma Contactor

At the end of the payload remote from the HV biassed spheres, a hollow cathode discharge source was installed. The operating gas in the device was Ar, planned to flow at 10 standard cc/min. In order to obtain a rapid start of the discharge it was covered by a plate, and maintained at a differential pressure of 2 psi above ambient. At third stage separation, the plate was to have been pulled away, and as the discharge region reached Paschen breakdown conditions, the discharge was to have started. Unfortunately the cover plate apparently jammed, and the pull wires snapped at separation, thereby preventing the plasma source from being exposed to the ionosphere.

2.2.8 Ambient Neutral Pressure

A cold cathode ionization gauge covering the pressure range 10^{-3} to 10^{-7} torr was installed on the forward payload bulkhead adjacent to the base of the sphere support boom. To ensure rapid starting of the ionization in the gauge it was launched filled with dry nitrogen and capped. At 171 sec (224km) the cap was removed, and as the gauge outgassed the cold cathode discharge was initiated immediately the pressure in the gauge reached a value corresponding to the Paschen minimum for the gauge geometry. The pressure signal was sampled with a time resolution of 1mS.

2.2.9 Ambient Plasma Density/Temperature

The ambient conditions of the plasma in the vicinity of the payload at times between HV discharges was monitored by a cylindrical Langmuir probe deployed radially outside the payload skin. The probe monitored electron density with a time resolution of 1mS except for periods when a sweep voltage was applied which enabled electron temperature to be deduced and positive ion density to be monitored. The sweeps from +5V down to -1V and back occurred over a period of 1 sec repeating every 2.3 sec.

2.2.10 Ion and Electron Detectors

Four imaging ion and electron detectors were flown to monitor energetic ion and electron fluxes in the energy ranges 2eV - 5keV and 10eV - 30keV at several different view directions relative to the axes of the instruments. The higher energy instruments had energy bandwidths of 11%, while the lower energy instruments had bandwidths of about 20%. The spectra were generated by stepping over the energy range in 32 steps, each energy being held for 1mS, thereby providing particle spectra with a 32mS time resolution.

A total of 26 channels were assigned to the four particle detectors which were arranged in two groups of two with their axes of symmetry viewing in opposite directions. The fields-of-view of each look direction were approximately 5° x 5°, and were oriented in directions relative to the rocket axis shown in Table 5 below.

Table 5. Look angles (degrees) relative to vehicle axis of particle detector channels for each of the four sensors.

Particle	Energy Range LO (2-5000eV)	HI (500eV-30keV)
Positive Ions	22.5	26.0
	45.0	36.0
	90.0	46.0
	112.5	56.0
		85.0
		95.0
		105.0
		115.0
Electrons	22.5	26.0
	45.0	36.0
	90.0	46.0
	112.5	56.0
		85.0
		95.0
		105.0
		115.0

2.2.11 VLF and HF Wave Detectors

Electric field measurements from DC to 30kHz were measured on a single axis utilizing two spheres each deployed one meter from the rocket skin. Both sphere to skin and sphere to sphere voltages were monitored with varying bandwidths up to 20kHz depending on parameters and channel sensitivities, while the full VLF signal from 20Hz to 30kHz was monitored on a wideband telemetry channel.

The supporting boom for the DC/VLF spheres was used as an antenna for a swept frequency HF receiver covering the frequency range 60kHz to 5MHz with a sweep period of 0.2 sec.

2.2.12 3-axis Magnetometer

A fluxgate magnetometer (Develco 9200C) was mounted in the payload covering the magnetic field strength range of ±0.6 Gauss in each of three orthogonal axes. The sampling frequency for each channel was 64 samples/sec.

3. Payload Engineering

3.1 Mechanical

The instruments described above in Section 2 were mounted in three sections. One was sealed and filled with sulphur hexafluoride to remain at one atmosphere during the flight. The other contained diagnostic instruments and was evacuated during the

rocket ascent. The plasma contactor formed a third payload section separated from the other two by the telemetry and ACS sections.

The general arrangement of the payload in the deployed configuration is shown in Figure 3-1.

3.1.1 Payload Skin Section

The payload skin sections including the pressure sealed joints on the HV power supply section were designed at USU, and fabricated by Bristol Aerospace Ltd. The skin sections were then delivered to USU for the installation of pressure bulkheads, doors, access ports and umbilical connectors.

3.1.2 Boom Deployment System.

The two current collecting spheres were mounted on a combination telescopic/folding boom system shown in the general assembly drawing in Figure 3-2. The telescopic portion of the boom was fabricated from G-10 fiberglass tube. In the launch configuration the telescoped section was held by a bolt which could be released by a pyrotechnic cutter. The two spheres mounted on the graded boom sections were folded down and the spheres held on pegs from which they were freed when the telescopic boom deployed. The booms were kept stowed against their internal spring forces by the deployment bolt. The booms were designed to withstand in their stowed configuration, the 580 pounds (2.58 kilo Newtons) exerted by the nosecone eject spring during the flight and the ejection action.

No latching was used to locate the deployed booms, their positions were held by residual forces applied from the telescoping and unfolding springs. The geometry of the deployed spheres is shown in the three views in Figure 3-3.

3.1.3 Graded Booms

In order to maintain a uniform decrease in electric potential along the sphere support booms, a graded ring structure was used with the potential of each ring determined by resistive coupling between the rings. In addition to performing this function the rings were shaped to prevent direct impact of electrons, accelerated to the collecting spheres, on the dielectric core of the graded boom.

The design and prototype fabrication of the graded boom were performed at the University of Texas, Arlington by Mr. W. Dillon under the direction of Dr. W. Nunnally. Details of the ring shape and the fabrication technique are shown in Figure 3-4. The rings were made from spun aluminum sheet which was subsequently nickel plated to reduce metallic outgassing and to provide a surface to which the inter-ring resistors could be soldered. The two flight booms were constructed at USU, requiring a period of about two weeks continuous effort to build the units.

The HV cable was located in the boom core center by using an epoxy resin filler surrounding the HV cable, stripped of its metallic outer braiding.

3.1.4 Current Collecting Spheres

The two 20cm diameter spheres to collect the plasma current were purchased as pairs of aluminum hemispheres. The hemispheres were machined to provide an

outgassing and access hole to attach the HV cable. In addition some internal structure was also welded inside as mechanical supports for attachment to the booms. The hemispheres were then welded together at their equator and smoothed to avoid any obvious harp protrusions on their surfaces. The finished spheres were then gold-plated to provide a stable current collecting surface.

3.2 Electrical

The overall inter-connection diagram of the SPEAR-1 payload is shown in Figure 3-5. The instrumented payload consisted of two modules; one, pressurized containing the HV power supply and capacitors, the other unpressurized containing some of the diagnostic instruments. The remaining diagnostic instruments were mounted on top of the pressurized power supply and electrical signals were routed through the pressurized section using hermetically sealed connectors at each end. Details of the SPEAR-1 power distribution and control are shown in the schematic diagram in Figure 3-6.

3.2.1 HV System.

A block diagram of the HV system contained in the sealed section of the payload is shown in Figure 3-7.

The prime power is the 28V battery on the lower left of the figure. The first step in generating the HV is to connect the 28V battery to the DC/AC connector and generate 110V AC at 60Hz. The delivery of this power to the HV power supply is under the control of an arming relay C4-3359. Upon receipt of the arm control signal the HV power supply is switched on and generates a no load voltage which would exceed 45kV. A series chain of stabilizer diodes was therefore added to clamp to HV supply output not to exceed the discharge capacitor working voltage. The delivery of the HV to the exposed spheres required two more steps. The closure of the charging relays KC1 and KC2 followed by the closing of the discharge (or fire) relays KF1 and KF2.

The timing and sequencing of the charging and discharging relays was under control of a mechanical cam system driving a group of microswitches. The internal impedance of the HV power supply was high, and the potential to which the discharge capacitors were charged was determined by the length of time KC1 or KC2 were closed. Since if both KC1 and KC2 are closed both capacitors are connected in parallel and to the HV power supply the charging rate will be about 0.5 times that when only one charging relay was closed. To enable a suitable set of cam times to be established the charging of the capacitors for predefined cam times was computed by a computer model based on the measured charging rate for the flight spare discharge capacitor.

Both KF1 and KF2 were triggered from the same cam microswitch to provide simultaneous capacitor discharges to within the variability in the relay pull-down times.

All of the circuitry associated with the HV generation and control was housed in a sealed section of the payload and operated at one atmosphere pressure in an environment of sulphur hexafluoride. This gas provides a high electron affinity, and will increase breakdown voltages by a factor of 2 - 2.5 over dry air.

The connection of the discharge relay to the sphere was made through HV cable the conductor of which remained unbroken up to the sphere. This was achieved by proving a

custom design hermetic seal for the HV cable as it emerged from the upper bulkhead of the sealed section. The outer, grounded metallic braid was retained on the cable up to the entry point into the graded boom. At that point the metallic braid was removed, and the cable was potted inside the dielectric boom supporting the grading rings.

Development problems were related to arcs within the HV structure which were triggered either on the Zener diode stabilizing chain, or on one occasion from an HV discharge relay to payload ground. On one occasion the current bypassed a 2kΩ current limiting resistor in series with each discharge capacitor. This had a major effect on low voltage electric circuits not directly connected to the discharge, but in the general vicinity. As a result of this problem the 2kΩ resistors were moved to connection points as close to the discharge capacitors as possible.

Once the problems referred to above had been corrected, the HV power system worked very well through the Plum Brook vacuum chambers tests and during the flight.

3.2.2 High Speed Data System

A high speed cache memory data collection system was included to measure the sphere - payload voltage and the capacitor current with a time resolution of 200nS. The size of the 8-bit memory into which the data were stored was 1024 bits, resulting in a window of 200μS. The memory was read out through the telemetry system at a rate of 1000 samples/sec, thereby requiring 10 sec to dump the memory after a discharge. This was quite consistent with the 15-20 sec cycle time to prepare the capacitors for another discharge.

The total current and HV signals were conditioned and delivered to a high speed 8-bit video digitizer. The digital data was then routed to the cache memory where a burst of samples was stored until the digitizer completed its task. The trigger to initiate the digitization and storage process was determined by level sensing the input signal.

The hardware used was largely copied from units successfully flown on the NASA CHARGE series of sounding rockets. The major difference was the provision of input level sensing as opposed to the computer generated trigger pulse used on the CHARGE flights.

A block diagram of the connection of the high speed data system to the signal sources and the interface to the telemetry system is shown in Figure 3-7.

The HV signals processed by two of the high speed data channels were conditioned by the same circuitry as was used for the low speed HV data. However, the source of the capacitor current signals were Rogowski coils around the capacitor output leads. The signals were fed directly from the coil to the video digitizer.

3.2.3 Langmuir Probe.

A block schematic diagram of the Langmuir probe is shown in Figure 3-8. The combination of the logarithmic amplifier and differential amplifier results in an electron current collection sensitivity from 10^{-10} amps to $5x10^{-5}$ amps and an ion current collection sensitivity from 10^{-7} amps to $5x10^{-9}$ amps. The asymmetry in the ranges is a result of the set point on the output voltage corresponding to zero net probe current (1.0 volts in this unit).

The function generator determines the voltage bias program applied to the probe. The waveform generated in the SPEAR-1 unit is shown in Figure 3-9. It can be seen that there is a period of 1.5 sec when the probe is biassed 5 volts positively with respect the vehicle body, and, if the vehicle is more positive relative to the ionosphere than -5 volts, then the probe will collect electrons and monitor the ambient electron density. At the end of each 1.5 sec fixed bias period the function generator provides a sweep voltage with a sweep period of 0.5 sec. During this time an analysis of the probe current enables the ionospheric electron temperature to be deduced. Also during the negative phase of the sweep ion currents can be monitored.

The schematic circuit diagram of the SPEAR-1 Langmuir probe is shown in Figure 3-10. It should be noted that the input current sensing electronics is temperature stabilized by a small oven to avoid ambient temperature sensitivity of the calibration of the unit.

3.2.4 Photometers

The schematic circuit diagram for one of the two pulse photon counting photometers is shown in Figure 3-11.

The electronics and photomultiplier tube were contained in a single box which was hermetically sealed and maintained at one atmosphere pressure in a dry air environment during the flight. This procedure prevented breakdown problems from the 800V accelerating potential applied to the photomultiplier dynode string.

The pulses of charge collected at the end of the dynode string were conditioned to generate standard waveform pulses having an amplitude of 5V and a pulse width of 40nS. These pulses were fed from a line driver to the payload telemetry system where they were accumulated for one half of a telemetry frame period (16mS) before being telemetered to ground as two 8-bit bytes forming a 16-bit accumulated value of the total counts during the integration period.

Other systems were either purchased as complete units or were supplied by subcontractors and will not be described in detail.

3.3 Integration and Testing

Integration and electrical testing of the payload up to the telemetry and timer interfaces took place at USU. A fully integrated and electrically tested science payload was delivered to AFGL for integration with the telemetry and ACS units.

The testing philosophy adopted was to test only newly developed units at sub-system level, proven instruments had their testing deferred until the all-up payload vibration test. Individual sub-systems were vibration tested at USU at qualification levels, but the prime flight testing was performed with the whole payload at WFF.

The boom deployment system was tested in two parts due to the design being for a weightless environment. The spring loaded deployment test of the graded booms was performed with the booms suspended horizontally using vertical cords to unload the boom joints. The telescopic boom was deployed independently and performed satisfactorily.

Following electrical integration at AFGL the payload was moved to the NASA Plum Brook facility at Sandusky, Ohio. At this facility the payload performed flight sequences, although the pressure was not as low as it is anticipated in recent months. Details of this test are given later in Section 6.

4. Data Collection

Three S-band telemetry senders were used on the SPEAR-1 payload operating with the following characteristics.

Table 6. S-band Telemetry Characteristics

Sender	Function	Frequency (MHz)	Power (W)
1	FM/FM	2251.5	10
2	FM/Video	2215.5	10
3	FM/PCM	2279.5	2

4.1 FM/FM Link

This link was used to transmit the data from the wave receiver experiment using IRIG channels with non-standard modulation indices. The details of the channel characteristics are listed below in Table 7.

Table 7. Wave Receiver Characteristics

Function	Channel	Frequency	Low Roll off	High Roll off	Modulation Index
AC coupled tip-to-tip high AGC	25	560. kHz	20 Hz	30. kHz	1.4
DC coupled tip-to-tip medium fixed gain	24	400.	-	20.	1.5
AC coupled tip-to-tip low AGC	23	300.	20 Hz	15.	1.5
DC coupled tip-to-tip low fixed gain	22	255.	-	10.	1.7
AC coupled tip-to-tip fixed gain	21	165.	1 Hz	5.	2.5
DC coupled tip-to-tip high fixed gain	20	124.	-	5.	1.9
Swept Frequency Analyzer	19	93.	-	3.4	2.0
DC coupled tip-to-skin	18	70.	-	1.	5.0
DC coupled tip-to-skin	17	52.5	-	1.	4.0
Automatic Gain Control levels for both ΔE1 and ΔE2	15	30.	-	1.	2.1
3-axis magnetometer	14	22.	-	330. Hz	5.0
Automatic Gain Control for ΔE1	13	14.5	-	220.	5.0
Automatic Gain Control for ΔE2	12	10.5	-	160.	5.0

4.2 FM/Video Link

This link was dedicated to the NTSC video signal generated by the LLLTV camera. The standard waveform from the camera was used to modulate the transmitter without intervening signal processing.

4.3 FM/PCM link

Data from experiments other than those listed above, and from payload systems was encoded into a fixed format, and the digitized values presented as a serial stream to modulate the third telemetry sender.

The format consisted of an array of 32 x 49 signals organized as shown in Figure 4-1. The mnemonics refer to specific channels of each individual subsystem in which the alphabetic prefixes have significance shown below in Table 8.

Table 8. Sub-system Mnemonics

Mnemonic	Sub-System
ac	attitude control
cm	cache memory
hv	high voltage
Lp	Langmuir probe
mg	magnetometer
np	neutral pressure
pc	plasma contactor
pd	particle detector
ph	photometer
pL	payload control
py	pyrotechnic control
tm	telemetry
tv	television
SFID	sub-frame identification (count)
vh	vehicle

5. Data Processing

5.1 SPEAR-1 PCM Data Reduction

Reduction of SPEAR-1 PCM data at USU was separated into four basic steps:

i) Conversion of data from sequential 9-track computer compatible tapes to random access disk files.
ii) Calibration and formatting of selected data channels.
iii) Further analysis (where required).
iv) Graphical display.

The first step, conversion from tape to disk files, was accomplished using FORTRAN programs written for the Center for Atmospheric and Space Sciences' Harris 800 computer. Depending on the source of the data tapes there were slight format differences either RDWFF.F or RDAFGL.F would be used (for tapes from Wallops Flight Facility and Air Force Geophysical Laboratory respectively) as the programs to generate the disk files. Both programs read in blocks of data from tape, strip off unused header blocks, converts the PCM data from VAX two-byte-integer to Harris one-byte-integer, converts the time from GMT in binary coded decimal (BCD) format to MET seconds stored as a Harris six-byte-real number, and writes the data to disk. The resulting disk file is random access and unformatted. Each record in the file contains the six byte MET and 49 x 32 bytes of uncalibrated PCM data.

The second step, conversion of unformatted uncalibrated data is accomplished using the menu-driven SPEAR-1 Calibration/Formatting program. Appendix B illustrates the screen output resulting from an interactive session on the Harris computer to select sphere current and voltage data for a specified time period, and output

it to a file for further processing or plotting. The output from this program is a formatted sequential file which contains columns of calibrated numbers.

The calibrated output can be reduced further when required. For example, to derive electron densities from the Langmuir probe data, a small FORTRAN program is used to convert measured current into plasma density.

Finally, the data is displayed in a graphical format. The formatted columns of data are amenable to plotting by plotting utilities. The two which are most commonly used for SPEAR-1 data at USU are Cricket Graph (Macintosh) and CASS*PLOT (Harris).

5.2 Video Processing

The output from the on-board video camera was recorded at WFF and transcribed to either U-matic (3/4 inch) format or VHS (1/2 inch) format video tapes. Some analog processing was performed at WFF in the tape copying process which resulted in some loss of frames which was not apparent during the viewing of the real-time transmission of the video signal during the flight.

5.2.1 Single Frame Images

The simplest processing of the video data was to use a VCR with stop frame and single frame advance capability to capture single frames during the discharge period. These frames could then be photographed and a permanent record of the discharge features around the sphere and booms retained.

The image noise problem seen in frozen frames can be reduced by using a time exposure and integrating many frames on the photographic film. This technique can be used to obtain images of non-varying features such as the general configuration of the booms and spheres while illuminated by the LED's and prior to the HV discharge.

5.2.2 TV Frame Image Processing

To obtain quantitative information from the television imagery data, individual video frames were digitized. This was carried out using digitizing hardware available in an Electrical Engineering microcomputer laboratory. Selected TV frames were digitized using a 256 by 256 pixel by 8 bit (256 gray levels) format resulting in a 65K byte data file. These data were written to floppy disk and subsequently transferred to the CASS H800 computer. Once in a digital format, the images were analyzed using a suite of image processing software developed on the Harris H800. A variety of image processing functions could be applied to the data including (but not limited to) edge detection, enhancement and filtering. Either the full image or selected portions of the image can be displayed on an AED-512 color display terminal which is a peripheral attached to the H800. Permanent copies of these images were made by photographing the color display with a 35-mm camera.

6. SPEAR-1 Chamber Test Results

6.1 Introduction

Early in the SPEAR-1 program it was decided that a chamber test of the fully integrated payload should be performed in a large space simulation vacuum chamber.

This testing was to be performed following successful electrical and mechanical integration of the complete payload, a vibration test of the complete payload followed by satisfactory post-vibration tests of the whole system. The principal purpose of the test was to verify the high voltage engineering and ensure that no unexpected discharges or arcs occurred in the high voltage wiring that was exposed to the ambient vacuum environment. In addition, it was hoped to gain some baseline information to which flight results could be compared.

In view of the high voltages being applied to the spheres during this test it was considered prudent to perform a pre-test in the same vacuum chamber with a mock-up of the SPEAR-1 payload having similar geometric characteristics and employing the prototype sphere grading ring boom assembly that had been developed earlier. This pre-test was performed and details on the method of testing and the results achieved are contained in a test report. The pre-test showed that when spheres of the same size as the SPEAR-1 spheres were biassed in the vacuum chamber that a glow discharge appeared around the spheres both in the presence of pure vacuum environment, and also when plasma was introduced by an external plasma generator. However, these discharges were not damaging to the system and although a moderately heavy current flowed from the spheres to the walls of the chamber this current was not an uncontrolled arc and nothing was observed that threatened the rest of the payload.

Both the pre-test and the payload test were performed at the NASA Lewis Plum Brook vacuum chamber facility using the vacuum chamber designated B-2. This consists of a large vacuum chamber ~38 ft. in diameter and 64 ft. high along the central axis of the chamber. The SPEAR-1 tests were performed immediately after a planned refurbishment of the chamber which was performed successfully and in time for the tests to occur as we had scheduled them. The pressure in the chamber was monitored by a Plum Brook staff and typically was operated at $\sim 10^{-5}$ Torr. The chamber also contained a mass spectrometer to monitor gas composition and vacuum conditions, and two hollow cathode plasma sources operated by NASA Lewis Research Center which could produce a background argon plasma in the chamber with a number density controllable from $\sim 10^{11}$ - 10^{12} particles per cubic meter. The plasma density was also monitored by NASA Lewis staff and this was performed during the payload tests by three Langmuir probes, one actually mounted on the payload skin and two others mounted in fairly close proximity to the SPEAR-1 payload.

6.2 Payload Configuration

The configuration of the SPEAR-1 flight payload for the chamber tests consisted of the high voltage booms in a deployed configuration, the high voltage power supply section, the diagnostic instrument section and the telemetry section. The attitude control system was not included in the payload build-up for these tests and the plasma contactor which normally is below the attitude control system was connected to the rest of the payload by a temporary adaptor ring. As far as the diagnostics were concerned there was no pressure gauge included on the payload nor were the energetic electric and ion particle detectors. Both of these latter instruments were omitted because of fears of contamination of sensitive surfaces within the instruments. The wave receiver booms were not deployed although the doors covering them were removed. The thermal electron Langmuir probe was deployed in the same fashion that it will be during the flight of the payload. The optical systems on the SPEAR-1 payload were activated although based on the perceived brightness levels during the pre-test it was decided not to completely remove any neutral filters from the low light TV system. One of the three neutral filters normally used to operate the camera under ambient lighting was retained on the face

plate of the camera containment vessel. The photometers were however uncovered and operated at full sensitivity.

The payload was mounted in the vacuum chamber at ~10° from the vertical with the booms pointing towards magnetic north in order to somewhat increase the distance perpendicular to B between the spheres and the plasma contactor. This mounting configuration is illustrated in Figure 6-1. The payload was grounded to the chamber and this was a permanent arrangement which could not be changed once the pressure was reduced inside the chamber. The telemetry signals and control signals for the experiments were brought out through umbilical connections to the payload and through the walls of the chamber. The support equipment for the telemetry and for the payload systems was set up on a level approximately half way up the chamber and all of the test operations were performed from that location. All umbilical connections remained attached during the whole testing period, and the payload was operated from both internal and external power supplies or batteries.

The high voltages generated and applied to spheres and the heavy weight of the fully assembled payload provided some safety hazards, and therefore a safety review had to be performed of the whole testing program. The report to support this safety review details the methods that were adopted to transfer the payload from the testing area outside the vacuum chamber into the vacuum chamber and also to secure the payload safely inside the vacuum tank.

6.3 Testing Schedule

The schedule for the test is shown in below in Table 9.

Table 9. Scheduled Major Activities for Chamber Test

Activity	Duration (hrs.)
Unpack	4
Assemble GSE	6
Build up payload outside chamber	8
Check payload outside chamber	4
Transfer payload to chamber	2
Orient and secure payload in chamber	2
Perform pre-pumpdown tests in chamber	4
Pump-down chamber	12
Perform chamber tests	8
Assess test results	4
Remove payload from chamber	2
Dismantle GSE	4
Pack	4

Table 9 shows that we called for a post-shipment test to ensure that the payload and its support equipment had survived the journey from AFGL to Plum Brook and this was performed outside the vacuum chamber. Safety considerations required that no high voltage be applied to the spheres during the period it was outside the vacuum chamber. Following successful testing as far as was possible the payload was built up and in a vertical orientation and then hoisted into the chamber through the top plate of the chamber which hinged back. Once inside the chamber the payload was tested in air and

the high voltage was applied to the spheres. The testing schedule for the pre-vacuum test is shown below in Table 10.

Table 10. Pre-pumpdown Test Schedule (11/10/87)

Test	Start Time	Function
1	19:09:58	One HV pulse, chamber open
2	21:50:43	One HV cycle, chamber open
3	22:18:59	One HV cycle, chamber closed

Details of the three tests performed before the chamber was pumped down were documented in an operational check sheet for all tests performed on the first day of testing prior to chamber pump-down. The tests were extended beyond the two planned tests of one pulse followed by one cycle because during the full cycle in air a discharge appeared to occur when the highest voltage was generated on the internal capacitors. Due to concern that this discharge may be external to the payload it was decided to close down the top of the vacuum chamber, cover all ports, shut all doors in order to darken the chamber and provide some opportunity for observing any flashes resulting from arcs or discharges when the full cycle was repeated. However, it was found that on repeating the full cycles of six discharges there was no evidence of any discharge occurring on the 44kV case and therefore no optical evidence of any effects were observed. To be doubly sure this full cycle was repeated a second time, again with the chamber darkened and all lighting removed. Again the test was successful, and it was therefore decided to proceed with the pump-down during the night and plan to perform the vacuum test starting the following morning.

The following morning the chamber pressure was down to the 10^{-5} Torr range and it was decided that the pressure was acceptable for this engineering test and plans were made to commence the vacuum testing. Again the full details of the testing are contained in the operational check sheet for the flight hardware tests for the tests performed on November 11, 1987. These tests, their start and stop times and chamber conditions are summarized in Table 11 below.

Table 11. Vacuum/Plasma Test Schedule (11/11/87)

Test #	Time (GMT) Start	Stop	Chamber Pressure(torr)	Plasma	Plasma Contactor	Function
1	15:00	15:03	2,-5	No	No	Set up check
2	15:13	15:16	1.8,-5	No	No	1 HV pulse
3	15:37	15:45	1.7,-5	No	No	Full HV cycle
4	18:45	18:50	3.3,-5	Yes	No	1 HV pulse
5	19:02	19:06	2.4,-5	Yes	No	1 HV pulse
6	20:31	20:43	2.5,-5	Yes	Yes	3 Full HV cycles

The same general philosophy was adopted as for the pre- vacuum tests that is to say first, one single pulse was operated, the results evaluated and then if no unexpected results were seen then we proceeded on to perform one complete cycle of six discharges applied to the spheres. This pattern of operation was performed firstly in vacuum, and then in a vacuum with a locally generated plasma and finally in a vacuum with the locally

generated plasma and with the payload plasma contactor operational. The final test with the plasma contactor operating was made to more simulate the period of operation of the actual flight of SPEAR-1. The six voltage program applied to the sphere was allowed to repeat three times to simulate the approximate duration of active operations during the flight of the payload.

6.4 External Diagnostics

In addition to the diagnostics that were included on the payload a number of external diagnostics were also included in or outside the vacuum chamber. The Langmuir probes used to monitor the ambient plasma density have already been mentioned earlier. In addition, several film cameras and TV cameras were used during the tests. One of the TV systems was a low light TV which was mounted inside the chamber to avoid problems of field-of-view obstruction by the rather small ports and the collimation produced by viewing through the liquid nitrogen shield inside the chamber. This low light TV system was mounted in a pressurized container to avoid discharge problems associated with the image intensifier that forms part of the TV camera. In addition to optical images the PCM data-stream was recorded, the wave data was recorded, and as far as the PCM is concerned some of this was produced as strip chart records. The TV images were all recorded on video tape and the film camera images were either printed or slides produced, depending on the type of film used in the camera.

6.5 Chamber Test Results

6.5.1 Sphere Currents and Voltages

The current and voltage variations for the spheres during a chamber test discharge were typically a series of impulsive breakdowns from the sphere to the chamber walls with an internal of approximately 50mS between breakdowns. Examples of the time variation of the total and boom currents and the sphere-rocket potential are shown in Figures 6-2 and 6-3.

Figure 6-2 is a case where the larger potential was applied to sphere-1. The heavy currents flowing in the discharge reduces the capacitor voltage to non-discharge levels in less than 1 sec. Figure 6-3 shows a similar plot for a case where sphere-2 had the larger potential applied, and it can be seen that the major features in the current and voltage variations are similar to the previous result.

Color photographs of the light emitted during the discharges shown in Figures 6-2 and 6-3 are shown in Figure 6-4. The photographs are time exposures integrating the effect of several of the impulsive discharges. The glow region is confined to the biassed sphere which differs in the upper and lower panels of Figure 6-4.

7. Flight Summary

7.1 Launch

SPEAR-I was launched from NASA Wallops Flight Facility on December 13, 1987 at 20:45 EST. It reached an apogee of 369km at 351 sec after launch. Details of the booster, launch and apogee coordinates and plots of the altitude and ground track are shown in Figure 7-1.

7.2 Attitude Program

Three observing attitudes were planned for SPEAR-I which oriented the payload with respect to the geomagnetic field such that the field lines were; a) near perpendicular to the line joining the spheres and to the payload axis, b) parallel to the line joining the spheres and near perpendicular to the payload axis and, c) parallel to the graded boom supporting sphere-1. These attitudes and the place in the trajectory when the maneuvers were initiated is shown schematically in Figure 7-2.

The details of the four maneuvers and the times to accomplish them are tabulated below in Table 12. Maneuver #1 was to reduce the 1 rps residual spin rate to zero rps and to return the vehicle to the same orientation as it was on the launch rail.

Table 12. SPEAR-I ACS Performance

ACS Pointing Maneuver	Time Occurred Sec.	Time To Complete Sec.	Pitch Position Deg.	Yaw Position Deg.	Roll Position Deg.
1	+129.0	9.0	0.0	0	+90
2	+151.5	21.0	+141.9	0	+90
3	+406.6	7.2	+110.4	0	0
4	+520.2	11.4	*56.0	27	0

*Note: With a 27° Yaw maneuver, the Pitch gyro TM will indicate 59° to achieve a true 56° Pitch angle due to cross coupling of the roll gimbal in the gyro.

7.3 Flight Timeline

The payload events were run from on-board timers, and the activities all occurred at the nominal times which are summarized below in Table 13.

Table 13. SPEAR-I Flight Sequence

Event	Time (Sec)	Alt (km)	Function
1	-600	0.0	ACS External
2	-180	0.0	Uncage Gyro - Slew Launcher
3	-120	0.0	ACS Internal
4	0	0.0	Terrier Ignition
5	+4.4	0.7	Terrier Burn Out
6	+12	3.0	Second Stage Ignition
7	+44.4	28.6	Second Stage Burn Out
8	+88	80.2	Second Stage Separation
9	+93	85.0	Third Stage Ignition
10	+110	113.2	Third Stage Burn Out
11	+113	119.4	Third Stage & Payload Despin
12	+115	123.6	Third Stage Separation
13	+116	125.6	LP and Wave Receiver Doors Eject
14	+117	127.7	Particle Detector Doors Eject
15	+118	129.7	Wave Receiver Booms Deploy
16	+129	151.6	ACS Position 1
17	+149	188.7	Nose Cone Eject
18	+151	192.2	ACS Position 2
19	+160	207.6	Part Detector HV On
20	+171	225.5	HV Booms Deploy, NPG uncover
21	+179	237.8	HV Experiment On
22	+350	369.2	Apogee
23	+403	358.5	Second Stage Impact
24	+405	357.6	ACS Position 3
25	+518	251.7	ACS Position 4
26	+601	103.4	Payload Starts Re-entry
27	+641	0.0	Payload Impact

7.4 High Voltage Timeline

The HV system operated from its own timer following activation of a relay at +179 sec indicated in Table 13 above. A total of 24 discharges were achieved during the flight, although the last discharge occurred during payload re-entry and breakup. The times, voltages measured on each sphere and the altitudes of each of the 24 discharges are listed below in Table 14.

Table 14. SPEAR-I HV Discharge Times Voltages and Altitudes

SPEAR-1 HV Sequence

MET	Peak Voltage Sphere 1	Sphere 2	Alt(km)
191.927	7098	21400	257
210.851	25660	200	285
229.800	36400	15000	303
248.342	13470	200	321
267.202	13650	15330	337
286.102	43860	200	350
304.590	7098	21500	359
323.391	24570	800	365
342.251	37860	15000	369
360.727	13290	300	369
379.506	13650	14800	366
398.344	45320	200	361
416.781	8008	22700	352
435.549	25120	200	340
454.387	36220	14600	325
472.847	13100	200	307
491.624	13650	15500	287
510.449	43320	800	263
528.900	7098	21600	235
547.658	24570	900	206
566.465	36400	14600	172
584.900	13290	200	**137
603.658	546	800	**97.7
622.452	728	800	**55.4

Note: Altitudes derived from preliminary, unsmoothed RADAR data, those marked ** are extrapolated from the un-smoothed data.

The 1-bit resolution of the HV monitor is about 200V.

7.5 Instrument Performance

In general, most instruments performed well throughout the flight. The most serious failure from the point-of-view of the original objectives was the lack of removal of the plasma contactor cap thereby preventing the planned low impedance path from the rocket body to the ionosphere. However, this failure did not prevent useful data from being achieved, and did enable the effects to be studied of both positive and negative high voltages being exposed to the space environment. One impact of this high negative potential was to prevent the VLF receiver measuring DC fields due to amplifier saturation. At the present stage of data analysis, the only other known failure was with 2 of the 26 particle detector channels.

7.7 Flight Results

7.7.1 Ambient Environment

The ambient conditions which contribute most to the possibility of an uncontrolled discharge triggered by electric fields in the space environment are ambient gas pressure, plasma density and magnetic field. Since no large currents were anticipated in the SPEAR-1 payload, it was assumed that the magnetic field would be the undisturbed geomagnetic field. This field was measured at a point remote from the possible discharge region, but only as a verification of vehicle attitude.

Measurements were also made of the ambient gas pressure close to the payload, and at as close a position to the biassed spheres as was possible without providing a target for potential discharges. The ambient ionosphere plasma properties were also measured close to the vehicle skin, and utilizing a Langmuir probe which was only able to monitor the local plasma in between sphere discharges.

7.7.2 Neutral Pressure

The results from the cold cathode ionization gauge are shown in Figure 7-3. The figure shows a plot of the gauge measurement as a function of flight elapsed time. For comparison, a second curve is plotted showing the expected ambient atmospheric pressure based on the MSIS-86 neutral atmosphere model run for the time and geophysical conditions corresponding to the SPEAR-1 flight.

As explained earlier, the procedure used to ensure rapid start-up of the gauge resulted in the initial period of operation corresponding to outgassing of the gauge ionization chamber. This is estimated to have lasted until approximately 300 sec, at which time the pressures inside and outside the gauge had equalized. It can be seen that from 30 sec to 590 sec the measured pressure was 3-4 orders of magnitude greater than ambient. During this period, there is a slow decline in pressure having an approximately t^{-1} time dependence. Eventually at about 590 sec the payload encountered an ambient atmospheric pressure which exceeded the local outgas pressure, and the gauge tracked ambient until it limited at 10^{-3} Torr for a short period before vehicle re-entry.

The high sampling rate and rapid (<10mS) response time of the gauge enabled transient pressure pulses to be searched for during ACS maneuvers and during HV discharges. In fact, no such transient pressure changes were observed at any time during the flight.

7.7.3 Plasma Density

The Langmuir probe functioned well throughout the flight, although vehicle charging prevented any electron data being measured during the HV discharges. The electron density profile during the periods when the probe was in an electron collecting mode is shown in Figure 7-4. The figure shows a plot of electron density as a function of altitude for both the upleg and downleg of the flight. The electron density was obtained by normalizing the electron density corresponding to the peak probe current to the F_2 peak density determined from an ionogram taken by an ionosonde located at the Wallops Island range just a few minutes prior to the flight time.

The asymmetry between upleg and downleg is the result of an attitude maneuver which occurred just after apogee and resulted in the probe being moved from the ram side of the vehicle into the plasma wake of the rocket body. The upleg electron density profile should therefore be taken as more representative of the ionospheric plasma density.

7.8 Electric Currents to HV Biassed Spheres

7.8.1 Steady State Currents

The nomenclature used for the steady state currents is that shown in Figure 2-2 with the addition of i(s) representing the plasma current collected by the sphere and grading rings.

An example of the measured currents and voltages for HV discharge at 286 sec is shown in Figure 7-5. The upper panel shows the current delivered to the sphere-1 circuit by the capacitor as a function of time, the center panel shows the boom current and the lower panel shows the voltage applied to the sphere. It can be seen that the voltage and currents show the exponential decay which is expected for a classical discharge of a capacitor into a linear resistor. The very small, short duration increases in current seen at around 288 sec in the figure are seen on other discharges sometimes greater in amplitude, but only rarely with amplitude comparable to the total current flowing. No fluctuations are seen in the HV measurement because the ΔVs produced by the Δs are below the quantization level of the telemetered HV signal. Another feature of the measured current which is seen on all discharges is the spike in current at the initial discharge time. Inspection of this feature on an expanded time scale shows it to be damped oscillatory current. An important feature of the boom current i(b) shown in Figure 7-5 is that it is entirely consistent with the ohmic current driven through the 1.1MΩ graded boom resistance. This shows that there is no breakdown of the region between the grading ring which could short circuit the grading resistance and destroy its effectiveness in providing a uniform potential gradient along the boom from sphere to ground.

A proportion of the current delivered by the capacitors flows through fixed resistors of known value, the 700kΩ and 1.1MΩ resistors in parallel shown in Figure 2-2. If we assume that these resistors remain at their nominal value during the voltage variation we can subtract the current through these resistors, and then the residual current represents plasma current flowing through the rocket body and sphere and grading ring sheath resistances in a series parallel combination shown in Figure 2-2. An example of the currents deduced by this method is shown in Figure 7-6 using the data shown in Figure 7-5. In this figure, the plasma current is plotted as a function of the voltage between the sphere and the rocket body. The stepped character of the data is a result of the quantization of the digitized current. It can be seen that this current voltage characteristic is approximately linear, and a fitted straight line shows a relationship which corresponds to a total plasma resistance of approximately 890kΩ .

The plasma current-voltage relationships for a number of other times in each of the three observing orientations in the flight are shown in Figure 7-7. Each of the discharges used in compiling Figure 7-7 corresponds to cases when only sphere-1 was biassed. The equivalent resistance of the best fit straight line shown on the figure is annotated on each panel.

While the plasma currents are generally well-behaved throughout the flight, there are some instances when a maneuver is not quite complete and the ACS thrusters are still firing when the HV is applied to the spheres. An example of this behavior is shown in Figure 7-8 where the sphere-1 and sphere-2 plasma currents are plotted as a function of time during a discharge made when sphere-1 was biassed to 7.1kV and sphere-2 to 21.6kV. Spikes in the plasma current can be seen at the same time for both spheres.

A complete set of plots of the measured sphere currents and voltages and the deduced plasma currents for each of the 24 discharges accompany the report as an addendum, bound separately.

7.8.2 Optical Signatures

The optical data from the LLLTV system produced clear images of sphere-1 and its graded boom from pre-lift-off throughout the flight until payload re-entry and burn-up. Unfortunately, a late-addition payload protection guide rod blocked the view of sphere-2 for most of the flight after sphere deployment.

The wide field-of-view of the camera was selected to observe the possibility of volume breakdown around the spheres. A full system space simulation chamber test during payload development did show such breakdown, filling the camera field-of-view with light for some discharges. However, during the SPEAR-1 space flight no optical evidence of large-scale breakdown was observed except for the last discharge prior to payload re-entry which occurred at 604 sec MET at an altitude of 98km when the ambient atmospheric pressure was measured to be 7×10^{-4} Torr.

The only repeatable optical feature seen when the discharges occurred was a small, localized glow around the grading rings, usually from the base of the sphere to about halfway down the graded boom, although on some discharges the glow extended to the base of the graded boom. The glow faded and moved towards the sphere with a time constant matching the decay of the applied rocket-sphere potential. Occasionally a slight flickering was observed in the light. An example of the glow surrounding the grading rings is shown in Figure 7-9 taken from one TV frame during the HV discharge at 286 sec MET (44kV, 350km).

Figure 7-10 shows an example of the results of image processing as applied to the television imagery data. Here, under conditions of no applied potential, an image of sphere 1 was digitized and the edges of the sphere were identified by the software. Using the digitized image of a second frame (acquired at 0148:121 UT) with 21.4kV applied to sphere-1 and 7kV to sphere-2, the location of the edges of the sphere were superimposed. From this superposition of the two images, it was determined that the glow discharge was directed from sphere-1 in the direction of sphere-2, a fact not readily apparent from the raw television data.

The intensity of the glow was very low. At present only qualitative estimates are available which show it to be comparable or less than the airglow emission which is clearly visible for most of the flight. The glow is also quite limited in spatial extent, typically becoming undetectable at a distance of 1-2 grading ring radii from the surface of the rings.

The field-of-view of the LLLTV encompasses the main fiberglass support boom and includes the metallic braiding of the HV cable which was attached to that boom. This part of the image and the base of the graded booms represent our only view of metallic

surfaces at the vehicle ground potential. During the discharges, no general arcing or discharging was observed on those surfaces even though they were estimated to charge several thousand volts negative relative to the ionosphere. In addition, the fiberglass boom surface represents a dielectric, possibly under high energy ion bombardment, again showing no detectable optical effects.

7.9 Vehicle Charging

It was expected that the rocket body would charge to negative potentials relative to the undisturbed ionosphere. If the plasma contactor had been exposed, this potential would have been in the 50-150 volt range, and could have become a large fraction of the applied voltage in the case of failure of the plasma contactor to operate correctly. To cover these possibilities a low energy and high energy differential ion detector was flown to measure the spectrum of incoming ions accelerated through the charge sheath around the rocket. The time resolution of this instrument was 32mS, consistent with the 1 sec decay time constant of the HV system under non-discharge conditions.

Two examples of ion spectra obtained during the discharge at 398 sec MET are shown in Figure 7-11. The plots show ion flux measured in ion/sec/cm^2/sr/eV as a function of ion energy measured by the high energy ion detector viewing at 34° from the geomagnetic field direction. The spectra were taken approximately one second apart during the decay of the applied voltage. It can be seen that the features associated with a cutoff in ion flux above a certain energy has moved to lower energies during this time. The high ion fluxes at lower energies are believed to be secondary ions resulting from the primary ion flux impinging on the vehicle skin.

Discussion of the feature which characterizes the potential of the vehicle will be deferred until Section 8 since no feature is sharp enough to give a very accurate measure of vehicle potential. Figure 7-12 shows two estimates of the vehicle potential obtained from the high energy cutoff seen in the ion spectrum, and also from the lower energy edge of the peak seen in the spectrum. It is thought these energies bracket of actual potential, and this is supported by theoretical calculations shown in the figure, and discussed later.

8. Discussion of Results

8.1 Ambient Environment

As shown in Figure 7-4, the ambient gas pressure measured at the location of the forward bulkhead of the payload never fell below 10-5 Torr, even though the modelled ambient atmospheric pressure was 3-4 orders of magnitude lower.

The slow fall-off in pressure during the period of the flight when ambient was below the local pressure has a t-1 dependence which is characteristic of outgassing surfaces. Due to the location of the gauge and the field-of-view of its ionization chamber, it is thought that the G-10 fiberglass boom supporting the spheres is the most likely source of gas.

The pressure at the spheres is expected to be related to this pressure by an inverse square relative to their separation from the rocket body since the mean free path of the outgas from the payload is much greater than the size of the system. If we estimate the payload radius as the rocket body radius of 0.22m, and the sphere to payload separation as 3m, then the pressure at the spheres is reduced by a factor of 0.005, that

is the gas pressure in the vicinity of the spheres is about 5 x 10^{-8} Torr. Thus we estimate the pressure at the spheres is quite close to ambient atmospheric pressure if the rocket body is the only source of outgassing. However, this is a lower limit since there will be outgassing from the grading rings and the sphere itself which will act to increase the gas pressure above the 5 x 10^{-8} Torr figure.

In summary, the most likely situation with regard to gas pressure is that the negatively charged part of the payload has a surrounding gas pressure of about 10^{-5} Torr, while the positively charged spheres have near surface pressure which are 1-2 orders of magnitude lower.

The ambient plasma density profile indicates a fairly typical mid-latitude night time ionosphere. The peak density was about 8 x $10^{10}m^{-3}$ occurring at an altitude of 240km. At apogee of 370km, the density had fallen to a value of about 3 x $10^{10}m^{-3}$. There was no evidence of sporadic -E ionization either from the Langmuir probe data or from an ionosonde operated at the launch site.

8.2 Plasma Currents

The plasma currents shown in Figure 7-8 indicate that the sum of the plasma sheath impedances controlling the flow of current from the sphere and to the rocket body via the ionosphere behaves as a linear resistance in the 100s of kΩ range. Due to the bipolar operation of the SPEAR-1 payload, as a result of the failure of the plasma contactor to be exposed to the ionosphere, the body and sphere have sheaths which interact. This linking of sheaths results in a complex behavior of the balanced currents to the sphere and rocket body described in detail by *Katz et al.* (1988). The situation is further complicated by a significant contribution to the body current by secondary electrons resulting from bombardment of the surface aluminum oxide by the incoming, energetic ionospheric ions attracted by the negatively charged rocket body.

The current levels are typical of space charge limited current from an ionospheric plasma of the number density measured, and in the presence of a low density neutral gas with a mean free path for the electrons much greater than expected sheath dimensions. However, caution should be exercised in comparing these currents to the limits predicted by the classical models of *Langmuir and Blodgett* (1924) or *Parker and Murphy* (1967), both of which are calculated for a unipolar system.

There is little evidence of any current enhancement due to sheath ionization except when one of the HV discharges coincides with vehicle ACS thruster firings as shown in Figure 7-9. The time coincidence for the widely differing voltages on the spheres indicates a temporary volume breakdown occurred during a transient ambient pressure increase as the thruster operated. Further studies are under way to ascertain if the enhanced current is a result of vehicle sheath impedance reduction, sphere sheath impedance reduction, or both.

The smaller changes in plasma current seen on many of the plots in Figure 7-8 appear to be associated with fluctuations in the glow around the grading rings, and may represent transient, small volume gas releases from the grading ring structure. Alternatively, they could result from surface discharges on the exposed parts of the negatively charged vehicle body. Such discharges have been reported for negatively biassed samples both in chamber tests and in space at bias voltages from a lower limit of -200V. We find no optical evidence of these discharges on negative vehicle surfaces in the field-of-view of the LLLTV system; however, those surfaces are limited in area to

parts of the grounded braid of the HV cables strapped to the outside of the main boom. However, even if the observed current fluctuations are due to surface discharges, their amplitude is so small that any EMI generated would be quite negligible. This is also supported by the fact that no interruption was observed in either the digital telemetry system or in an on-board computer controlling the particle detector.

8.3 Vehicle Charging

As has been discussed earlier the vehicle charged to a negative potential necessary to collect ions and generate secondary electrons to balance the electron flux collected by the positively biassed spheres. The data shown in Section 7.9 shows that the general characteristic of the positive ion spectra measured by the charged particle detectors supports the conclusion that the vehicle was at a negative potential relative to the distant ionosphere by several kilovolts.

The measured spectra show that the energization process for the ions collected by the detector is not a straightforward acceleration from the ionosphere thermal ion population to an energy equal to the negative potential on the vehicle. If this was the case, all of the ionosphere ions would fall within one of the kV energy channels of the detector and there would be a cutoff of particle fluxes at higher energies. In fact, although the cutoff can be clearly seen in the spectra, there is no narrow peak in the flux. Furthermore, there is a continuum of energies below the cutoff. This latter flux is probably the result of secondary ions produced as a result of the impact of the primary particles on the vehicle surface, and returned to the surface by the electric field due to the vehicle charge. The broadness of the peak is not understood at present, but could represent a more complex, dynamic character to the ion sheath around the rocket in which wave particle interactions result in a smearing of the classical monoenergetic ion flux expected from steady state electrostatic considerations.

Figure 7-12 shows two estimates of the vehicle potential based on the ion spectrum characteristic for a body-sphere potential also shown on the plot. It can be seen that the vehicle potential tracks the applied potential well, again supporting the linearity of the vehicle sheath impedance. Calculated values of vehicle potential using the NASCAP/LEO (*Katz et al.*, 1988) show that the lower bound of the vehicle potential is probably more representative of the actual static vehicle potential. The ion energization above this value is probably achieved by dynamic processes within the sheath region around the vehicle.

In summary, we found that both the observations and the theoretical model supported vehicle potentials of several kV negative with respect to the undisturbed ionosphere. However, the exact values are difficult to ascertain without further studies of the particle data and a better understanding of the dynamics of the positive charge sheath around the vehicle.

The flight component of the SPEAR-1 project provided some valuable data points verifying the capability of modelling the interaction between high voltages on conducting electrodes and the ambient space environment at LEO altitudes. In particular the flight achieved the following specific items:

i) Measured current collected when voltages up to 10s of kV were exposed to LEO environment.

ii) Showed negligible volume discharge effects when the HV interacted with the LEO environment in the geometrical configuration used.

iii) Showed that the plasma currents to the bipolar system were generally low compared to possible load currents even after the short space exposure time of a sounding rocket.

iv) Showed that for the size and geometry of the SPEAR payload, the net space load placed on the power supply was well represented by a linear resistance having values in the 500-1000kΩ range.

v) Showed that exposed negative potentials of up to -10kV resulted in no adverse system effects resulting from transient surface discharges.

vi) Showed transient discharge currents could be triggered by vehicle gas release during ACS operations during discharge cycle.

vii) Demonstrated feasibility of using high energy, high voltage capacitors on a space vehicle.

The SPEAR-1 results have provided new insight on the interaction of HV with the space environment. However, the results have raised questions which will need further investigation in the space environment. The most immediate are:

i) Will the plasma currents remain low if the vehicle is clamped close to ionospheric potential by an exposed plasma contactor?

ii) Will the plasma current remain low if a significant fraction of field-of-view of the exposed HV electrode contains a physical, conductive cathode?

iii) What is the time history of the development of the steady state plasma currents on a sub-microsecond time scale?

iv) What visible discharge phenomena can be observed for exposed HV negative potentials, and how do these differ from the same positive potential applied to the same collector-vehicle geometry?

We hope that observations to provide answers to these questions will be possible on future sounding rocket flights.

9. References

Katz, I., G. A. Jongeward, V. A. Davis, M. J. Mandell, R. A. Kuharski, J. R. Lilley, Jr., W. J. Raitt, D. L. Cooke, R. B. Torbert, G. Larson and D. Rau, Structure of the bipolar plasma sheath generated by SPEAR 1, *J. Geophys. Res.*, (accepted) 1988.

Langmuir, I. and K. Blodgett, Current limited by space charge flow between concentric spheres, *Phys. Res., 2*, 49, 1924.

Parker, L. W. and B. L. Murphy, Potential buildup on an electron-emitting ionospheric satellite, J. *Geophys. Res., 72*, 1631, 1967.

10. Figures

Fig. 1-1 Simplified schematic diagram of voltage distribution between the SPEAR-1 payload and the space environment.

Fig. 2-1 Planned voltage levels of discharge capacitors for each sphere for each of the 6 steps in the cyclic biassing sequence.

Fig. 2-2 Schematic diagram of one of the SPEAR-1 HV biassing system indicating current paths and monitoring points for voltage and current.

Fig. 3-1 Schematic diagram of the flight configuration of the SPEAR-1 payload showing approximate dimensions and locations of the major elements of the system.

Fig. 3-2 Assembly drawing showing the complete configuration of the telescopic and folding boom assembly used to deploy the spheres.

Fig. 3-3 The geometrical arrangement of the deployed spheres shown in three views; a) from above, b) from the side and c) from the front.

Fig. 3-4 Detail of the shape of the grading rings, and the construction technique used to divide the potential of the sphere relative to the payload evenly between the rings.

Fig. 3-5 Block diagram of science section of the SPEAR-1 payload

Fig. 3-6 Schematic diagram of the SPEAR-1 power distribution scheme.

Fig. 3-7 Block diagram of the SPEAR-1 HV system.

Fig. 3-8 Block diagram of the SPEAR-1 Langmuir probe.

Fig. 3-9 Voltage program applied to the SPEAR-1 Langmuir probe.

Fig. 3-10 Schematic circuit diagram of the SPEAR-1 Langmuir probe.

Fig. 3-11 Schematic diagram of the SPEAR-1 pulse counting photometer.

Fig. 4-1 SPEAR-1 PCM telemetry format. The 32x49 format is shown in two segments; a) columns 1-24 and b) columns 25-49.

Fig. 6-1 Arrangement of SPEAR-1 payload within the Plum Brook vacuum chamber for performance of the complete payload vacuum tests.

Fig. 6-2 Example of current and voltage signatures for sphere-1 during a discharge in the vacuum chamber.

Fig. 6-3 Example of current and voltage signatures for sphere-2 during a discharge in the vacuum chamber.

Fig. 6-4 Photographs of the discharges corresponding to the currents and voltage shown in Figures 6-2 and 6-3 taken by a film camera using a time exposure.

Fig. 7-1 Details and plots of the launch data and trajectory for SPEAR-1.

Fig. 7-2 Diagram illustrating the attitude maneuvers and their location in the trajectory for SPEAR-1.

Fig. 7-3 Plot of the pressure determined by the SPEAR-1 cold cathode ionization gauge located on the payload and the ambient atmospheric pressure predicted by the MSIS-86 model atmosphere. Both are plotted as a function of elapsed time from launch.

Fig. 7-4 Plot of electron density determined by the Langmuir probe during the flight. The electron density is plotted as a function of altitude for both the upleg and downleg.

Fig. 7-5 Plots of the discharge capacitor current (upper panel), graded boom current (center panel) and capacitor potential (lower panel) as a function of MET following the connection of the capacitor to sphere-1.

Fig. 7-6 Plots of the plasma current flowing to the spheres and grading rings for sphere-1 at two different altitudes. The plasma currents are plotted as functions of capacitor potential.

Fig. 7-7 Collection of plasma current plots organized in columns corresponding to each of the three observing altitudes used in the SPEAR-1 flight.

Fig. 7-8 Plots of plasma currents measured by sphere-1 (upper panel) and sphere-2 (lower panel) during a period when ACS thruster gas was being emitted to stabilize the payload attitude.

Fig. 7-9 Images from the TV data showing the glow surrounding the grading rings for discharges of similar voltage but as different altitudes.

Fig. 7-10 Computer generated display of the light detected by the TV camera after the frame had been image processed to highlight boundaries, and superimpose the location of the sphere and boom centerline determined a few frames prior to the discharge.

Fig. 7-11 Plots of the ion energy spectrum measured at the skin of the payload at two times during the exponential decay of voltage on the capacitor. The upper panel corresponds to the higher capacitor voltage.

Fig. 7-12 Two estimates of vehicle potential derived from ion spectra similar to those shown in Figure 7-11 are shown in the two lower curves. The upper curve is the decaying voltage on the discharge capacitor. The three black circles show theoretical computation of the vehicle potential by the NASCAP/LEO computer model.

SPEAR-1

Simplified Schematic Diagram of Voltage Distribution

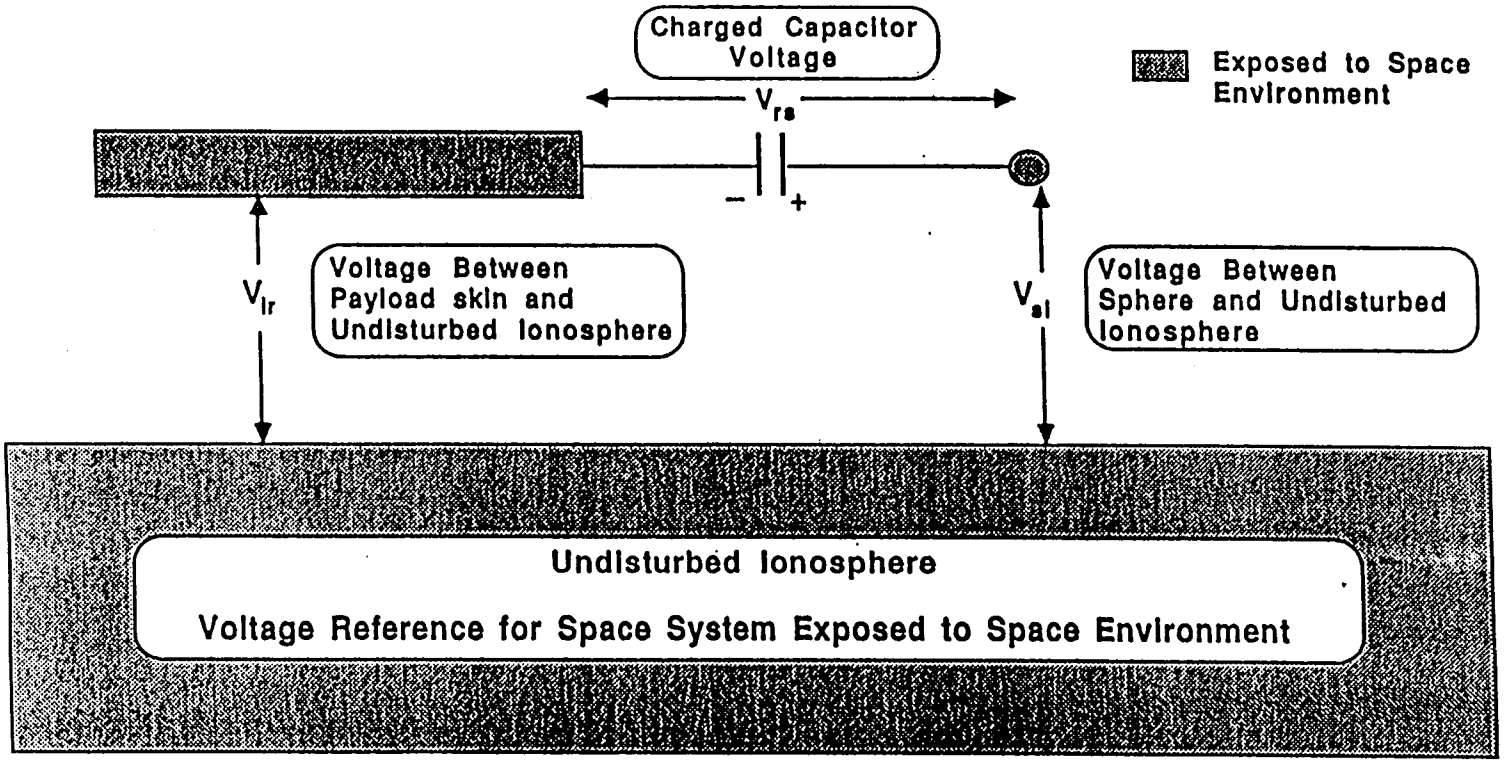

Figure 1-1

Basic Relationship $V_{lr} + V_{rs} + V_{sl} = 0$

For Example, using standard convention to define sign of electrical potential difference:

If $V_{rs} = -45$ kV and $V_{lr} = +10$ kV then $V_{sl} = (45 - 10) = +35$ kV

SPEAR-1

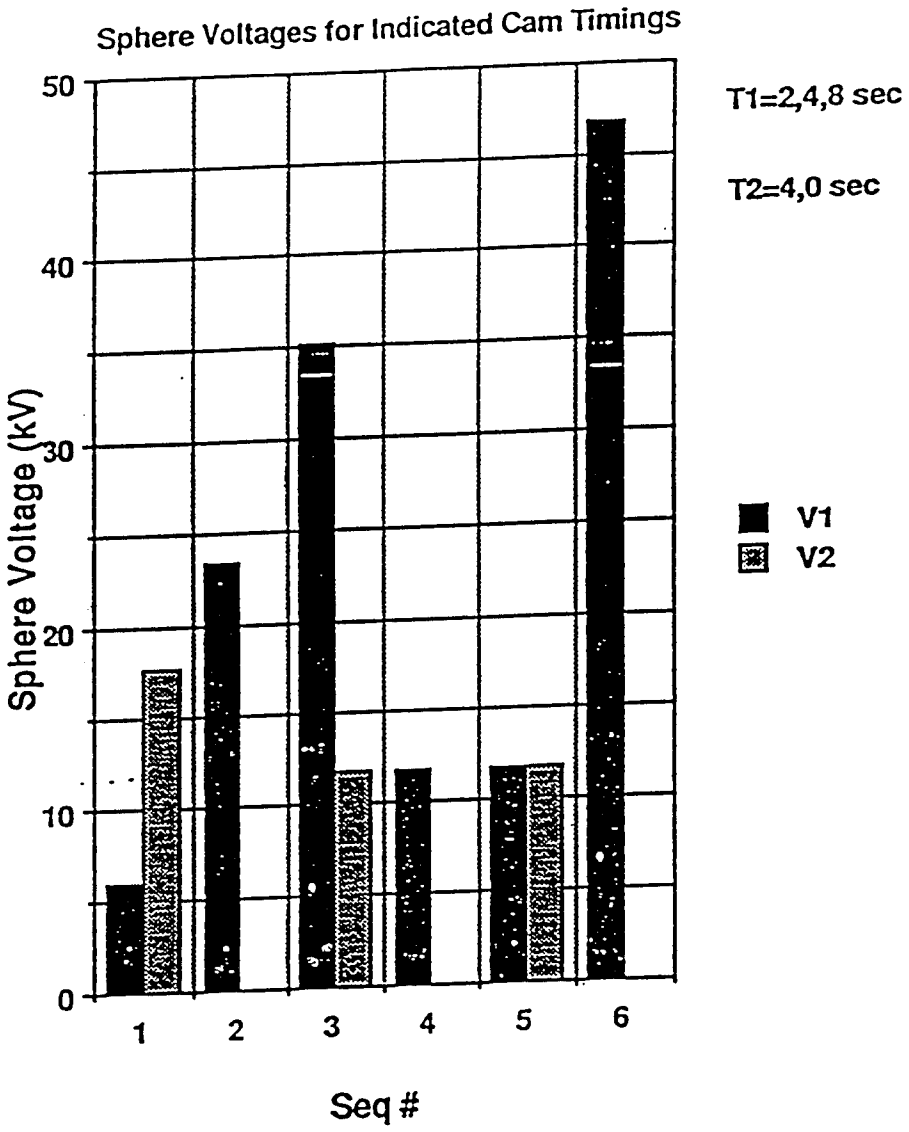

Figure 2-1

SPEAR-1

HV System - Schematic Diagram

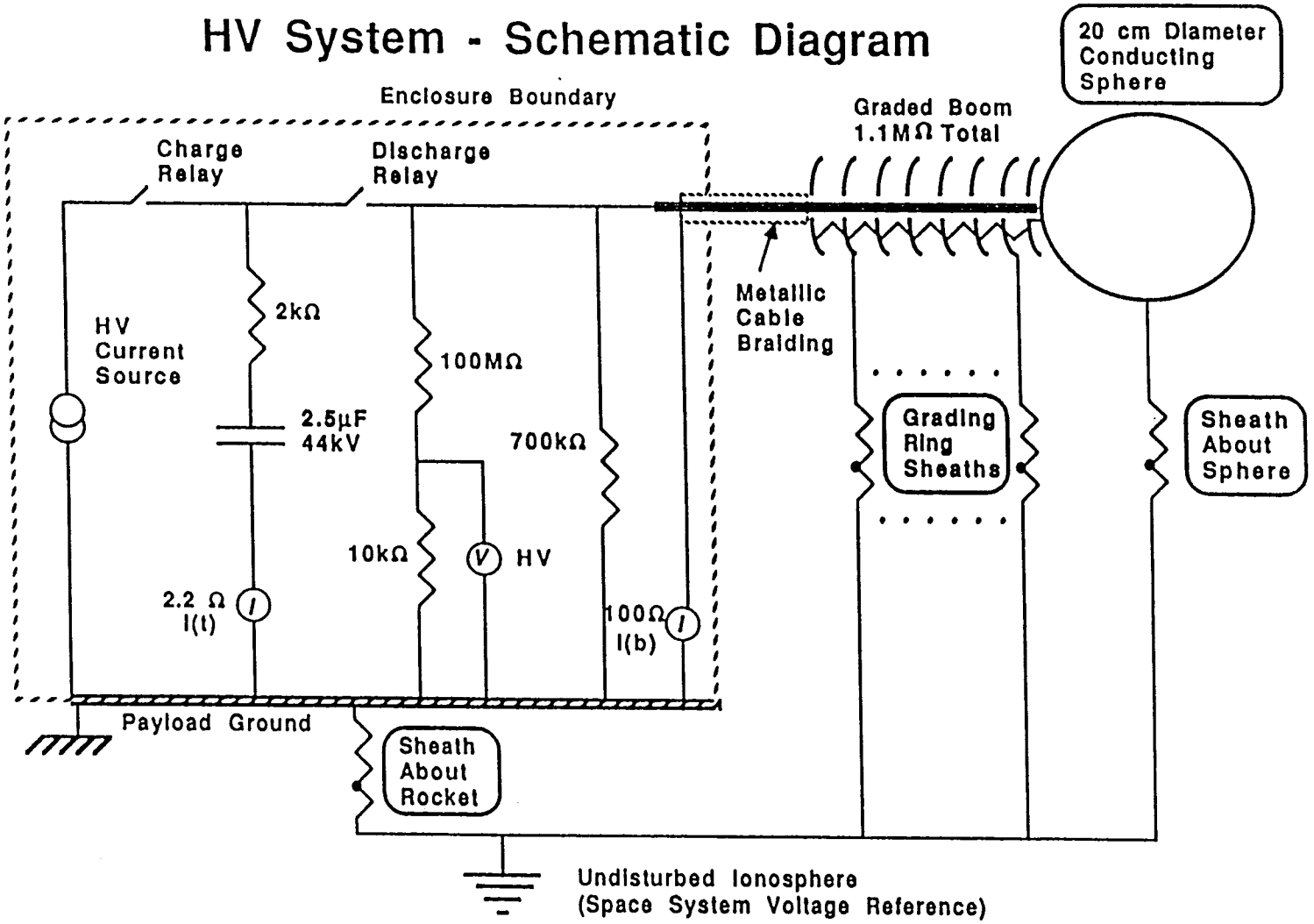

Figure 2-2
A-39

SPEAR-1

Schematic Diagram of Front View of Payload

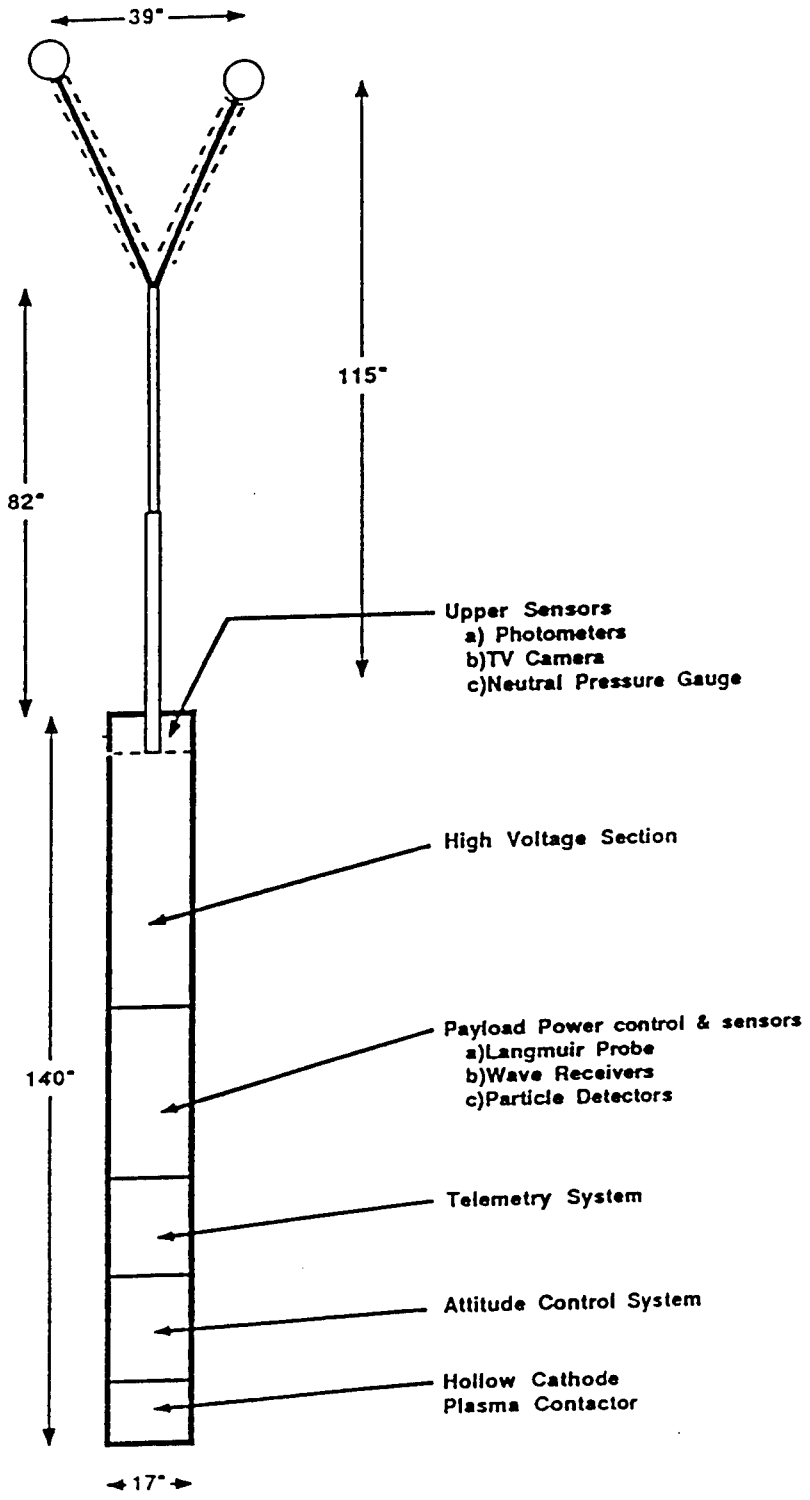

Figure 3-1

SPEAR-1

HV Booms in Stowed Configuration

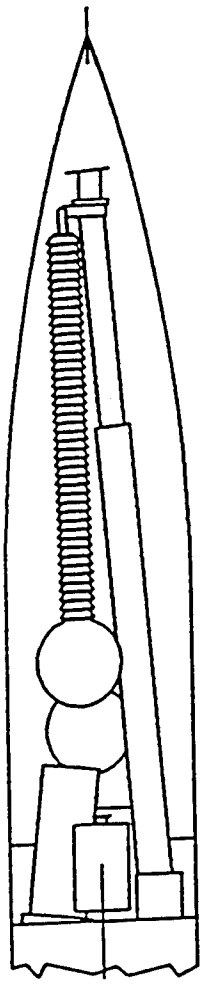

Figure 3-2

SPEAR-1

Sphere Geometry (Top View)

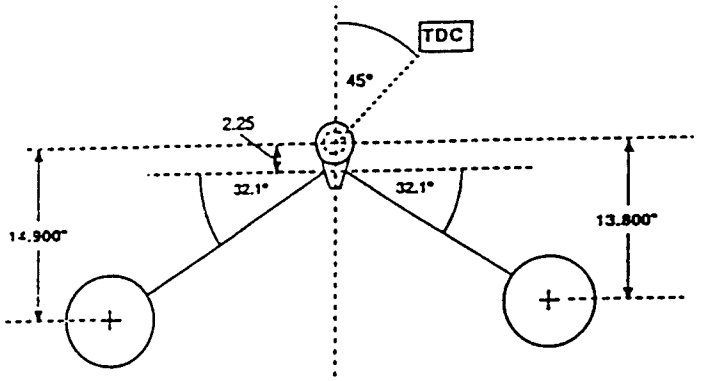

SPEAR-1

Sphere Geometry (Side View)

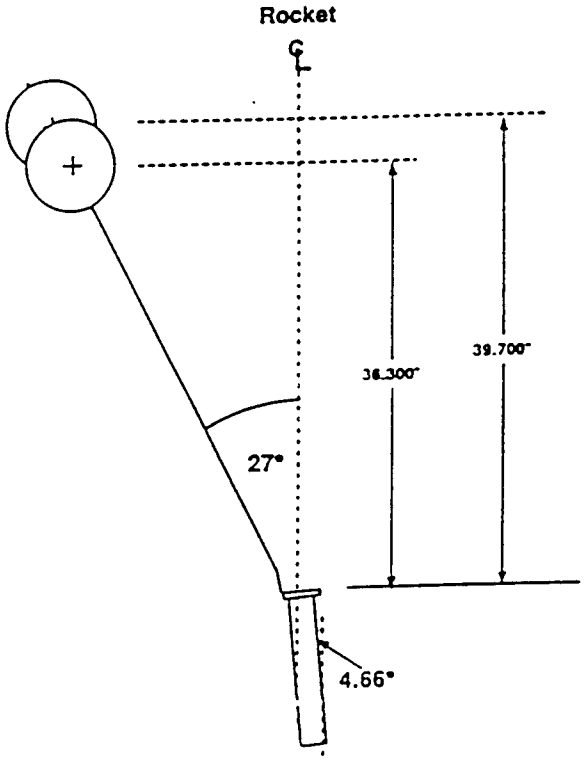

SPEAR-1

Sphere/Boom Geometry (View from Front)

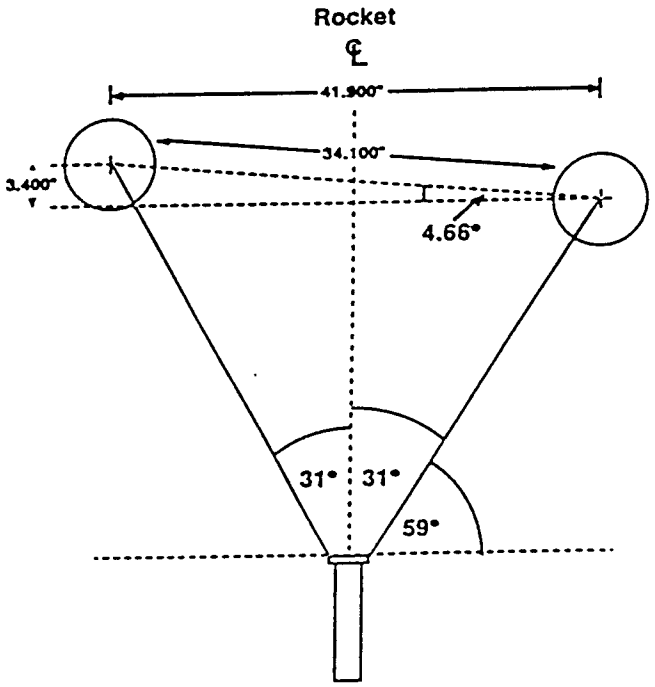

Figure 3-3

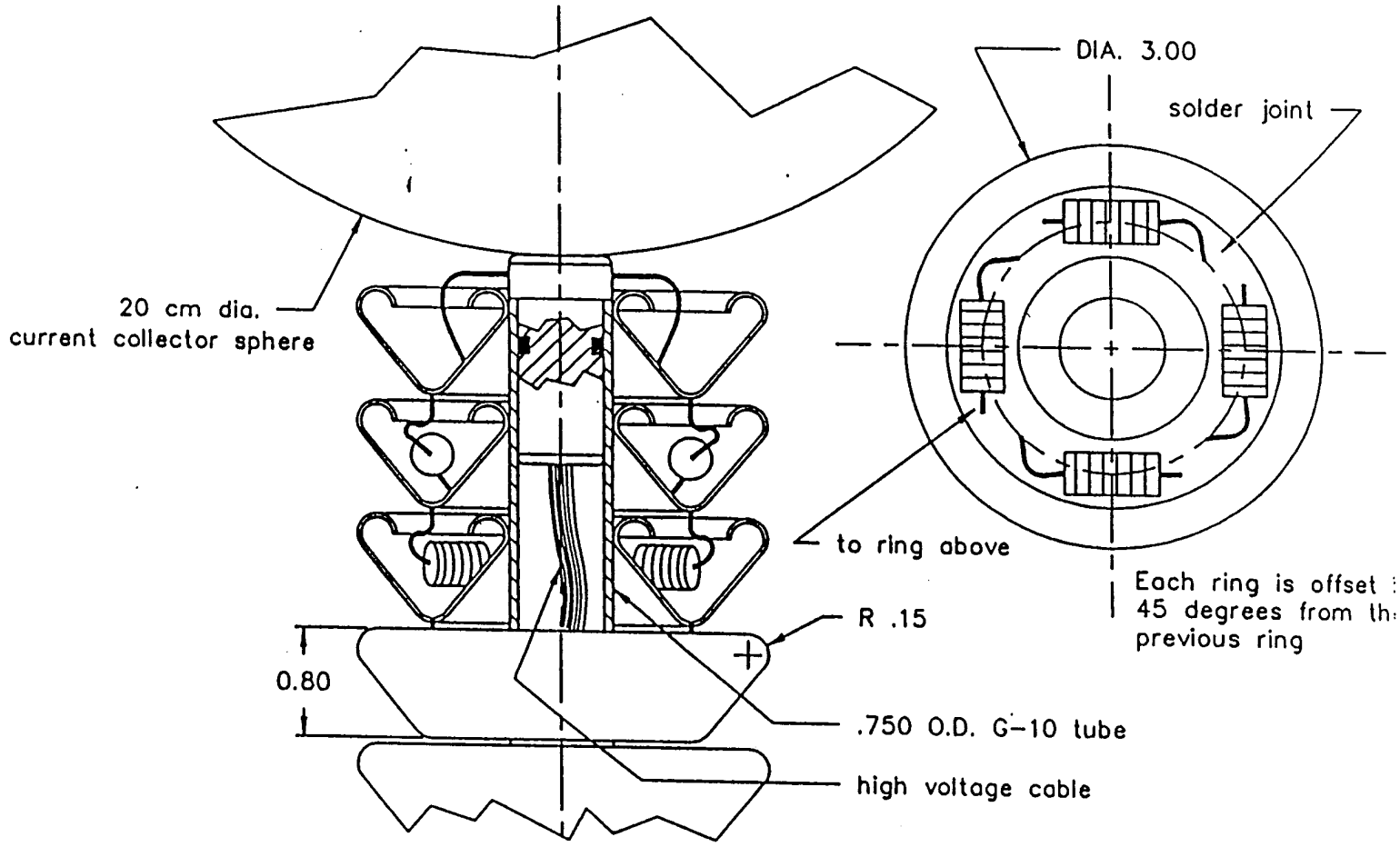

DETAIL OF SPEAR-1 BOOM GRATING RINGS

Figure 3-4

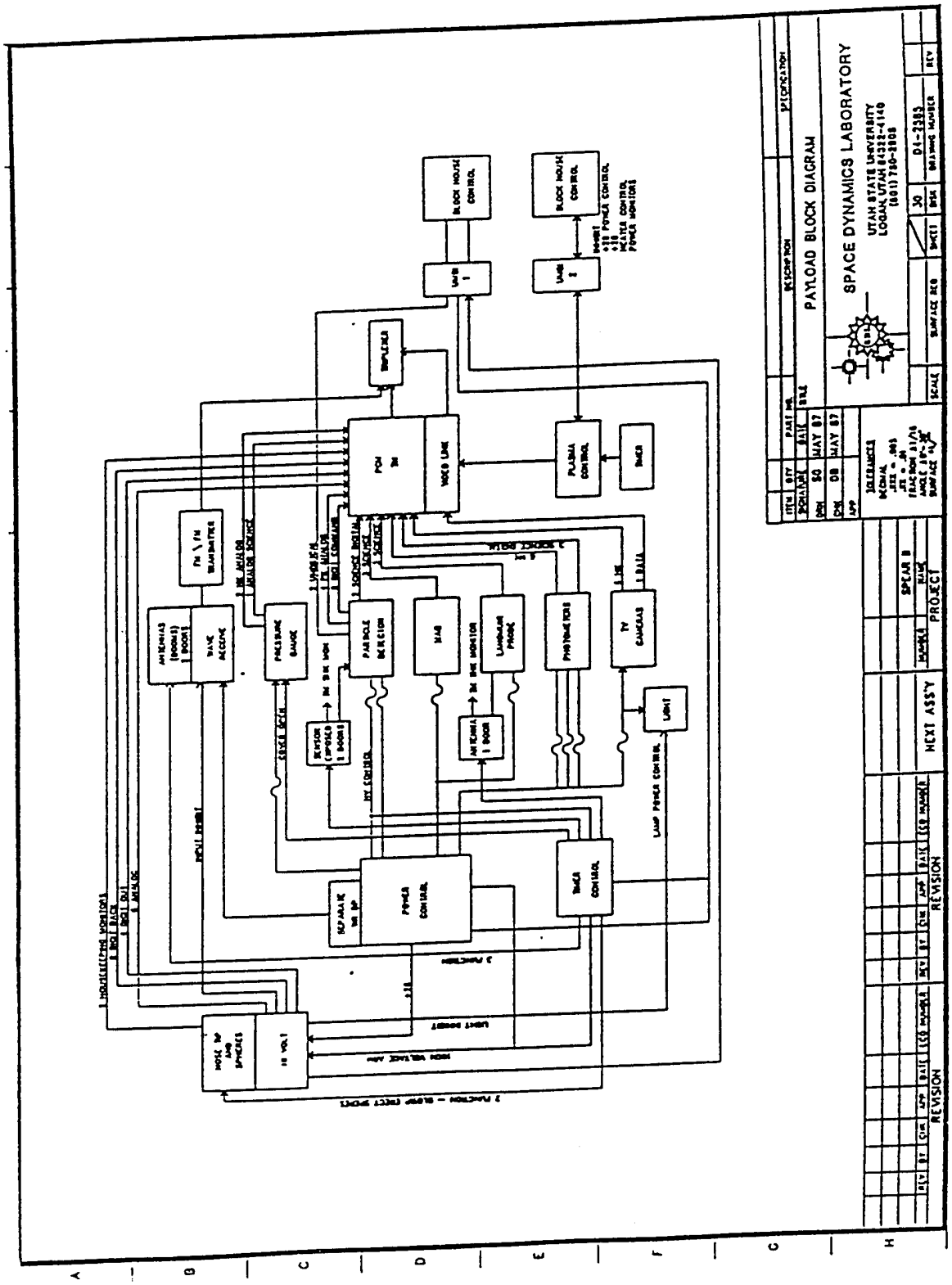
PAYLOAD BLOCK DIAGRAM
SPACE DYNAMICS LABORATORY
UTAH STATE UNIVERSITY
LOGAN, UTAH 84322-4140
(801) 750-3808
SPEAR II
PROJECT
NEXT ASSY
REVISION
DESCRIPTION
BLOCK HOUSE CONTROL
PCM
VIDEO LINE
PAYLOAD CONTROL
TRACK
PRESSURE GAUGE
PHOTOMETER
TV CAMERAS
LIMIT
POWER CONTROL
TRACK CONTROL

Figure 3-5

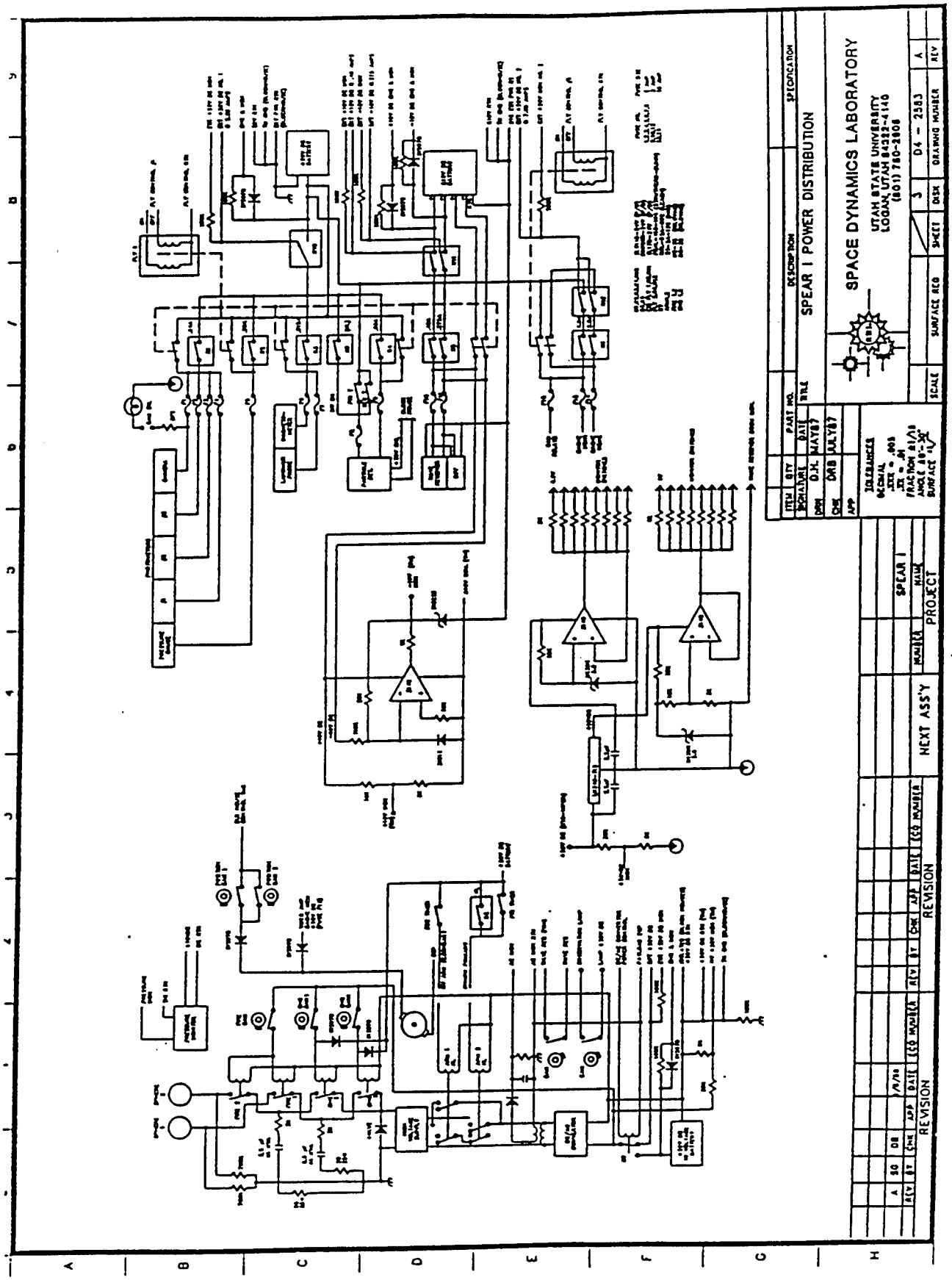
SPACE DYNAMICS LABORATORY
UTAH STATE UNIVERSITY
LOGAN, UTAH 84322-4140
(801) 750-2906
SPEAR I POWER DISTRIBUTION
SPEAR I
PROJECT
NEXT ASS'Y
REVISION

Figure 3-6

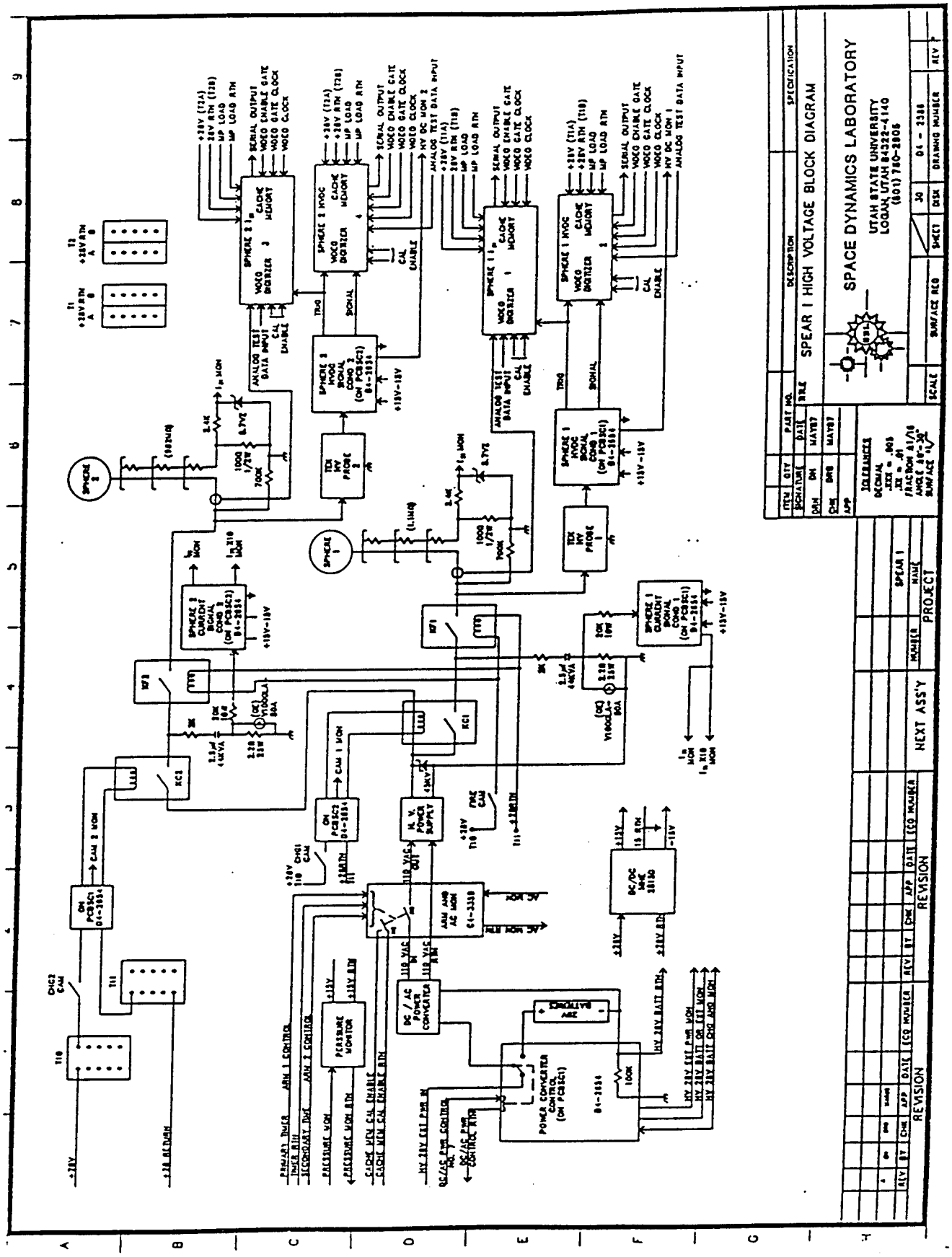

Figure 3-7
A-46

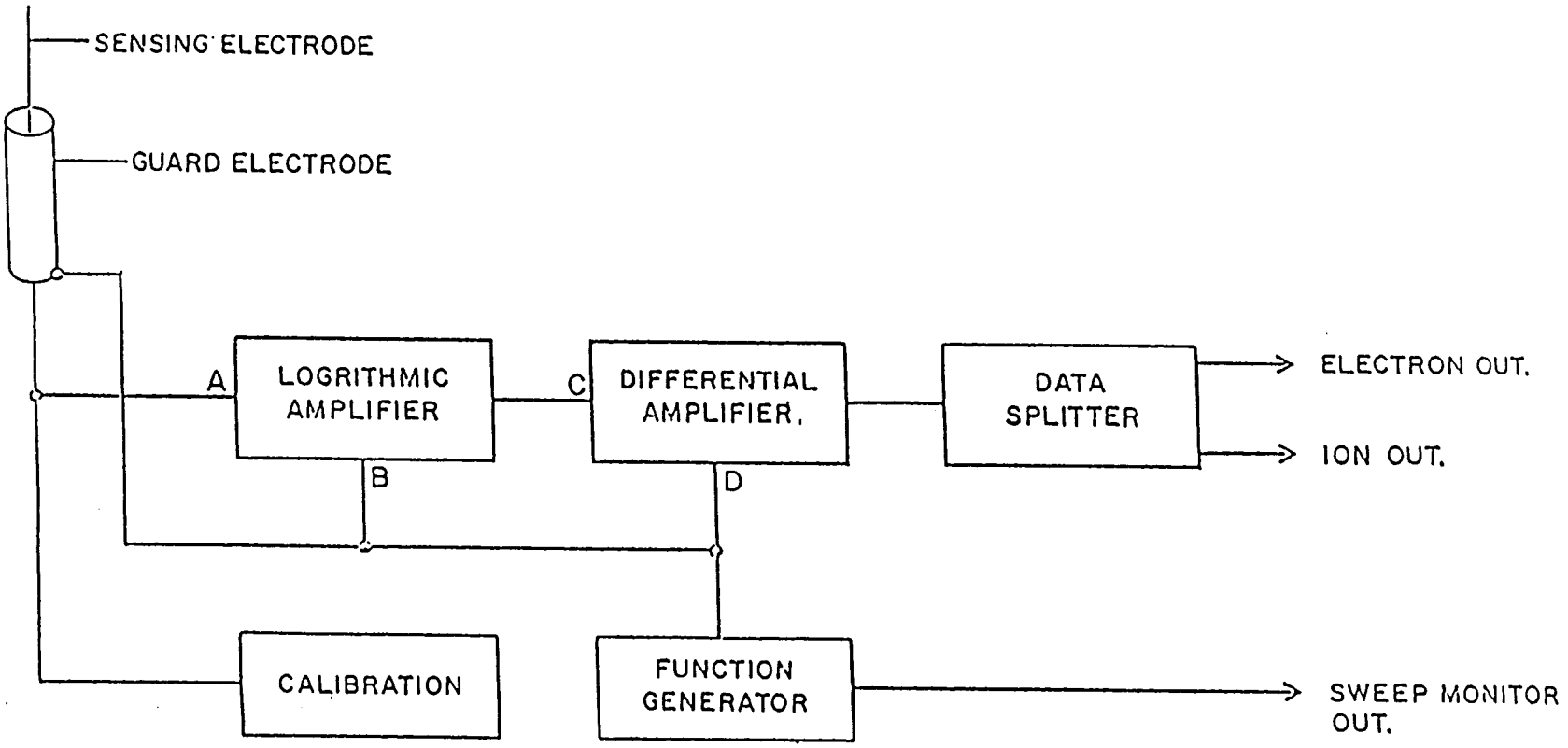

Figure 3-8
A-47

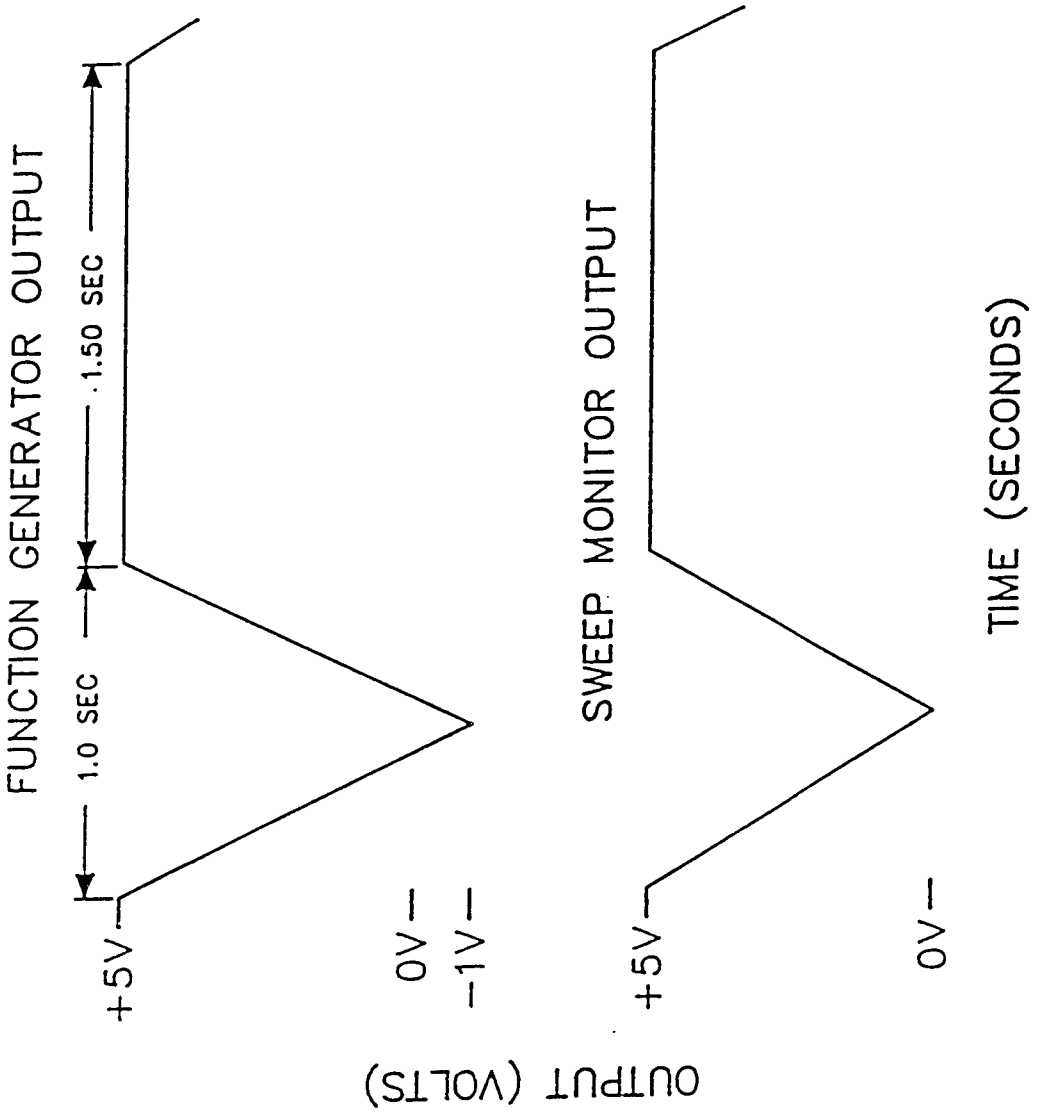
FUNCTION GENERATOR OUTPUT
1.0 SEC
1.50 SEC
+5V
0V
-1V
SWEEP MONITOR OUTPUT
+5V
0V
TIME (SECONDS)
OUTPUT (VOLTS)

Figure 3-9

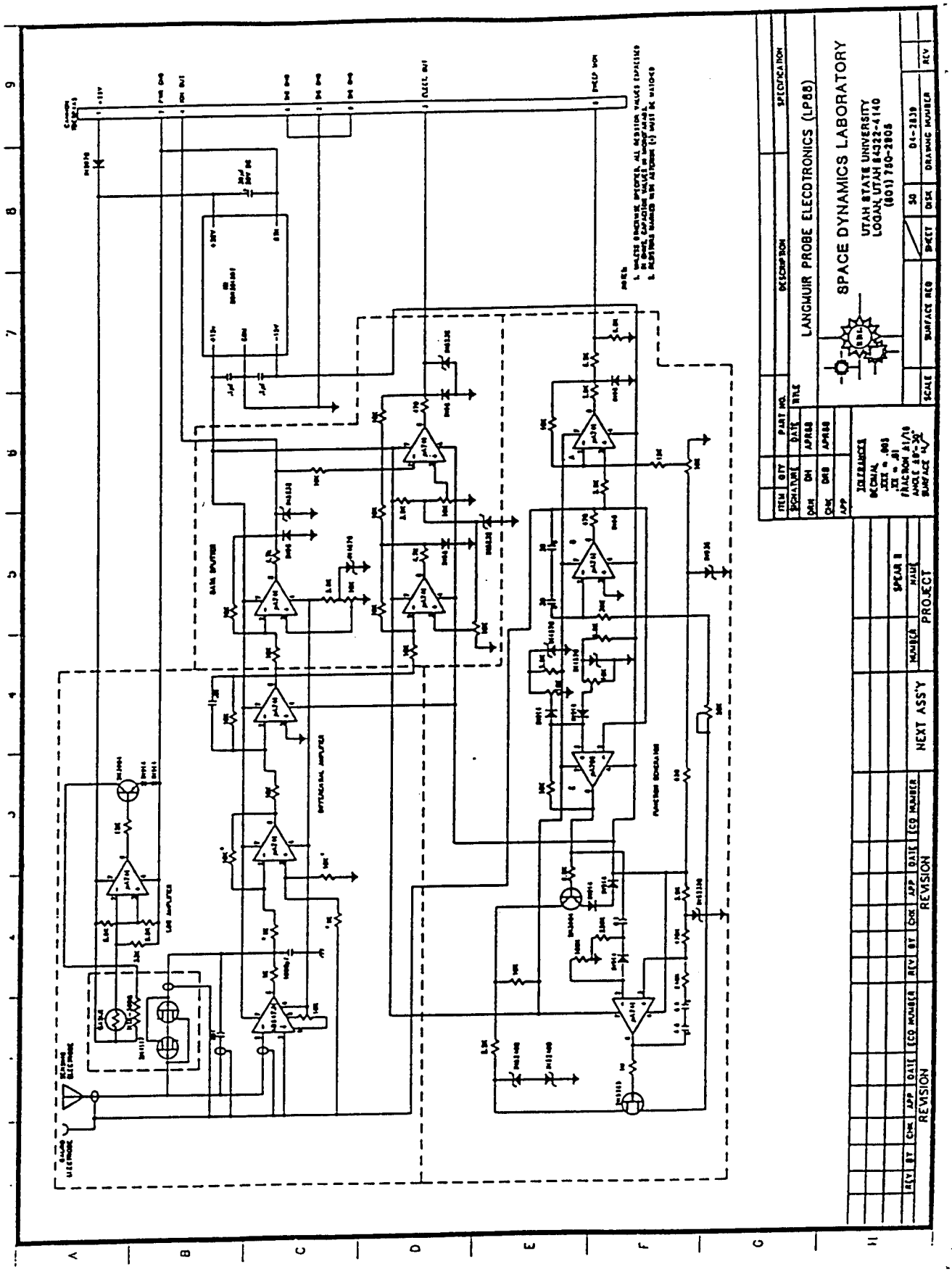

Figure 3-10
A-49

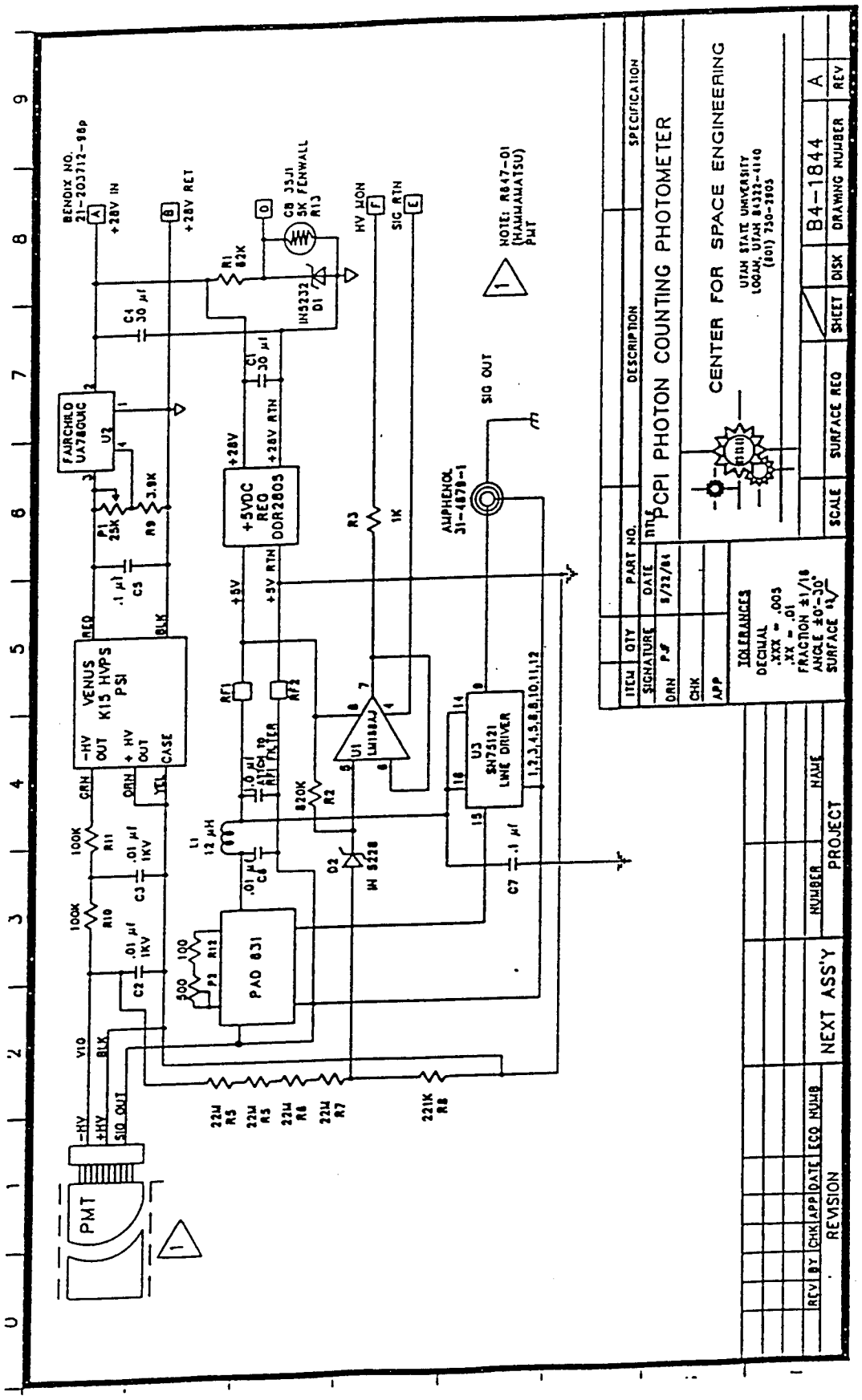
PCPI PHOTON COUNTING PHOTOMETER
CENTER FOR SPACE ENGINEERING
UTAH STATE UNIVERSITY
LOGAN, UTAH 84322-4140
(801) 750-2905
B4-1844
DRAWING NUMBER
SURFACE REQ
SCALE
SHEET
DISK
DESCRIPTION
SPECIFICATION
PART NO.
DATE
ITEM
QTY
SIGNATURE
DRN
CHK
APP
TOLERANCES
DECIMAL
.XXX = .005
.XX = .01
FRACTION ±1/16
ANGLE ±0°-30'
SURFACE
REVISION
REV
BY
CHK
APP
DATE
ECO NUMB
NEXT ASS'Y
NUMBER
NAME
PROJECT
PMT
VENUS K15 HVPS PSI
-HV OUT
+ HV OUT
CASE
FAIRCHILD UA78GUC
PAD 831
LM185AJ
SN75121 LINE DRIVER
+5VDC REG ODR2803
AMPHENOL 31-4870-1
BENDIX NO. 21-203712-16P
+28V IN
+28V RET
HV MON
SIG RTN
SIG OUT
CB 33J1 5K FENWALL
1N5232 D1
NOTE: R847-01 (HAMAMATSU) PMT

Figure 3-11

Spear-1 PCM format 11-20-87

	1	2	3	4	5	6	7	8	9	10	11	12	13	14	15	16	17	18	19	20	21	22	23	24
1	pd1	pd14	hv1	SFID	pd2	pd15	cm1	Lp1	pd3	pd16	hv2	pd27	pd4	pd17	hv3	Lp2	pd5	pd18	cm2	pd28	pd6	pd19	hv4	pd7
2								ph1h								ph2h								
3								Lp1								Lp2								
4								ph1L								ph2L								
5								Lp1								Lp2								
6								spare								spare								
7								Lp1								Lp2								
8								spare								spare								
9								Lp1								Lp2								
10								mgx								mgy								
11								Lp1								Lp2								
12								vh1								vh2								
13								Lp1								Lp2								
14								vh4								vh5								
15								Lp1								Lp2								
16								np2								tv2								
17								Lp1								Lp2								
18								ph1h								ph2h								
19								Lp1								Lp2								
20								ph1L								ph2L								
21								Lp1								Lp2								
22								spare								spare								
23								Lp1								Lp2								
24								spare								spare								
25								Lp1								Lp2								
26								mgx								mgy								
27								Lp1								Lp2								
28								ac2								ac3								
29								Lp1								Lp2								
30								ac5								ac6								
31								Lp1								Lp2								
32								ac8								ph11								

Figure 4-1a

Spear-1 PCM format 11-20-87

25	26	27	28	29	30	31	32	33	34	35	36	37	38	39	40	41	42	43	44	45	46	47	48	49
pd20	np1	pd8	pd21	hv5	Lp3	pd9	pd22	cm3	ph21	pd10	pd23	hv6	pd29	pd11	pd24	hv7	ph22	pd12	pd25	cm4	pd30	pd13	pd26	hv8
					ph3h				ph31								ph32							
					Lp3				pc1								pc2							
					ph3L				pc3								pc4							
					Lp3				pc5								pc6							
					tv1				pc7								pL1							
					Lp3				pL2								pL3							
					ac1				pd31								pc8							
					Lp3				pL4								pL5							
					mgz				pL6								pL7							
					Lp3				pL8								pL9							
					vh3				pL10								spare							
					Lp3				hv9								hv10							
					vh6				hv11								tm1							
					Lp3				tm2								tm3							
					tv3				pd31								tm4							
					Lp3				tm5								tm6							
					ph3h				tm7								tm8							
					Lp3				tm9								tm10							
					ph3L				tm11								tm12							
					Lp3				tm13								tm14							
					tv1				tm15								tm16							
					Lp3				tm17								tm18							
					ac1				pd31								tm19							
					Lp3				tm20								tm21							
					mgz				tm22								tm23							
					Lp3				tm24								tm25							
					ac4				tm26								tm27							
					Lp3				py1								py2							
					ac7				tm28								tm1							
					Lp3				pL11								pL12							
					ph12				pd31								spare							

Figure 4-1b
A-52

SPEAR-1

Schematic Diagram showing Payload location in NASA Plum Brook Chamber-B

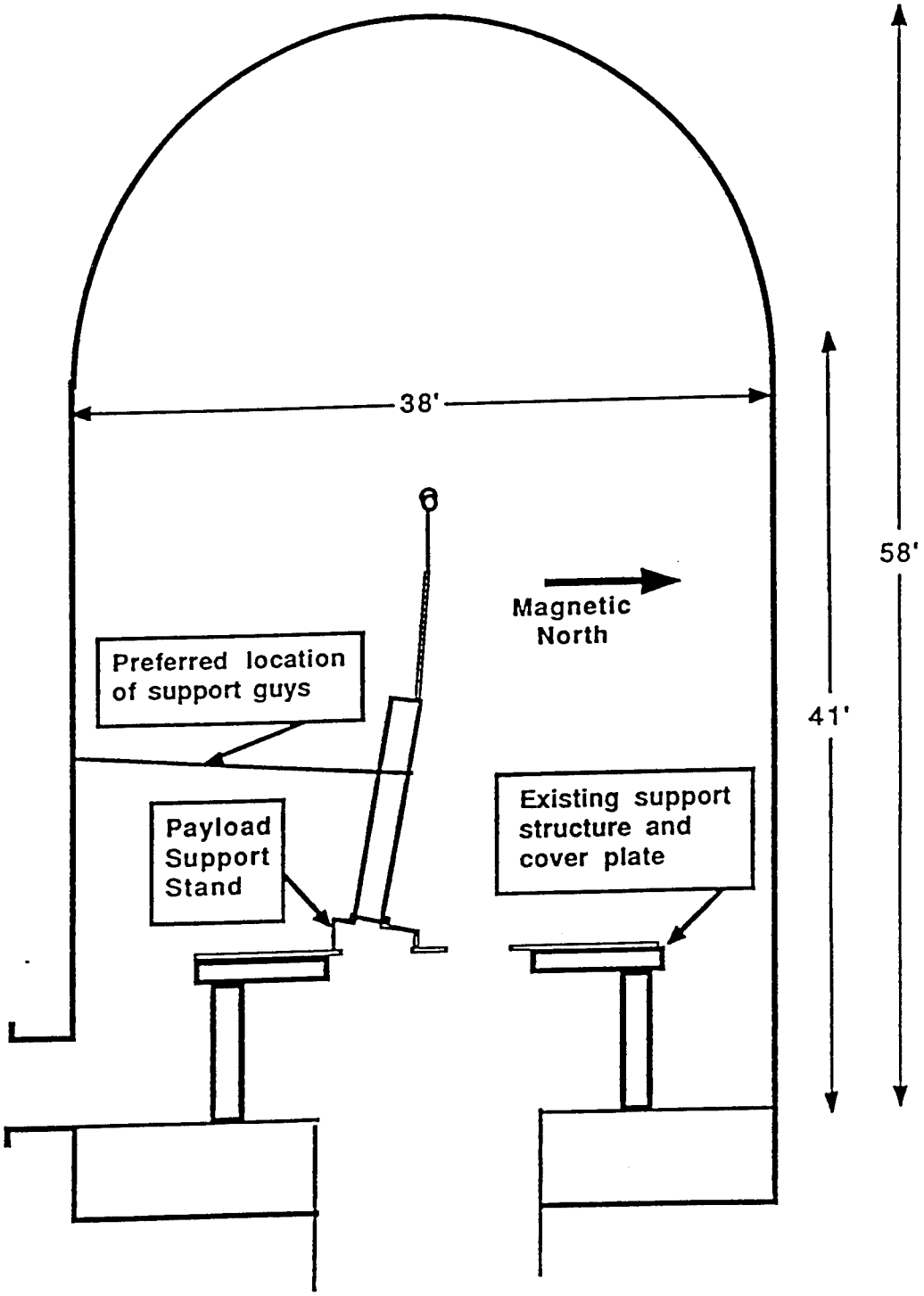

Figure 6-1

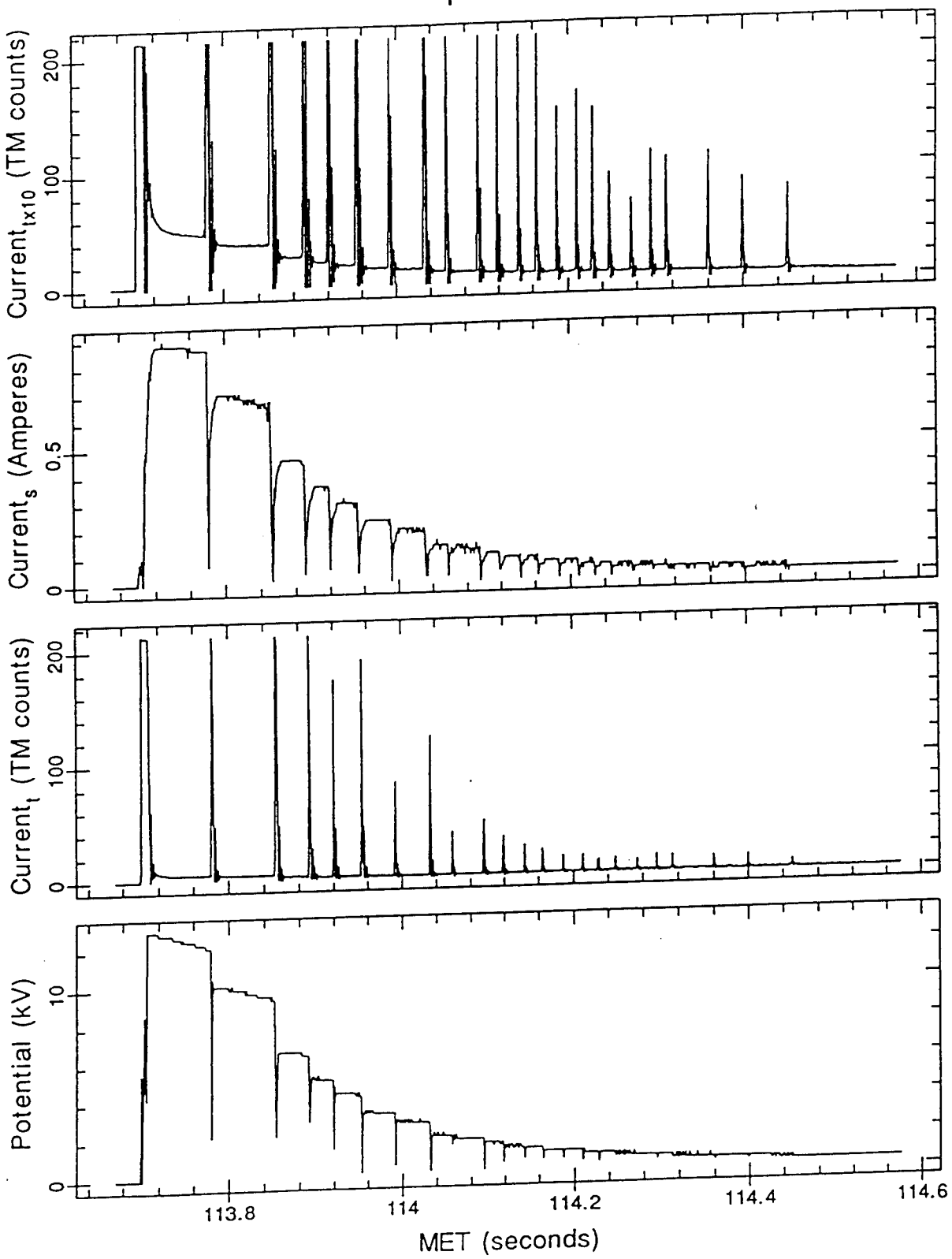
SPEAR-1 HV Monitors
Sphere 1
Current$_{tx10}$ (TM counts)
0
100
200
Current$_s$ (Amperes)
0
0.5
Current$_t$ (TM counts)
0
100
200
Potential (kV)
0
10
113.8
114
114.2
114.4
114.6
MET (seconds)

Figure 6-2

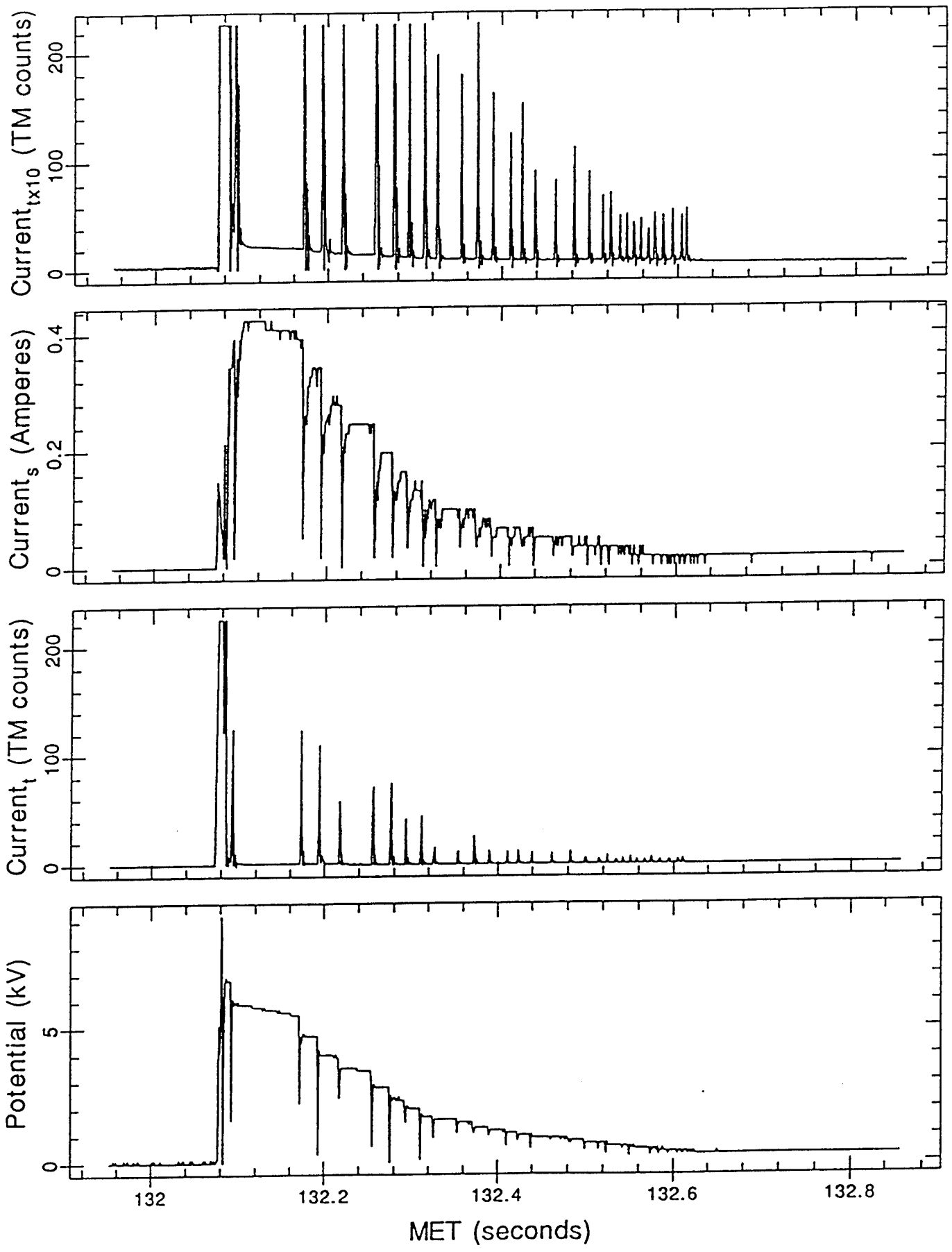
SPEAR-1 HV Monitors
Sphere 2
Current$_{Ix10}$ (TM counts)
0
100
200
Current$_s$ (Amperes)
0
0.2
0.4
Current$_t$ (TM counts)
0
100
200
Potential (kV)
0
5
132
132.2
132.4
132.6
132.8
MET (seconds)

Figure 6-3

SPEAR-1

Diffuse Discharge Glow - Photographic Time Exposures
NASA Plumbrook Chamber Test November, 1987

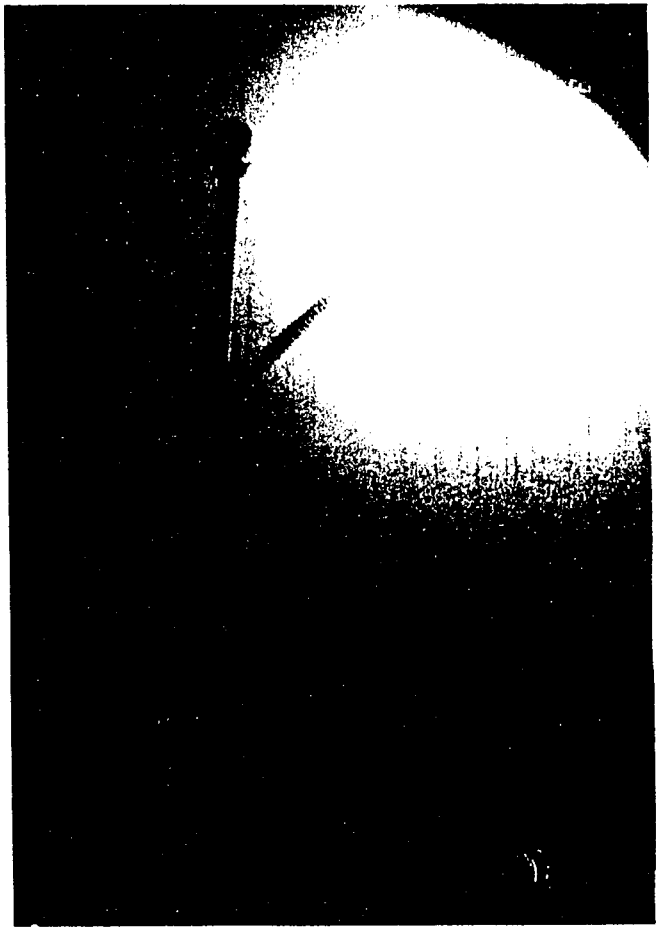

SPHERE-1 13kV

Discharge time: 315/20:38:53
Plasma gen. ON Plasma cont. ON

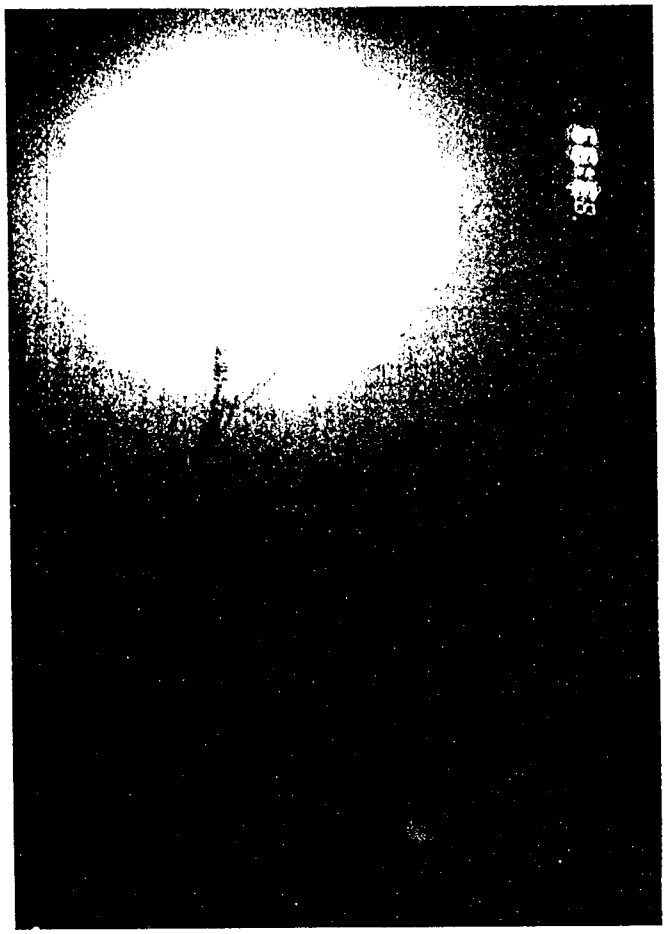

SPHERE-2 6kV

Discharge time: 315/20:39:12
Plasma gen. ON Plasma cont. ON

Figure 6-4

SPEAR - 1

LAUNCH DATA

ROCKET BOOSTER : Black Brant 10
3 Stage Solid Fuel — Terrier Booster
— Black Brant 5c
— Nikha
Rocket Diameter 17 inches

LOCATION : WALLOPS ISLAND RANGE, VIRGINIA
Lat : 37° 50' Long : -75° 28' Mag Lat : 51° 48'
Mag Inclination : 68° 30' Mag Declination : 8° 30'

DATE & TIME : December 14, 1987, 01:45 GMT (12/13/87, 20:45 EST)

TRAJECTORY :

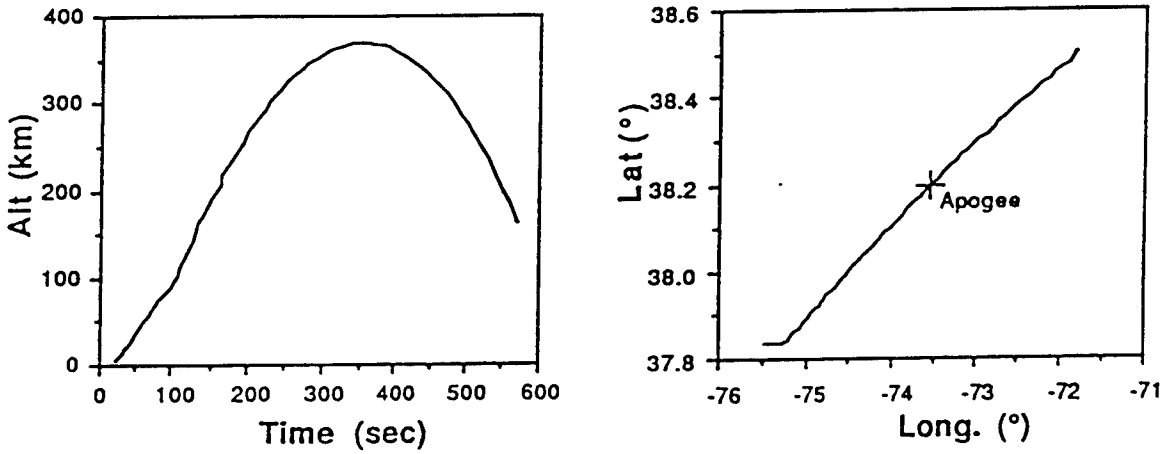

APOGEE : 369 km at 351 sec
Lat : 38° 12' Long : -75° 26' Mag Lat : 52° 50'

Figure 7-1

SPEAR - 1

Vehicle Attitudes

- Payload Axis remains in magnetic meridian
- Schematic views of payload relative to geomagnetic field (from East)

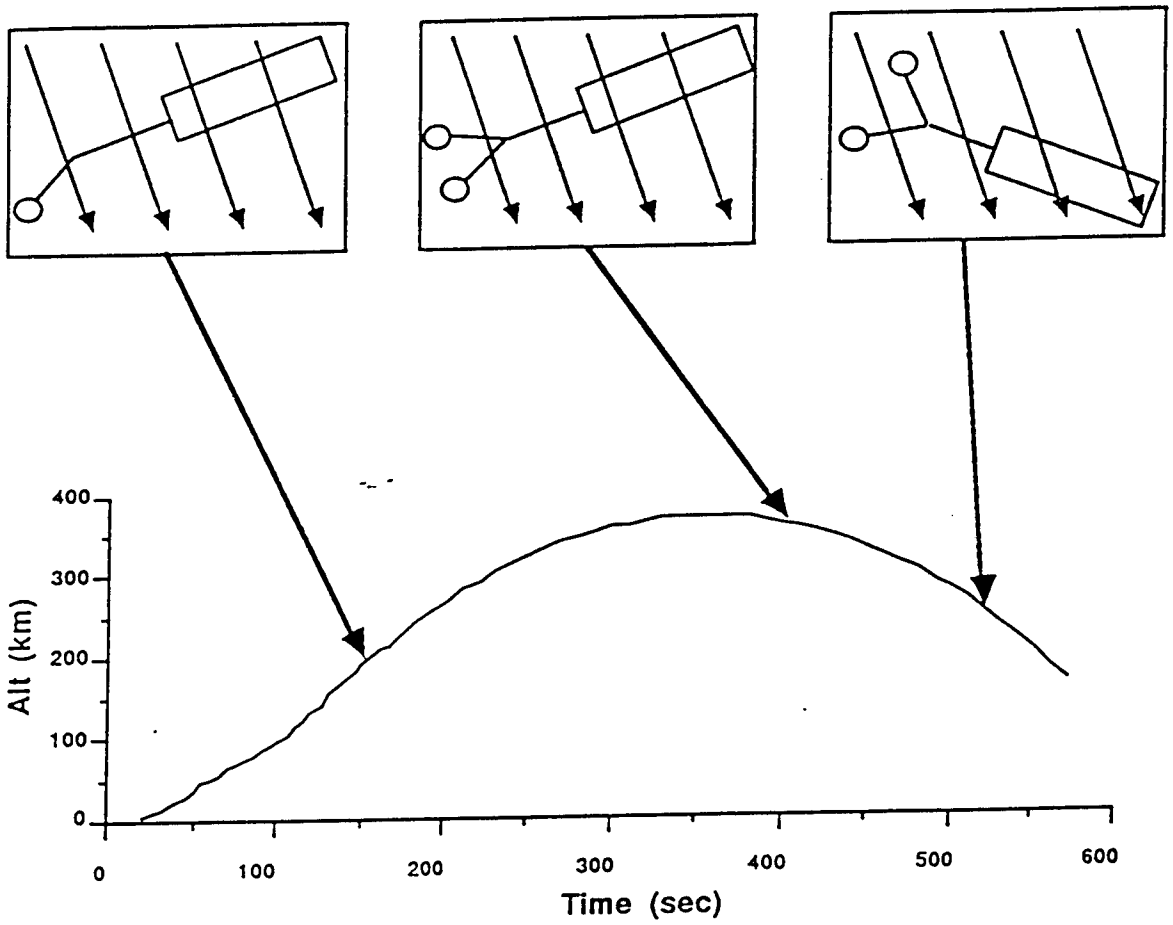

Figure 7-2

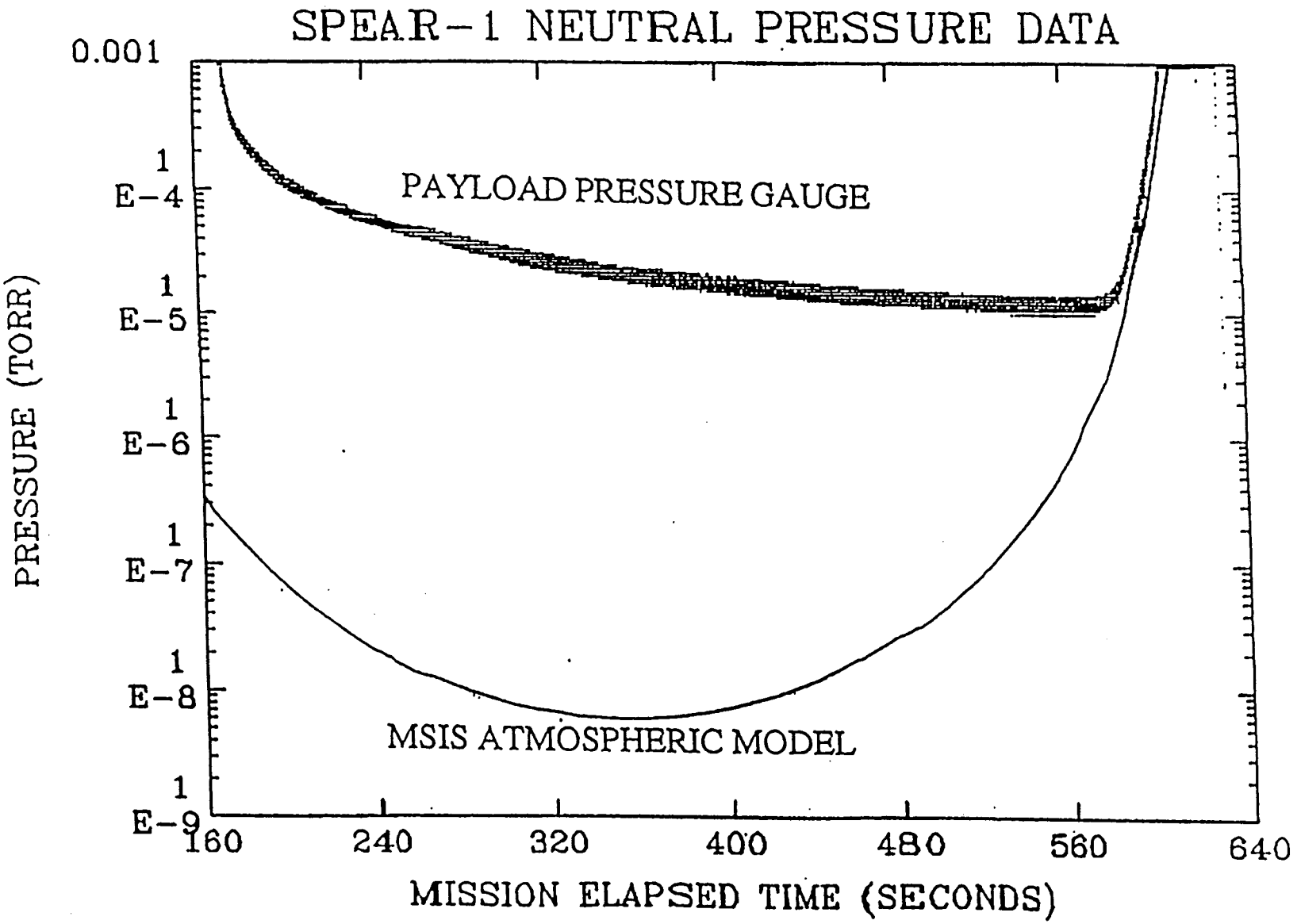

Figure 7-3
A-59

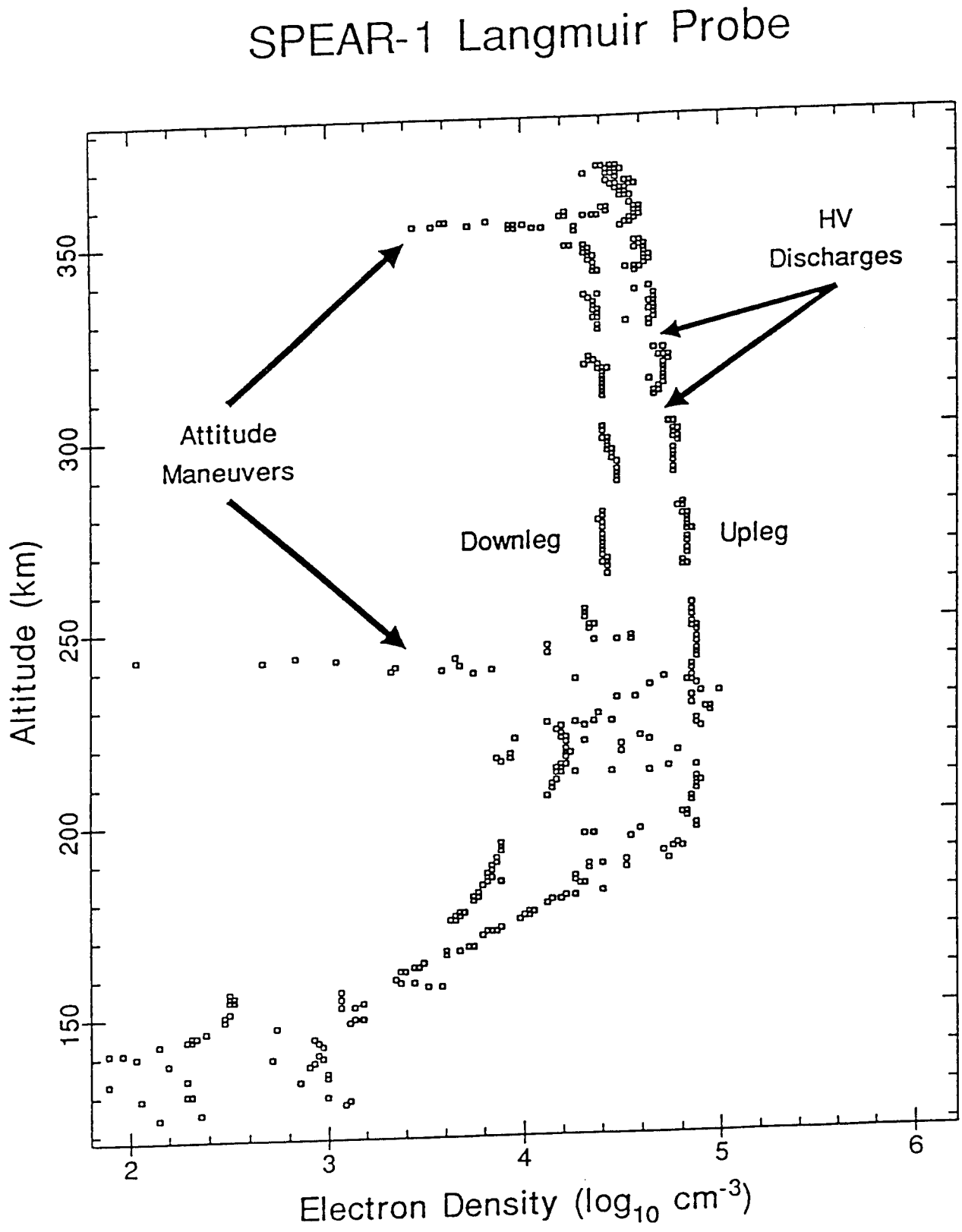
SPEAR-1 Langmuir Probe
HV
Discharges
Attitude
Maneuvers
Downleg
Upleg
Altitude (km)
350
300
250
200
150
2
3
4
5
6
Electron Density (log_{10} cm^{-3})

Figure 7-4

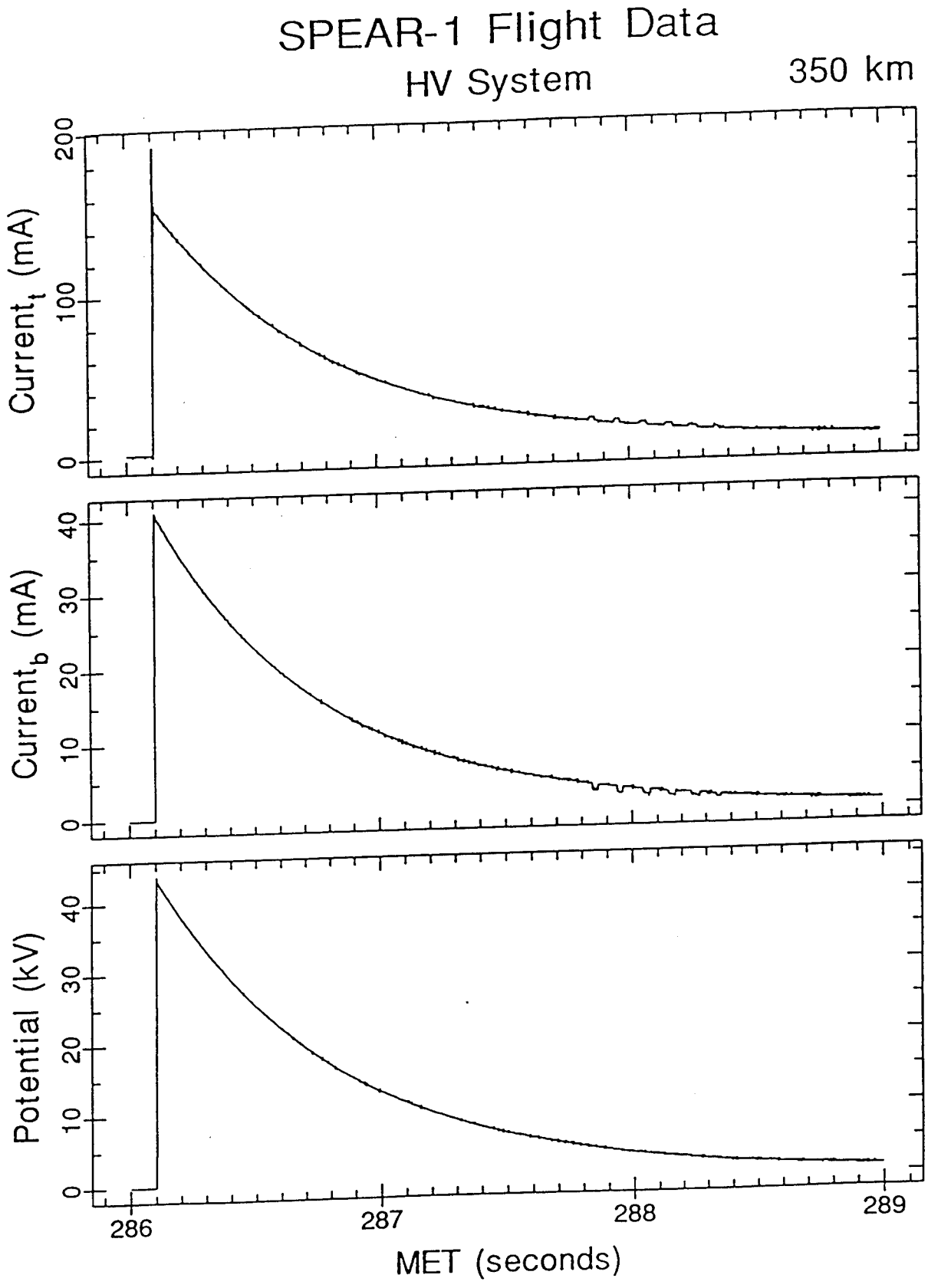
SPEAR-1 Flight Data
HV System
350 km
Current$_t$ (mA)
200
100
0
Current$_b$ (mA)
40
30
20
10
0
Potential (kV)
40
30
20
10
0
286
287
288
289
MET (seconds)

Figure 7-5

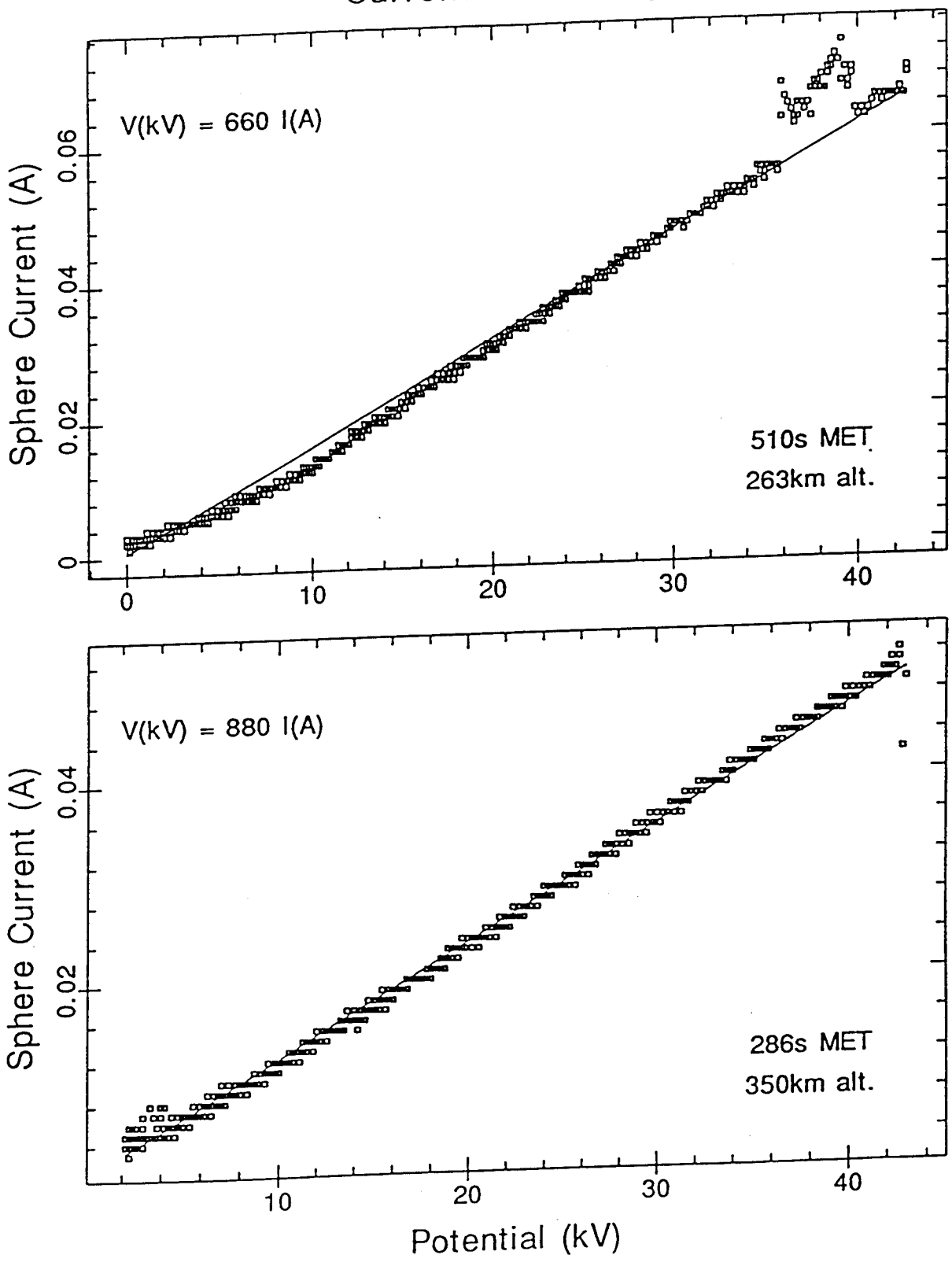
SPEAR-1
Current vs. Voltage
V(kV) = 660 I(A)
510s MET
263km alt.
V(kV) = 880 I(A)
286s MET
350km alt.
Sphere Current (A)
Potential (kV)
0
0.02
0.04
0.06
10
20
30
40

Figure 7-6

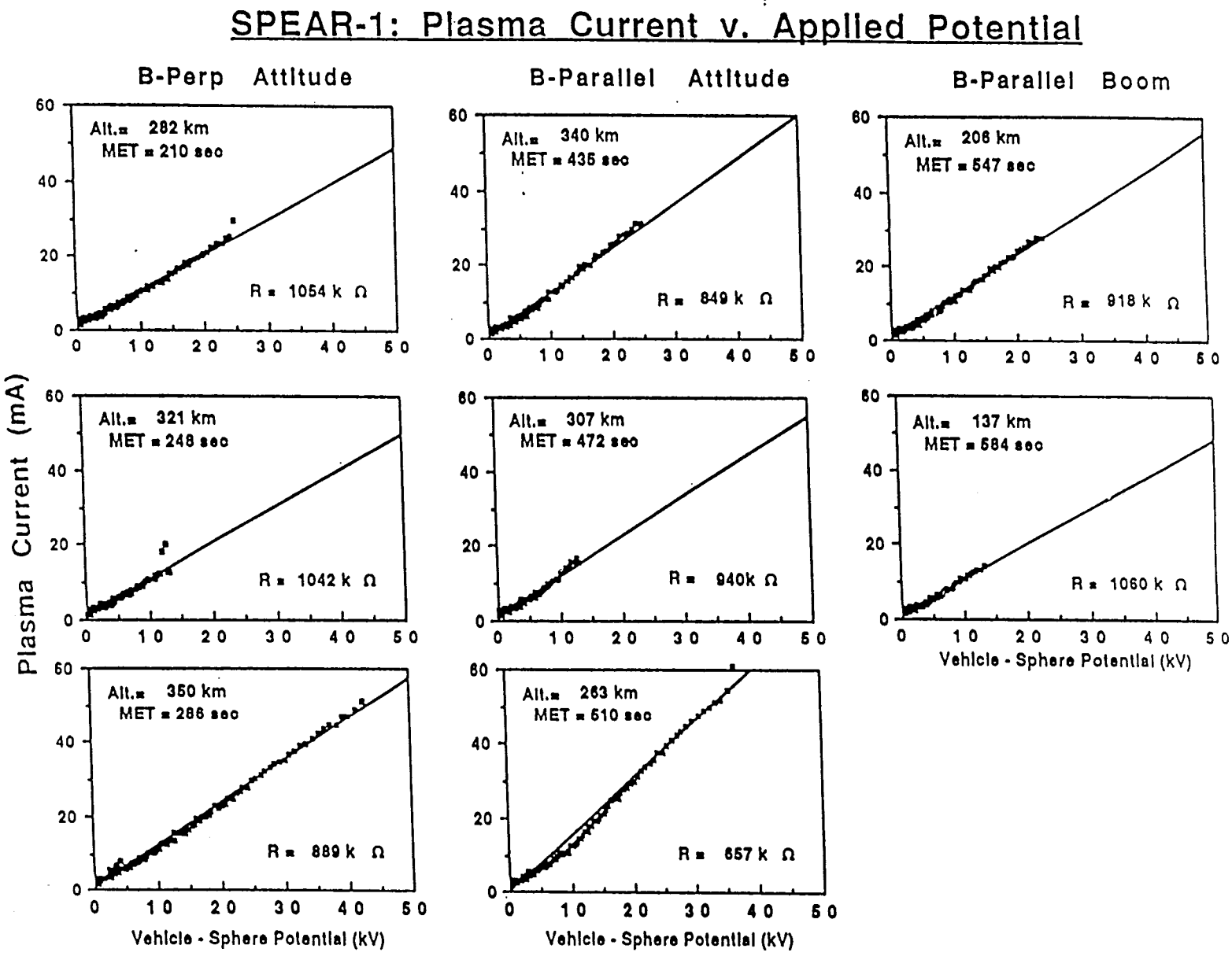

Figure 7-7
A-63

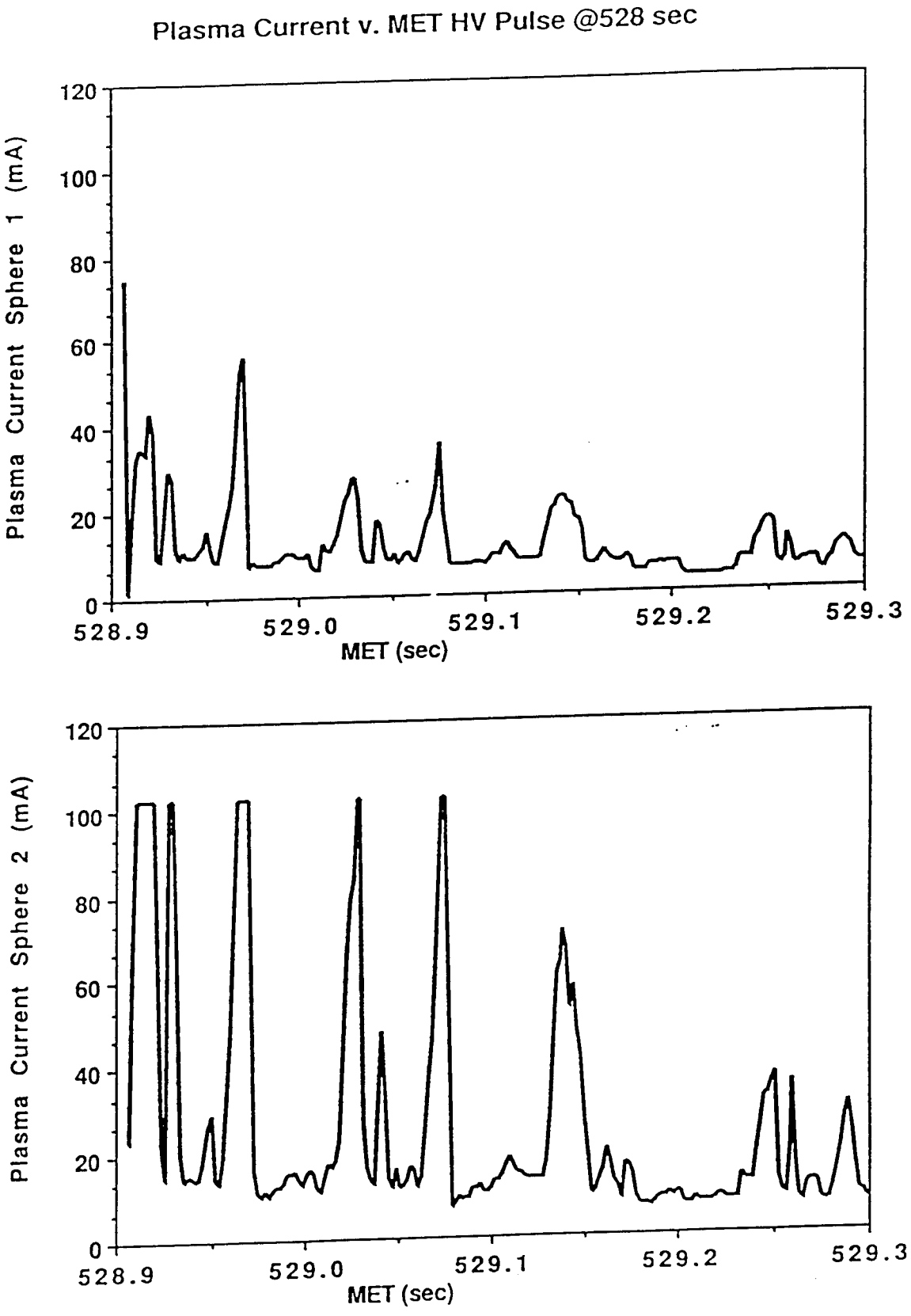
Plasma Current v. MET HV Pulse @528 sec
Plasma Current Sphere 1 (mA)
120
100
80
60
40
20
0
528.9
529.0
529.1
529.2
529.3
MET (sec)
Plasma Current Sphere 2 (mA)
120
100
80
60
40
20
0
528.9
529.0
529.1
529.2
529.3
MET (sec)

Figure 7-8

SPEAR-1 LLLTV Single Frame Images

City Lights Glow around Sphere 1 Edge of airglow layer

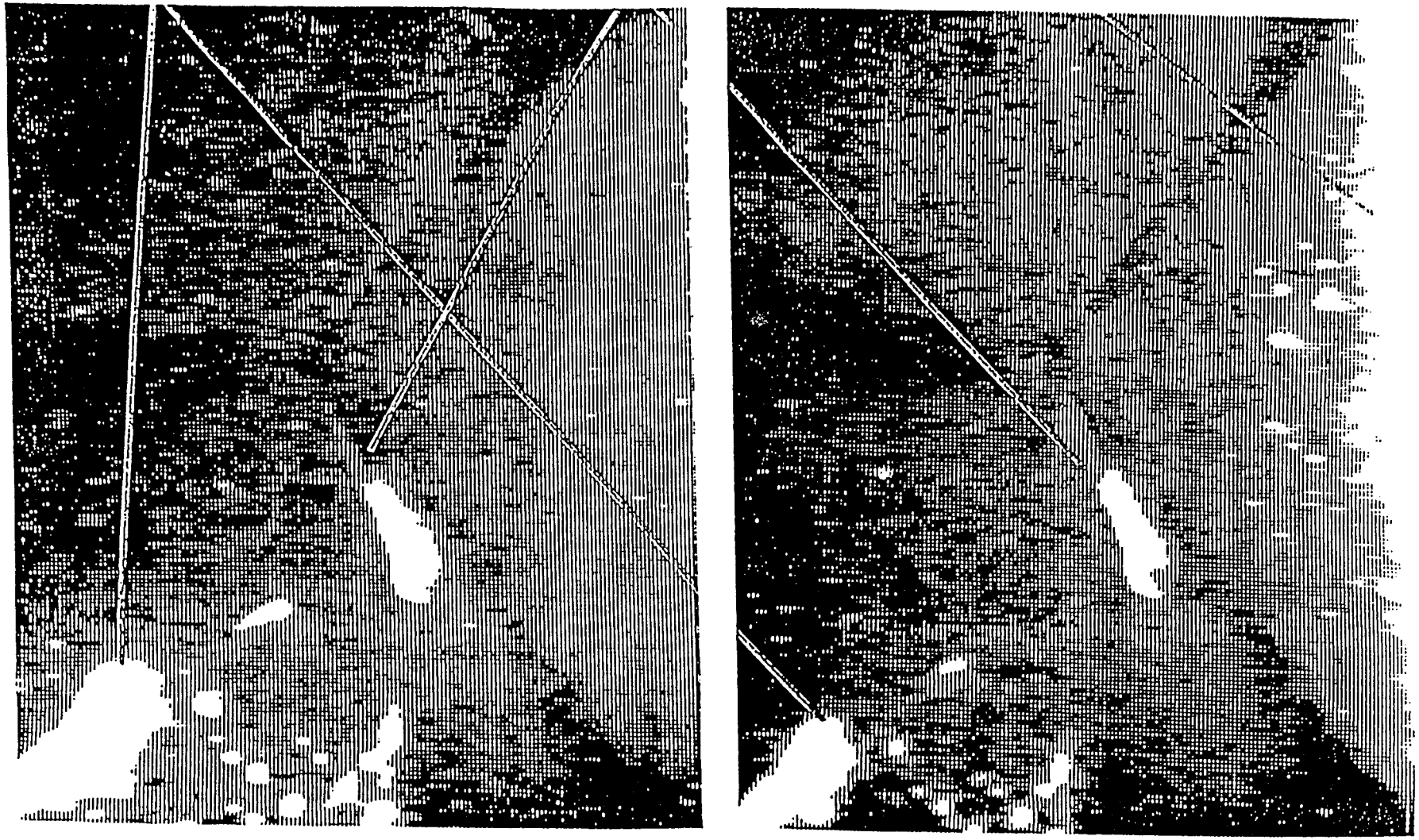

MET 211 sec Alt-282km V_1 = 25,600V

MET 323 sec Alt-365km V_1 = 24,570V

Figure 7-9

Figure 7-10

Ion Flux Energy Spectra to Vehicle during 398sec Discharge

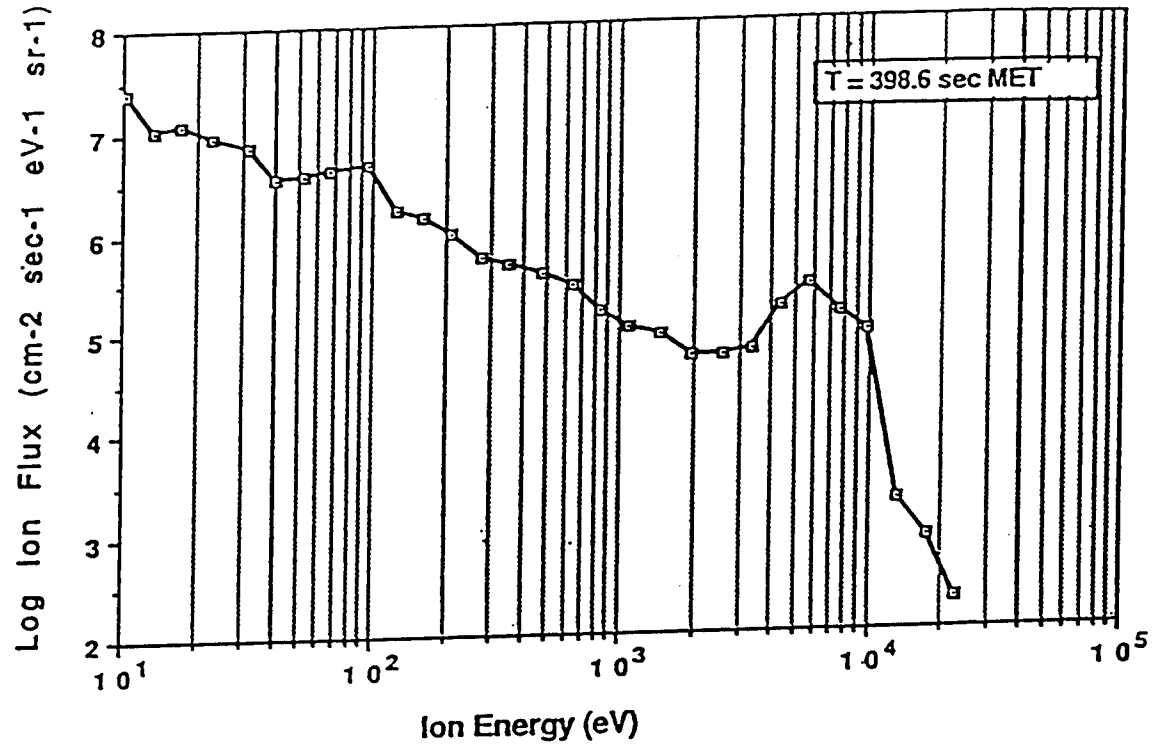

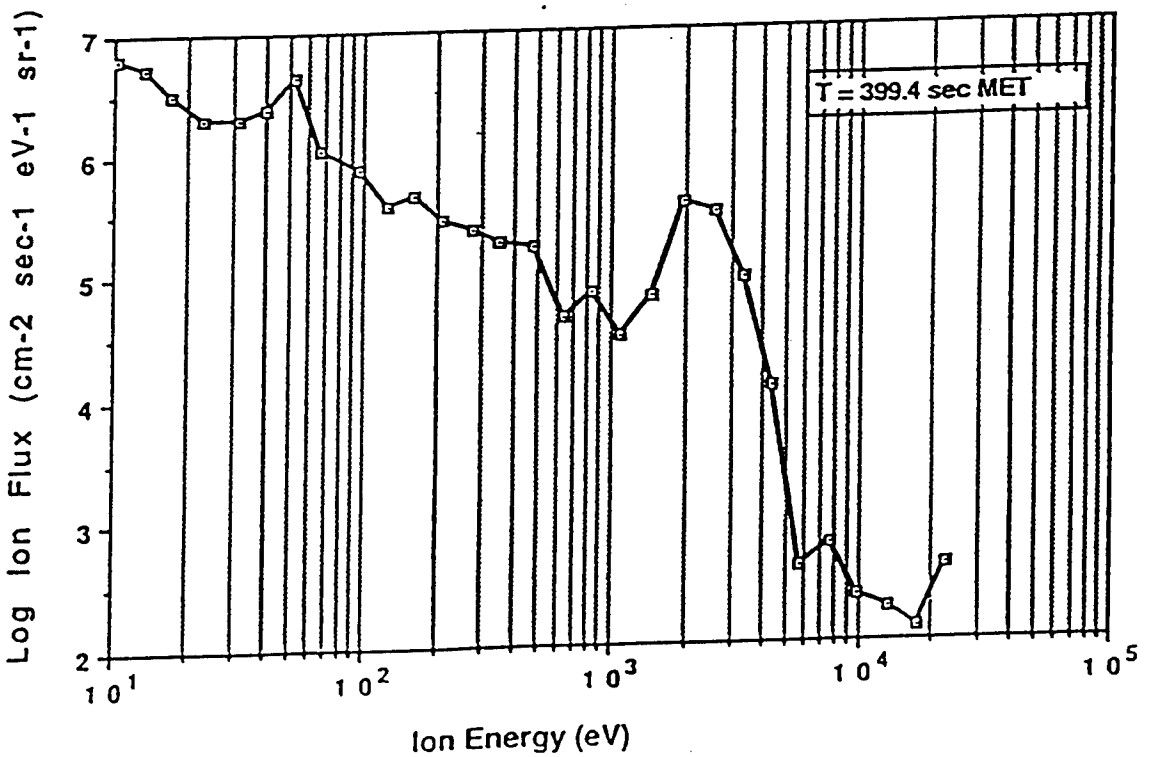

Figure 7-11

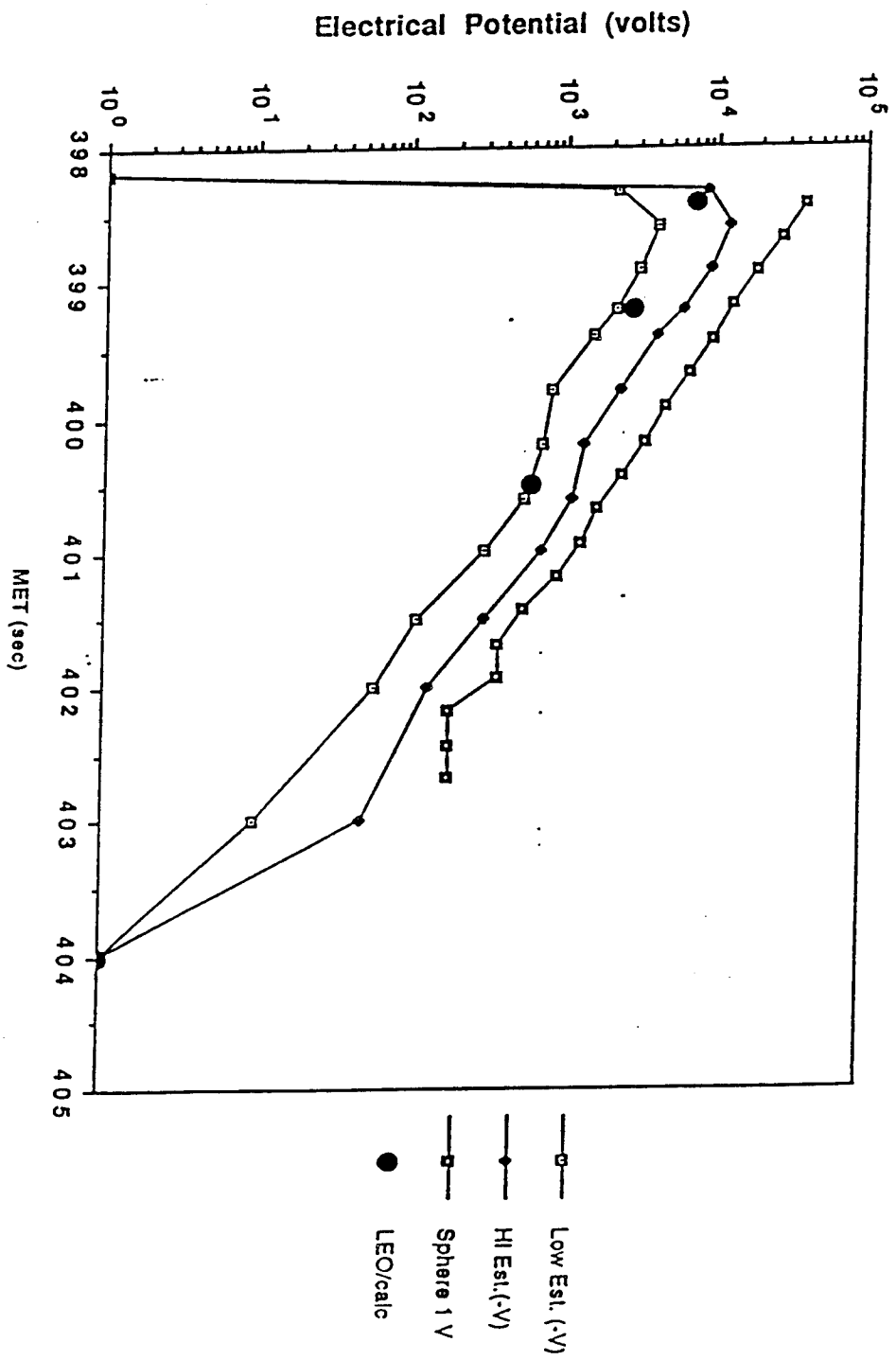
SPEAR-I Vehicle Potential and Sphere-1 Potential
Electrical Potential (volts)
10^0
10^1
10^2
10^3
10^4
10^5
398
399
400
401
402
403
404
405
MET (sec)
Low Est. (-V)
HI Est.(-V)
Sphere 1 V
LEO/calc

Figure 7-12

APPENDIX B

HOW TO USE THE SPEAR-1 FORMATTING/CALIBRATING PROGRAM

How To Use The SPEAR-1 Formatting/Calibrating Program

The formatting/calibrating program for SPEAR-1 PCM data is available on the Center for Atmospheric and Space Sciences Harris 800 computer. To use it, log on the Harris, change default directory (MO QL=0252PCM) and run the program (RUN PCM). After initializing, the program displays the following menu:

```
WHICH DATA DO YOU WANT TO PROCESS?

  1. PREDEFINED DATA SETS    2. CACHE MEMORY          3. HV SYSTEM MONITOR
  4. PHOTOMETERS             5. LANGMUIR PROBE        6. MAGNETOMETER
  7. PLASMA CONTACTOR        8. NEUTRAL PRESSURE      9. PARTICLE DETECTORS
 10. PAYLOAD CONTROL        11. PYRO CONTROL         12. TELEMETRY
 13. TELEVISION CAMERA      14. ATTITUDE CONTROL     15. VEHICLE
 16. DERIVED QUANTITIES     17. VARIATIONS ON TIME

 44.  CLEAR DATA STREAMS
 55.  OPEN ANOTHER INPUT DATA FILE:(SPR1.FLT)
 66.  OPEN ANOTHER OUTPUT FILE:    (PCM.DAT )
 77.  SET START AND STOP TIMES:    74.58100000        643.8750000
 88.  SET SAMPLE FREQUENCY:  EVERY         1
 99.  SELECTED DATA STREAMS:

            Data not yet output!

999.  QUIT
```

and awaits the user to input an integer number. To access the data under the general heading HV SYSTEM MONITOR enter the number 3. The appropriate sub-menu is the displayed:

```
HV SYSTEM MONITOR

ENTER A NUMBER

  1. DC SPH1 I(T)
  2. DC SPH1 I(S)
  3. DC SPH1 HV
  4. DC SPH2 I(T)
  5. DC SPH2 I(S)
  6. DC SPH2 HV
  7. DC SPH1 I(T) X 10
  8. DC SPH2 I(T) X 10
  9. HV +28 V DC
 10. HV AC VOLTAGE
 11. HV PRESSURE

 99.  RETURN TO MAIN MENU
```

To chose data streams within the sub-menu, enter the number corresponding to the channel desired. Up to 10 data channels may be selected from any combination of sub-menus. To return from the current sub-menu to the main menu, enter 99. For example, the main menu would appear as below if the numbers 1,2,3, and 99 were entered. Note that the selected data channels are displayed in the main menu. The hilighting is not shown on the user terminal but is included here for emphasis.

```
WHICH DATA DO YOU WANT TO PROCESS?

  1. PREDEFINED DATA SETS   2. CACHE MEMORY          3. HV SYSTEM MONITOR
  4. PHOTOMETERS            5. LANGMUIR PROBE        6. MAGNETOMETER
  7. PLASMA CONTACTOR       8. NEUTRAL PRESSURE      9. PARTICLE DETECTORS
 10. PAYLOAD CONTROL       11. PYRO CONTROL         12. TELEMETRY
 13. TELEVISION CAMERA     14. ATTITUDE CONTROL     15. VEHICLE
 16. DERIVED QUANTITIES    17. VARIATIONS ON TIME

 44.  CLEAR DATA STREAMS
 55.  OPEN ANOTHER INPUT DATA FILE:(SPR1.FLT)
 66.  OPEN ANOTHER OUTPUT FILE:    (PCM.DAT )
 77.  SET START AND STOP TIMES:    74.58100000        643.8750000
 88.  SET SAMPLE FREQUENCY:  EVERY          1
 99.  SELECTED DATA STREAMS:     SPH1_I(T)     SPH1_I(S)        SPH1_HV

             Data not yet output!

999.  QUIT
```

When the program initializes it chooses start and stop times corresponding to the first and last record in the chosen data file. Generally only a small subset of the entire mission is required. To change the start and stop time enter 77 in the main menu. The program will prompt for the desired start and stop times in MET seconds. After entering, for example, 190 and 191 seconds for the start and stop time respectively, the main menu will appear as:

```
WHICH DATA DO YOU WANT TO PROCESS?

  1. PREDEFINED DATA SETS   2. CACHE MEMORY          3. HV SYSTEM MONITOR
  4. PHOTOMETERS            5. LANGMUIR PROBE        6. MAGNETOMETER
  7. PLASMA CONTACTOR       8. NEUTRAL PRESSURE      9. PARTICLE DETECTORS
 10. PAYLOAD CONTROL       11. PYRO CONTROL         12. TELEMETRY
 13. TELEVISION CAMERA     14. ATTITUDE CONTROL     15. VEHICLE
 16. DERIVED QUANTITIES    17. VARIATIONS ON TIME

 44.  CLEAR DATA STREAMS
 55.  OPEN ANOTHER INPUT DATA FILE:(SPR1.FLT)
 66.  OPEN ANOTHER OUTPUT FILE:    (PCM.DAT )
 77.  SET START AND STOP TIMES:    190.0000000          191.0000000
 88.  SET SAMPLE FREQUENCY:  EVERY          1
 99.  SELECTED DATA STREAMS:     SPH1_I(T)    SPH1_I(S)      SPH1_HV

             Data not yet output!

999.  QUIT
```

In similar fashion, one may change the output data file, the input data set and the sample frequency. The sample frequency defaults to the maximum telemetered rate (every 1) but may be slowed (every 2, every 3, ...,every 1000,...) if the full rate is not required. When all parameters are as desired, enter the value 99 and the program will read the chosen data channels from the unformatted input file, calibrate, and write the data to the formatted output file over the range of chosen MET times. The menu will then appear with a message indicating that the data has been output:

```
WHICH DATA DO YOU WANT TO PROCESS?

  1. PREDEFINED DATA SETS    2. CACHE MEMORY           3. HV SYSTEM MONITOR
  4. PHOTOMETERS             5. LANGMUIR PROBE         6. MAGNETOMETER
  7. PLASMA CONTACTOR        8. NEUTRAL PRESSURE       9. PARTICLE DETECTORS
 10. PAYLOAD CONTROL        11. PYRO CONTROL          12. TELEMETRY
 13. TELEVISION CAMERA      14. ATTITUDE CONTROL      15. VEHICLE
 16. DERIVED QUANTITIES     17. VARIATIONS ON TIME

 44.  CLEAR DATA STREAMS
 55.  OPEN ANOTHER INPUT DATA FILE:(SPR1.FLT)
 66.  OPEN ANOTHER OUTPUT FILE:    (PCM.DAT )
 77.  SET START AND STOP TIMES:    190.0000000        191.0000000
 88.  SET SAMPLE FREQUENCY:  EVERY          1
 99.  SELECTED DATA STREAMS:    SPH1_I(T)   SPH1_I(S)     SPH1_HV

          this data set has been output.

999.  QUIT
```

Enter ing 999 returns the user to the Harris operating system. The contents of the output file may be viewed by typing `TY PCM.DAT`.

APPENDIX C

SPEAR-1, COLLECTION OF ALL DISCHARGE/CURRENT AND VOLTAGE PLOTS

SPEAR-1

Collection of all discharge/current and voltage plots

October 1988

SPEAR-1

Discharge current and voltage plots

This addendum to the SPEAR-1 final report contains plots of current and voltage for each of the discharges of the capacitors during the SPEAR-1 flight.

The upper six panels show the measured voltage and currents for the two spheres. The time resolution of the data sampling is approximately 1mS, but in plotting the data this has been reduced to 3mS to more closely match the plotting resolution.

The currents and voltages are shown in engineering units derived from pre-flight calibration of the data channels. They are plotted as a function of mission elapsed time (MET), being the time elapsed since the rocket lift-off. The absolute time origin of MET is December 14, 1987 01:45:00 GMT. The panels of potential show the electrical potential applied between the vehicle body and the appropriate sphere. As explained in the report, this potential is distributed between a rocket body-plasma potential and a sphere-plasma potential.

Below the six parameter plots as a function of time, the altitude of the payload and the attitude of the payload is shown. The three attitude indications have the meanings:

$B \perp S_2\text{-}S_1$	Geomagnetic field perpendicular to the line joining spheres 1 and 2.
$B \parallel S_2\text{-}S_1$	Geomagnetic field parallel to the line joining spheres 1 and 2.
B||Boom	Geomagnetic field parallel to the axis of the graded boom supporting sphere 1.

The two lower panels show the current-voltage characteristics for the plasma current flowing in the rocket-capacitor-sphere system for each of the spheres. The regular patterning seen on these plots is a result of the discrete steps in the digitization of the currents and voltages. Reference to the report will explain that for every alternate discharge sphere-2 was not biassed, in these cases no current-voltage plots were generated.

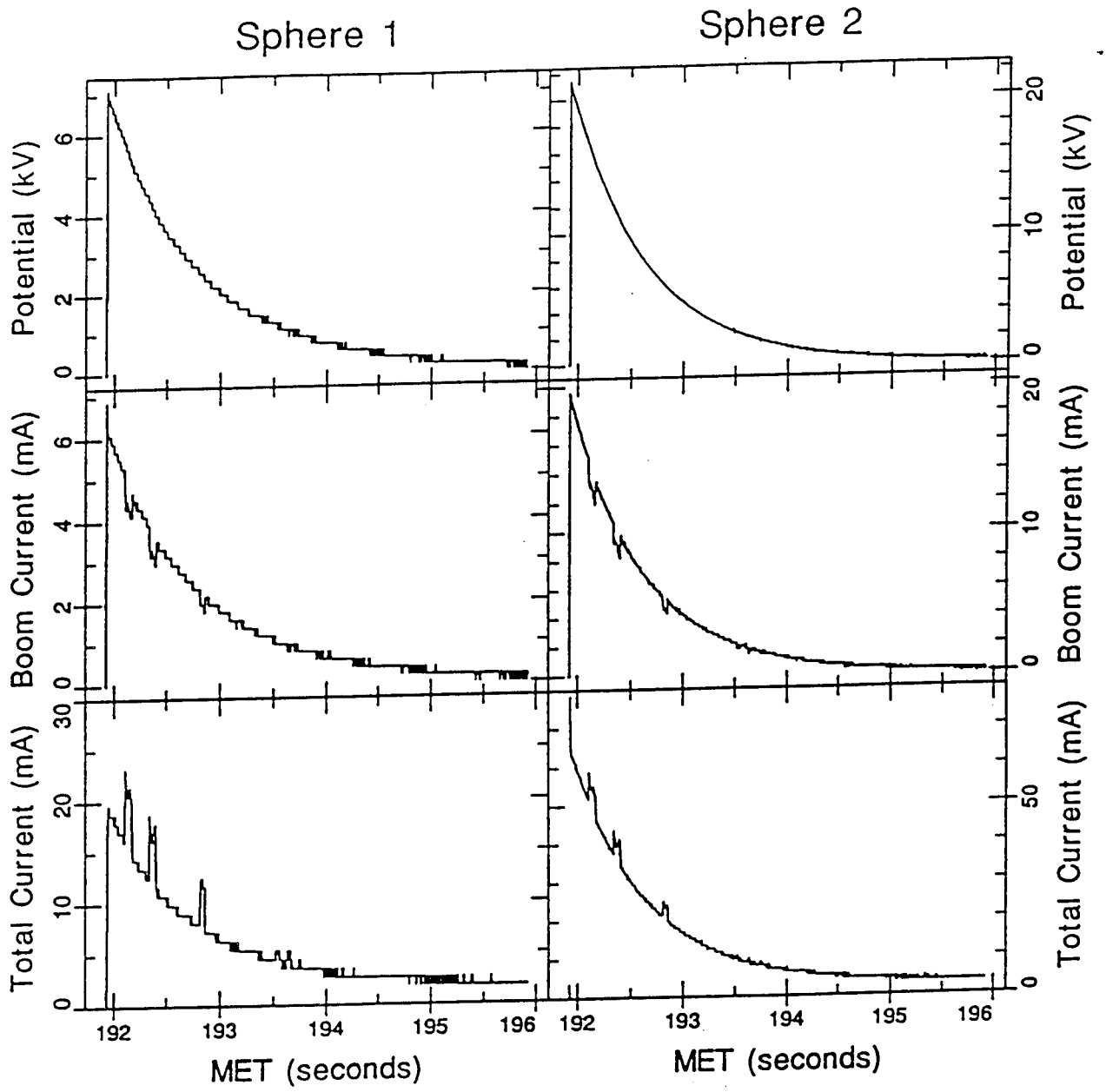
Sphere 1
Sphere 2
Potential (kV)
Boom Current (mA)
Total Current (mA)
MET (seconds)
192
193
194
195
196

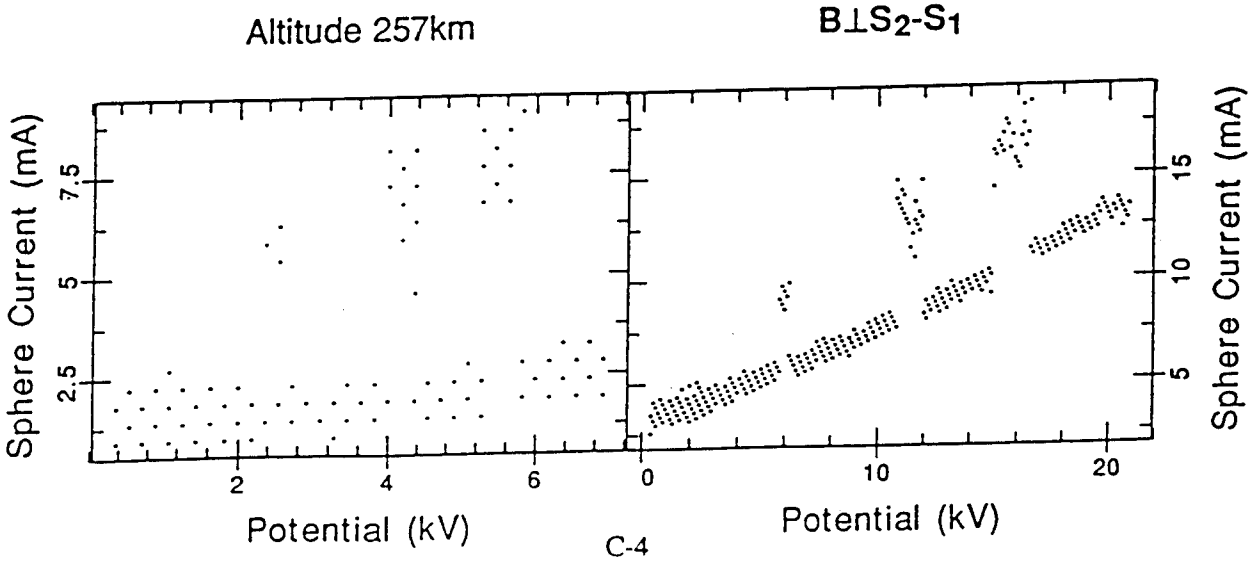
Altitude 257km
B⊥S2-S1
Sphere Current (mA)
Potential (kV)

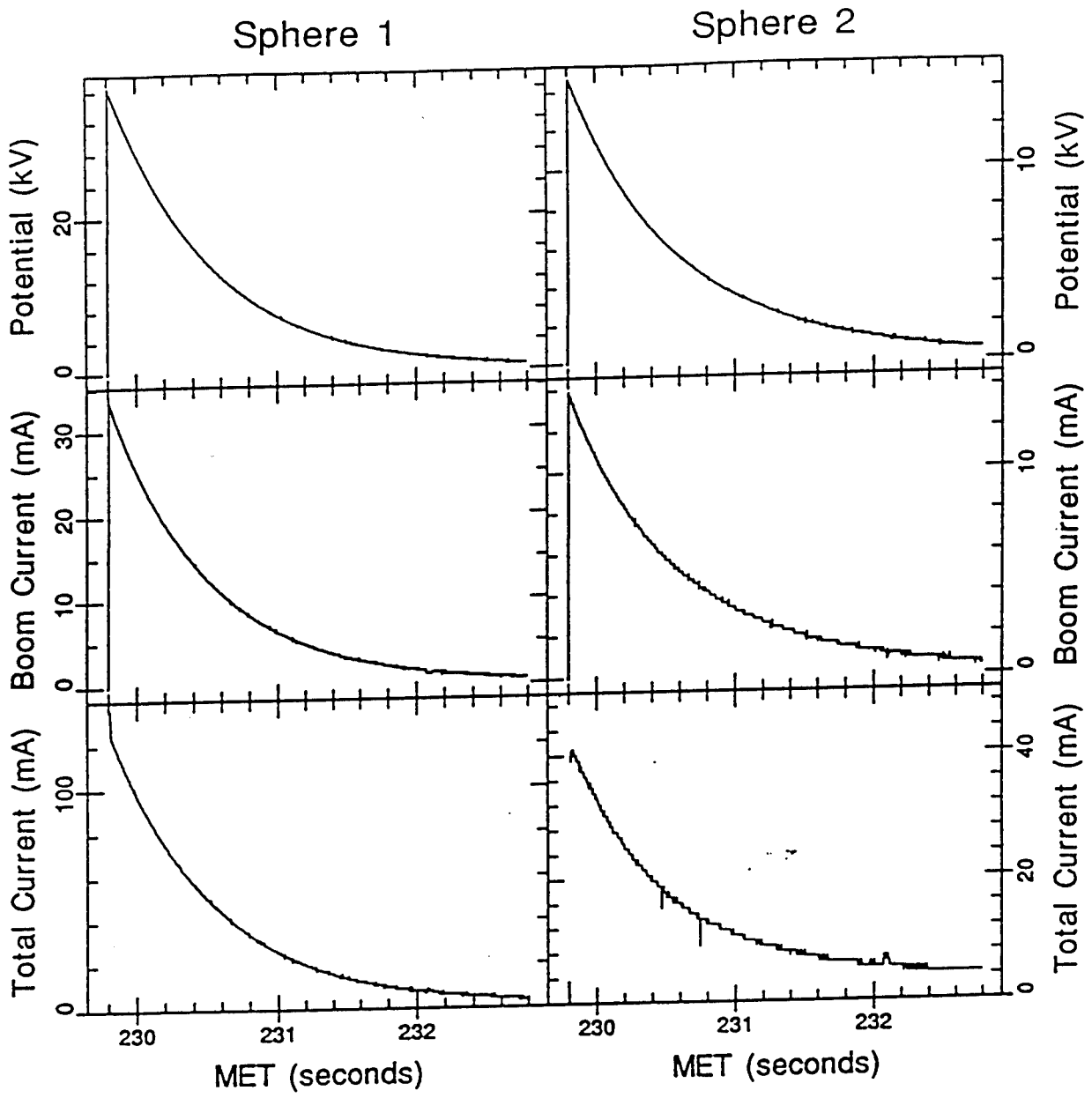

Altitude 303km

$B \perp S_2\text{-}S_1$

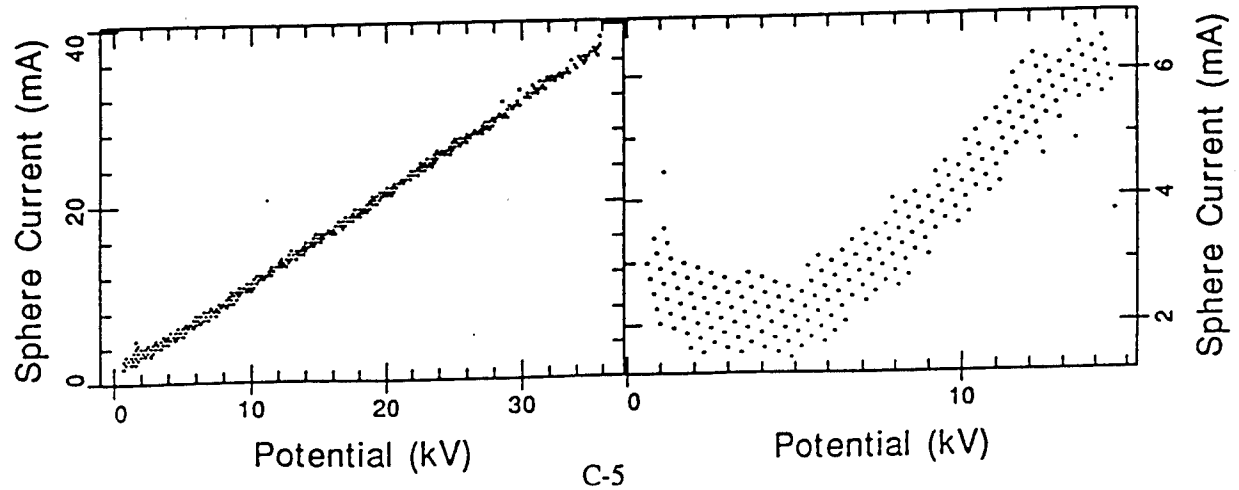

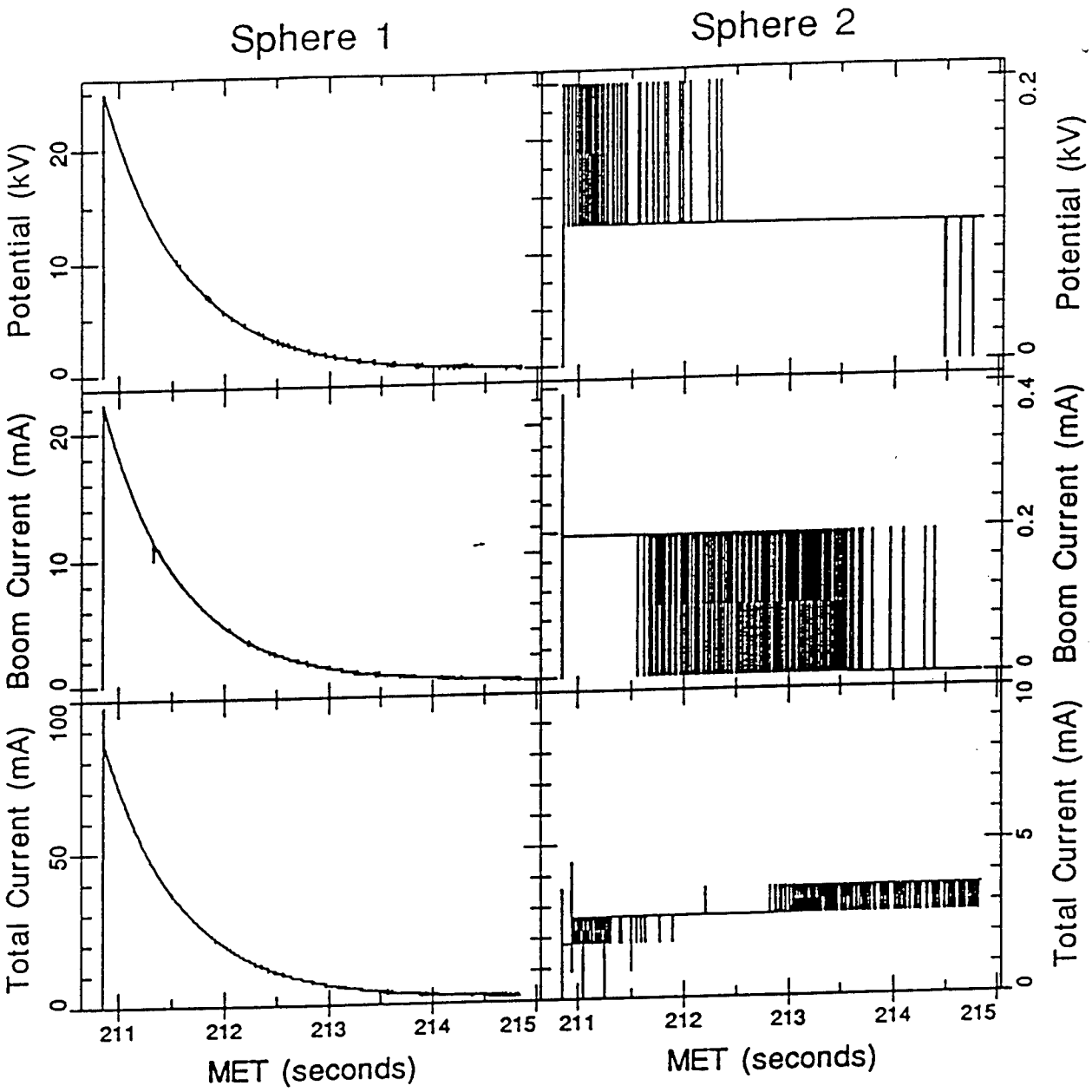

Altitude 282km

$B \perp S_2\text{-}S_1$

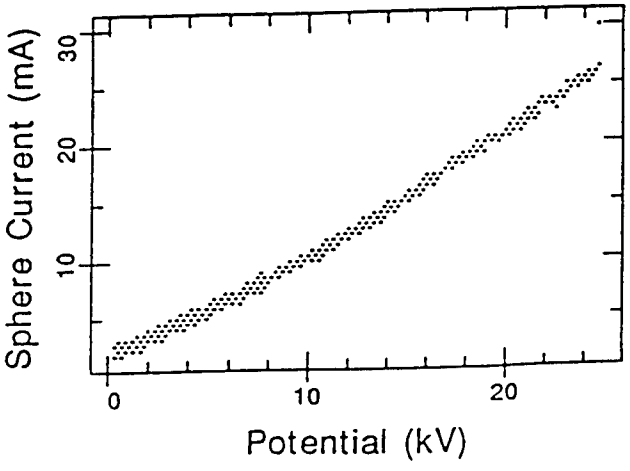

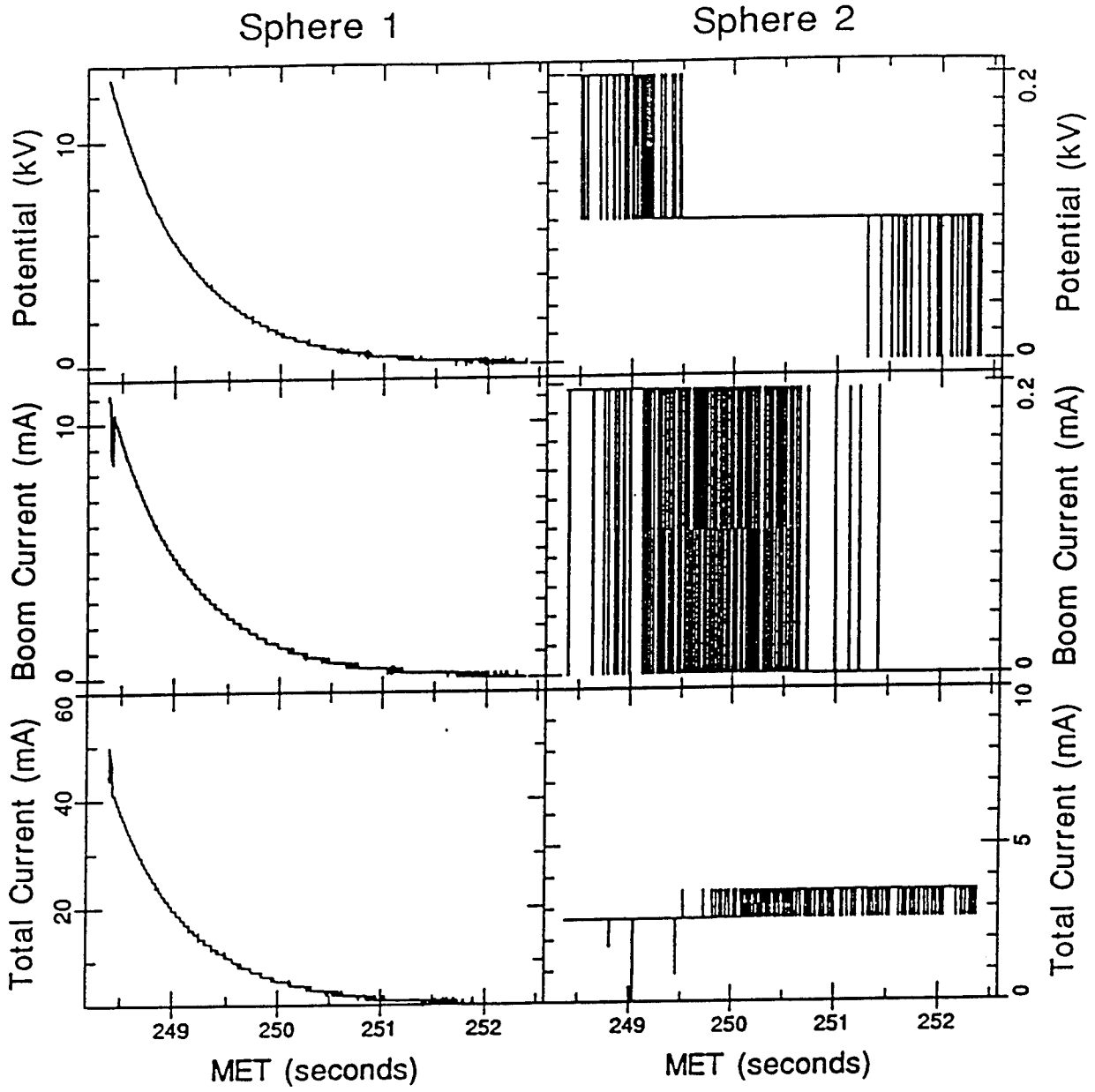

Altitude 321km

$B \perp S_2\text{-}S_1$

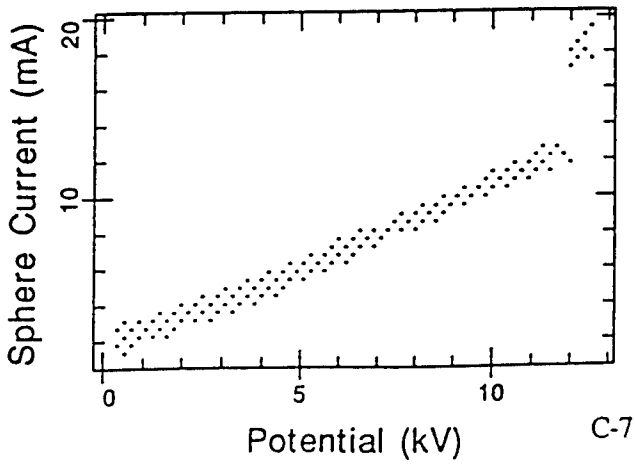

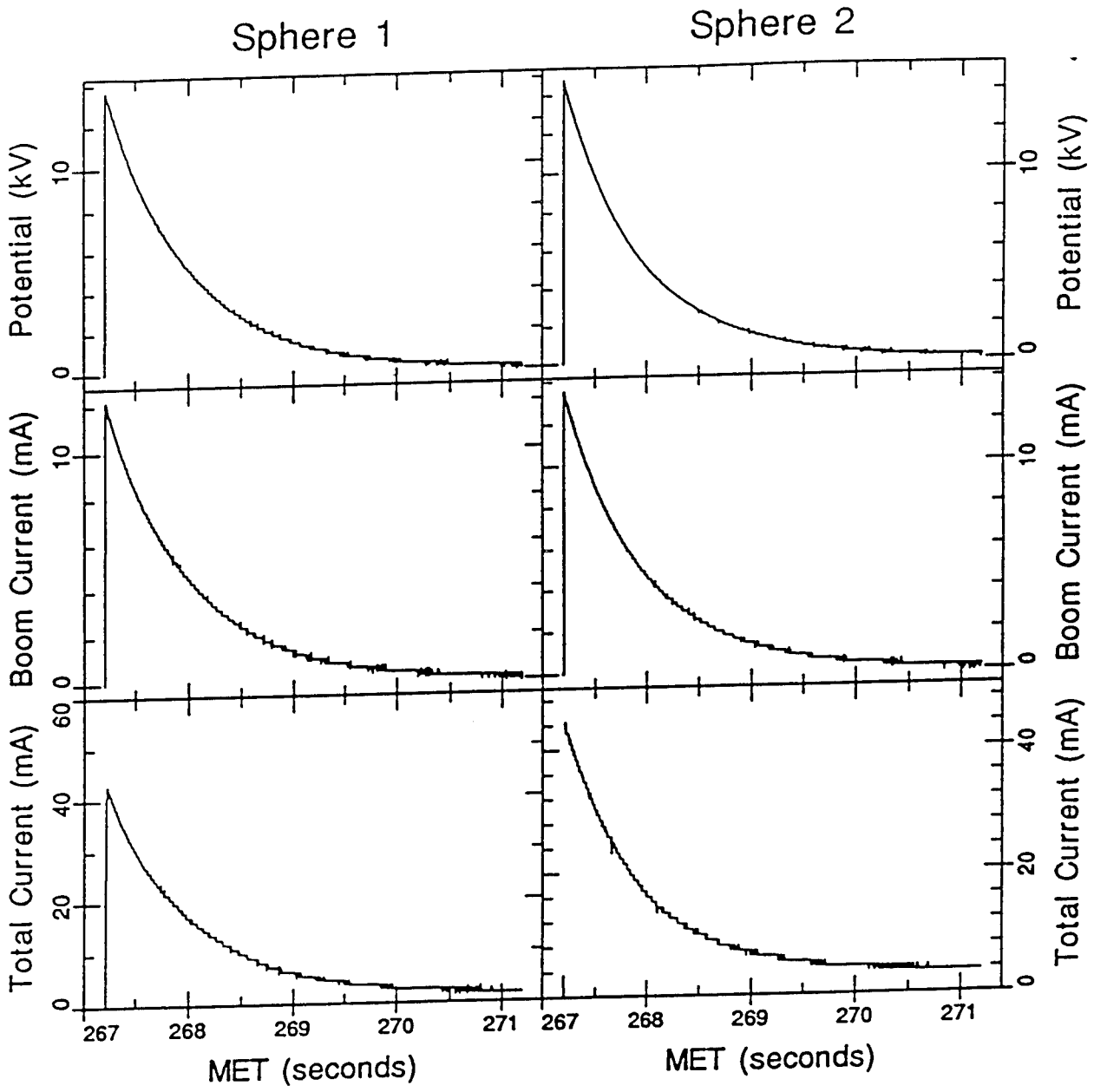

Altitude 337km

$B \perp S_2\text{-}S_1$

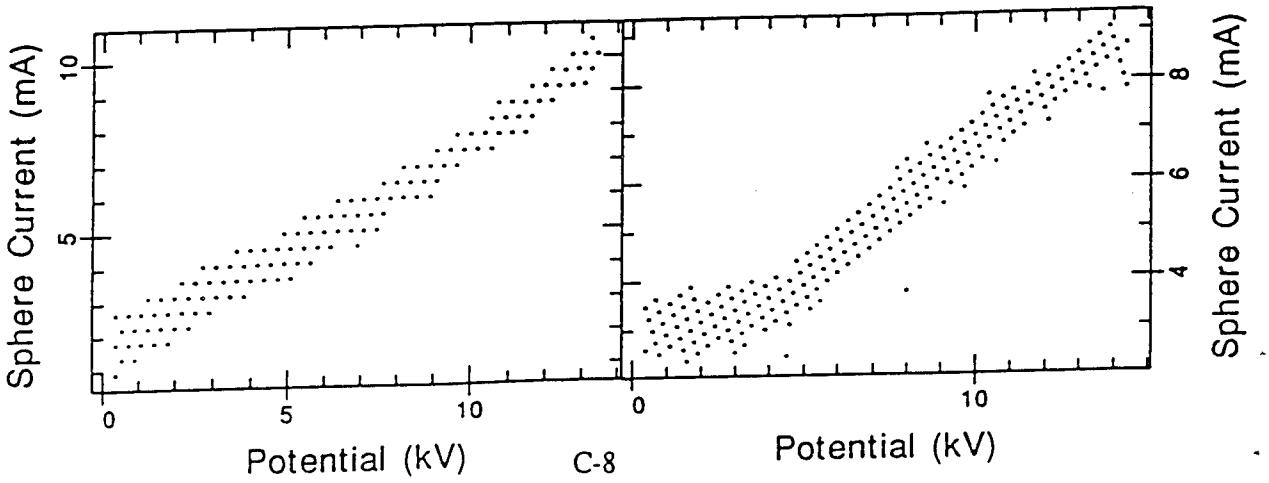

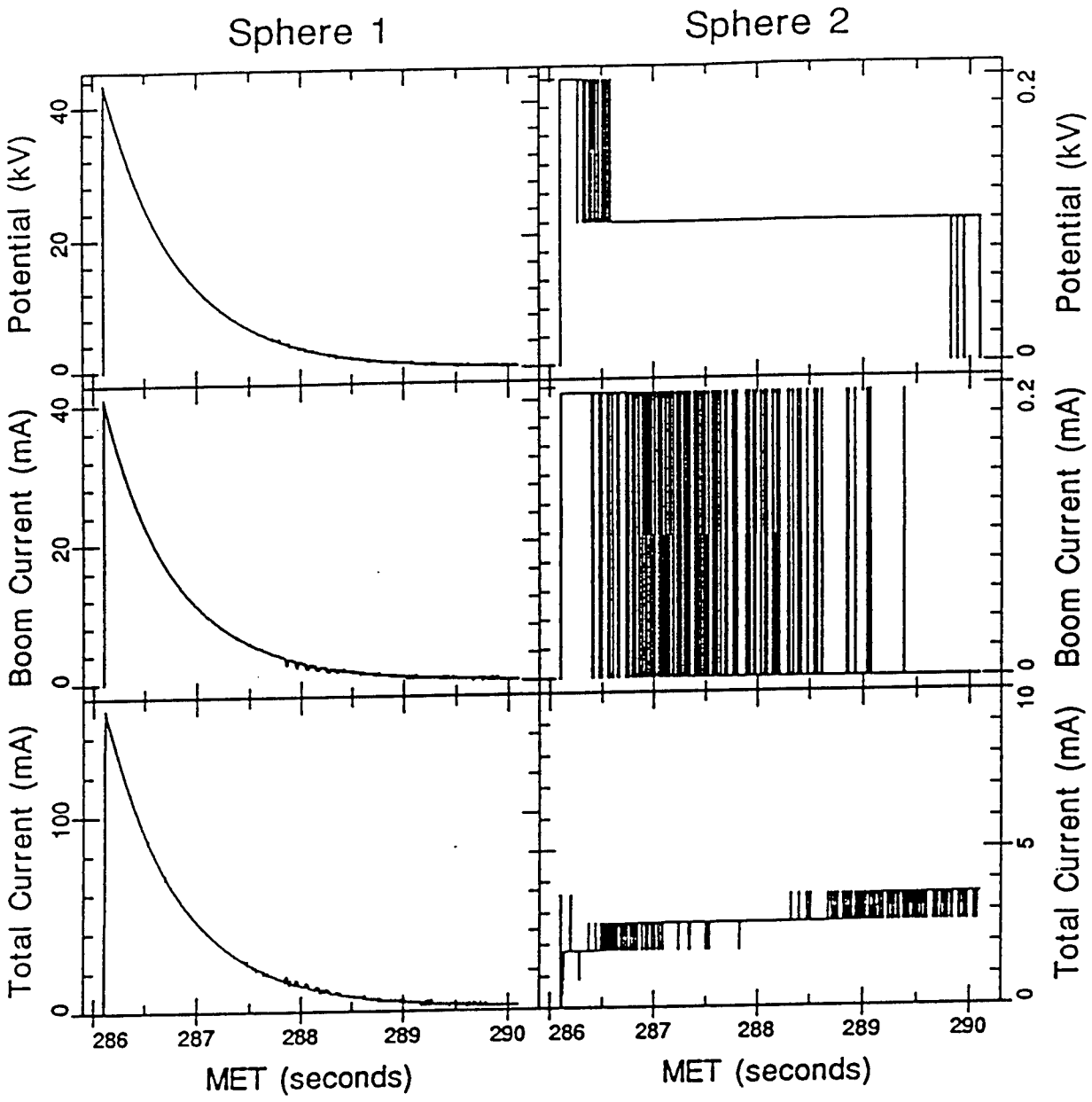

Altitude 350km

$B \perp S_2\text{-}S_1$

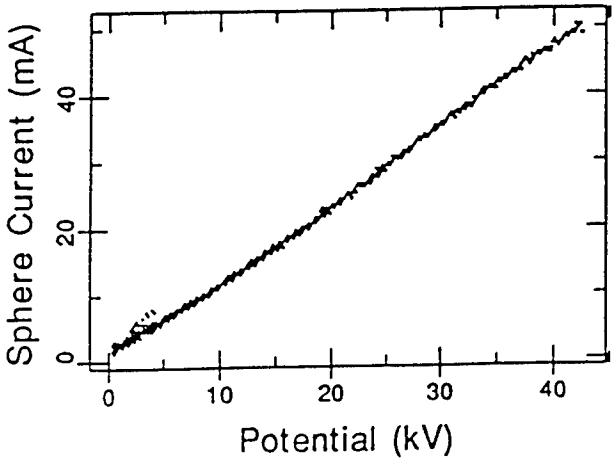

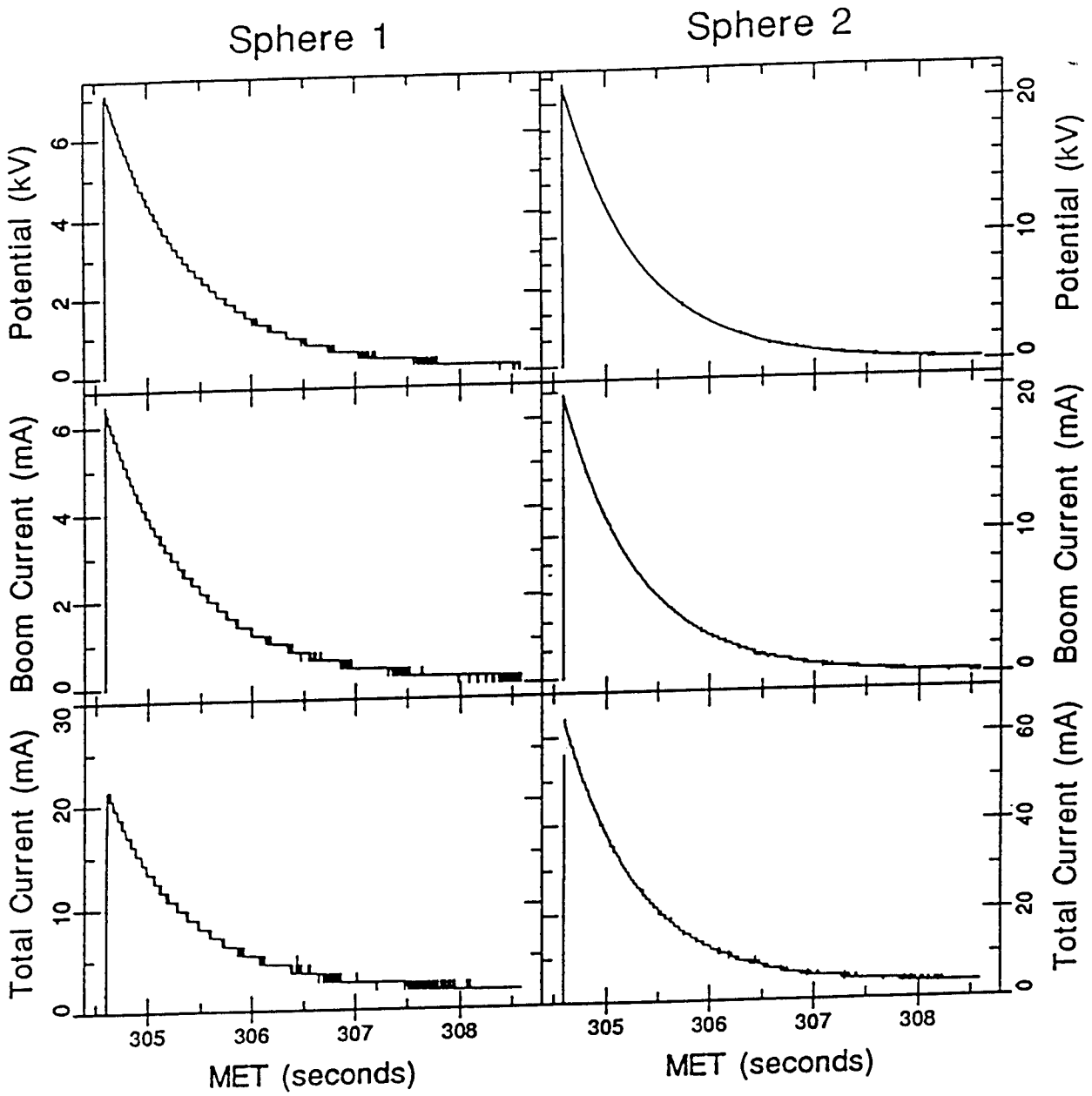

Altitude 359km

$B \perp S_2\text{-}S_1$

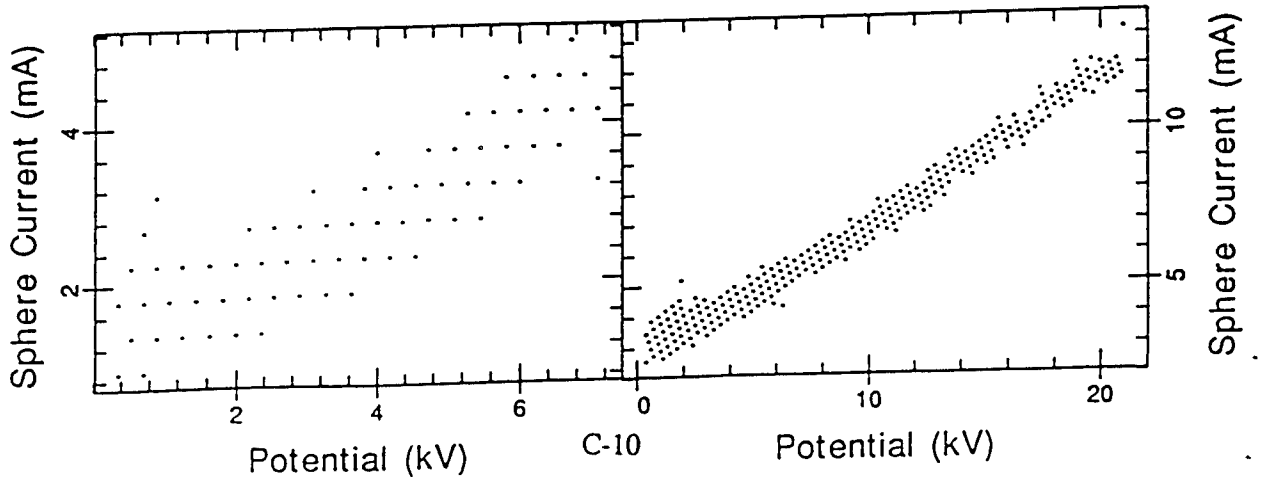

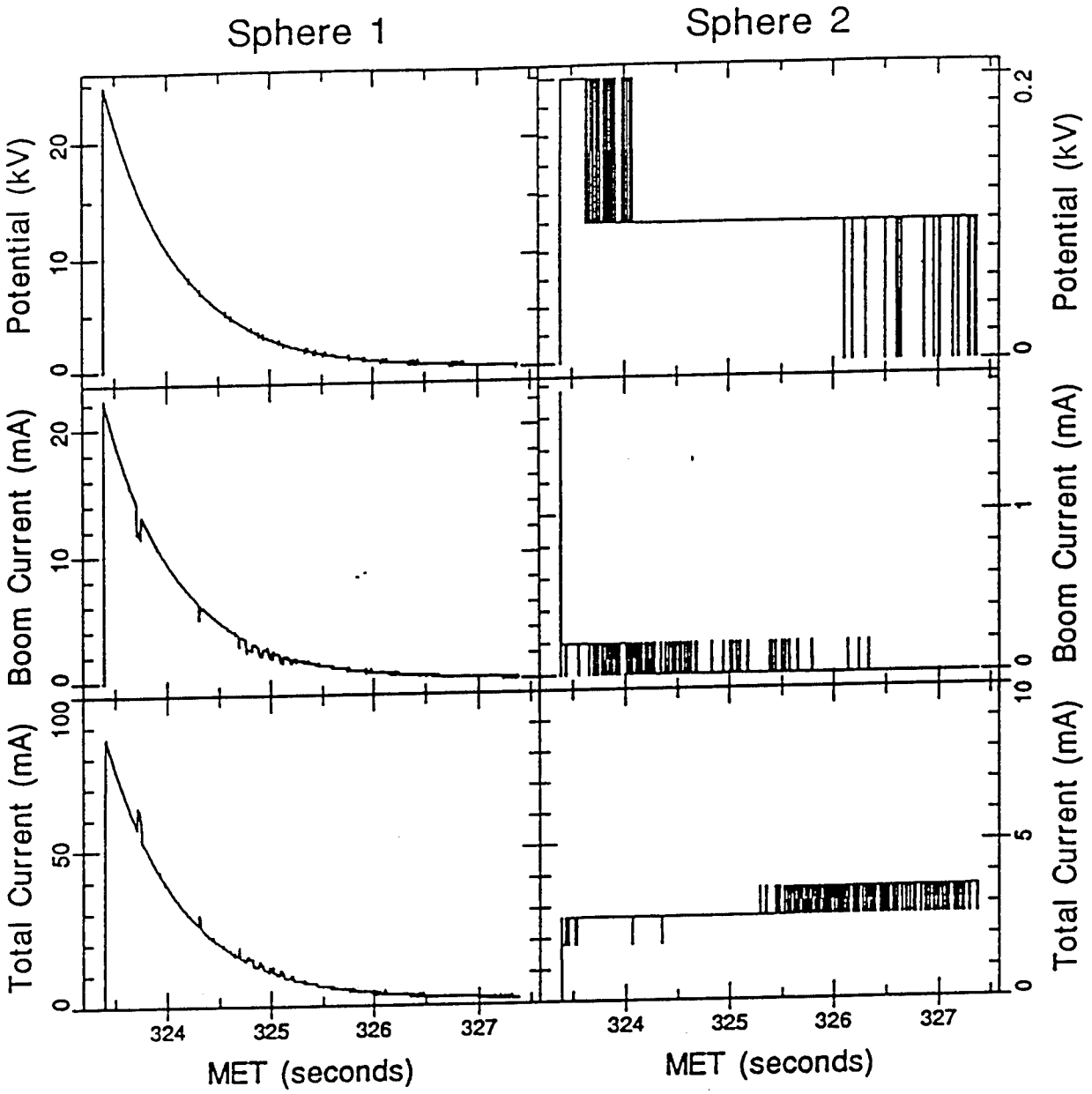

Altitude 365km

$B \perp S_2\text{-}S_1$

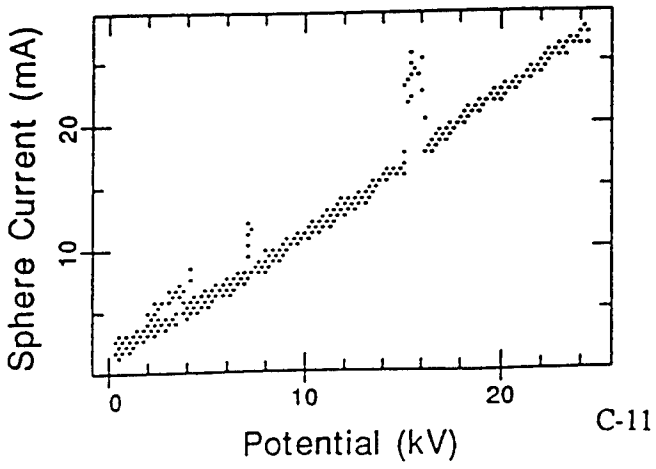

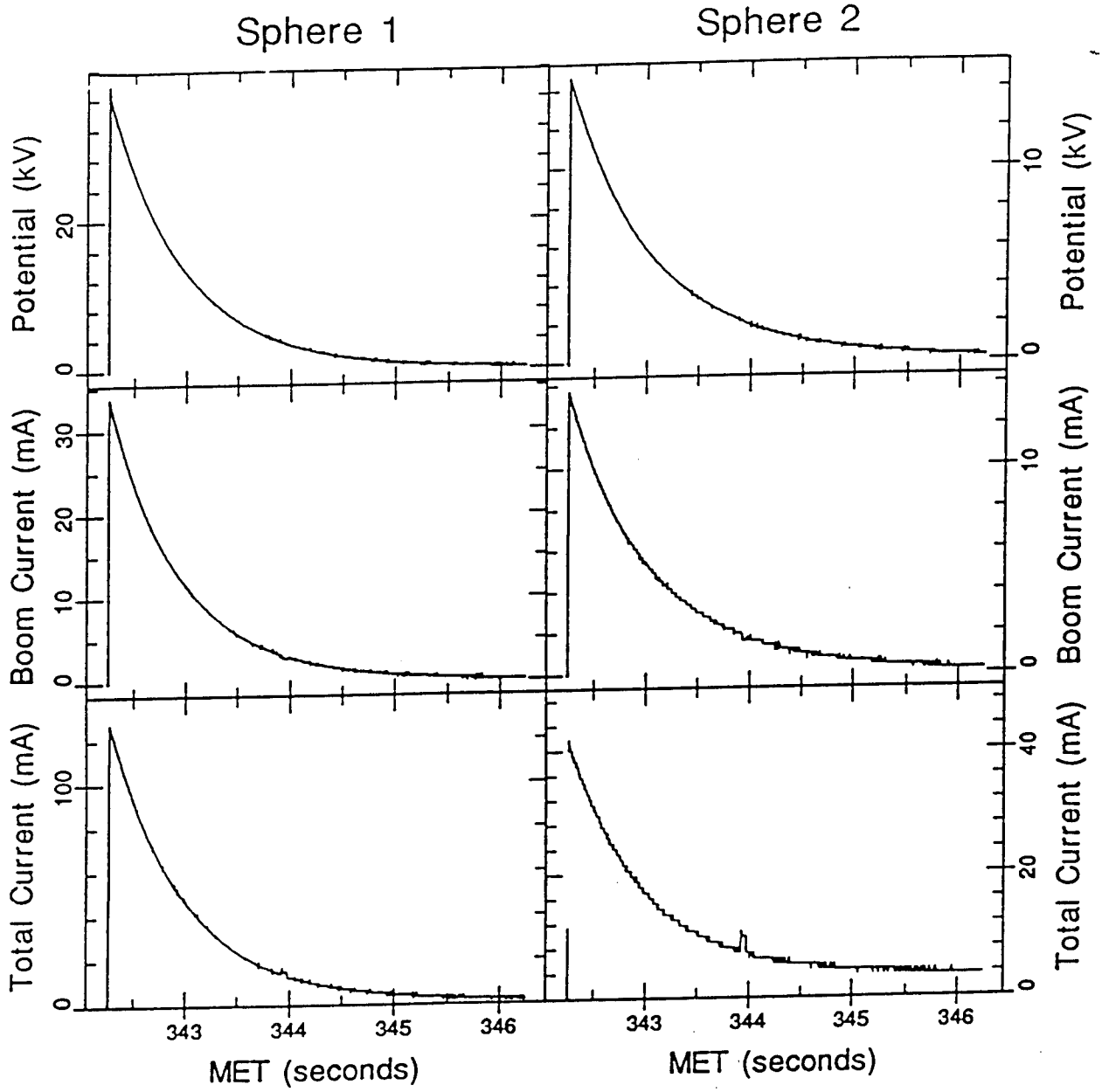

Altitude 369km

$B \perp S_2\text{-}S_1$

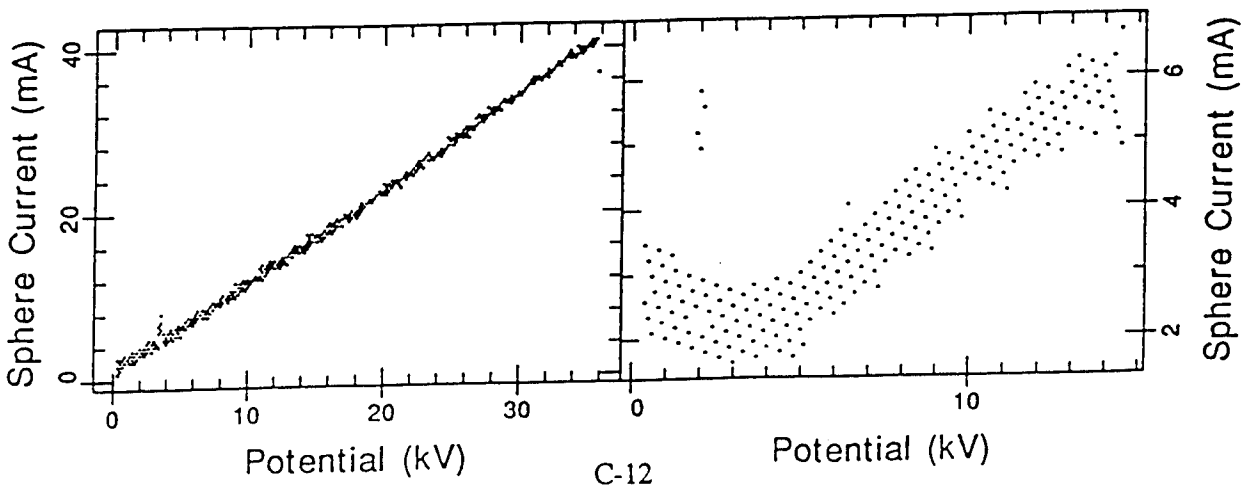

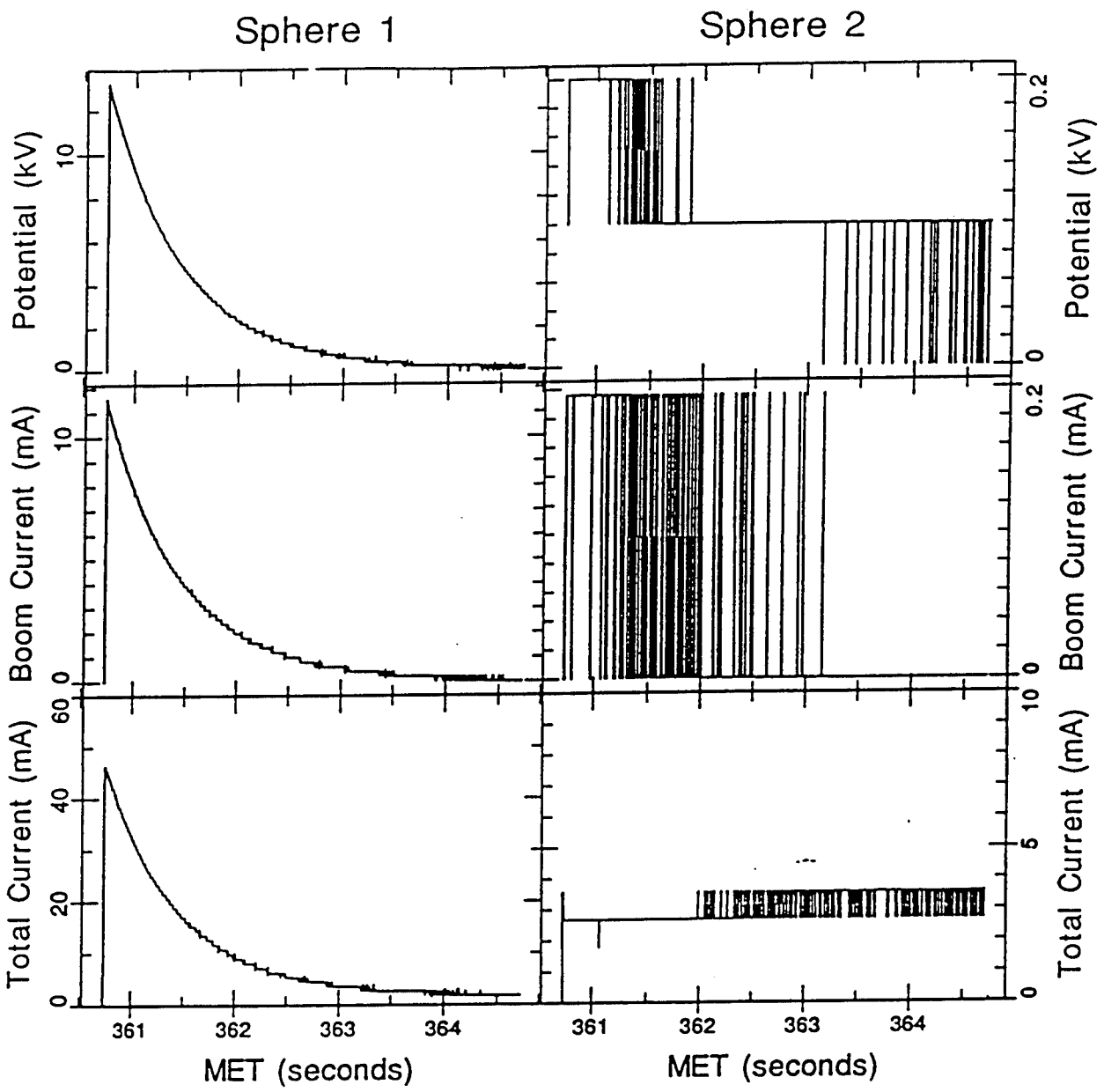

Altitude 369km

$B \perp S_2\text{-}S_1$

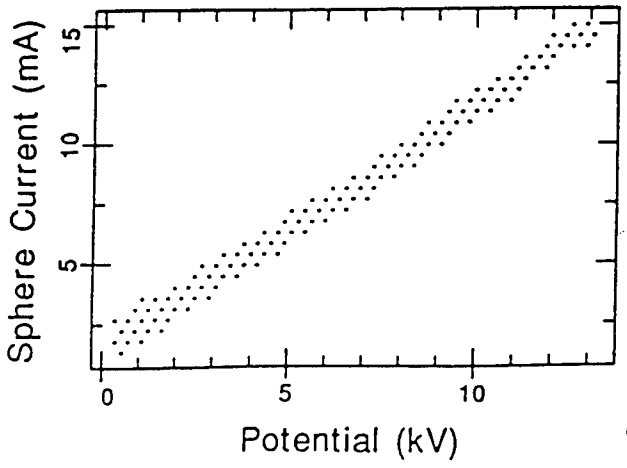

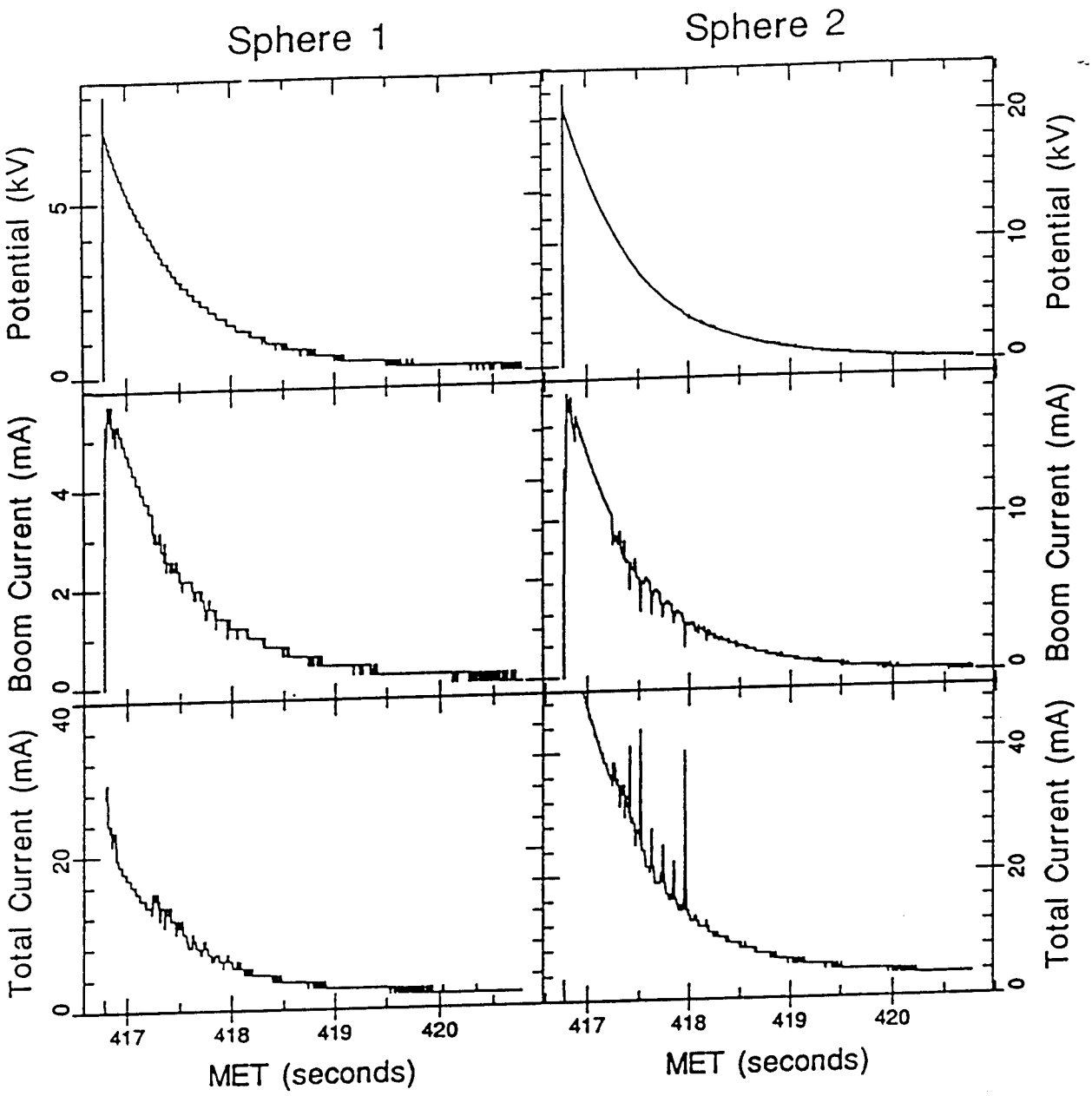

Altitude 352km

$B \| S_2\text{-}S_1$

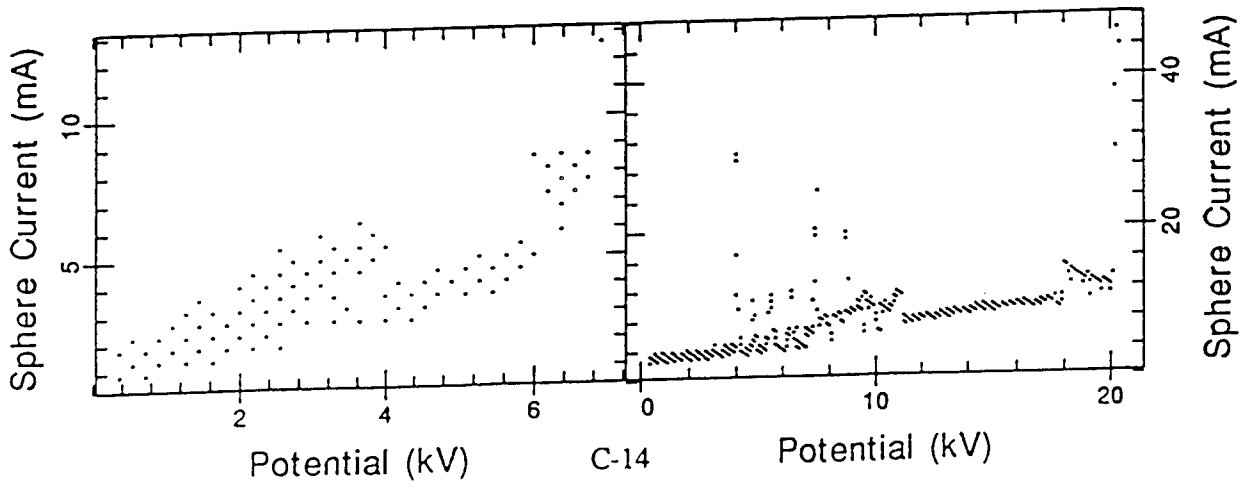

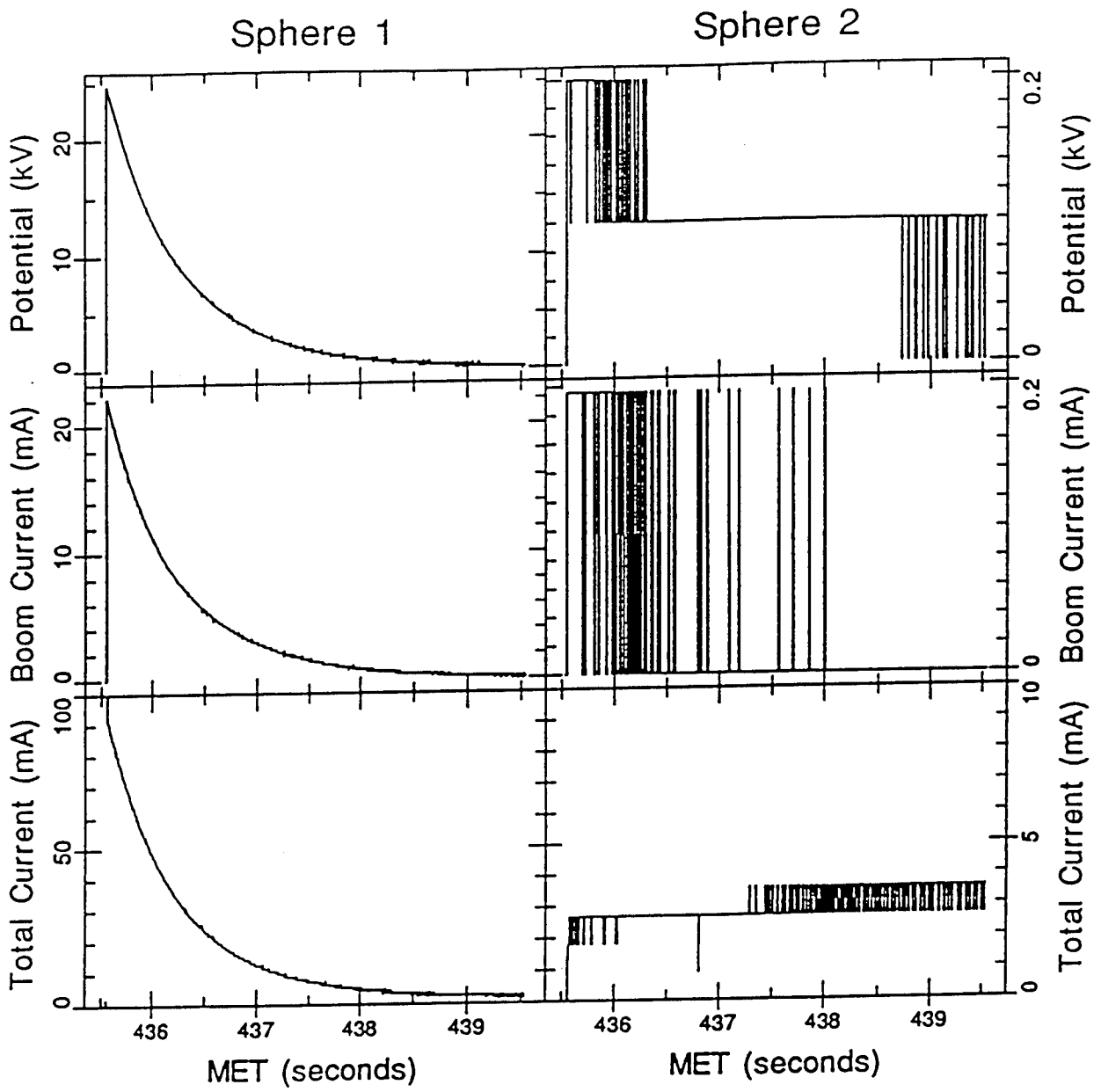

Altitude 340km

$B \| S_2\text{-}S_1$

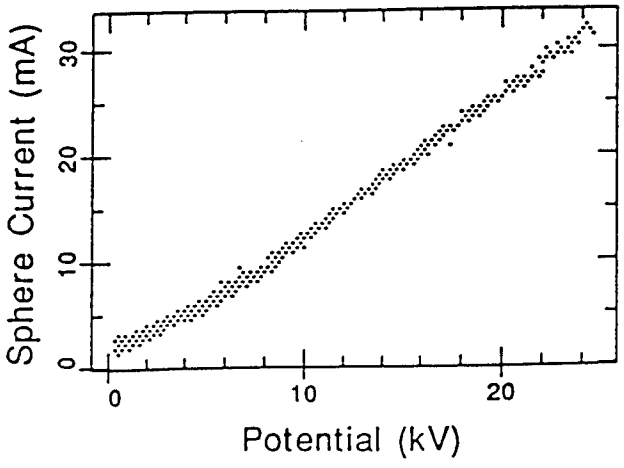

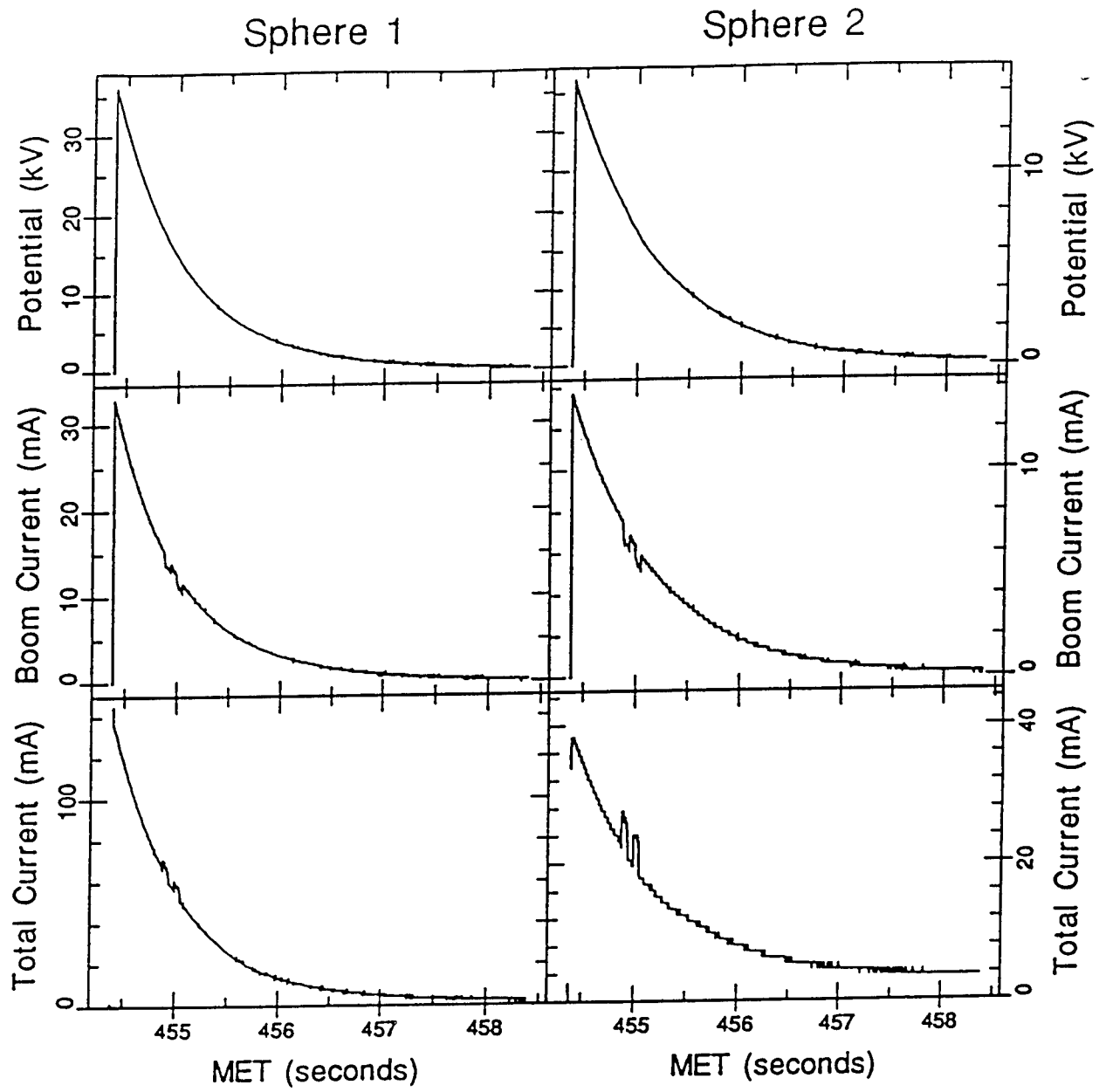

Altitude 325km

$B \| S_2\text{-}S_1$

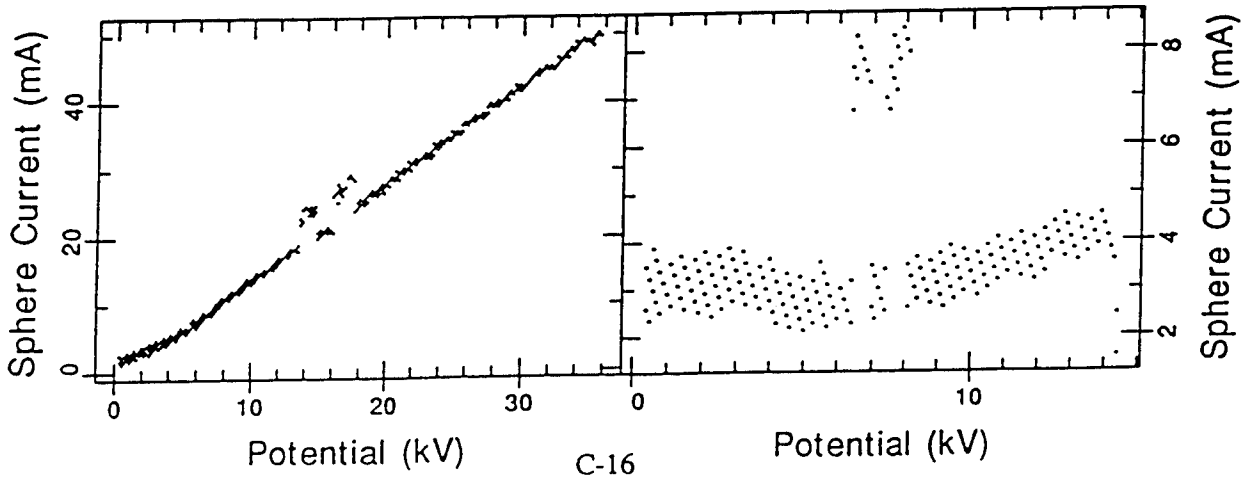

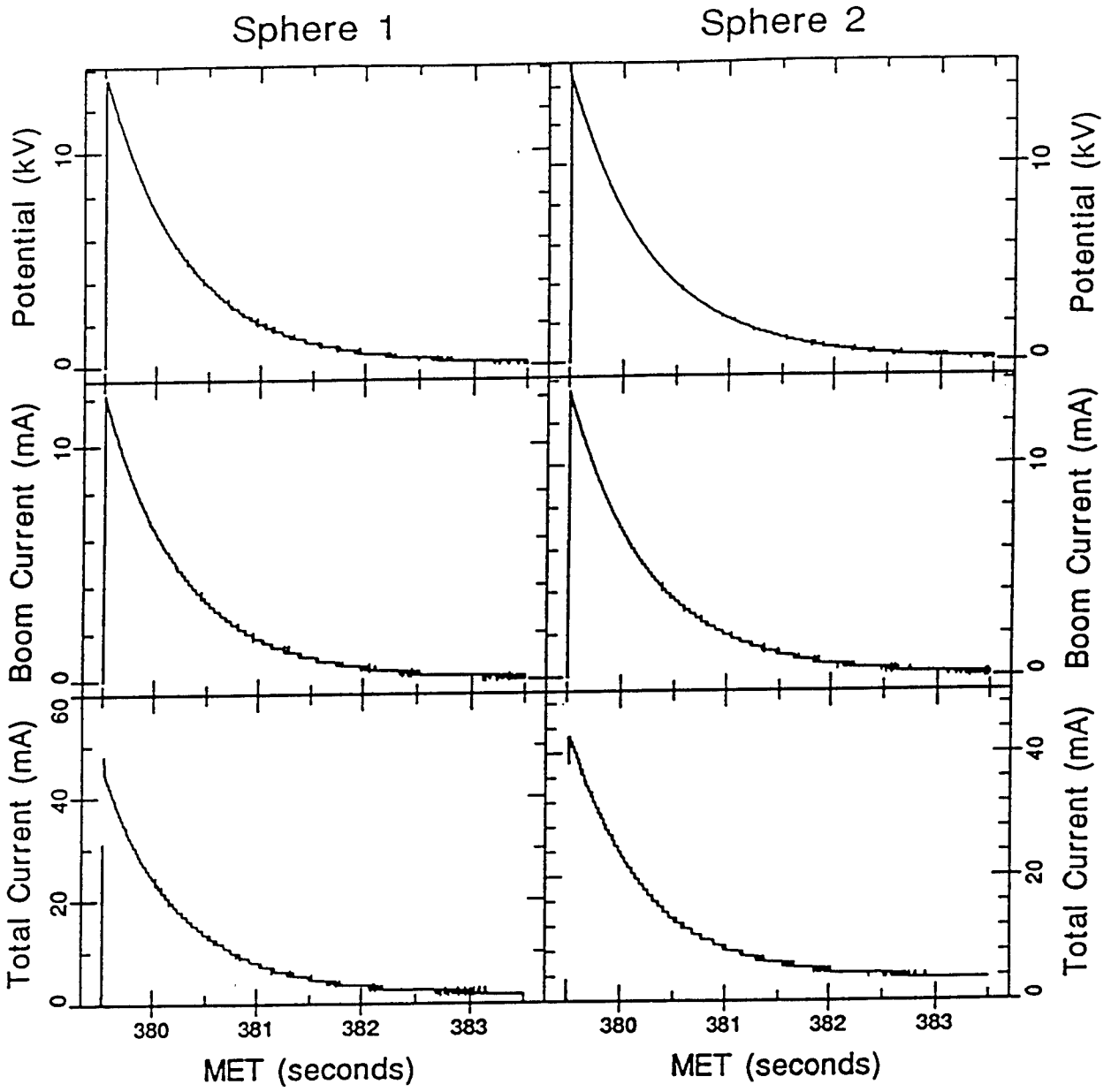

Altitude 366km

$B \perp S_2\text{-}S_1$

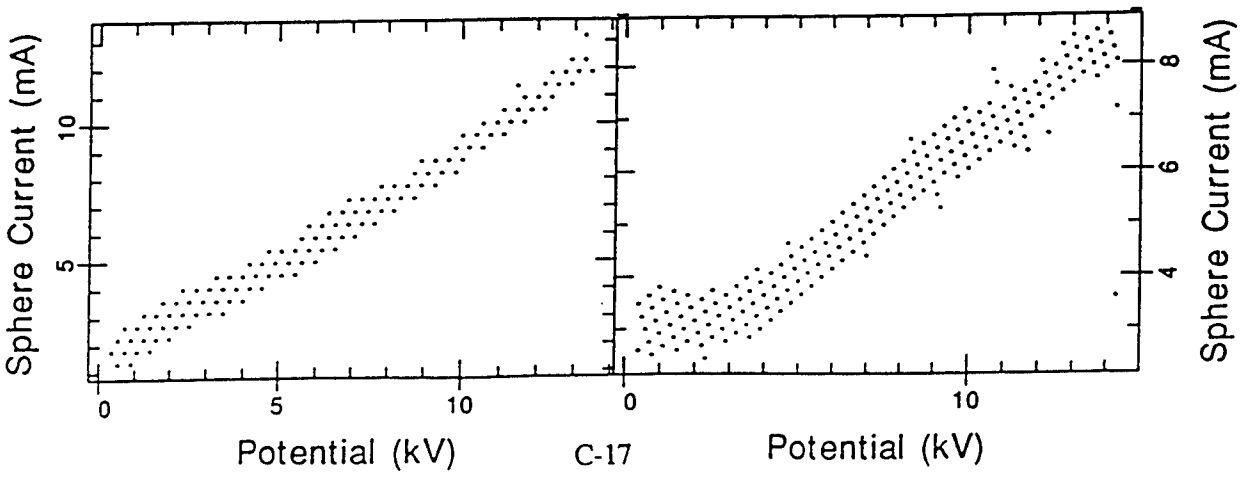

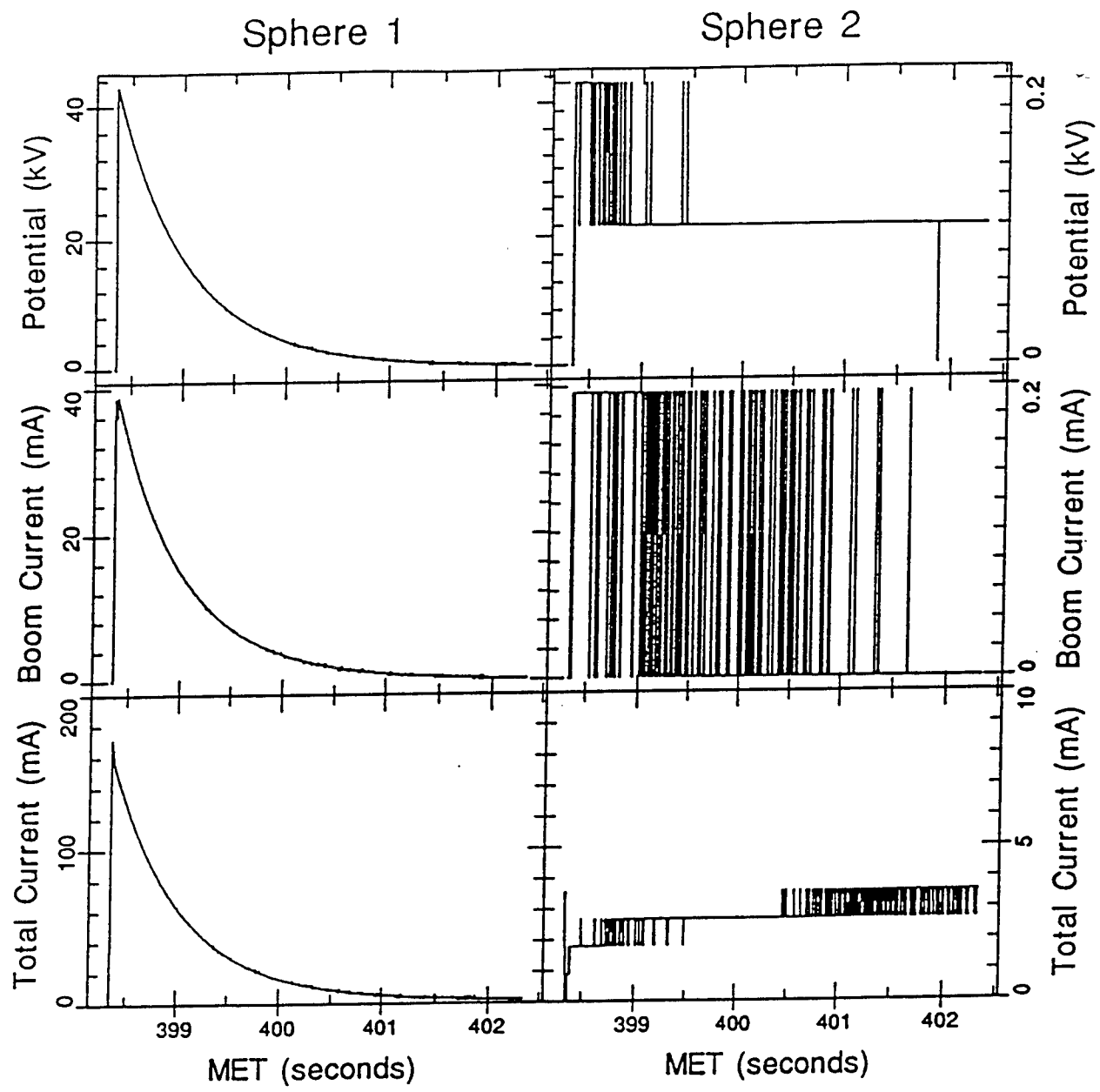

Altitude 361km

B⊥S2-S1

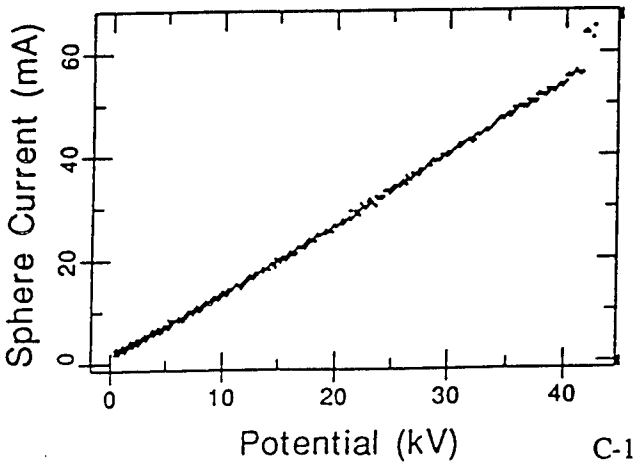

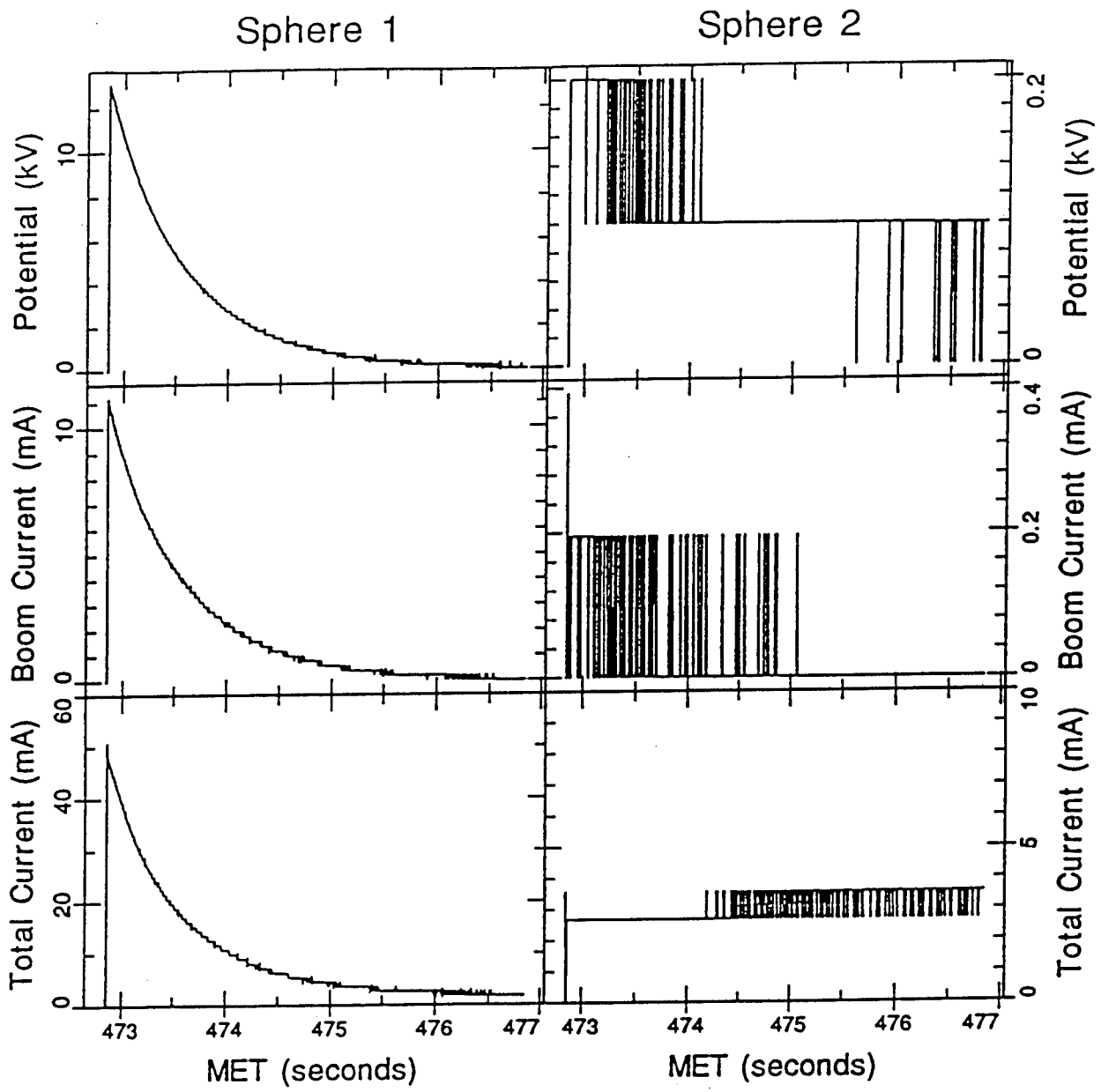

Altitude 307km

$B \| S_2\text{-}S_1$

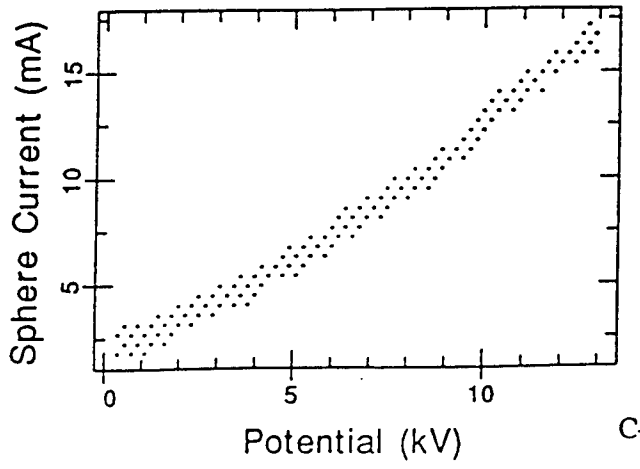

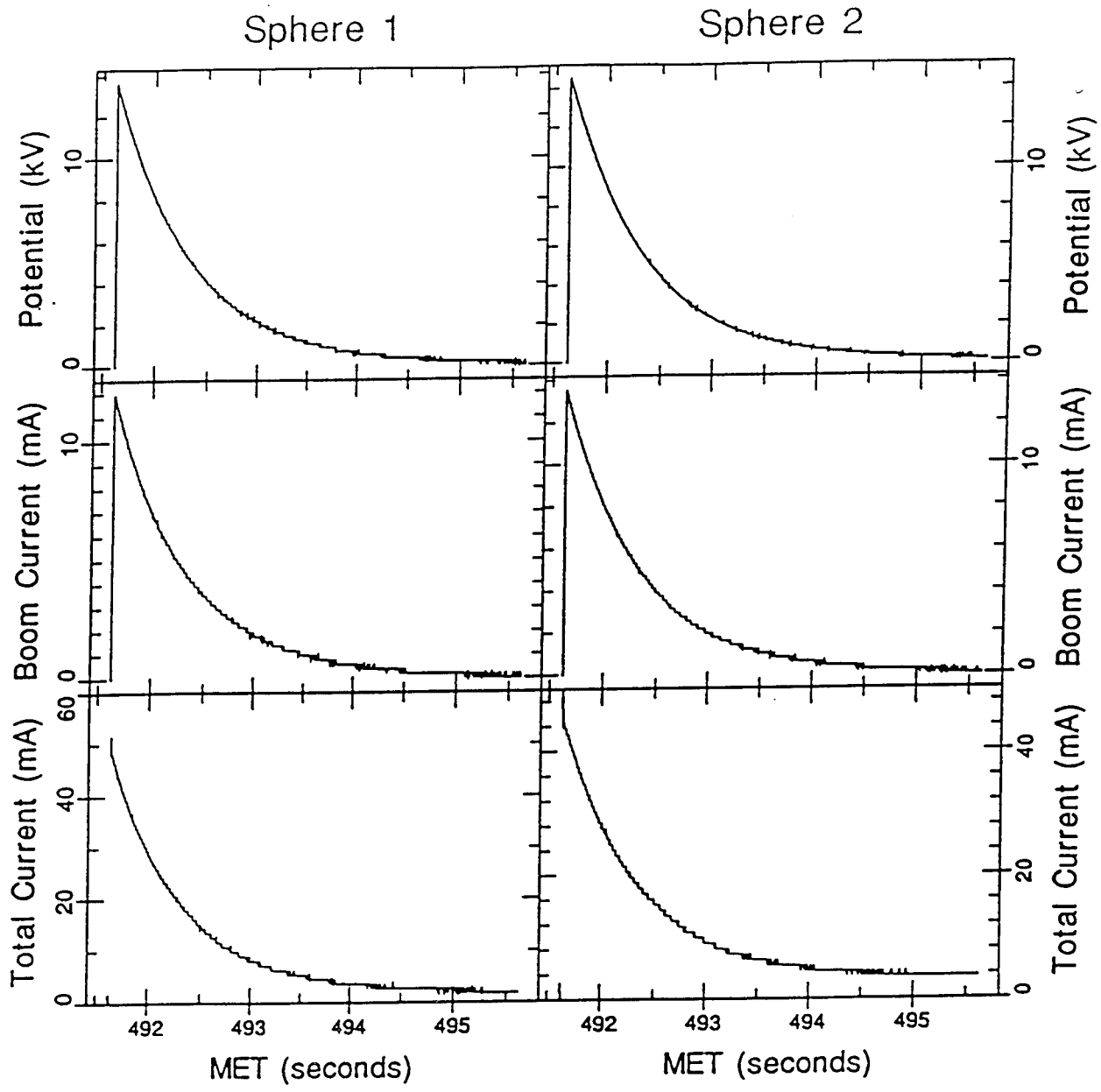

Altitude 287km

$B \| S_2\text{-}S_1$

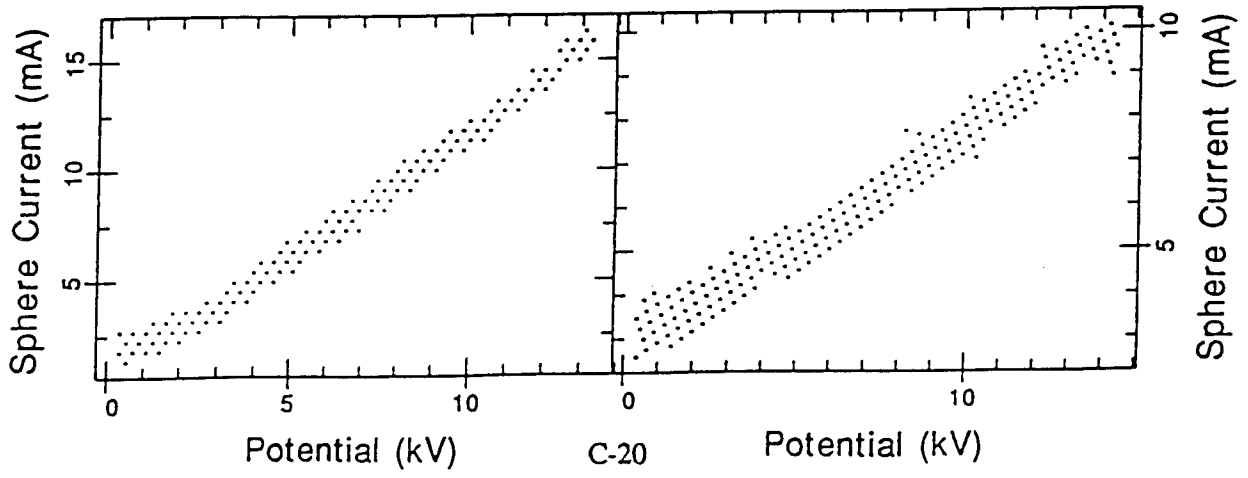

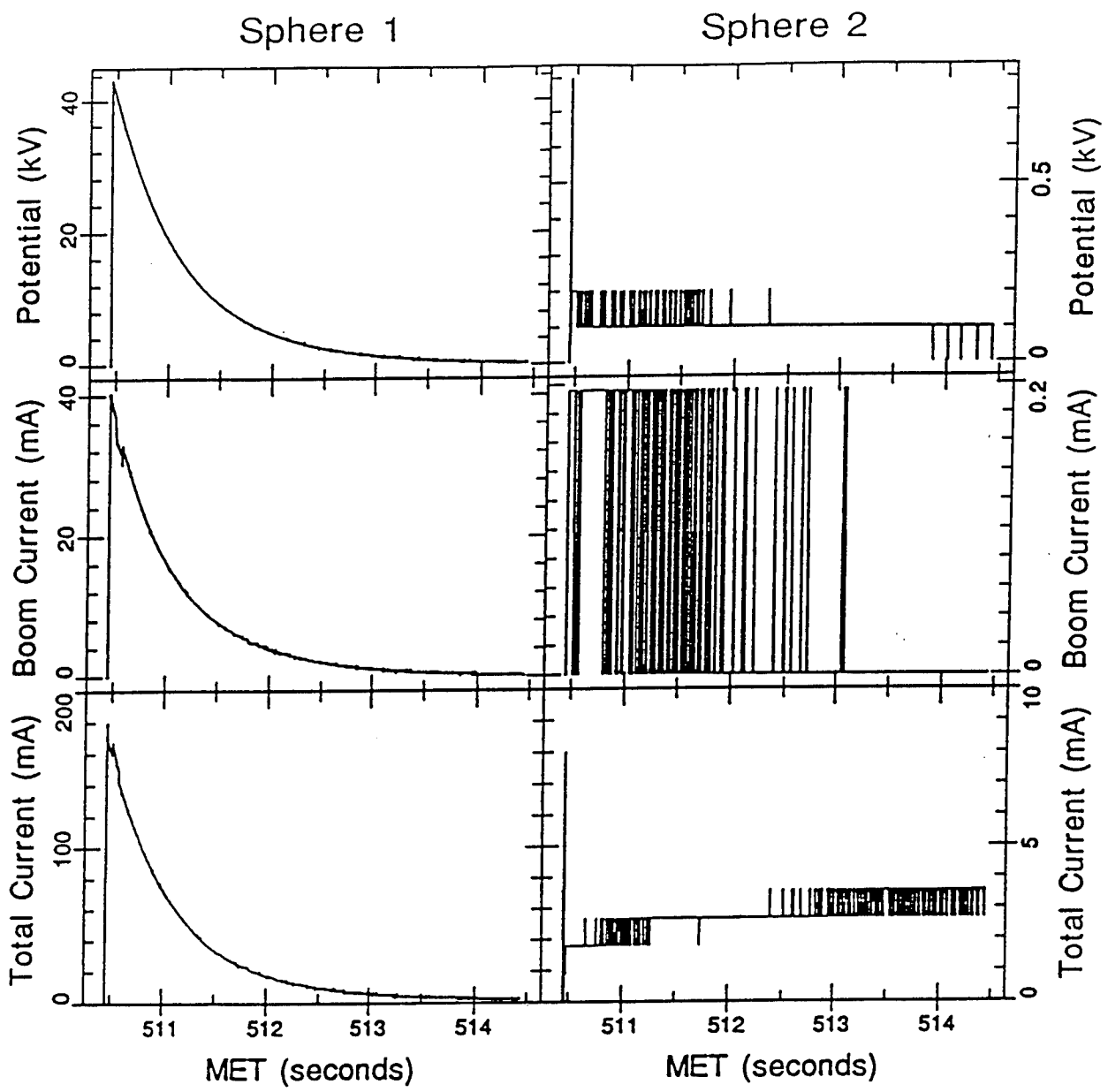

Altitude 263km

$B \| S_2\text{-}S_1$

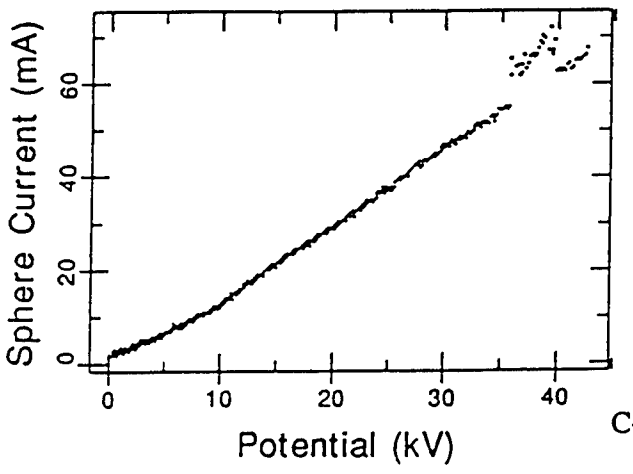

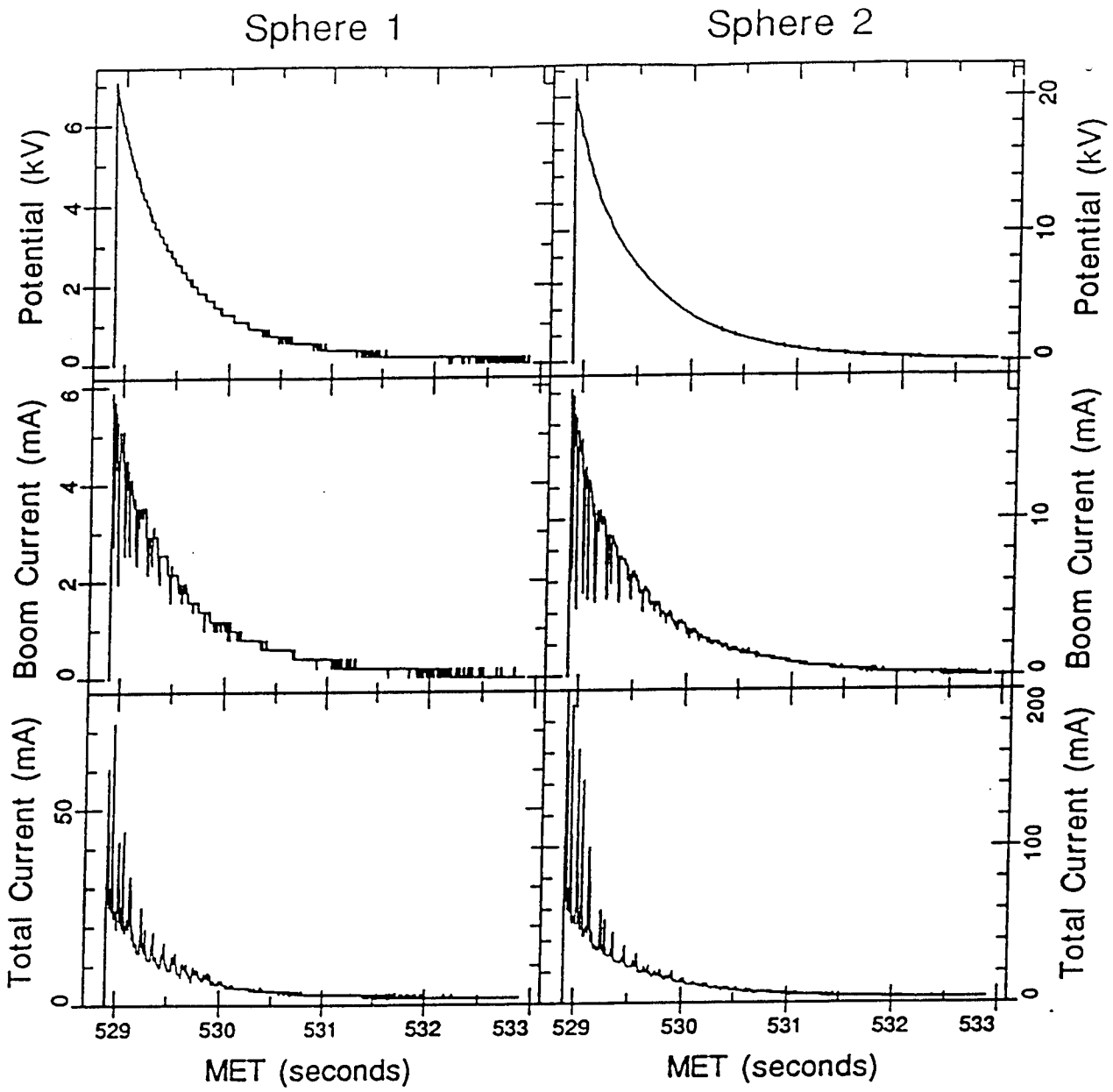
Sphere 1
Sphere 2
Potential (kV)
Boom Current (mA)
Total Current (mA)
529
530
531
532
533
MET (seconds)
Altitude 235km
B||Boom

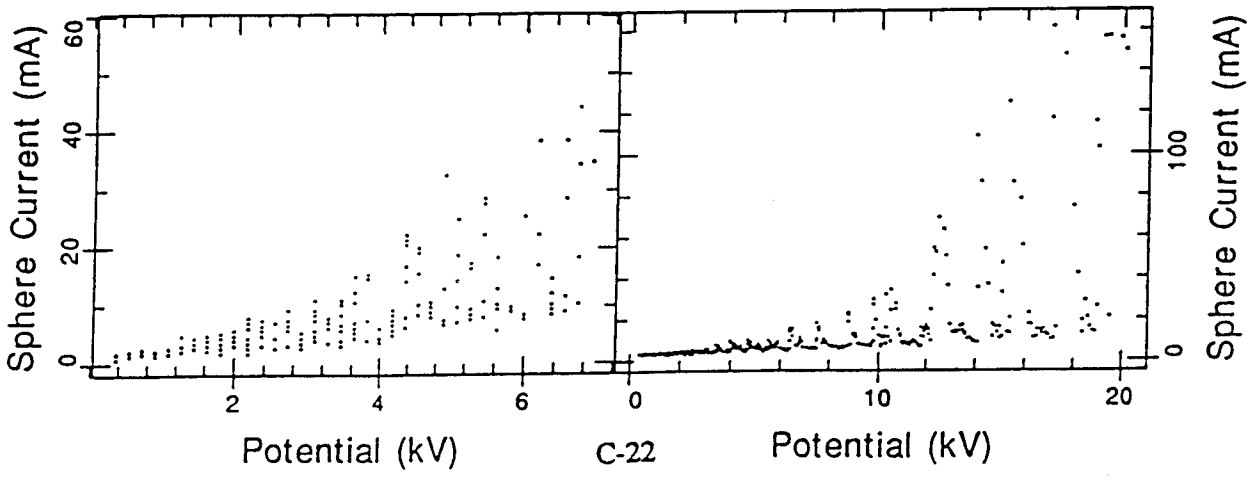
Sphere Current (mA)
Potential (kV)
Potential (kV)
Sphere Current (mA)

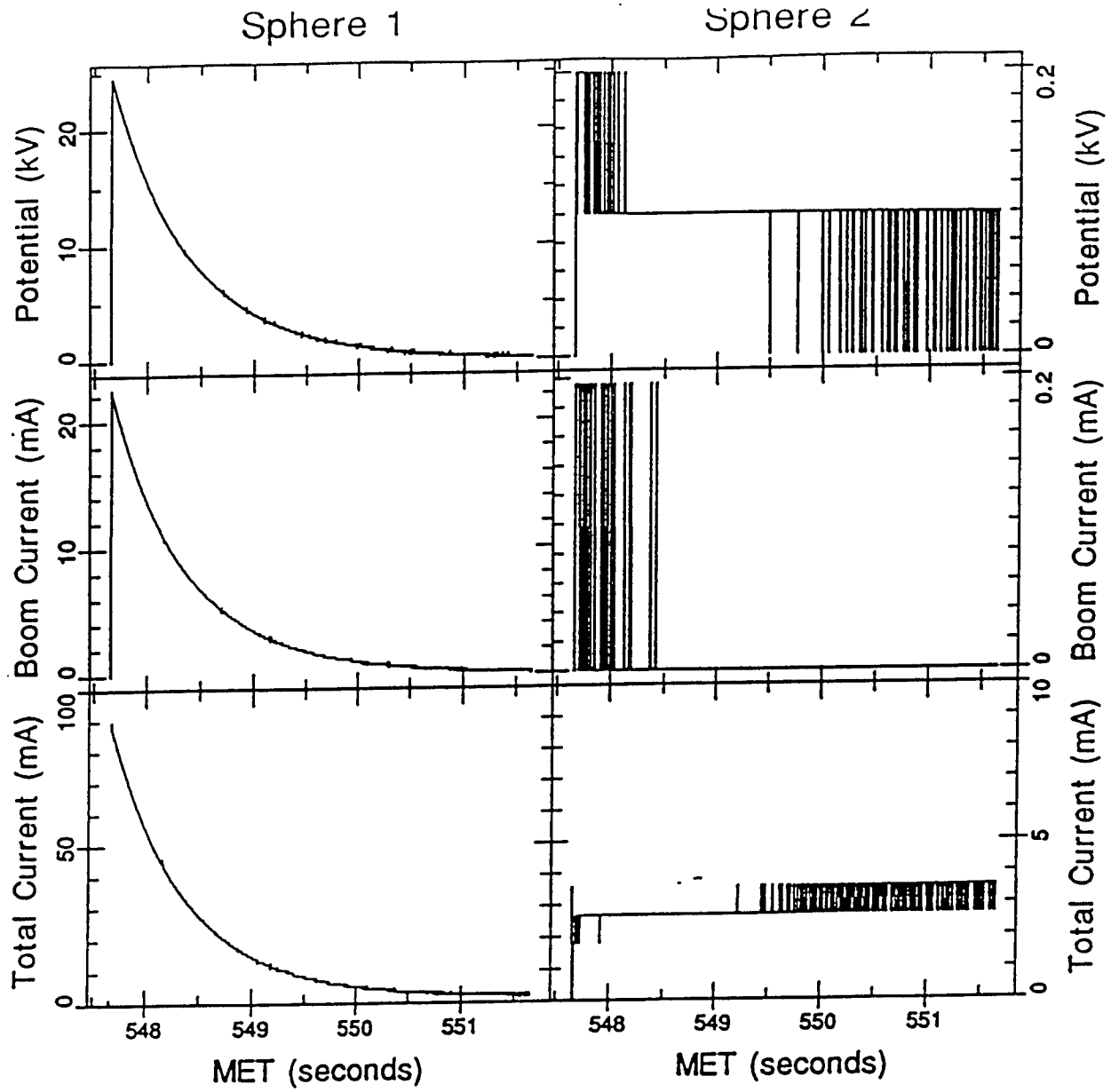
Sphere 1
Sphere 2
Potential (kV)
Boom Current (mA)
Total Current (mA)
MET (seconds)
548
549
550
551
Altitude 206km
B||Boom

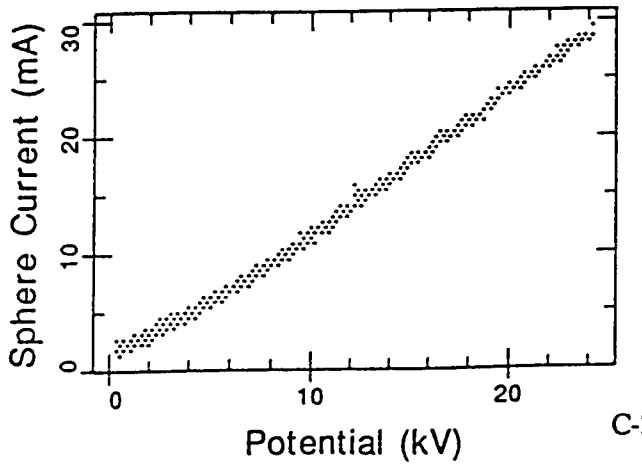
Sphere Current (mA)
Potential (kV)

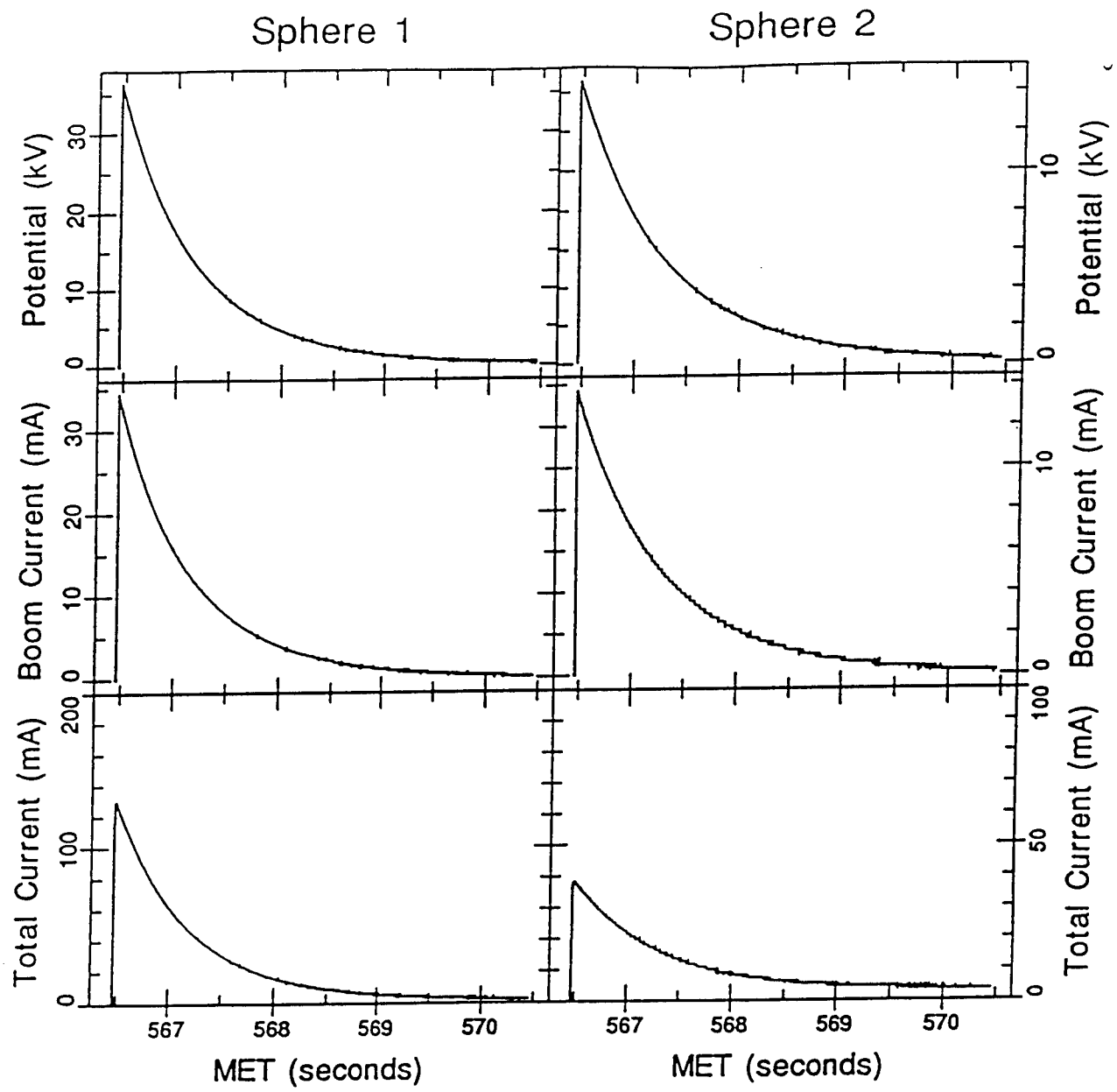

Altitude 172km

B||Boom

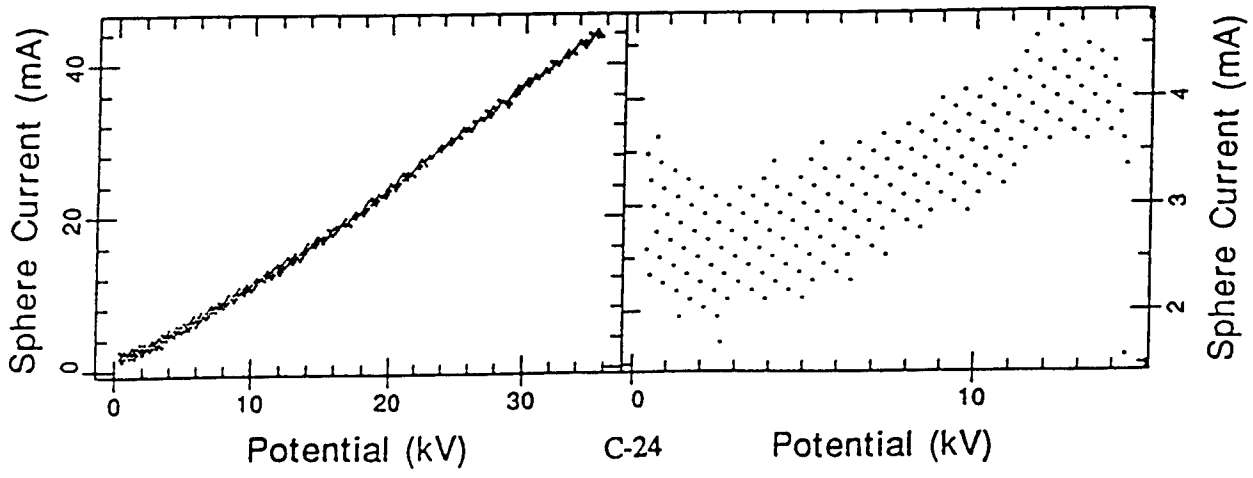

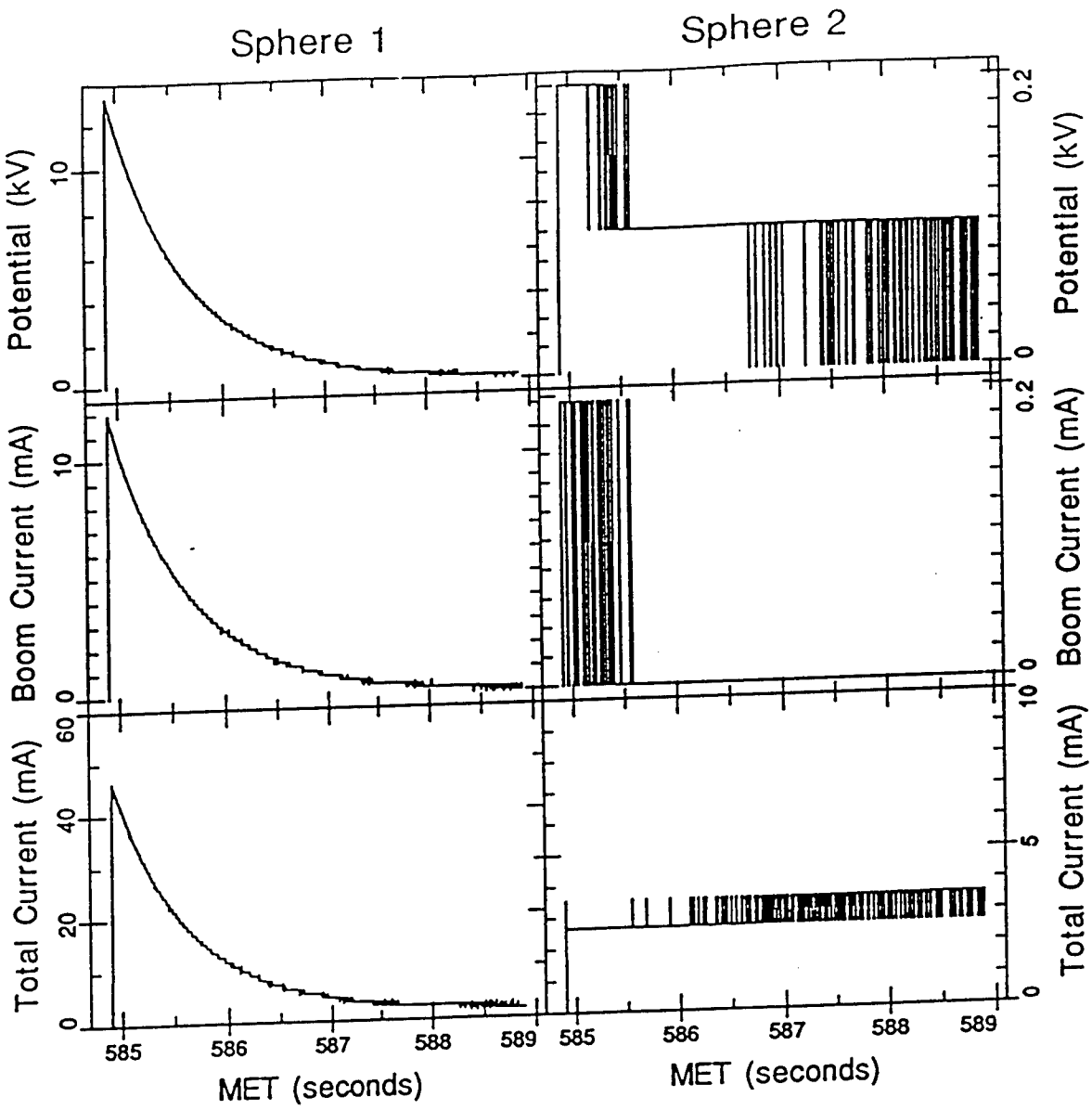

Altitude 137km

B||Boom

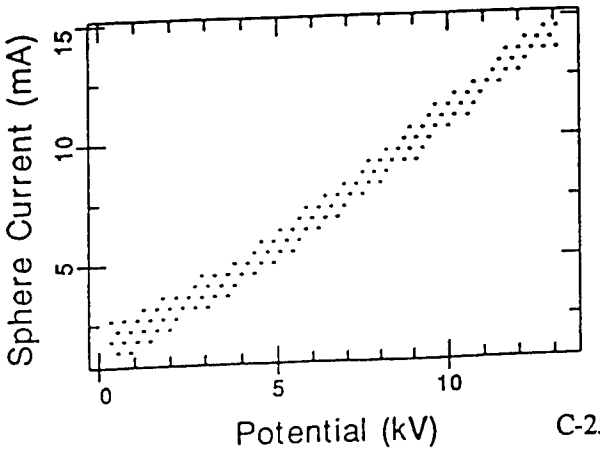

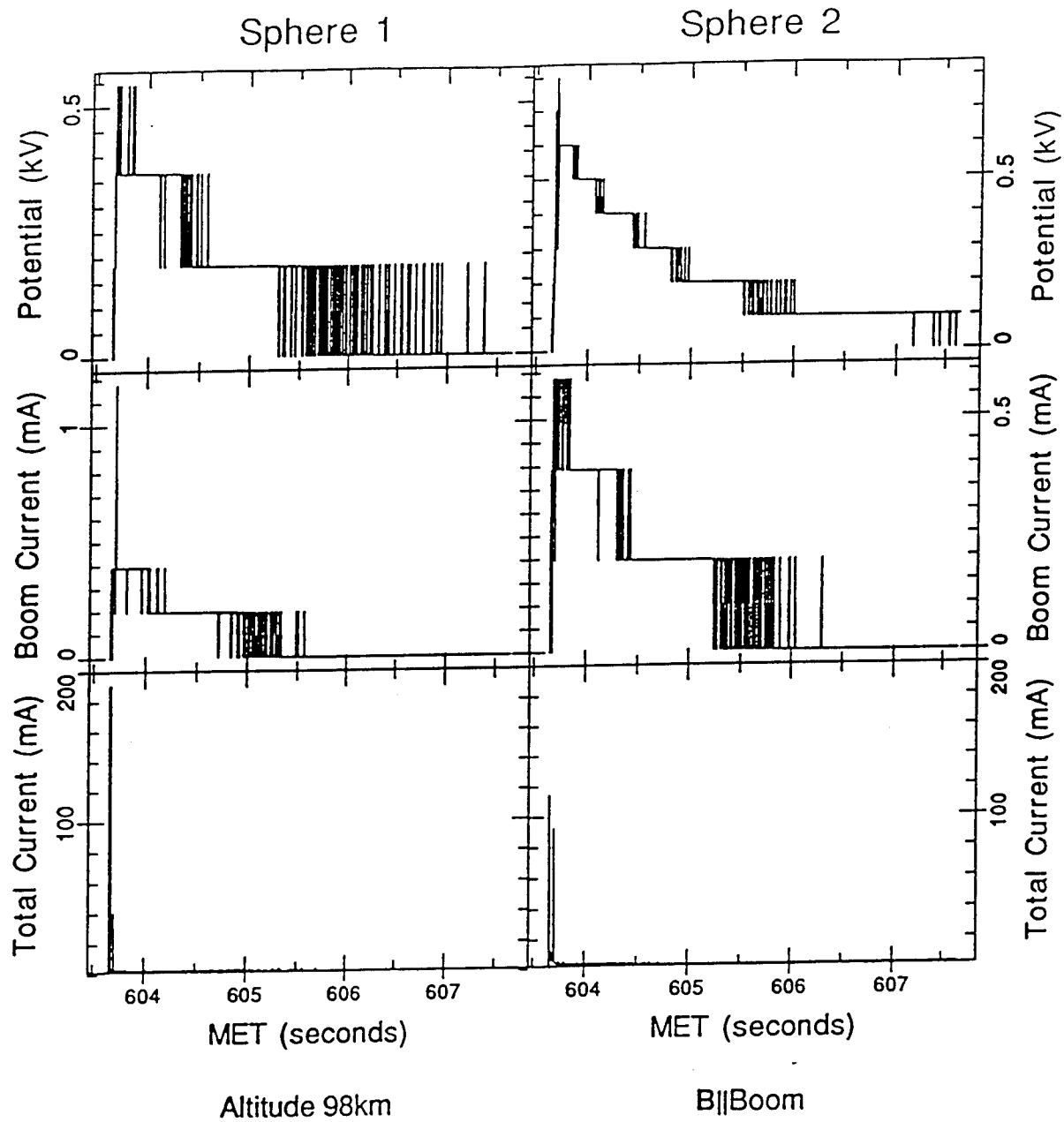
Sphere 1
Sphere 2
Potential (kV)
Boom Current (mA)
Total Current (mA)
0.5
1
200
100
604
605
606
607
MET (seconds)
Altitude 98km
B||Boom

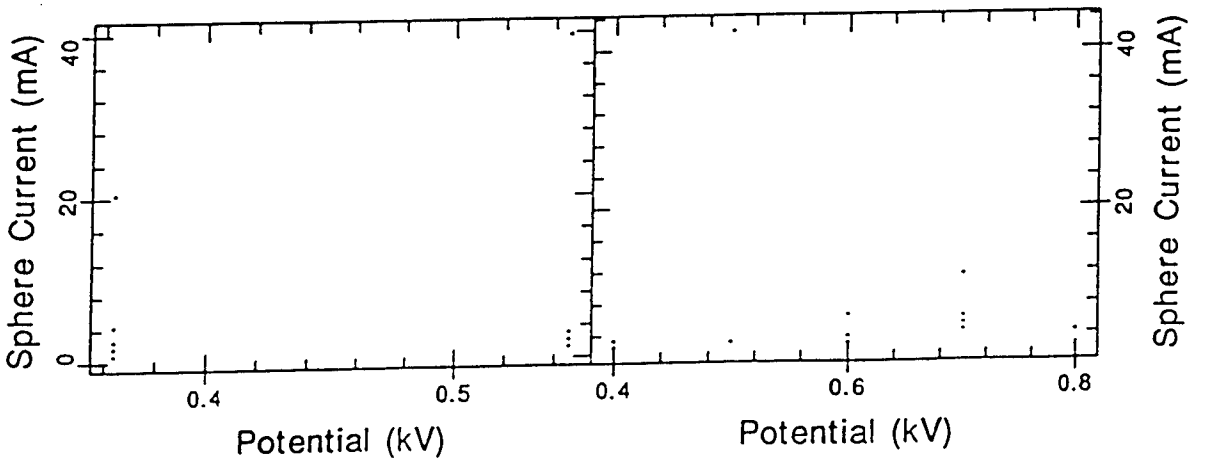
Sphere Current (mA)
40
20
0.4
0.5
0.6
0.8
Potential (kV)